

# Dynamics of wind-induced coastal upwelling and interbasin exchange in Lake Geneva during winter: Implications for deepwater renewal

Présentée le 10 septembre 2021

Faculté de l'environnement naturel, architectural et construit  
Laboratoire de technologie écologique  
Programme doctoral en génie civil et environnement

pour l'obtention du grade de Docteur ès Sciences

par

## Rafael Sebastian REISS

Acceptée sur proposition du jury

Prof. F. Porté Agel, président du jury  
Prof. D. A. Barry, directeur de thèse  
Prof. M. Wells, rapporteur  
Prof. S. G. Schladow, rapporteur  
Prof. A. J. Wüest, rapporteur





# Acknowledgements

First and foremost, I want to thank my supervisor, David Andrew Barry, for giving me the opportunity to join his group and discover the fascinating world of science in general and physical limnology in particular. I greatly appreciate your keen and wide interest in science, your fine sense of when to let your PhD students explore the world alone and when to mount some pressure to steer the work into the right direction (although the appreciation for the latter generally came in hindsight), and last but not least your good sense of humor. I sincerely enjoyed our meetings and discussions, be they of scientific nature or not, and have certainly learned tremendously over the last five years.

This thesis would not have been possible without the great support of my unofficial second supervisor Ulrich Lemmin. Your vast experience played a crucial role in planning and preparing the field experiments, resulting in some of the finest mooring designs and deployment techniques the limnological world has seen thus far - in my humble and perhaps somewhat biased opinion that is. In any case, I took great pleasure in this part of the work and am grateful to have had the opportunity to learn from one of the grand masters of the field. I greatly appreciate your help with structuring, improving and proofreading the manuscripts, especially during the last, most intense weeks of the project. The discussions with you and Andrew were invaluable in not getting lost amidst the vast amount of data and keeping track of the big picture of this thesis.

I would like to thank the members of the thesis committee for their interest in my work and the constructive comments and questions during the defence: Alfred Johny Wüest, Mathew Wells, S. Geoffrey Schladow and Fernando Porté-Agel.

A big thank you goes out to all former and current ECOL members, who made the last five years a memorable and highly enjoyable journey: My first office mates, Abolfazl Irani and Mohsen Cheraghi, who warmly welcomed me to the group and, seemingly knowing every single person at EPFL and in the greater Lausanne area, made the start so much easier. Andrea Cimatoribus, without whom the modeling part of this thesis would not be what it is today. My other office mates: Mehrshad Foroughan, whose good nature and calm attitude I greatly appreciate, as well as Qihao Jang, Haoran Shi, and Zhaoyang Luo. Mahmood Ziabari, who is not only a bottomless source of good tea, but also a great sparring partner for intense discussions

about life, politics and science. Frédéric Soullignac, with whom I spent countless hours philosophizing about the value and beauty of superb beer and the making thereof. Benjamin Graf, who was a great, reliable help in the field and served as a compendium for questions related to programming and electronics. A special thanks to Htet Kyi Wynn, whose great experience and meticulous planning were vital in the success of our many field campaigns. And last but not least, thanks to François Mettra and Violaine Piton, who helped to greatly improve the final presentation of this thesis and whose easygoing nature brought new vigor to the group.

I am grateful for the administrative support and problem solving by Marie Sudki over the past five years, especially at the beginning and during the last year while working from home.

Thank you to my dear colleagues and friends from APHYS, Hugo and Oscar, with whom one can equally well enjoy a beer, a coffee, or a scientific/philosophical discussion. Thanks to all my teammates from the Persepolis de Lausanne football club, notably Amin. I fondly remember the many training sessions (if one can call them such) and matches we had together.

I want to express the deepest gratitude to my family, parents, siblings and friends, who might not have directly contributed to this thesis, but shaped the person who wrote it, and without whom I would not be who I am today.

Saving the best for last: Infinite thanks to my beloved wife Caroline, who laid the groundwork for this thesis by “luring” me to Switzerland in the first place. Without your unconditional support during the most stressful periods, this invaluable journey would not have been possible.

# Abstract

Water quality in lakes is closely linked to hydrodynamics and often dominated by stratification, limiting the exchange between the epi- and hypolimnion. Thus, the vertical redistribution of biogeochemical tracers such as dissolved oxygen and nutrients by convective overturning during winter is an important process in annual lake cycles. In deep, monomictic lakes convective cooling often does not reach the deepest layers. Studies have shown that climate change will further reduce the efficiency of this process, motivating a good understanding of alternative deepwater renewal mechanisms.

Combining field observations, three-dimensional (3D) hydrodynamic modeling, and particle tracking, this thesis explores wind-induced transport processes contributing to vertical exchange in Lake Geneva during winter. A first focus is on Ekman-type coastal upwelling at the northern shore. Then, wind-induced interbasin exchange and hypolimnetic upwelling between the *Petit Lac* (depth 75 m) and *Grand Lac* (depth 309 m) basins of Lake Geneva are investigated. Finally, the effect of stratification in the *Petit Lac* on the latter phenomenon is revealed by model-based momentum budget analysis.

Coastal upwelling at the northern shore of Lake Geneva was investigated in the winter 2017/2018. Following a strong alongshore wind, nearshore temperatures decreased and remained low for 10 days, with the lowest temperatures corresponding to values found at 200-m depth. Current measurements at 30-m depth showed dominant alongshore currents with episodic upslope transport of cold hypolimnetic water in the lowest 10 m. Model results suggest that upwelled waters spread over ~10% of the *Grand Lac*'s surface area. Furthermore, particle tracking confirmed that upwelled waters originated from far below the thermocline and descended back to these layers after the wind ceased.

Exchange and upwelling between the lake's two basins was investigated in the winter 2018/2019. Following a strong along-axis wind, a two-layer flow established, with the downwind surface drift into the *Grand Lac* being balanced by opposing bottom currents into the *Petit Lac* and the current reversal occurring around the thermocline depth. Bottom temperatures at

the confluence gradually decreased to values found in the deep *Grand Lac* hypolimnion. Furthermore, particle tracking revealed a current loop, whereby hypolimnetic water from below 150-m depth first upwelled into the *Petit Lac*, intruding ~10 km, i.e., half its length, and then descended back into the *Grand Lac* hypolimnion. Model results indicated a temporary doubling of the *Petit Lac* hypolimnetic volume during the upwelling.

The observed interbasin upwelling occurred only during early winter, with the bottom inflow of deep hypolimnetic water driven by baroclinic pressure gradients at the confluence, produced by upwind upwelling at the western end of the *Grand Lac*. Once the *Petit Lac* was fully mixed, the wind-induced net volume exchange between the basins was reduced by > 50% and deep hypolimnetic interbasin upwelling was suppressed altogether.

This thesis shows that wind-induced coastal upwelling and hypolimnetic interbasin exchange are complex 3D processes, regularly occurring during winter and providing important mechanisms for deepwater renewal in Lake Geneva. They cannot be represented by one-dimensional models frequently employed to predict climate change induced shifts and merit further attention when assessing deepwater renewal in large, deep lakes.

## Keywords

Lake Geneva, coastal upwelling, interbasin upwelling, interbasin exchange, multi-basin lake, deepwater renewal, Coriolis, 3D modeling, particle tracking, momentum budget analysis

# Zusammenfassung

Wasserqualität in Seen wird stark von hydrodynamischen Prozessen beeinflusst und ist eng mit der Temperaturschichtung verknüpft, welche den Austausch zwischen dem Epi- und Hypolimnion einschränkt. Die vertikale Zirkulation von Sauerstoff und Nährstoffen ist daher ein wichtiger Bestandteil des jahreszeitlichen Zyklus von Seen. In tiefen monomiktischen Seen erreicht die winterliche Konvektion die tiefsten Schichten oft nicht. Studien zeigen, dass Konvektion durch den Klimawandel zunehmend schwächer wird. Ein gutes Verständnis alternativer Mechanismen der Tiefenwassererneuerung ist daher unabdinglich.

Mittels Feldmessungen, dreidimensionaler (3D) hydrodynamischer Modellierung und model-basierter Partikelverfolgung erkundet diese Dissertation wind-induzierte Transportprozesse, die zu vertikalem Austausch im Genfersee im Winter beitragen. Zunächst wird Coriolis-bedingter Küstenauftrieb am Nordufer untersucht. Danach wird der wind-induzierte Tiefenwasseraustausch zwischen den beiden Becken des Genfersees, dem *Petit Lac (PL)* (Tiefe 75 m) und dem *Grand Lac (GL)* (Tiefe 309 m), beleuchtet. Abschliessend wird mittels Impulsbilanz der Einfluss der Temperaturschichtung auf den Austausch zwischen den beiden Becken untersucht.

Küstenauftrieb am Nordufer wurde im Winter 2017/2018 untersucht. Starker küstenparalleler Wind führte dazu, dass die küstennahen Temperaturen abfielen und für 10 Tage tief blieben. Die niedrigsten Temperaturen entsprachen dabei Werten in ~200 m Tiefe. Messungen in 30 m Tiefe zeigten überwiegend küstenparallele Strömungen mit episodischem Küstenquertransport von kaltem Tiefenwasser in den unteren 10 m. Modellergebnisse zeigten, dass sich das aufgetriebene Wasser über ~10% der Fläche des *GL* verteilte. Die Ergebnisse der Partikelverfolgung bestätigten den tiefen Ursprung des aufgetriebenen Wassers und zeigten ausserdem, dass dieses in die tiefen Schichten zurückkehrte nachdem der Wind nachliess.

Tiefenwasseraustausch zwischen den beiden Becken wurde im Winter 2018/2019 untersucht. Starker, küstenparalleler Wind erzeugte eine Zweischichtenströmung. Dabei wurde die in Windrichtung gerichtete Oberflächenströmung in den *GL* von einer entgegengesetzten Bodenströmung in den *PL* ausgeglichen. An der Mündung zwischen den Becken sanken die bodennahen Temperaturen auf Werte die denen des tiefen Hypolimnions entsprachen. Die Ergebnisse

der Partikelverfolgung zeigten, dass sich eine „Strömungsschleife“ einstellte: Tiefenwasser ( $> 150$  m) aus dem *GL* strömte zunächst in den flachen *PL*, wo es daraufhin  $\sim 10$  km (die halbe Länge des *PL*) weit eindrang, bevor es anschliessend in die tiefen Schichten des *GL* zurückfloss. Gemäss den Modellergebnissen verdoppelte sich das Hypolimnionvolumen des *PL* temporär während dieses Prozesses.

Wind-induzierter Tiefenwasseraustausch zwischen den Becken fand nur im frühen Winter statt. Die starke Bodenströmung in den *PL* wurde dabei von baroklinen Druckgradienten an der Mündung getrieben, welche wiederum von windwärtigem Auftrieb am westlichen Ende des *GL* verursacht wurden. Im Spätwinter, sobald der *PL* vollständig durchmischt war, d.h. ohne Baroklinität, reduzierte sich der Volumenaustausch zwischen den Becken um 50% und Tiefenwasseraustausch fand nicht mehr statt.

Diese Dissertation zeigt, dass wind-induzierte Tiefenwasserauftriebsphänomene im Genfersee komplexe 3D Prozesse sind, die häufig im Winter vorkommen und somit potenziell wichtige Mechanismen zur Tiefenwassererneuerung darstellen.

## Stichwörter

Genfersee, Küstenauftrieb, Beckenaustausch, Temperaturschichtung, Tiefenwassererneuerung, Coriolis, 3D Modellierung, Lagrange-Partikelverfolgung, Impulsbilanz

# Contents

<b>Acknowledgements.....</b>	<b>i</b>
<b>Abstract .....</b>	<b>iii</b>
<b>Zusammenfassung.....</b>	<b>v</b>
<b>Chapter 1      Introduction.....</b>	<b>1</b>
1.1    Lakes in a nutshell: Stratification and how it governs water quality .....	2
1.2    Rotational effects on fluid motion.....	4
1.3    Coastal upwelling .....	5
1.4    Interbasin exchange .....	7
1.5    Lake Geneva.....	8
1.5.1 Thermal structure and deepwater renewal .....	9
1.5.2 Typical winds during winter .....	11
1.5.3 The importance of rotational effects in Lake Geneva.....	11
1.5.4 Thermal response to climate change.....	11
1.6    Research objectives and approach.....	13
<b>Chapter 2      Wintertime coastal upwelling in Lake Geneva: An efficient transport                   process for deepwater renewal in a large, deep lake .....</b>	<b>15</b>
2.1    Introduction .....	18
2.2    Materials and methods.....	20
2.2.1 Study site.....	20
2.2.2 Field observations .....	23
2.2.3 Hydrodynamic model.....	24
2.2.4 Particle tracking .....	25
2.3    Results .....	27
2.3.1 Thermal stratification of Lake Geneva .....	27
2.3.2 Meteorological data .....	27
2.3.3 Temperature and current moorings.....	29
2.3.4 Model results.....	32
2.3.5 Particle tracking results.....	35

2.4	Discussion .....	37
2.4.1	Observed temperature peaks near the shore during the active upwelling phase .....	37
2.4.2	Wintertime coastal upwelling as a pathway for deepwater renewal.....	41
2.5	Summary and conclusions.....	43
<b>Supporting Information for Chapter 2 .....</b>		<b>51</b>
<b>Chapter 3 Wind-induced hypolimnetic upwelling between the multi-depth basins of Lake Geneva during winter: An overlooked deepwater renewal mechanism?.. 63</b>		
3.1	Introduction .....	65
3.2	Materials and methods.....	67
3.2.1	Study site.....	67
3.2.2	Field observations .....	69
3.2.3	Hydrodynamic model.....	70
3.2.4	Particle tracking .....	70
3.3	Results and discussion.....	72
3.3.1	Field observations .....	72
3.3.2	Model results.....	75
3.3.3	Particle tracking .....	79
3.4	Summary and conclusions.....	88
<b>Supporting Information for Chapter 3 .....</b>		<b>95</b>
<b>Chapter 4 What role does stratification play in wind-induced hypolimnetic upwelling between the multi-depth basins of Lake Geneva during winter? ..... 107</b>		
4.1	Introduction .....	109
4.2	Materials and methods.....	111
4.2.1	Study site.....	111
4.2.2	Field observations .....	112
4.2.3	Hydrodynamic model.....	113
4.2.4	Particle tracking .....	115
4.3	Results and discussion.....	116
4.3.1	Field observations .....	116
4.3.2	Model results.....	119
4.3.3	Effect of stratification on interbasin exchange and hypolimnetic upwelling .....	131
4.4	Summary and conclusions.....	134
<b>Supporting Information for Chapter 4 .....</b>		<b>141</b>
<b>Chapter 5 Conclusions and Outlook .....</b>		<b>153</b>



5.1	Summary and conclusions.....	154
5.2	Future work .....	157
5.2.1	The role of wind-induced upwelling processes in energizing and mixing the deep hypolimnion layers in Lake Geneva.....	157
5.2.2	Field observations of deepwater ventilation by wind-induced upwelling processes in Lake Geneva.....	158
5.2.3	The role of <i>Bise</i> winds in generating coastal upwelling in Lake Geneva..	158
<b>Bibliography .....</b>		<b>161</b>
<b>Curriculum Vitae .....</b>		<b>162</b>



# Chapter 1    Introduction

---

”A lake is the landscape's most beautiful and expressive feature. It is earth's eye; looking into which the beholder measures the depth of his own nature.” (Thoreau 1854).

”Lakes are formed when depressions are filled with water. [...] Different physical, chemical, and biological processes take place in lakes [...]” (Bengtsson et al. 2012)

One can argue who has really grasped the true nature of lakes, the writer or the scientist. However, it is the latter who, by studying the “*different physical, chemical, and biological processes*”, generates the knowledge and understanding that is essential for developing sustainable lake management and conservation strategies. This is especially true in the light of climate change, which has begun and will continue to alter lakes in many ways. Besides inspiring writers and keeping scientists busy, lakes are complex ecosystems of great economic and societal value, e.g., by supplying water for drinking and agricultural use, and supporting recreational activities, tourism, fishing, and transport.

This thesis aims to contribute to a better understanding of “*the landscape's most beautiful and expressive feature*”, as Thoreau put it, by exploring different physical processes and their ecological implications in Lake Geneva, Western Europe’s largest lake.

## 1.1 Lakes in a nutshell: Stratification and how it governs water quality

Lakes are stratified water bodies exhibiting a distinct vertical structure of physical and biogeochemical properties, typically subject to a pronounced seasonal cycle. The latter is largely shaped by climatic conditions such as air temperature and wind forcing, and by lake depth. The annual thermal cycle of warm monomictic lakes, such as Lake Geneva, can be summarized as follows (e.g., Bohrer and Schultze 2009):

The upper layers of the water column are directly affected by momentum and heat exchange with the atmosphere. In summer, this results in a warmer, well-mixed surface layer (epilimnion), “floating” on top of a colder, denser bottom layer (hypolimnion). The transition layer

(thermocline or metalimnion) is characterized by strong density gradients, limiting vertical exchange between the epi- and hypolimnion. Atmospheric cooling and often increased wind speeds during autumn lead to a gradual erosion of the stable thermal structure and deepening of the well-mixed layer. In comparably shallow lakes and/or under strong cooling, the stratification is gradually eroded during autumn and winter cooling, resulting in a fully-mixed water column. In very deep lakes, on the other hand, a weak thermal stratification is often maintained throughout the winter season. Warming of the upper layers during spring and summer gradually reestablishes the stable thermal structure and the annual cycle begins anew.

In the upper, well-mixed and sunlit layers, dissolved oxygen (DO) is maintained near saturation levels by gas exchange with the atmosphere and photosynthesis. In the hypolimnion, on the other hand, no active reoxygenation takes place. Instead, DO is consumed by microbial mineralization of organic matter within the water column and in the upper sediment layers, and by biochemical processes in the lower sediments (e.g., Schwefel et al. 2017, 2018). Due to the high DO consumption and limited vertical exchange with the well-aerated epilimnion, DO concentrations in the hypolimnion are often low during the stratified period. On the other hand, nutrients such as phosphorus and nitrogen are assimilated during primary production by photosynthesis in the epilimnion and released by mineralization of organic matter in the hypolimnion (e.g., Krishna et al. 2021). As a result, the vertical temperature structure of a stratified lake is strongly reflected in many biogeochemical parameters such as DO and nutrients, making vertical exchange, especially during the unstratified period, an important process in the annual cycle of a lake.

In deep, monomictic lakes, such as Lake Geneva, convective cooling during winter often does not reach the deepest layers (e.g., Livingstone 1993; Coats et al. 2006; Lemmin 2020). Furthermore, driven by the temperature differences between the atmosphere and the lake surface, convective cooling is expected to become even less efficient in the future with potentially milder winters due to climate change (Goldman et al. 2013), making a good understanding of alternative deepwater renewal mechanisms crucial.

This thesis investigates the as yet little-known dynamics of wind-induced coastal upwelling and wind-induced hypolimnetic exchange between the two basins of Lake Geneva during winter. These processes have in common that they are highly complex, transient, and three-dimensional (3D). They occur regularly during winter in Lake Geneva, driving significant horizontal and

vertical exchange, with vertical excursions often exceeding 100 to 150 m, and thus may contribute to deepwater renewal even during periods of incomplete vertical convective mixing.

In sections 1.2 to 1.5 some key concepts that are at the heart of this thesis are introduced and the characteristics of the study site Lake Geneva are presented. The research objectives and the structure of this thesis are outlined in section 1.6.

## 1.2 Rotational effects on fluid motion

All large-scale motion in oceans and very large lakes, such as the Laurentian Great Lakes, is strongly modified by the Coriolis force, resulting in a rightward (leftward) deflection perpendicular to the direction of motion in the Northern (Southern) Hemisphere. In “large” lakes, Coriolis effects also play an important role, however, what “large” means in this context is not always well defined and sometimes blurred in the literature, as discussed by Amadori et al. (2020).

The internal wave field of a stratified lake is strongly modified by the Coriolis force when the characteristic horizontal scale of the basin,  $L$ , is close to or larger than the internal Rossby radius, defined as  $R_i = c_i f^{-1}$ , where  $c_i$  is the baroclinic phase speed and  $f$  is the inertial frequency (Antenucci 2009). In basins with  $L > R_i$  or  $L \approx R_i$ , long internal waves can take the form of internal Kelvin and Poincaré waves (e.g., Lemmin et al. 2005; Bouffard et al. 2012; Bouffard and Lemmin 2013; Flood et al. 2020; Roberts et al. 2021).

Closely related to the Rossby radius is the Rossby number, which relates advection to the Coriolis force and is defined as  $Ro = u_x f^{-1} L_x^{-1}$ , where  $u_x$  and  $L_x$  are a characteristic velocity and horizontal length scale of the flow, respectively (Cushman-Roisin and Beckers 2011).  $Ro$  is often used to describe the significance of Coriolis effects in the context of large-scale currents such as gravity currents, with small numbers indicating that the Coriolis force is important (e.g., Roget and Colomer 1996; Jazi et al. 2020).

On the other hand, the extent to which the (steady state) wind-driven circulation in narrow, elongated basins is modified by rotation is better described by the Ekman depth  $d_E = \sqrt{2K_v f^{-1}}$ , where  $K_v$  is the vertical eddy viscosity (e.g., Hutter et al. 2011). The dimensionless Ekman number relating frictional forces to the Coriolis force is defined as  $Ek = K_v f^{-1} D^{-2}$ , where  $D$  is a typical depth scale (e.g., the maximum or mixed layer depth, respectively), with

large numbers indicating that the flow is governed by friction and vice versa (e.g., Kämpf 2010). In narrow, elongated basins where the maximum depth is larger than  $d_E$ , axial wind stress can induce a transversal secondary circulation, which in turn has significant consequences for the vertical current structure (e.g., Winant 2004; Sanay and Valle-Levinson 2005) and can result in up- and downwelling along the lateral boundaries (Toffolon 2013; Piccolroaz et al. 2019).

The definitions and nomenclature of the length scales and dimensionless numbers used to characterize Coriolis effects in lakes can vary in the literature. However, it is important to note that, especially in medium-sized basins, there is not only one single criterion that defines whether the circulation is modified by rotation. Instead, it depends on the process that is considered.

An elegant way to assess the importance of Coriolis effects in complex, realistic flows is by momentum budget analysis based on a 3D hydrodynamic model (chapter 4). The wind-induced circulation in both basins of Lake Geneva is strongly modified by the Coriolis force in different ways, as discussed in chapters 2 to 4.

### 1.3 Coastal upwelling

Wind-driven coastal upwelling in lakes and the ocean occurs when surface waters are transported away from the shore, creating a nearshore divergence in the surface layers that is balanced by upwelling of colder waters from below. Depending on the basin size and shape, and the fetch length, coastal upwelling in lakes takes on different forms, as illustrated in Figure 1.1.

In small lakes (in terms of Rossby radius), direct upwelling occurs at the upwind end (e.g., Mortimer 1952; Coman and Wells 2012), generally accompanied by downwelling at the downwind end (Figure 1.1a). Depending on the basin shape and fetch length, the same type of upwelling can occur in larger lakes in which Coriolis force-induced Poincaré and/or Kelvin waves are observed, such as Lake Simcoe (Cossu and Wells 2013), Lake Tahoe (Schladow et al. 2004; Steissberg et al. 2005; Roberts et al. 2021), and Lake Biwa (Homma et al. 2016). In the ocean and large (elongated) lakes with sufficiently long fetch, persistent along-shore wind stress results in surface layer transport that is perpendicular to the direction of the wind (to the right in the Northern Hemisphere; Figure 1.1b). This so-called Ekman transport (Ekman 1905) causes divergence or convergence near the shore (depending on the wind direction), resulting in Ekman-type coastal upwelling or downwelling, respectively (e.g., Csanady 1977; Rowe et

al. 2019; Reiss et al. 2020). Note that several studies have employed remote sensing technologies, i.e., airborne or spaceborne thermal imagery, to investigate coastal upwelling and downwelling based on the induced surface temperature patterns, both in small (e.g., Pöschke et al. 2015) and large (e.g., Steissberg et al. 2005; Plattner et al. 2006; Troitskaya et al. 2015; Bouffard et al. 2018) lakes.

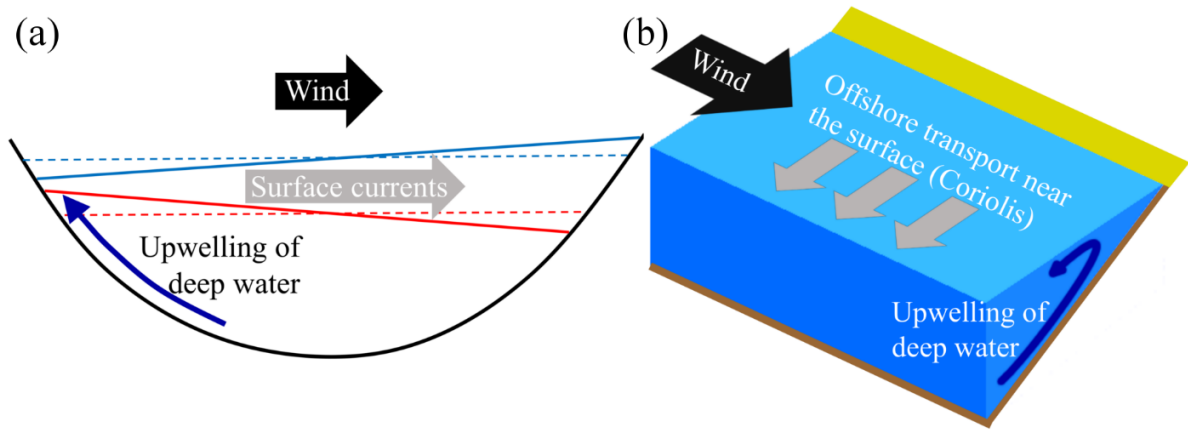


**Figure 1.1.** Schematics illustrating (a) direct and (b) Ekman-type coastal upwelling. The blue and red lines in (a) mark the level of the free surface and thermocline, before (dashed lines) and during (solid lines) the wind event.

Coastal upwelling is an efficient transport process that can induce large vertical motions in deep, stratified lakes (Schladow et al. 2004; Reiss et al. 2020; Roberts et al. 2021), bringing large amounts of deep, hypolimnetic waters in contact with the “fresher” upper layers and the atmosphere. Furthermore, upwelling by definition induces large isotherm excursions, which upon relaxation of the wind stress, generate baroclinic motions such as internal waves and coastal jets (e.g., Beletsky et al. 1997; Boegman 2009; Roberts et al. 2021). Strong shear and density inversions during coastal upwelling events and the subsequent relaxation processes can lead to diapycnal mixing between upwelled and ambient waters, directly affecting water quality, e.g., by supplying the upper photic layers with nutrients and ventilating the hypolimnetic layers. Similar to wind-driven coastal upwelling, coastal downwelling can be an important mechanism for deepwater ventilation in deep lakes by transporting fresher surface waters down to great depths (e.g., Amadori et al. 2018, 2020; Piccolroaz et al. 2019). Furthermore, pelagic



upwelling and downwelling in cyclonic and anti-cyclonic gyres (generally caused by the prevailing wind patterns), respectively, can also enhance vertical exchange between the hypolimnion and epilimnion during the stratified period (e.g., Troitskaya et al. 2015).

In the ocean, large-scale coastal upwelling systems significantly contribute to the redistribution of nutrients and DO (e.g., Kämpf and Chapman 2016). Furthermore, oceanic coastal upwelling plays an important role in modulating estuarine exchange by changing pressure gradients at the estuary mouth (e.g., Giddings and MacCready 2017). In lakes, on the other hand, the effects of coastal upwelling on water quality, and especially deepwater renewal, are often less well understood (e.g., Roberts et al. 2021), partly due to their complex, transient nature, which depends on many parameters such as basin size and shape, stratification, and the local wind field.

Thus far, coastal upwelling in lakes has mainly been studied during the strongly stratified summer period (e.g., Rao and Murthy 2001; Corman et al. 2010; Troy et al. 2012; McKinney et al. 2018; Bouffard et al. 2018; Hlevca et al. 2018; Soullignac et al. 2018; Valipour et al. 2019). Coastal upwelling during the weakly stratified winter period, on the other hand, has received little attention, even though it is under these conditions that wind stress effects penetrate the deepest into the water column and therefore can “lift” very deep water masses up to the surface layers (e.g., Schladow et al. 2004), potentially contributing to deepwater renewal. Chapter 2 of this thesis addresses this research gap and investigates wind-induced coastal upwelling in large, deep Lake Geneva during winter.

## 1.4 Interbasin exchange

As outlined in section 1.1, stratified lakes are generally dominated by vertical gradients. However, in multi-basin lakes, large horizontal gradients in water quality can exist, e.g., due to (i) localized nutrient loading (Hamidi et al. 2015), (ii) differences in the thermal structure and productivity (Bartish 1987), or (iii) different seasonal mixing regimes in adjacent basins of different depths (Lake Garda: Salmaso 2005; Lake Geneva: CIPEL 2016). Consequently, exchange processes between sub-basins, especially between their hypolimnia, can have significant ecological consequences (Jabbari et al. 2019, 2021) and contribute to deepwater renewal (Boyce et al. 1980; Ahrnsbrak and Wing 1998).

One major driver for interbasin exchange is wind stress, which can act indirectly through internal wave pumping (van Senden and Imboden 1989; Umlauf and Lemmin 2005; Flood et al.

2020) and geostrophic adjustment processes after the relaxation of coastal upwelling fronts (Jabbari et al. 2021). Furthermore, in the presence of stratification, along-axis winds can produce direct two-way advective exchange, where the mean downwind surface drift towards one basin is balanced by a hypolimnetic counterflow into the other basin (Laval et al. 2008; Niu et al. 2015).

The importance of wind-driven coastal upwelling in lakes due to its potential role in nutrient cycling and vertical and horizontal exchange has long been recognized and made it the subject of many studies (albeit mainly during the stratified season; see section 1.3). On the other hand, wind-induced interbasin exchange, in particular, hypolimnetic upwelling between basins of different depths has received little attention, with the exception of shallow Lake Erie (Boyce et al. 1980; Bartish 1987; Saylor and Miller 1987; Jabbari et al. 2021) and narrow Quesnel Lake (Laval et al. 2008). Chapters 3 and 4 of this thesis seek to bridge this gap in the literature by exploring the dynamics of wind-induced interbasin exchange between the two multi-depth basins of deep Lake Geneva during winter, with a focus on the deepwater renewal potential of this process.

## 1.5 Lake Geneva

Lake Geneva (local name: *Lac Léman*) is a crescent shaped, warm monomictic lake situated on the border between Switzerland and France. With a surface area of 580 km<sup>2</sup> and a volume of 89 km<sup>3</sup>, it is not only Western Europe’s largest lake but also of great regional socio-economic and ecological importance, providing drinking water for more than 900,000 people (CIPEL 2019). Lake Geneva is composed of two basins with a total length of 73 km: the large, eastern *Grand Lac* (maximum width 14 km and depth 309 m) and the small, western *Petit Lac* (maximum width 5 km and depth 75 m). The “confluence” between the two basins is approximately 3.5 km wide, with a maximum depth of 65 m (Figure 1.2).

The Rhône River is the main inflow and only outflow, entering the basin at the eastern end and leaving it at the western end, where a weir controls the lake’s water level. River throughflow leads to a theoretical residence time of about 11 years (CIPEL 2019).

A systematic monitoring program of the lake’s water quality exists since 1957 (Commission Internationale pour la Protection des Eaux du Léman – [CIPEL](#); last accessed 17 May 2021).

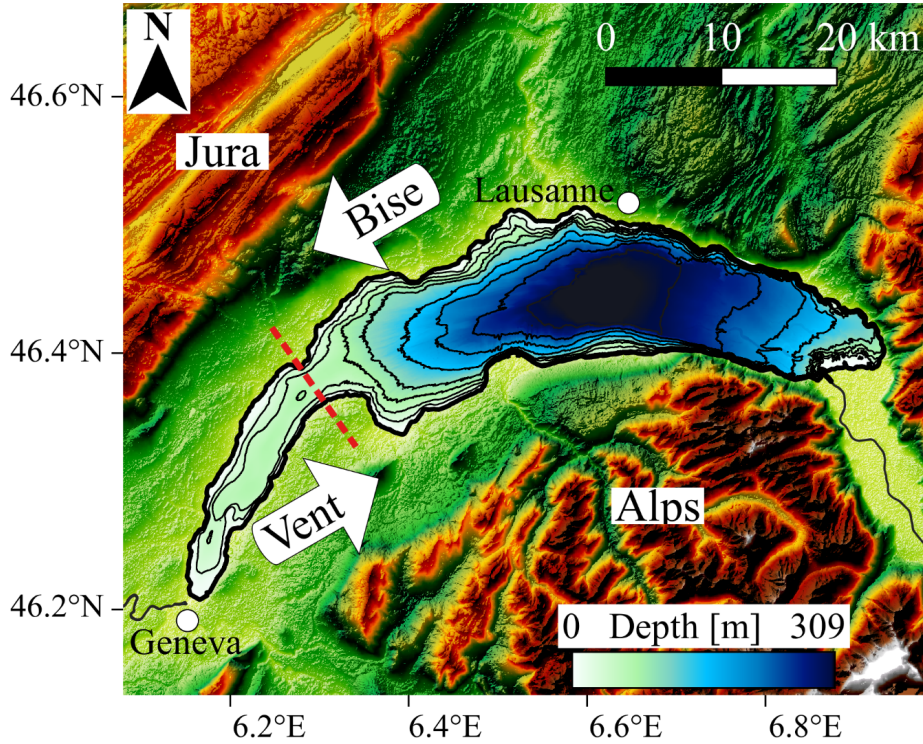


**Figure 1.2.** Bathymetric map of Lake Geneva including the surrounding topography and schematics of the two dominant large-scale winds, namely the *Vent* from the southwest and the *Bise* from the northeast. The red dashed line approximately delimits the two basins, i.e., the small, western *Petit Lac* and the large, eastern *Grand Lac*. Depth is given in meters in the colorbar legend and by the isobath contours (0, 25, 50, 75, 100, 150, 200, 250, and 300 m).

### 1.5.1 Thermal structure and deepwater renewal

Lake Geneva is strongly stratified in summer with a thermocline at approximately 20-m depth. Convective cooling during fall and winter gradually erodes the stable thermal structure, however, due to its great depth and the mild climate, the deep main basin remains stratified during most years, with the maximum mixing depth of 100 to 150 m typically reached by the end of February or beginning of March. Full-depth convective overturning occurs only during severely cold winters (CIPEL 2019). However, even during years of incomplete vertical mixing, heat is transferred down to the deepest layers by internal mixing processes, which are not fully understood yet but appear to be mainly related to internal wave breaking and frictional decay of inertial motions (Lemmin 2020). The result is a “saw-tooth” temperature pattern in the deep hypolimnion that is characterized by multiannual periods of warming followed by a sudden cooling during extremely cold winters, as is typical for deep, warm monomictic lakes (Livingstone 1997; Coats et al. 2006; Ambrosetti et al. 2010). Note that field observations show that sediment-laden gravity currents (i.e., underflows) from the Rhône River, as well as

turbidity currents due to slope failure in the Rhône delta region occasionally reach the deepest layers of Lake Geneva (Lambert and Giovanoli 1988; Giovanoli 1990). While the understanding of how important these currents are for warming and ventilating the deep hypolimnion remains elusive (largely due to the lack of conclusive field observations), they are limited in frequency and intensity, indicating that their contribution is likely minor. Furthermore, sediment-laden gravity currents are generally related to discharge peaks of the Rhône river, e.g., due to intense rainfall, and as such are absent in winter (Giovanoli 1990; Loizeau and Dominik 2000). The warming of the deep layers, on the other hand, occurs throughout the year (Lemmin and Amouroux 2013), indicating that internal mixing processes are the dominant source.

Due to the annual complete vertical mixing of the shallow *Petit Lac* basin (maximum depth 75 m), water quality parameters such as DO (higher values) and nutrient concentrations (lower values) differ from those in the deep *Grand Lac* hypolimnion (e.g., CIPEL 2016; Lavigne and Nirel 2016). Hypolimnetic exchange processes between the two basins could therefore have important ecological effects.

The aeration of the deepest layers has long been attributed to full-depth convective mixing during severely cold winters only. However, recently it was shown (Lemmin 2020) that (i) in cold winters, vertical DO profiles with high concentrations near the bottom and a pronounced minimum in the bulk water of the deep hypolimnion can occur, suggesting the lateral advection of oxygen-rich water along the lakebed; (ii) near-bottom DO concentrations at the central 300 m deep plateau in the *Grand Lac* basin can show a significant spatial variability; and (iii) a small increase of the DO concentrations at the deepest point of the lake (309 m) occurs every winter, even under incomplete vertical convective cooling.

Altogether, there are strong indications that deepwater renewal in Lake Geneva is not only controlled by vertical convective mixing but also, to some extent, by diverse 3D processes such as differential cooling (Fer et al. 2002a; b) or wind-induced upwelling (Reiss et al. 2020). However, the details of the dynamics in the deep hypolimnion remain not fully understood, largely due to the lack of spatially and temporally resolved in situ observations in the deepest layers and systematic 3D modeling studies.

### 1.5.2 Typical winds during winter

Lake Geneva is bordered by the Alps in the south and Jura mountains in the northwest (Figure 1.2). The surrounding topography creates a “corridor” that guides two strong, large-scale winds, namely the *Bise* from the northeast and the *Vent* from the southwest, both approximately aligned with the main axis of the western half of Lake Geneva. Both winds are characterized by a long fetch and high wind speeds ( $5 - 15 \text{ m s}^{-1}$ ) lasting for several days and generate most of the large-scale circulation in the lake (e.g., Lemmin et al. 2005; Umlauf and Lemmin 2005; Bouffard and Lemmin 2013; Bouffard et al. 2018; Reiss et al. 2020).

### 1.5.3 The importance of rotational effects in Lake Geneva

Rotational effects strongly modify the internal wave field in Lake Geneva, giving rise to internal Poincaré and Kelvin waves (Lemmin et al. 2005; Bouffard and Lemmin 2013), which in turn can generate high-frequency internal waves (Thorpe et al. 1996) and enhance interbasin exchange (Umlauf and Lemmin 2005). Cimattori et al. (2018) showed by 3D numerical modeling that the time- and depth-averaged circulation in the lake’s interior, i.e., away from the shallow shore regions, is in near-geostrophic balance throughout the year. Furthermore, *Vent* winds generate Ekman-type coastal upwelling in the central *Grand Lac* (Bouffard et al. 2018; Soulignac et al. 2018; Reiss et al. 2020). Coastal upwelling in the shallow, narrow *Petit Lac* (max. width 5 km) during summer, manifesting in sudden nearshore temperature drops of  $\sim 10^\circ\text{C}$ , has attracted media attention<sup>1,2</sup> and was reproduced by 3D numerical modeling (Baracchini et al. 2020). While the near-surface temperature patterns during coastal upwelling at the northern shores of the *Petit Lac* and *Grand Lac* resemble each other, the underlying mechanisms appear to be different, at least during winter, as discussed in chapters 3 and 4.

### 1.5.4 Thermal response to climate change

Climate change and global warming have impacted lake ecosystems worldwide (e.g., Goldman et al. 2013). However, the effects are complex and the individual response on a lake

---

<sup>1</sup> <https://www.letemps.ch/sciences/leman-un-froid-abyssal-glace-eaux-genevoises>; last accessed 18 May 2021

<sup>2</sup> <https://www.meteosuisse.admin.ch/home.subpage.html/fr/data/blogs/2017/7/21-degres.html>; last accessed 18 May 2021

level may depend on many parameters, such as lake depth, surface area, and surrounding topography (e.g., Shimoda et al. 2011; Kraemer et al. 2015; Mesman et al. 2021). The most obvious effects of climate change on the physical properties of lakes are globally increasing surface water temperatures (O'Reilly et al. 2015). Furthermore, broader changes to the thermal structure of lakes have been documented such as reduced ice-cover, prolonged periods of stratification, and reduced maximum mixing depths (e.g., Livingstone 2003; Coats et al. 2006; Austin and Colman 2008). In Lake Geneva, both increasing surface temperatures (e.g., Molinero et al. 2007; Lemmin and Amouroux 2013) and a lengthening of the stratified period over the past decades (e.g., Anneville et al. 2013) have been observed.

Global warming effects on Lake Geneva's thermal structure between 1970 and 2010 were summarized by Lemmin and Amouroux (2013). Their analysis demonstrated that the Lake Geneva region has experienced a warming trend, which was most pronounced in the nighttime air temperatures, leading to reduced convective cooling. A comparable warming trend (albeit with considerable interannual variability) was observed in the upper 100 m of the water column, indicating that this was the depth range directly affected by global warming-induced changes to the atmospheric forcing. In contrast, the deep hypolimnion showed a weaker warming trend compared to the upper layers. Furthermore, the multiannual, continuous warming of the deepest layers (i.e., the rising flank of the saw-tooth temperature pattern; section 1.5.1) was much stronger than the long-term trend (see also Lemmin, 2020), with a comparable rate before and after the onset of climate change (Lemmin and Amouroux 2013). The latter led the authors to conclude that the internal mixing processes causing the multiannual warming in the deep hypolimnion have not been directly impacted by climate change.

Climate change-induced atmospheric warming will continue to affect lakes, raising the important question, how the already documented alterations to the thermal structure will play out in the future. For Lake Geneva, it has been shown by one-dimensional (1D) modeling that convective cooling will further reduce in strength, resulting in: (i) a prolonged stratified period, (ii) less frequent complete vertical overturning, and (iii) a reduced maximum mixing depth (Perroud and Goyette 2012; Schwefel et al. 2016). However, 1D models cannot represent complex, transient 3D processes, such as density currents, coastal upwelling, and wind-induced interbasin exchange. Since 3D processes appear to play a significant role in the deepwater dynamics of Lake Geneva and other large, deep lakes (e.g., Fer et al. 2002a; Peeters et al. 2003; Schladow et al. 2004; Piccolroaz et al. 2019; Lemmin 2020; Reiss et al. 2020; Roberts et al. 2021) further, more mechanistic investigations are required.

## 1.6 Research objectives and approach

Lake Geneva is a particularly interesting lake to investigate wind-induced upwelling and interbasin exchange processes during winter because it regularly features strong, along-axis winds and consists of two basins of different depth and width. While the large, deep *Grand Lac* is wide enough that Coriolis force strongly modifies the circulation, the situation in the narrow, shallow *Petit Lac* is less obvious. Furthermore, due to its great depth the *Grand Lac* remains stratified in most years, whereas the *Petit Lac* fully mixes every winter.

This thesis aims to develop a better mechanistic understanding of wind-induced interbasin exchange and coastal upwelling processes that regularly occur in Lake Geneva during winter by: (i) analyzing in detail their transient 3D dynamics, (ii) investigating how they contribute to horizontal and vertical exchange between the epi- and hypolimnion, and (iii) exploring the implications of these processes for the deepwater renewal dynamics in Lake Geneva during winter.

Extensive in situ observations, based on moored Acoustic Doppler Current Profilers (ADCPs) and thermistor lines, were combined with synoptic Conductivity Temperature Depth (CTD) profiling campaigns to form the basis for (i) describing in detail the hydrodynamics at carefully selected study sites, and (ii) validating a 3D hydrodynamic model ([MITgcm](#)). The latter provided the vehicle to investigate these complex and transient processes on a basin-wide scale. Furthermore, the modeled 3D velocity field was used to reveal dominant transport pathways and source regions of upwelled waters by Lagrangian particle tracking, which allowed drawing conclusions on the deepwater renewal potential of the considered upwelling processes. Finally, model-based momentum budget analysis was employed to investigate the underlying driving mechanisms and forces, and their dependency on stratification.

This dissertation is structured as follows:

**Chapter 2** is dedicated to wind-driven Ekman-type coastal upwelling at the northern shore of Lake Geneva. Field observations near the shore during the winter 2017/2018 revealed frequent upwelling of cold, hypolimnetic waters, with upward excursions of  $\sim 100$  to 150 m. The temporal development and spatial extent of the coastal upwelling were studied by 3D hydrodynamic modeling, and the origin and fate of upwelled waters were revealed by particle tracking. Finally, combining model and particle tracking results, a rough order-of-magnitude estimate of

the hypolimnetic ventilation potential by these regularly occurring coastal upwelling events was provided.

**Chapter 3** focuses on wind-induced interbasin exchange and hypolimnetic upwelling between the basins of Lake Geneva during early winter, i.e., when both basins are weakly stratified. Field observations taken during the winter 2018/2019 revealed frequent upwelling of cold, hypolimnetic *Grand Lac* water from depths around 150 to 200 m into the bottom layers of the *Petit Lac*. The spatiotemporal development of this “interbasin upwelling”, with a focus on the origin and fate of upwelled waters, was studied with field observations, 3D modeling, and particle tracking. Based on the latter two, coastal upwelling at the northern *Petit Lac* shore, which occurred at the same time as interbasin upwelling, was investigated, and a mechanistic explanation was proposed.

**Chapter 4** builds on the findings of chapter 3 and investigates the effect of stratification on wind-induced exchange between the two basins. Parts of the observational data set discussed in chapter 3 are revisited, focusing on the differences between early and late winter, i.e., when the *Petit Lac* is either weakly stratified or fully-mixed. Furthermore, two 3D hydrodynamic simulations were performed, with identical, realistic meteorological forcing, but different initial temperature fields, representative of the early and late winter thermal structure of Lake Geneva, respectively. For both simulations, the temporal development of the wind-induced, transversal and axial circulations at the confluence are discussed with the help of model-based momentum budget analyses. Furthermore, the role of stratification in modifying the net volume exchange between the basins and the potential for deepwater renewal was revealed.

Finally, **Chapter 5** brings together the key findings of this dissertation and outlines possible research questions to be addressed in the future.

Chapters 2 to 4 are based on manuscripts that have been published in or submitted to peer-reviewed journals.



# Chapter 2     Wintertime coastal upwelling in Lake Geneva: An efficient transport process for deepwater renewal in a large, deep lake

---

Rafael Sebastian Reiss, Ulrich Lemmin, Andrea Cimatoribus, and David Andrew Barry

Ecological Engineering Laboratory (ECOL), Faculty of Architecture, Civil and Environmental Engineering (ENAC), Ecole Polytechnique Fédérale de Lausanne (EPFL), Lausanne, Switzerland

Published in *Journal of Geophysical Research: Oceans*:

Reiss, R. S., U. Lemmin, A. A. Cimatoribus, and D. A. Barry. 2020. Wintertime coastal upwelling in Lake Geneva: An efficient transport process for deepwater renewal in a large, deep lake. *Journal of Geophysical Research: Oceans* **125**. doi:[10.1029/2020JC016095](https://doi.org/10.1029/2020JC016095)

## Abstract

Combining field measurements, 3D numerical modeling and Lagrangian particle tracking, we investigated wind-driven, Ekman-type coastal upwelling during the weakly stratified winter period 2017/2018 in Lake Geneva, Western Europe's largest lake (max. depth 309 m). Strong alongshore wind stress, persistent for more than 7 d, led to tilting and surfacing of the thermocline (initial depth 75-100 m). Observed nearshore temperatures dropped by 1°C and remained low for 10 d, with the lowest temperatures corresponding to those of hypolimnetic waters originating from 200-m depth. Nearshore current measurements at 30-m depth revealed dominant alongshore currents in the entire water column (maximum current speed 25 cm s<sup>-1</sup>) with episodic upslope transport of cold hypolimnetic waters in the lowest 10 m mainly during the first 3 d. The observed upwelling dynamics were well reproduced by a 3D hydrodynamic model (RMSE 0.2°C), whose results indicated that upwelled waters spread over approximately 10% of the lake's main basin surface area. Model-based Lagrangian particle tracking confirmed that upwelled waters originated from far below the thermocline, i.e., > 150-m depth and descended back to around 150 to 200-m depth over a wide area after wind stress ceased. Observational and particle tracking results suggest that wintertime coastal upwelling, which can occur several times during winter, is an overlooked transport process that is less sensitive to the effects of global warming than convective cooling. It can provide an effective, but complex 3D pathway for deepwater renewal in Lake Geneva, and other large, deep lakes with a sufficiently long wind fetch.

## Plain Language Summary

Freshwater lakes are increasingly important as drinking water sources and for societal and economic activities. To maintain good water quality, deepwater renewal is essential for lake ecosystems. Traditionally, convectively driven vertical mixing during wintertime is considered as one of the main processes for deepwater renewal. In deep lakes, this mixing often cannot reach down to the deepest layers.

Since this situation is expected to worsen due to climate change-induced warming, a good understanding of alternative deepwater renewal processes is crucial. We investigate wind-driven coastal upwelling of hypolimnetic water during the weakly stratified winter period. The study

was carried out in monomictic Lake Geneva, a large, deep lake (depth 309 m), combining field observations, 3D hydrodynamic modeling and Lagrangian particle-tracking, an effective combination for addressing the complex 3D upwelling dynamics over a large area of the lake. We show that coastal upwelling can lift water masses from far below the thermocline up to the surface in the nearshore region, where they spend up to 5 d before descending back to the deeper layers. Our results demonstrate that wintertime coastal upwelling, an as yet overlooked transport process, can efficiently contribute to the renewal and aeration of the deepwater layer in deep lakes.

## 2.1 Introduction

Convective winter cooling is an important process in the annual cycle of many lake ecosystems. It transports oxygen-rich waters from the surface to the deeper parts and recycles nutrients. However, in deep monomictic lakes, convectively-induced vertical transport and mixing are often not sufficient to reach the lake's deepest layers (Livingstone 1993; Coats et al. 2006; Perroud et al. 2009). Driven by the temperature differences between the atmosphere and the lake surface, convective cooling is expected to become even less efficient in the future with potentially milder winters due to climate change (Ambrosetti and Barbanti 1999; Adrian et al. 2009; Goldman et al. 2013; Sahoo et al. 2013; Wahl and Peeters 2014; O'Reilly et al. 2015). Such a reduction of convectively-induced deepwater renewal might result in lower Dissolved Oxygen (DO) concentrations, causing potentially negative effects for the lake's ecological health (e.g., Likens 2010; Friedrich et al. 2014).

In large, deep lakes, two other processes originating in the coastal zone can significantly contribute to deepwater renewal during wintertime: density currents on the lateral slopes caused by differential cooling between the shallow littoral zone and the deep off-shore region (Fer et al. 2002a; Peeters et al. 2003) and upwelling of deepwater masses over the lateral slopes, which results from wind forcing and may be affected by Coriolis forcing (e.g., Csanady 1977; Schladow et al. 2004). The former is a special case of convective cooling, and as such may decrease in importance because of climate change. The latter, on the other hand, is wind-driven and thus less sensitive to increasing air temperatures.

Observations and qualitative descriptions of coastal upwelling in the ocean date back more than a century (e.g., Thorade 1909; McEwen 1912; Schulz 1917). The phenomenon could be explained by Ekman's then recent work on the influence of the earth's rotation on ocean currents (Ekman 1905), whereby persistent wind stress results in surface layer transport that is perpendicular to the direction of the wind (to the right in the Northern Hemisphere). In the nearshore region, this divergence in the surface layers must be compensated for by upwelling of colder waters from below or by downwelling of near-surface water masses, depending on the direction of the wind. Upwelling events are classified as "partial" (the thermocline does not reach the surface) or "full" (the thermocline surfaces) (Csanady 1977).

Depending on the basin size and fetch length, coastal upwelling in lakes takes on different forms. In small (in terms of Rossby radius) lakes, direct upwelling occurs at the upwind end (Mortimer 1952; Coman and Wells 2012). Pöschke et al. (2015) used airborne thermal imagery

and in situ temperature observations to investigate upwelling in two small temperate lakes. They concluded that wind-driven upwelling could be at least as important as convective cooling for deep mixing and hypolimnetic oxygen renewal during the spring overturn in such systems. The same type of upwelling takes place in larger lakes in which Coriolis force-induced Poincaré and/or Kelvin waves are observed, but which have limited fetch, such as Lake Simcoe (Cossu and Wells 2013), Lake Tahoe (Steissberg et al. 2005) and Lake Biwa (Homma et al. 2016). Similar to the ocean, Ekman-type upwelling occurs in large, deep lakes with sufficiently long fetch (e.g., Csanady 1977; Wang et al. 2000; Rao and Murthy 2001; Amadori et al. 2018).

Upwelling in large lakes has mainly been studied during the strongly stratified summer period, when it is associated with nearshore-offshore exchange (McKinney et al. 2018; Valipour et al. 2019), cross-shore thermal variability (Troy et al. 2012), increased horizontal and vertical mixing (Rao and Murthy 2001), flushing of harbor embayments (Hlevca et al. 2018) and nutrient and phytoplankton transport (Corman et al. 2010). In Lake Geneva, Ekman-type upwelling appears to be relevant for spatio-temporal heterogeneity of surface phytoplankton during the summer period (Bouffard et al. 2018; Soulignac et al. 2018). Upwelling is therefore generally considered ecologically beneficial. However, in some cases, upwelling of deep, anoxic waters can lead to a deterioration of the surface water quality and even fish kills, e.g., Lake Erie, whose deep waters regularly undergo severe hypoxia (Rao et al. 2014; Jabbari et al. 2019).

On the other hand, wind-driven Ekman-type coastal upwelling during the weakly stratified winter period has received little attention, even though it is under these conditions that wind stress effects can penetrate the deepest into the water column and consequently can “lift” very deep water masses up to the surface layers. Schladow et al. (2004) reported on an extraordinary large upwelling event in Lake Tahoe (max. depth 500 m) in winter lasting for 4 d, observed by means of in situ measurements and surface temperatures deduced from satellite imagery. They concluded that the amplitude of the upwelling covered the full water depth and affected 50% of the lake’s surface. Although this was considered an extraordinary event, their findings vividly illustrate the potential role of wintertime coastal upwelling in affecting the hypolimnetic dynamics in large, deep lakes.

In the present study, we aim to investigate the as yet little-known dynamics of wintertime coastal upwelling and address the following questions: (i) Does Ekman-type coastal upwelling occur in Lake Geneva, Western Europe’s largest lake during the weakly stratified winter period? (ii) If so, can it provide an efficient pathway for hypolimnetic-epilimnetic exchange under

favorable wind conditions? and thus (iii) Does it contribute to deepwater renewal and re-oxygenation in the deep hypolimnion? To achieve this, we combined detailed field observations, three-dimensional (3D) numerical modeling, and model-based Lagrangian particle tracking.

The paper is organized as follows: The characteristics of Lake Geneva, the observational data, the 3D numerical model and the particle tracking algorithm are described in Section 2.2. In Section 2.3, the prevailing thermal stratification and meteorological data are introduced. Field observations and hydrodynamic model results are presented and analyzed, and the origin and fate of upwelled deepwater masses are determined based on Lagrangian particle tracking results. The results and their implications are discussed in Section 2.4, followed by the conclusions in Section 2.5. A Supporting Information (SI) section provides additional clarifications/details on certain topics mentioned in the text.

## 2.2 Materials and methods

### 2.2.1 Study site

Located between Switzerland and France, Lake Geneva (local name: *Lac Léman*) is often considered the birthplace of limnology (Forel 1892) and is Western Europe’s largest lake. Lake Geneva is crescent-shaped and consists of two basins: a small, narrow western basin called the *Petit Lac*, with a maximum depth of 75 m, and a large eastern basin called the *Grand Lac* with a mean depth of 170 m and a maximum depth of 309 m (Figure 2.1a). The lake has a surface area of 580 km<sup>2</sup>, a length of 73 km along its major axis, a maximum width of 14 km and is classified as warm monomictic. The shallow *Petit Lac* basin regularly destratifies every winter. The deep *Grand Lac* basin of Lake Geneva, however, remains (thermally) stratified during most years, with a thermocline typically in the range of 100 to 150-m depth during winter cooling and complete vertical destratification only occurring during severely cold winters (CIPEL 2019).

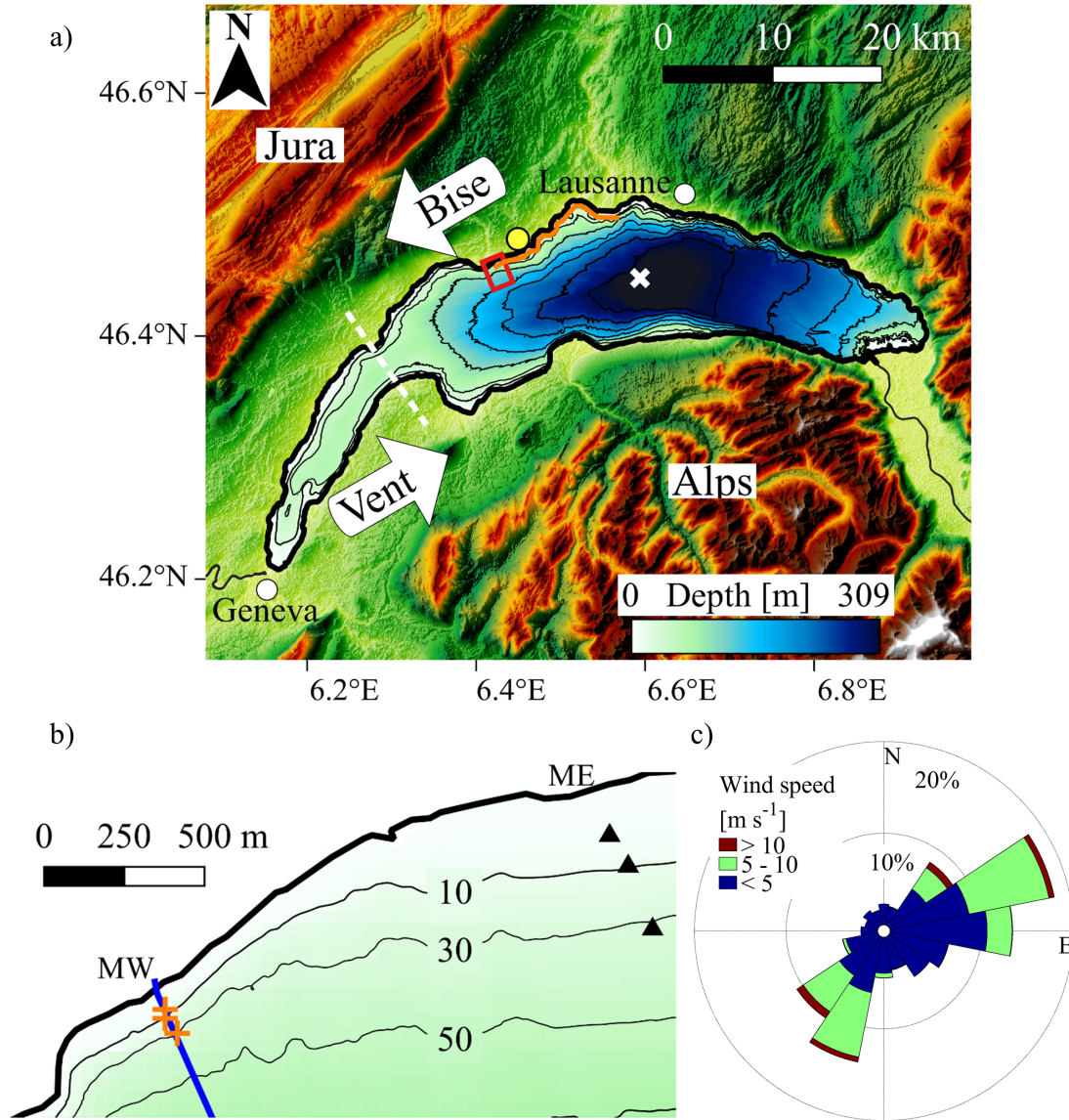


**Figure 2.1.** **a.** Bathymetric map of Lake Geneva including the surrounding topography. The Jura and Alp mountains create a wide “corridor” through which two strong, dominant winds, namely the *Vent* from the southwest and the *Bise* from the northeast, blow over most of the lake surface. The white dashed line approximately delimits the two basins, i.e., the small *Petit Lac* and the large *Grand Lac*. Full-depth temperature profiles were taken at CIPEL station SHL2 (white X; depth 309 m). Meteorological data were recorded at the MeteoSwiss St. Prex station (yellow circle). The red rectangle and orange line in **a** show the study site location and the alongshore extent of the particle tracking seeding area (for details, see Section 2.2.4), respectively. Depth is given in meters in the colorbar legend and by the isobath contours (25, 50, 100, 150, 200, 250, 300 m), **b.** Close-up of the study site during winter 2017/2018 giving an overview of the western (MW1, MW2, MW3; orange crosses) and eastern (ME1, ME2, ME3; black triangles) mooring sites. The blue line shows the first 500 m of the DTS fiber-optic cable, and **c.** Wind-rose depicting the prevailing mean wind directions and strength during the observation period (1 December 2017 to 31 March 2018) recorded at the nearby meteorological station (yellow circle in **a**).

Full depth profiles taken by the Commission Internationale pour la Protection des Eaux du Léman (CIPEL) on 21 December 2017, prior to the coastal upwelling event investigated in this study, show DO concentrations of  $6 \text{ mg L}^{-1}$  at 200-m depth, decreasing to approximately  $3 \text{ mg L}^{-1}$  at the bottom (CIPEL 2019). The ventilation of these deep layers is generally attributed to complete vertical overturning due to convective cooling during severely cold winters. Recently it was shown (Lemmin 2020) that: (i) In cold winters, vertical DO profiles with a pronounced minimum in the bulk water of the deep hypolimnion persisting for several months and higher DO concentrations towards the lake bottom occur, suggesting the lateral advection of oxygen-rich water along the lakebed, (ii) A significant spatial variability of the DO concentrations in the near-bottom layer exists as revealed by measurements taken along submarine dive tracks across the central 300 m deep plateau in the *Grand Lac* basin, and (iii) An increase in DO levels at the deepest point of the lake (309 m) can be observed every year, even during mild winters with incomplete vertical convective mixing. Field measurements (Giovanoli 1990) indicate that dense, sediment-laden turbidity currents from the lake's main tributary, the Rhône River, occasionally reach the deepest layers. However, due to the limited frequency and intensity of these events, their contribution to deepwater renewal can be considered minor. Altogether, there is strong evidence suggesting that deepwater renewal in Lake Geneva is not only governed by vertical convective mixing but also, to some extent, by 3D processes such as differential cooling or wind-driven coastal upwelling.

River throughflow is small, leading to a flushing time (also referred to as theoretical residence time in the literature; Monsen et al. 2002) of approximately 11 y (CIPEL 2019). The inertial period at the latitude of Lake Geneva is approximately 16.5 h. Numerous observational and numerical studies have shown that Coriolis force effects play an important role in determining the lake's hydrodynamics (e.g., Bauer et al. 1981; Lemmin et al. 2005; Bouffard and Lemmin 2013; Cimattoribus et al. 2018, 2019; Lemmin 2020).

Lake Geneva is subject to a variety of winds (local fishermen distinguish over 20 different winds by name) generated by differential heating, pressure differences across the Alps and/or large-scale atmospheric pressure gradients (Bohle-Carbonell 1991). The channeling effect created by the surrounding topography, i.e., the Jura and Alp mountains, guides two strong, dominant pressure-gradient winds over most of the lake surface, namely the *Vent*, blowing from the southwest and the *Bise*, from the northeast (Figure 2.1a). These winds are fairly homogenous in space and steady in time for several days, typically reaching wind speeds between 5 and  $15 \text{ m s}^{-1}$  (e.g., Lemmin and D'Adamo 1996; Lemmin et al. 2005). Both have a long fetch and are



almost aligned with the shore of the western and central parts of the *Grand Lac* basin, which in turn favors the development of upwelling events. The coastal upwelling on the northern shore investigated in this study is generated under *Vent* wind conditions.

### 2.2.2 Field observations

A field measurement campaign was carried out at two sites, hereinafter referred to as Western (MW1, MW2, MW3) and Eastern Moorings (ME1, ME2, ME3) during the winter of 2017/2018 near the northern shore of Lake Geneva, 20 km west of Lausanne (Figure 2.1a, b). The western mooring site had three vertical thermistor lines with a total of 34 temperature loggers (RBRsolo T and Seabird SBE-56) that were deployed from December 2017 to April 2018 at 5 m (MW1), 10 m (MW2) and 30-m depths (MW3), respectively. The moorings were aligned along a transect perpendicular to the shoreline. The 30-m depth mooring (MW3) was additionally equipped with an Acoustic Doppler Current Profiler (ADCP) (Nortek Signature 1000).

A similar set of three moorings, ME1, ME2 and ME3, was deployed 1.5 km east of the western mooring site, at the same depths. Current velocities at the 30-m depth mooring (ME3) were recorded by a combination of a Teledyne RDI Workhorse Sentinel (300 kHz) and a Nortek Aquadopp-HR Profiler that was added to resolve the near-bottom currents within the blanking distance (approximately 4 m) of the RDI instrument.

All thermistors had an accuracy of  $\pm 0.002^{\circ}\text{C}$  and sampled every 2-5 s. Prior to analyzing the data, 10-min moving averages were applied to all temperature measurements. The accuracy of all current velocity measurements was in the order of  $0.5 \text{ cm s}^{-1}$ . To facilitate the comparison between the two mooring sites, the current coordinate systems were rotated to be aligned with the orientation of the local shoreline (alongshore, positive to the east; cross-shore and upslope, positive to the north) and are given as “flowing towards.” Details of the mooring configurations and the instrument settings are summarized in Table 2.1.

Table 2.1. Details of the moorings.

Moorings	Depth [m]	Instruments and settings
MW1	5	4 RBRsolo T, vertical spacing 1 m
MW2	10	15 RBRsolo T, vertical spacing 60 cm
MW3	30	12 RBRsolo T, 3 Seabird SBE-56, vertical spacing 1-3 m Nortek Signature 1000: 26 bins of 1 m, 2 min averaging interval, 10 min measurement interval
ME1	5	4 RBRsolo T, vertical spacing 1 m
ME2	10	15 RBRsolo T, vertical spacing 60 cm
ME3	30	12 RBRsolo T, 3 Seabird SBE-56, vertical spacing 1-3 m Nortek Aquadopp HR Profiler: 18 bins of 15 cm, 90 s averaging interval, 5 min measuring interval Teledyne RDI Workhorse Sentinel (300 kHz): 12 bins of 2 m, 20 min averaging/measurement interval

In addition to the moored temperature and current instruments, near-bottom water temperatures at the western mooring site were obtained from a 1.8 km long fiber-optic based Distributed Temperature Sensing (DTS) system (Selker et al. 2006; van de Giesen et al. 2012). The DTS system measured temperatures along a fiber-optic cable that was laid down on the lakebed perpendicular to the shoreline, starting at the shore, with spatial and thermal resolutions of 1 m and 0.1°C, respectively (Figure 2.1b). Knowing the approximate position of the cable and the local bathymetry, we mapped distances along the cable to the corresponding depths.

Wind speed and direction were recorded every 10 min at a meteorological station at St. Prex operated by the Swiss National Weather and Climate Service ([MeteoSwiss](#)), located approximately 3 km east of the study site (Figure 2.1a). Hourly moving averages were applied to the meteorological data prior to the analysis. The data sets were complemented by CTD (Conductivity Temperature Depth) profiles taken on a regular basis at the deepest point of the lake (SHL2 in Figure 2.1a) by [CIPEL](#) (CIPEL 2019), which monitors water quality in Lake Geneva (Rimet et al. 2020).

### 2.2.3 Hydrodynamic model

To simulate the hydrodynamics of Lake Geneva, we employed a hydrostatic version of the MITgcm, which solves an incompressible Boussinesq form of the 3D Navier-Stokes equations (Marshall et al. 1997). This code is widely used in the oceanographic community and has successfully been applied to lakes (Dorostkar and Boegman 2013; Djournna et al. 2014;

Dorostkar et al. 2017), and recently to Lake Geneva (Cimatoribus et al. 2018, 2019). Following Cimatoribus et al. (2018), we ran a Low-Resolution (LR) and a High-Resolution (HR) version of the 3D model.

The LR model (curvilinear grid, horizontal resolution 173-260 m, 35  $z$ -layers, integration time step 20 s) was initialized from rest on 15 December 2016 at 12:00 (local time) with a horizontally homogenous temperature initial condition, derived from the temperature profile at SHL2 on that date. The LR model was run until 25 October 2017, 00:00.

The interpolated 3D temperature field from the LR model served as initial condition for the HR model, which was started from rest on 25 October 2017 at 00:00 and was run for five months. The HR model adopted a Cartesian grid with a constant horizontal resolution of 113 m, 50 size-varying  $z$ -layers (30 cm at the surface, 10 m at the deepest point) and an integration time step of 8 s. The starting date for the HR model was selected such that the preceding days were characterized by calm wind conditions, allowing the model to adjust to the initial conditions. Both model versions were forced at the free surface by the output of the COSMO-1 numerical weather model provided by MeteoSwiss covering the lake surface with a 1.1 km grid. We used the assimilated outputs (called reanalysis data), based on observational data, rather than pure forecast data (Voudouri et al. 2017). Quadratic bottom drag and free-slip conditions at the lateral boundaries were employed in all cases.

The model configurations were adapted from Cimatoribus et al. (2018) and Cimatoribus et al. (2019). The former study describes the configurations in detail and provides an in-depth model validation using: (i) temperature and current velocity time series, and vertical temperature profiles, both recorded at a number of monitoring stations and moorings located around the entire lake, and (ii) temperature variance and kinetic energy spectra. In Figure S2.1 in the SI, the temperature profile measured at SHL2 approximately one month after the beginning of the high resolution (HR) modeling is compared with the one obtained by the numerical model for that day. Good agreement is found.

#### 2.2.4 Particle tracking

Lagrangian particle tracking is used for analyzing the velocity output of lake or ocean circulation models. Van Sebille et al. (2018) presented the fundamentals of the Lagrangian analysis, code availability, and a variety of applications in the ocean. When combined with 3D numerical modeling, it can identify preferential transport pathways and determine the origin

(backward tracking) and fate (forward tracking) of upwelled water masses in coastal regions of the ocean. In this context, particle tracking has been applied on seasonal/regional scales (e.g., Rivas and Samelson 2011; Viglione and Thompson 2016) and for long-term global ocean circulation studies with time-scales in the order of 100 y (Tamsitt et al. 2017). Recently, Amadori et al. (2018) used particle tracking to study transport processes in Lake Garda (Italy) and found that Ekman-type coastal upwelling/downwelling along the steep shores of the lake resulted in large vertical displacement of particles, i.e., water masses.

The particle tracking code employed in this study uses the method described by Döös et al. (2013), whereby particle trajectories are calculated based on the 3D velocity field output from a hydrodynamic model, applying linear interpolation in time (between model outputs) and space (between grid points). Cimatoribus (2018) implemented the algorithm using the Python language and validated it against the analytical results discussed by Döös et al. (2013). The code was recently applied to Lake Geneva in an investigation of the dispersion of water originating from the lake's main tributary, the Rhône River (Cimatoribus et al. 2019).

Here, we used particle tracking to determine the pathways followed by hypolimnetic water masses during a 10-d coastal upwelling in January 2018. Particles were continuously released during the first 3 d (hereinafter referred to as active upwelling phase) at every grid point of the upper 15 m of the water column in an approximately 13 km alongshore by 1.5 km cross-shore nearshore region surrounding our study site (Figures 2.1a and S2.2). The seeding region was chosen based on the maximum alongshore extent of the surface temperature anomalies computed by the hydrodynamic model during the upwelling period. The origin and fate of upwelled water masses were investigated employing backward and forward tracking, respectively, and filtering the trajectories by initial and final depths.

The computed particle trajectories were used to estimate the time that particles spend in the upper layers of the water column, before descending back to greater depths. This surface exposure time has ecological implications, since it represents the time that water masses spend in contact with the atmosphere and are thus subject to heat and gas exchange.

The sensitivity of the analysis to the number of released particles was tested by varying the seeding interval between 0.5 and 2 h, yielding between 230,000 to 890,000 particles in total. Since we were interested in the deterministic advection of water masses resolved by the hydrodynamic model, diffusion (e.g., in the form of random particle displacements) was not considered.

## 2.3 Results

### 2.3.1 Thermal stratification of Lake Geneva

Figure 2.2 shows the temperature profile taken by CIPEL at SHL2 on 21 December 2017. At that time, that is, three weeks before the upwelling event investigated in this study, a weak thermocline remained between 75 m and 100 m. The following three weeks were characterized by rather mild air temperatures ( $T_{\text{mean}} = 5.2^\circ\text{C}$ ). Therefore, this profile will be considered representative for the stratification conditions during the coastal upwelling period investigated here.

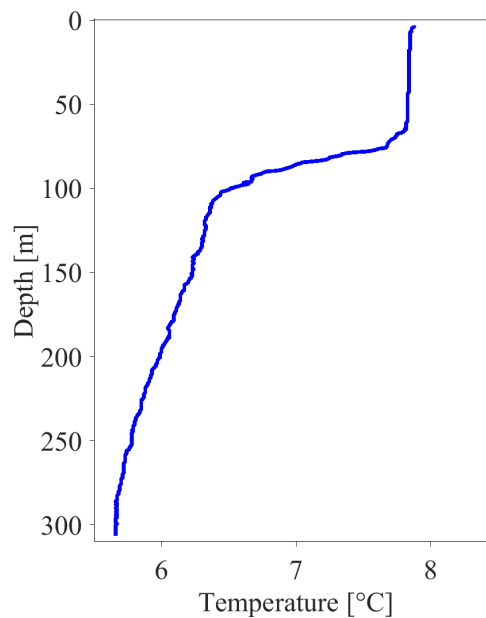


**Figure 2.2.** Temperature profile taken at the SHL2 station on 21 December 2017. For station location, see Figure 2.1a.

### 2.3.2 Meteorological data

Prevailing measured wind speeds and directions from 1 December 2017 to 31 March 2018 are displayed in the wind-rose in Figure 2.1c. Wind directions in degrees refer to the direction the wind originates from. *Vent* events, which may generate coastal upwelling along the northern shore of Lake Geneva, occurred during 25% of the time. The *Vent* event analyzed in this study lasted from 16 to 26 January 2018. Wind speed and direction for that period are shown in Figure 2.3a, b, respectively. The wind blew steadily in a northeasterly direction for 7.5 days with maximum wind speeds exceeding  $16 \text{ m s}^{-1}$  and a mean value of  $7.2 \text{ m s}^{-1}$ . The

two-dimensional (2D) wind field over the lake derived from COSMO-1 data, and typical for most of that period, showed a spatially relatively homogenous wind blowing parallel to the main axis of the central part of the lake (Figure 2.4), thus generating favorable conditions for coastal upwelling at our study site.

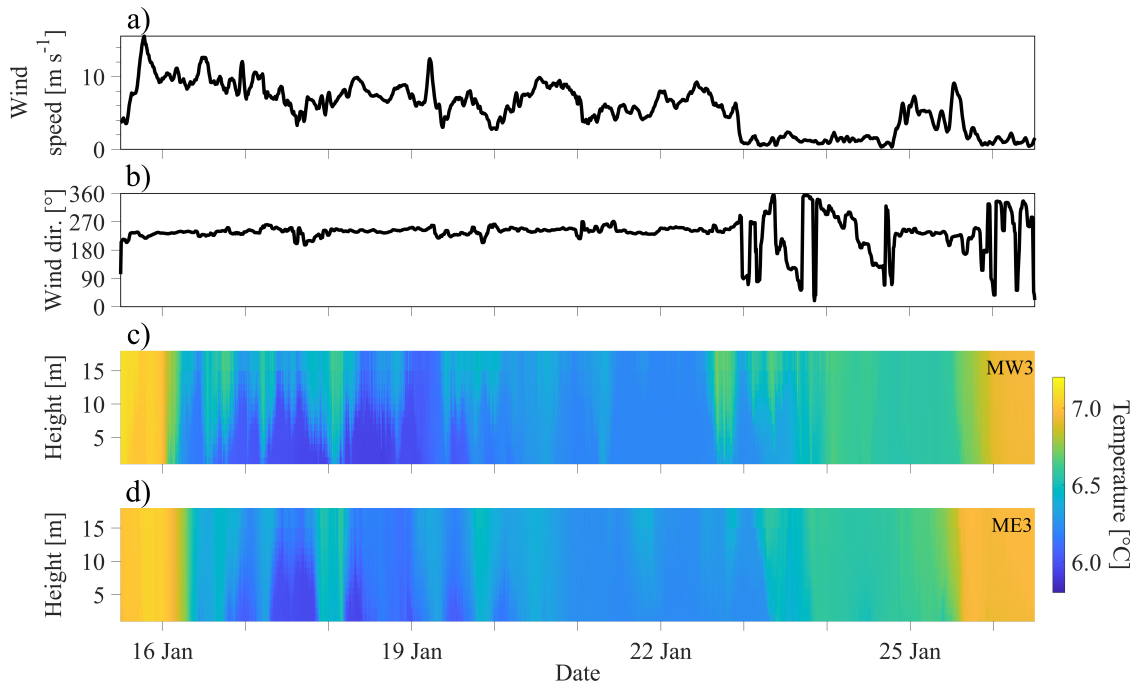


**Figure 2.3.** **a.** Wind speed and **b.** wind direction, both recorded during the upwelling period by the MeteoSwiss station at St. Prex. **c.** and **d.** Contour plots of the temperature time series recorded at the 30 m moorings MW3 and ME3, respectively. The colorbar gives the water temperature. Height is indicated in meters above the lakebed. The dates on the horizontal axis refer to the year 2018. See Figure 2.1 for station and mooring locations.

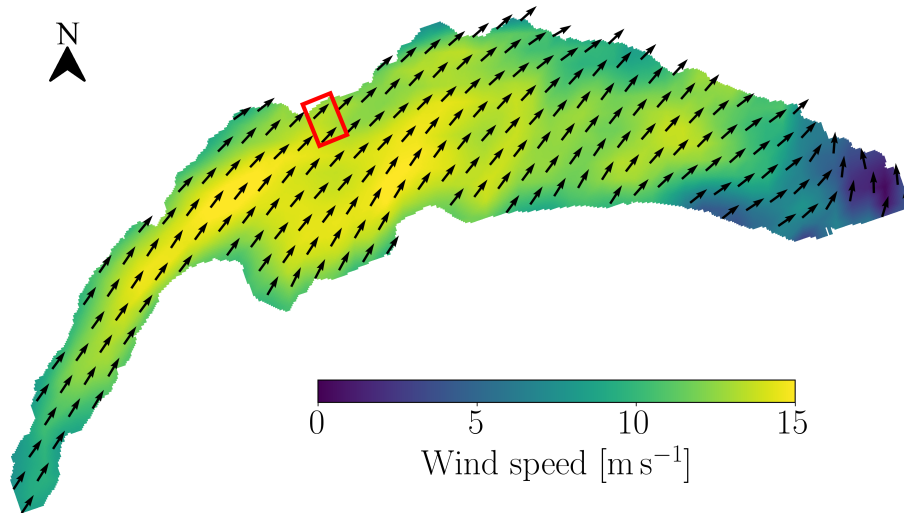


**Figure 2.4.** Two-dimensional (2D) wind field during the upwelling event on 16 January 2018 at 12:00 (local time) derived from the COSMO-1 meteorological model. The normalized black arrows show a northeasterly wind direction ( $V_{ent}$ ) over most of the lake. The red rectangle marks the area where the moorings were deployed (Figure 2.1b). The colorbar gives the wind speed. For clarity, not all wind vectors are shown.

### 2.3.3 Temperature and current moorings

The  $V_{ent}$ -induced upwelling was seen at all moorings. The time series of selected DTS temperatures between 35-m depth and the end of the cable (130-m depth) are shown in Figure 2.5. Prior to this full coastal upwelling event, a temperature difference of less than  $0.1^{\circ}\text{C}$  between 35 and 75-m depth and a stronger change in temperature between 75 and 100-m depth indicate a thermocline depth between 75 and 100 m, in good agreement with the SHL2 profile from 21 December 2017 (Figure 2.2). Starting on 16 January at 00:00 at approximately  $7^{\circ}\text{C}$ , temperatures at 35, 50 and 75-m depths suddenly dropped by  $0.6^{\circ}\text{C}$  within the first 6 h. This sudden temperature drop was most likely caused by the alongshore advection of cold-water masses that underwent upwelling further west, as suggested by the dominant eastward along-shore currents at this time (discussed below). The arrival of the upwelled cold water mass lagged behind the peak in wind speed by approximately 12 h.

All DTS temperatures then gradually decreased further to below  $6^{\circ}\text{C}$  on 18 January at around noon (Figure 2.5). This period will be considered the “active upwelling” phase. The temperature pattern suggests that during that period cold hypolimnetic water masses were continuously transported to the nearshore region by wind-driven Ekman-type coastal upwelling. During the

following week, wind speeds progressively decreased and temperatures slowly rose to approximately the values recorded before the upwelling. The minimum temperature of 5.71°C recorded at the end of the DTS cable during the upwelling period (Figure 2.5; 130-m depth) corresponds to the water temperature at a depth of approximately 270 m at the SHL2 station on 21 December 2017 (Figure 2.2), suggesting that, albeit not having reached the surface, even the deepest layers of the lake were affected by this upwelling.

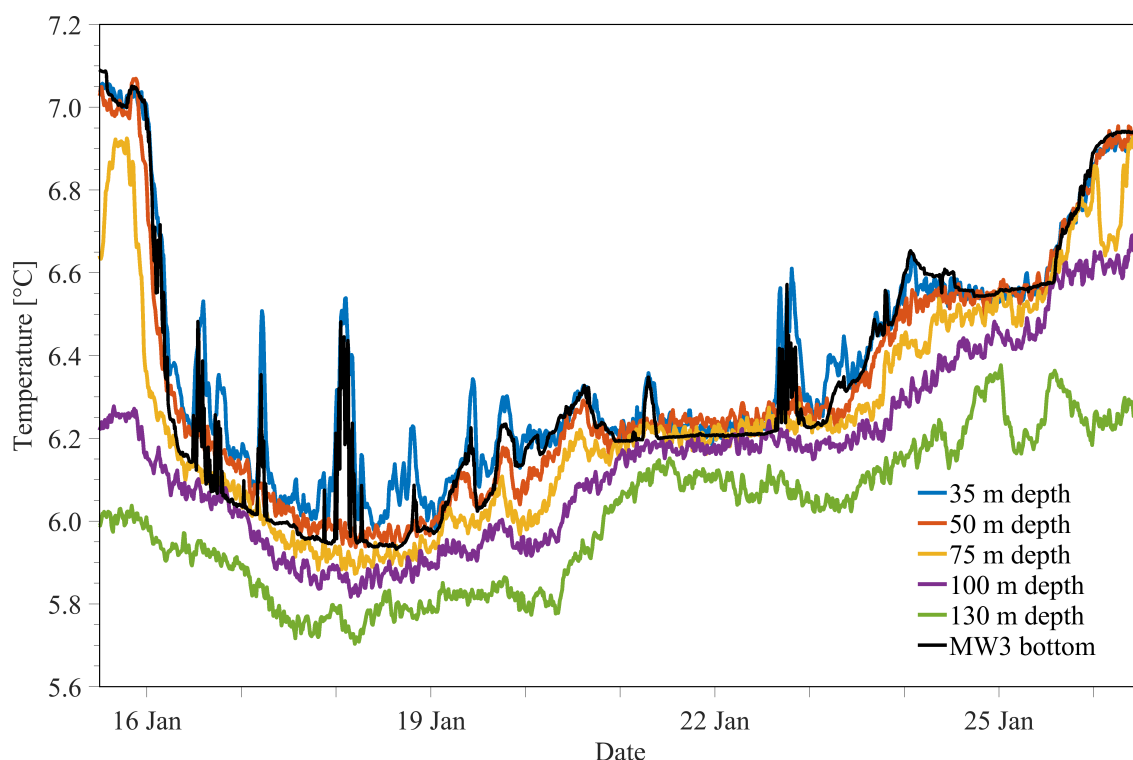


**Figure 2.5.** Temperature time series recorded by the DTS system at the western mooring site, between 30 and 130-m depth. The depth was estimated by using the approximate position of the cable and a map of the local bathymetry (Figure 2.1). The temperatures recorded at the bottom of the nearby ME3 mooring (30-m depth) are also shown. The different depths are given in the legend. The dates on the horizontal axis refer to the year 2018.

Prior to the *Vent* event, all 68 thermistors at the eastern and western mooring sites showed similar temperatures within a range of 0.05°C, illustrating vertical and horizontal well-mixed conditions (Figure 2.3c, d). Following the onset of the *Vent* event, nearshore temperatures at all instruments first suddenly dropped, then remained low during the active upwelling phase and finally began to gradually increase towards the end of the upwelling period. This time development corresponds to the one seen in the DTS recording (Figure 2.5). The time series of near-bottom temperatures measured by the bottommost thermistor of the mooring MW3 agreed well



with the temperatures recorded at the nearby DTS system at 35-m depth (Figure 2.5, black line). During the active upwelling phase, several short events of warming are evident, some reaching down to the lakebed. These coincide with the peaks in the 35 m temperature record of the DTS (Figure 2.5) and will be further analyzed in Section 2.4.1.

During the upwelling period, a weak stratification of less than  $0.5^{\circ}\text{C}$  often remained between the top- and bottom-most thermistors at the 30 m (Figure 2.3c, d) and 10-m depth moorings (Figure S2.3). Temperatures at the 5-m depth moorings were essentially vertically uniform (Root Mean Square Error, RMSE, between the bottommost and topmost thermistor signal was  $0.02^{\circ}\text{C}$ ), and were close to the ones observed at the topmost thermistors at the 10 m and 30 m moorings, respectively. A minimum temperature of  $5.93^{\circ}\text{C}$  was observed 1 m above the lakebed at MW3. This temperature is close to the lowest temperature recorded by the DTS (Figure 2.5) and corresponds to values found below depths of 200 m, as indicated by the temperature profile at SHL2 for 21 December 2017 (Figure 2.2).

Figure 2.6 shows the observed current velocities at MW3 and ME3 during the 3-d active upwelling phase as current roses. To illustrate the prevailing processes, the water column was divided into: (i) an upper layer that is  $> 15$  m above the lakebed and (ii) a lower layer that is  $< 8$  m above the lakebed. The mean values over the 3-d period are displayed for each layer. At both mooring sites, northeastward alongshore currents (i.e., aligned with the mean wind stress) dominated over the entire water column, with maximum values exceeding  $25\text{ cm s}^{-1}$  in both layers. The gradually decreasing water temperatures during the first 3 d (Figure 2.5) could be explained by episodic cross-shore, upslope currents seen in the bottom layers of both moorings that carry cold-water masses from the hypolimnion towards the shore, particularly at the western mooring site (Figure 2.6c, d). The observed spatial heterogeneity of the current speeds between the two moorings is likely due to a combination of effects, including the spatially varying wind velocity (Figure 2.4), shoreline irregularities close to the western study site and differences in the bed slope (Figure 2.1b).

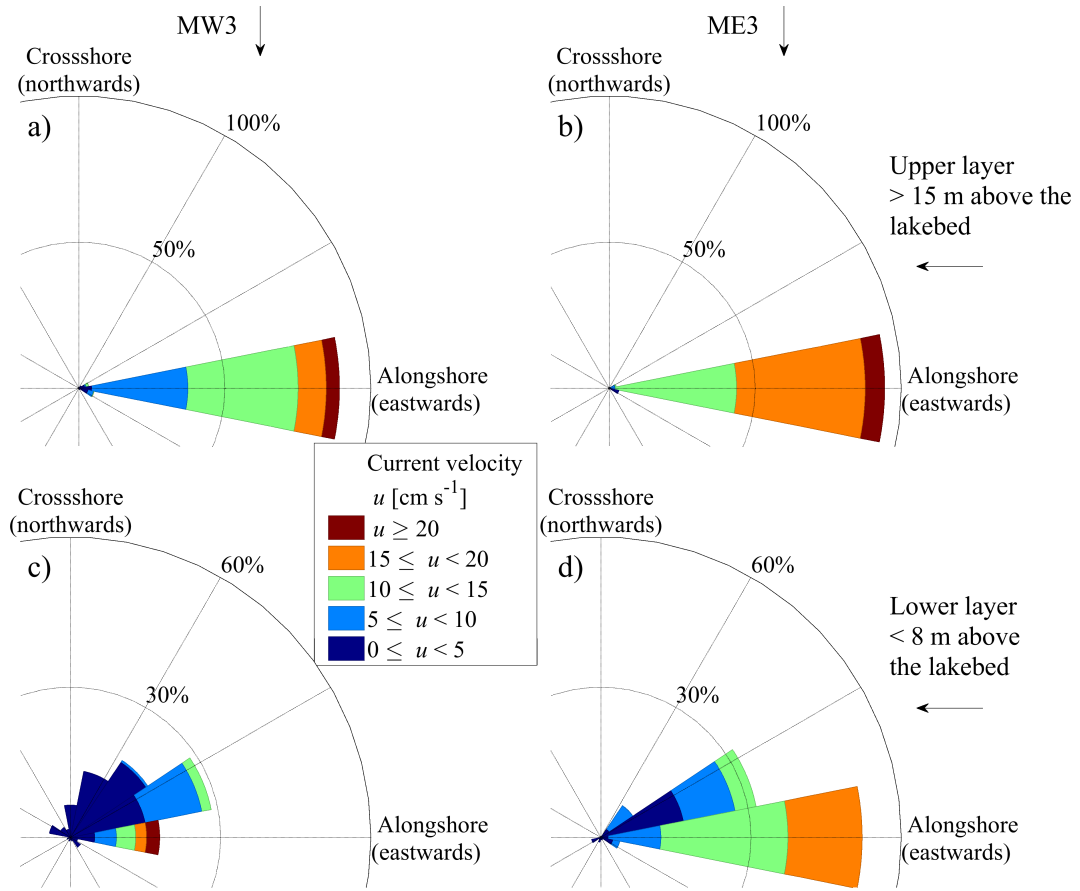


**Figure 2.6.** Current roses at MW3 (left panels) and ME3 (right panels) for the upper (a, b) and the lower (c, d) layers during the active upwelling phase from 15 January, 15:00 (onset of *Vent* event) to 18 January 2018, 12:00 (end of active upwelling phase). Current vectors were projected onto the local alongshore axis. Note that the scales in the top and bottom panels are different.

#### 2.3.4 Model results

Figure 2.7 shows the vertical average of the temperature signal in the lower layer of the water column (approximately between 2 to 8 m above the lakebed) recorded at mooring ME3 (blue) and computed by the HR model (red) from 13 to 28 January 2018. Due to the discretization of the bathymetry, the depth in the HR model at this location is approximately 26 m. Even though the model grid is too coarse to resolve all the details of this complex nearshore bathymetry, the model overall reproduces the upwelling event well in terms of absolute temperatures and temporal variability, and the modeled temperatures are in good agreement with field observations (RMSE approximately  $0.2^\circ\text{C}$ ). The initial rapid temperature drop due to northeastward alongshore advection of previously upwelled cold-water masses and the gradual temperature increase during the relaxation phase are both captured by the model. Furthermore,

field observations and numerical modeling results show several significant temperature peaks during the active upwelling phase. These were due to temporary downwelling close to the shore and are discussed in Section 2.4.1. The overall agreement between observational data and numerical modeling results, allowed us to investigate further the 3D structure of the upwelling. It should be emphasized that this would not have been possible by only using the point measurements of the field observations.

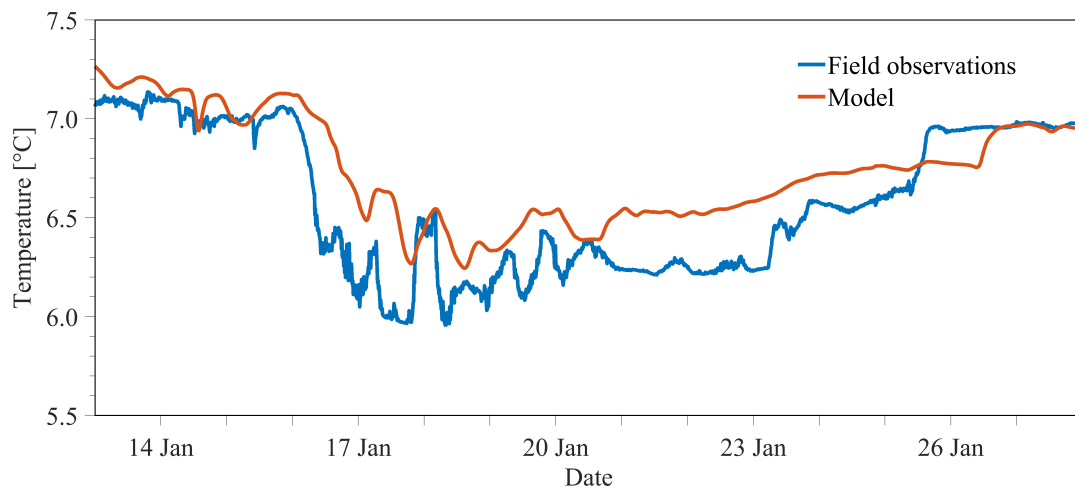


**Figure 2.7.** Temperature time series in the lower layer of the water column (approximately 2 to 8 m above the lakebed) as recorded at ME3 (blue) and as computed by the High Resolution (HR) model (red). The dates on the horizontal axis refer to the year 2018.

Maps of the modeled near-surface temperatures at 1-m depth before (16 January 2018, 00:00), during (19 January 2018, 00:00) and after (28 January 2018, 00:00) the upwelling period, as well as vertical temperature slices at selected locations are displayed in Figure 2.8. In order to estimate the surface area affected by this event, we considered the surface temperature anomaly (i.e., local surface temperatures minus basin-wide averaged surface temperature) as a proxy for upwelled water masses. By assuming that the upper layer was well mixed before the onset of the *Vent* event (Figure 2.3), a surface temperature anomaly of  $-0.2^{\circ}\text{C}$  indicates that these surface water masses originated from well within the thermocline (75 to 100-m depth; Figure 2.2). The modeling results suggest that, based on this choice of threshold, an area of up to  $50 \text{ km}^2$  was affected by the upwelling (black contoured area in Figure 2.8c). This corresponds to approximately 10% of the surface area of the *Grand Lac* basin. It should be noted that comparably lower surface temperatures in some parts of the lake prior to the *Vent*-induced upwelling (Figure 2.8a) were not related to coastal upwelling. Instead, they could be attributed to: (i) differential

cooling of the shallow *Petit Lac* basin and shallow nearshore regions of the *Grand Lac*, and (ii) a counterclockwise rotating gyre in the central part of the *Grand Lac*. Upwelling in the center of the gyre resulted in a local dome-shaped thermocline (eastern-most slice in Figure 2.8b) and was a remnant of a previous wind event.

Vertical temperature slices at selected locations on 19 January 2018 at 00:00 (Figure 2.8d) revealed a significant tilt of the thermocline perpendicular to the wind stress and thus are in agreement with our field measurements above, indicating that the cold temperatures observed near the northern shore were due to a full upwelling event (i.e., the thermocline reached the surface). The shape of this modeled transect across the lake illustrates the tilting and surfacing of the thermocline that was generated by a sufficiently strong and long-lasting *Vent* wind event. The shape was confirmed experimentally by north-south CTD transects in this part of the lake taken during a similar coastal upwelling event in December 2018 (Figure S2.4).

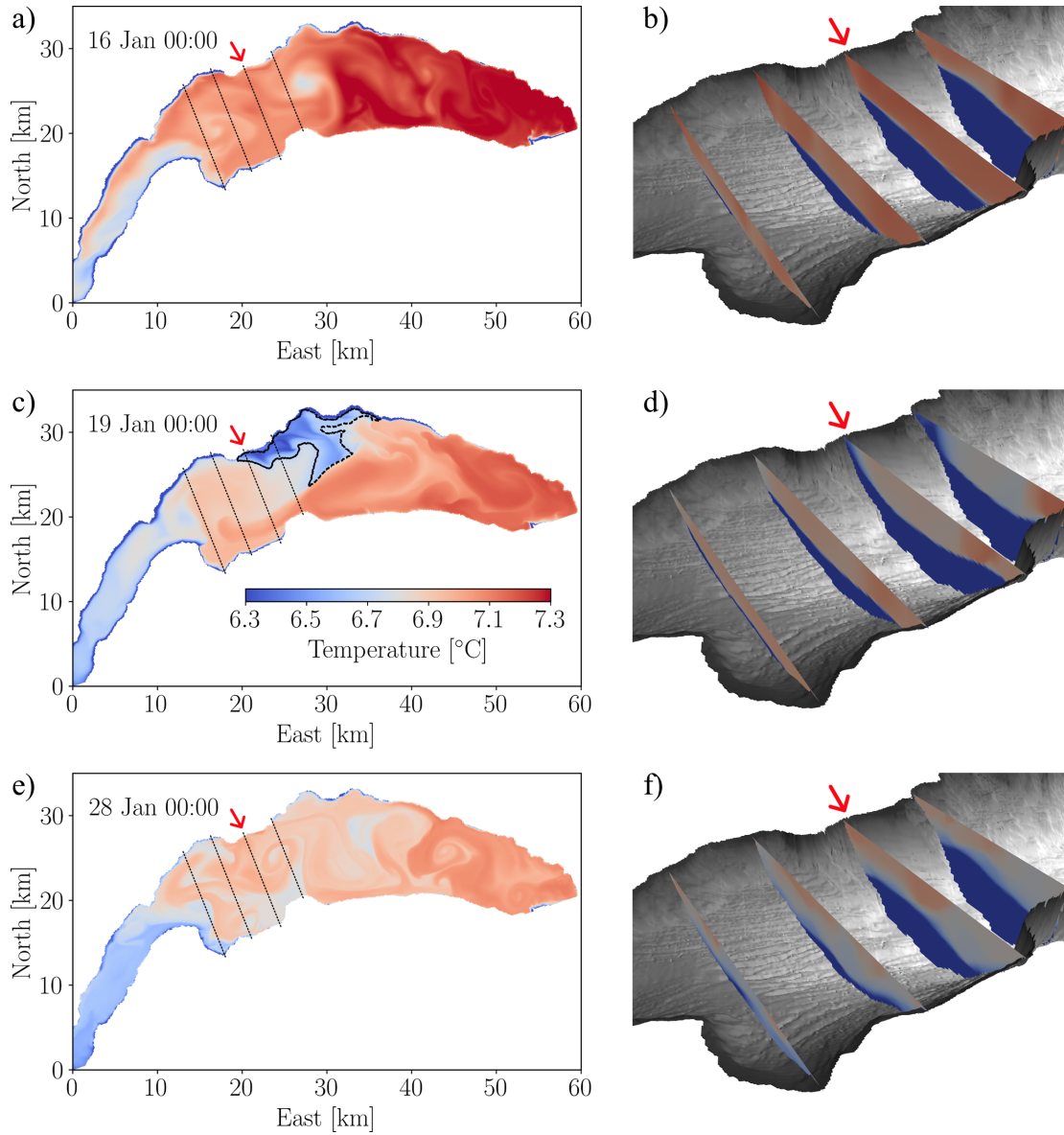


**Figure 2.8.** Modeled near-surface temperatures (**a**, **c**, **e**) and vertical full-depth temperature slices at selected locations (**b**, **d**, **f**) before (16 January 2018, 00:00), during (19 January 2018, 00:00) and after (28 January 2018, 00:00) the upwelling period. The locations of the vertical slices are marked in the surface contour plots by the black lines. The red arrow indicates the mooring sites. The colorbar in **c** gives the temperature range for all panels.

### 2.3.5 Particle tracking results

Observed and modeled temperatures near the northern shore of the lake show that water masses from far below the thermocline reached the nearshore surface, confirming that wintertime coastal upwelling is an effective transport process for hypolimnetic-epilimnetic water exchange. To further assess the upwelling pathways, i.e., the origin and fate of the upwelled water masses in our study area, we employed backward and forward particle tracking. The

computed Lagrangian trajectories with an origin (backward tracking) or final (forward tracking) depth below the thermocline (i.e., 100-m depth), were calculated for a total of approximately 230,000 released particles. Doubling (tripling) the number of released particles by reducing the seeding interval by a factor of two (three) did not change the results of the particle trajectory analysis, thus indicating their statistical robustness. For better visualization, random subsets of 10,000 (Figure 2.9a, c) and 30 (Figure 2.9b, d) particles are shown. Figure S2.5 shows all 230,000 particle trajectories for both backward and forward tracking.

The analysis of the backward tracking trajectories revealed that approximately 30% of all particles released near the shore between 0 and 15-m depth during the active upwelling phase originated from the hypolimnion. The maximum computed origin depth of approximately 200 m is in good agreement with our field observations. Likewise, forward particle tracking confirmed that a similar fraction of the particles released near the shore descended back down into the hypolimnion after wind stress ceased, reaching a maximum depth of more than 200 m.

A clear difference can be seen in the particle motion pattern of the upward motion during the initiation of upwelling and downward motion during the relaxation period (Figure 2.9). As would be expected, most of the upward motion of the deep waters is generated over the lateral slope in close proximity to the nearshore upwelling zone (Figure 2.9a, b). In contrast, the trajectories of the downward motion spread out over a much wider region covering a large portion of the *Grand Lac* basin (Figure 2.9c, d). Furthermore, when tracking only a limited number of particles (Figure 2.9d), it becomes obvious that a significant number of them are entrained into the large-scale gyres in this area, as detailed by Cimattoribus et al. (2019). Thus, the gyre motion field provides for an efficient spreading of the oxygen enriched water masses that originated in the 15-km long nearshore zone of our study site within most of the *Grand Lac* basin.

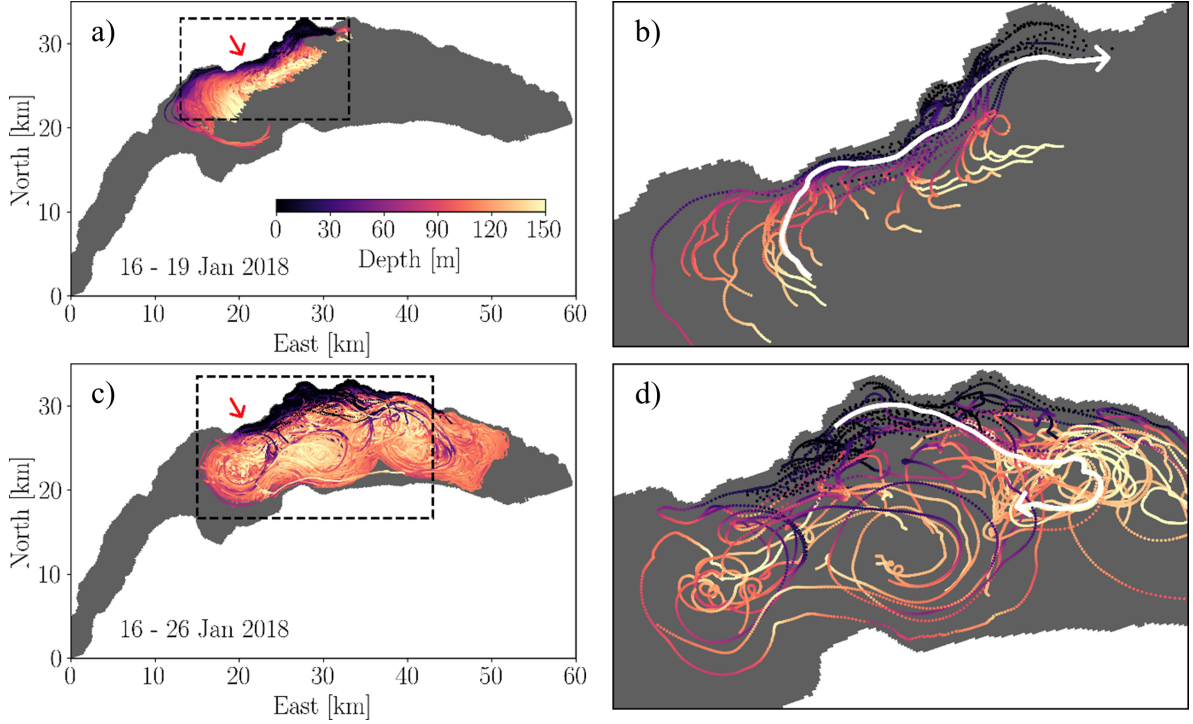


**Figure 2.9.** **a.** Backward tracking (from 19 to 16 January) and **c.** forward tracking (from 16 to 26 January) of particles during the upwelling event from 16 to 26 January 2018. For better visualization, a random subset of 10,000 particles was selected prior to plotting. **b.** and **d.** Close-ups of the areas delimited by the black dashed lines in **a)** and **c)** showing, respectively, backward and forward tracking with a random subset of 30 particles. The white arrows indicate the travelling direction of the released particles along one exemplary trajectory, reflecting the movement of water parcels. The swirling motions in panel **d)** are due to large-scale gyres. Particles were continuously released in the nearshore study site (marked by the red arrow) within the upper 15 m of the water column (Section 2.2.4). Only particles with an origin depth (backward tracking) or a final depth (forward tracking) of more than 100 m are displayed and all trajectories shown in **d)** end on 26 January. Particle depth is given in the colorbar legend in **a)**. Note that the size of the areas in panels **b)** and **d)** is different.

## 2.4 Discussion

### 2.4.1 Observed temperature peaks near the shore during the active upwelling phase

Coastal upwelling of cold hypolimnetic water manifested itself during the active period as cross-shore upslope currents in an approximately 10-m thick bottom boundary layer at both moorings MW3 and ME3 (Figure 2.6). Comparing the contour plots of water temperature and current velocities at ME3 (Figure 2.10a, b), it is evident that the two were strongly correlated, which is confirmed by normalized cross-correlation coefficients of 0.67 and 0.85 for the upper and lower layers, respectively. In particular, it can be seen that after the onset of the

upwelling, events of high current velocity occur simultaneously with an increase of nearly  $0.5^{\circ}\text{C}$  in water temperature in the whole bottom boundary layer. The near-bottom temperatures overall decreased during the active upwelling phase, producing a strong gradient between the top and the bottom layer (Figures 2.5 and 2.10c). However, during this phase, the temperatures in the bottom boundary layer sporadically approached again those that were measured in the top layer (Figure 2.10c). This suggests that warm near-surface waters descended down to 30-m depth.

In order to determine the paths followed by these water masses, the current directions in the top and bottom layers of the eastern mooring ME3 are plotted in Figure 2.10d. Overall, current directions, particularly in the top layer, are oriented alongshore. However, superimposed on this long-term trend, current directions in the bottom layer are downslope-oriented during the warming events, whereas those in the top layer are pointing slightly towards the shore. This is a current pattern characteristic of downwelling where near-surface water is pushed towards the shore by the wind and then down the slope. The full-depth current profiles for this downwelling event document the flow direction reversal between the top (onshore) and bottom (off-shore/downslope) layers, as well as the high velocities (red curve in Figure 2.11; red arrow in Figure 2.10). In contrast, the full-depth direction profiles measured during the active upwelling phase (black curve in Figure 2.11; black arrow in Figure 2.10) show the inverse with offshore movement in the top layer and upslope motion in the bottom layer.

An analysis of the time development of the COSMO-1 wind field over the lake in the vicinity of our study area during these downwelling events confirms that the spatially-averaged wind over an area of  $3\text{ km} \times 3\text{ km}$  is oriented onshore and can therefore push warmer near-surface waters towards the shore (Figure 2.10e, f). Maps of the instantaneous wind pattern in the area confirm the change in orientation with a significant onshore component during these events when compared to the pattern when upwelling is dominant and most vectors are oriented along the shore (Figure 2.10g, h). Thus, while the general wind pattern is that of a *Vent*, causing upwelling in the nearshore area, temporal variability in the wind orientation can generate short events of downwelling (Movie S2.1).

In Figure 2.10b, the near-bottom temperature at the western mooring MW3 also shows these warm water peaks at the same time, thus indicating that these downwelling events covered the full lateral extent of the study area. These peaks also coincide with the peaks seen in the DTS temperature recording at 35-m depth. The DTS near-bottom temperatures below 50-m depth,



i.e., further than 300 m offshore, continuously decreased and showed no sign of warmer surface water intrusions (Figure 2.5). This confirms the nearshore nature of these downwelling events. During these events, oxygen-saturated near-surface water is rapidly pushed to greater depths. The alternating interplay between upwelling and downwelling in this lateral boundary layer causes strong mixing in the whole area and can further increase the oxygen content of these water masses which, as was seen in the particle-tracking analysis above (Figure 2.9), will eventually descend down into the deep hypolimnion. It should be noted, that the numerical model reasonably well reproduced the temperature peaks (Figure 2.7), and thus the downwelling events, despite its limited resolution close to the shoreline.

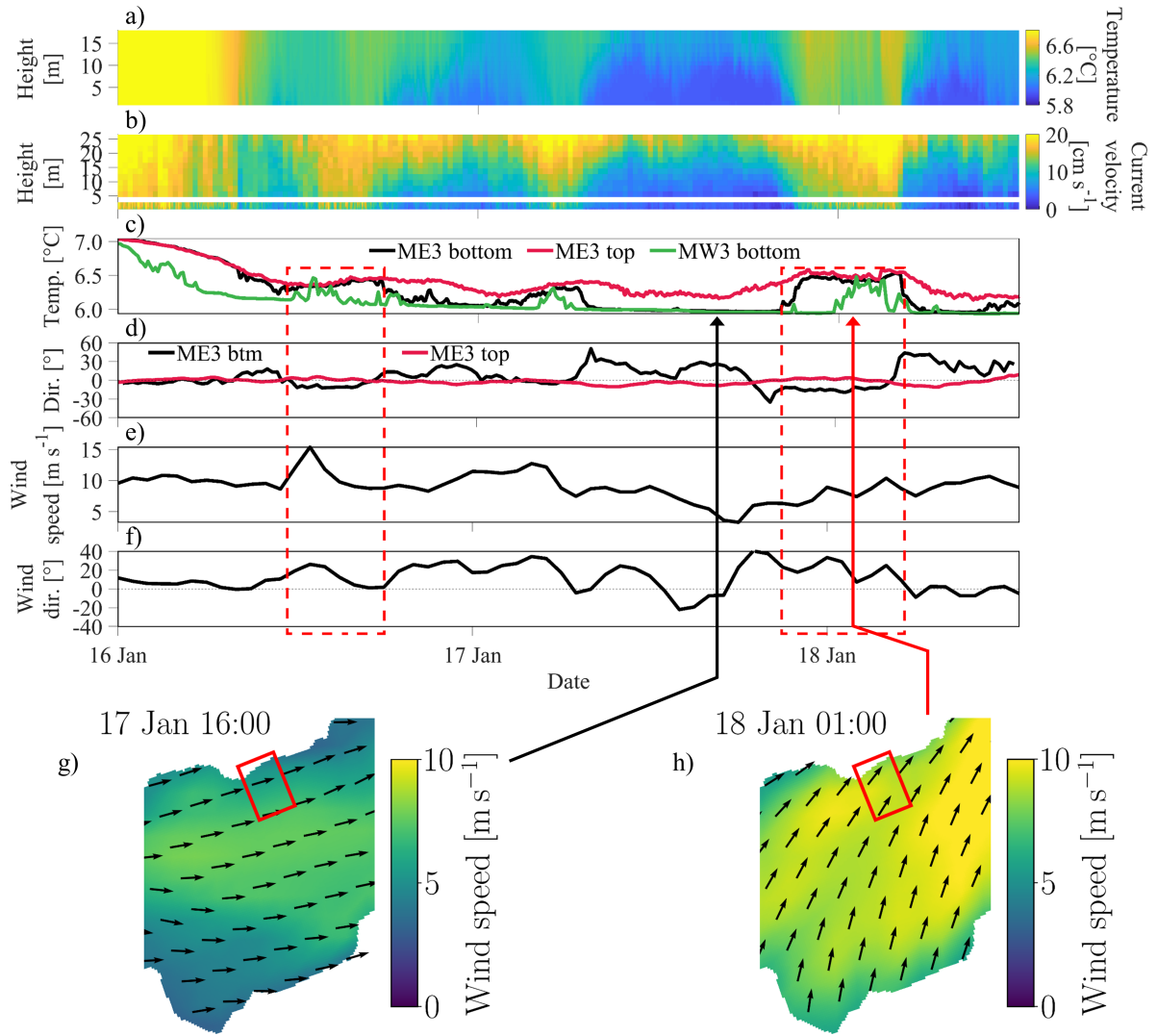


**Figure 2.10.** **a.** Contour plot of the temperature recorded at ME3 during the active upwelling phase, **b.** Contour plot of the current velocity recorded at ME3; height is given in meters above the lakebed, **c.** Temperature time series recorded at ME3 and MW3 for selected heights. The temperatures of the bottom- and topmost thermistors, respectively (MW3 btm: 0.3 m; ME3 btm: 1 m, top: 18 m above the lakebed) are given. **d.** Median-filtered current direction recorded at ME3 in the lower ( $< 10$  m height; black curve) and upper ( $> 15$  m height; red curve) part of the water column. **e.** and **f.** Wind speed and direction derived from the COSMO-1 meteorological model and spatially averaged over the red rectangle shown in **g)** and **h)**. Current (and wind) directions are expressed as divergence from the alongshore direction:  $0^{\circ}$  corresponds to an eastward alongshore flow (wind), whereas positive numbers reflect a shift in the current (wind) direction towards cross-shore and upslope (onshore). The dates on the horizontal axis refer to the year 2018. **g.** and **h.** 2D COSMO-1 wind field on 17 January at 16:00 (active upwelling) and 18 January at 01:00 (downwelling), respectively. The corresponding measured current velocity profiles are shown in Figure 2.11. The red rectangles in **g)** and **h)** indicate the areas where the moorings were deployed. Red dashed-line rectangles in **c)** - **f)** mark downwelling events. Temperature, current velocity and wind speed are given in the colorbar legends.

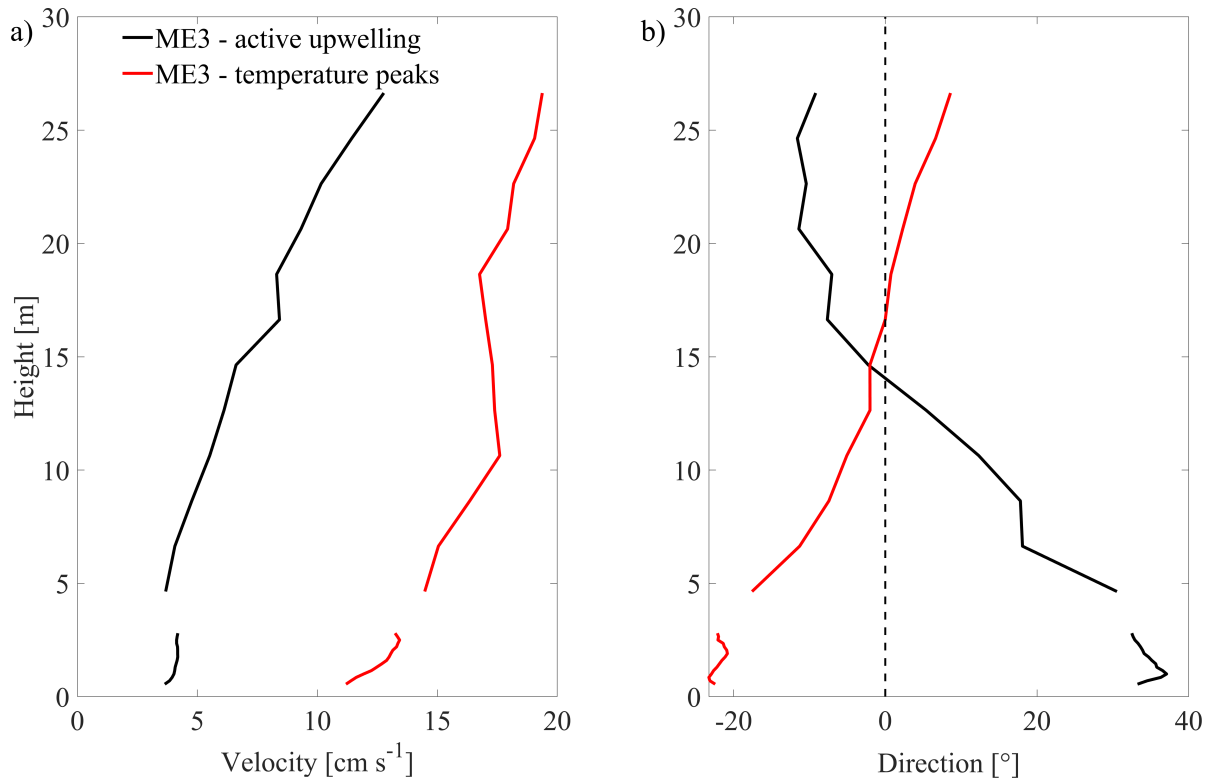


**Figure 2.11.** Profiles of **a.** current velocity and **b.** current direction, both recorded at mooring ME3. The profiles are representative for periods of downwelling related to the observed temperature peaks (red curves) and active upwelling (black curves). The corresponding times are marked in Figure 2.10 by the long red and black arrows. Current directions are plotted as divergence from the alongshore direction: 0° corresponds to an eastward, alongshore flow, whereas positive values reflect a shift in the current direction towards cross-shore and upslope. Height is given in meters above the lakebed.

#### 2.4.2 Wintertime coastal upwelling as a pathway for deepwater renewal

As indicated by the field observations and confirmed by Lagrangian particle tracking, hypolimnetic water from as deep as O(200 m) was transported upslope during the upwelling period. The particle tracking results also suggest that most of the water masses upwelled in the nearshore area descended back to a maximum depth O(200 m) after the wind stress had ceased (Figures 2.9 and S2.5b). The trajectories of these descending water masses were found to be strongly affected by the dynamics of the large-scale motions in the lake, often characterized by large gyres (Cimatoribus et al. 2019), as seen in Figures 2.9c, d and S2.5b. Forward particle tracking shows that due to the presence of these large-scale gyres, descending particles rapidly spread over a wide area in the *Grand Lac* basin, thus demonstrating that coastal upwelling during wintertime, even in a limited nearshore area, is an effective contributor to deepwater renewal over a much larger area.

Once brought to the surface, i.e., in direct contact with the atmosphere, the upwelled water is subject to heat and gas exchange. Hence, the time upwelled water masses spend near the surface appears to be of interest when considering the ecological implications of this physical process. By integrating the time that particles spent in the upper 15 m of the water column, we estimated a surface exposure time for particles with an origin and final depth below the thermocline, i.e., for approximately 30% of all released particles. We found that these upwelled particles spent on average about 1 d near the surface before descending back below the thermocline. Approximately 25% of the upwelled particles spent more than 1.5 d and the maximum observed surface exposure time was more than 5 d.

While the surface exposure time might be limited to a few days, conditions for air-water oxygen exchange are highly favorable during wintertime upwelling due to: (i) high wind speeds which cause intense mixing and large gas transfer velocities, (ii) high values of oxygen saturation concentrations at low in situ temperatures (i.e., high solubility of oxygen) and finally, (iii) low measured in situ concentration of oxygen in upwelled hypolimnetic water (about 6 mg L<sup>-1</sup> at 200-m depth). A rough, order-of-magnitude estimation of the oxygen exchange indicates a DO flux of 23 t km<sup>-2</sup> d<sup>-1</sup> or an oxygen injection of about 1,000 t in our study area for the conditions specified above. However, great care has to be taken when interpreting such average values (for details, see Text S2.1 in the SI). Upwelling also occurs simultaneously in other sections of the northern shore of Lake Geneva, thus increasing the total oxygen input during the surface exposure of the deepwater masses.

Moreover, a number of other processes that may further enhance the air-water oxygen exchange estimated above take place at the same time in this near surface layer:

(i) Air injection by bubbles caused by breaking or whitecapping waves increases the rate of oxygen exchange (e.g., Woolf 1993).

(ii) In addition to direct air-water gas exchange, significant turbulent mixing between upwelled hypolimnetic (low in DO) and DO-saturated epilimnetic water can be expected, considering the high levels of turbulence induced by wind stress and bottom friction in the shallow nearshore region.

(iii) The nearshore downwelling events discussed in Section 2.4.1 brought near-surface water masses down to a depth of 30-40 m, thus contributing to additional mixing, and

(iv) Results of the 3D modeling indicate that the cold upwelled hypolimnetic water can spread over a large surface area. This spreading leads to an unstable stratification in the surface layer, which results in convective downward motion of these cold waters. It was previously observed that this downward motion often occurs in large size convective plumes (several meters in diameter) that have been estimated to cover up to 10% of the lake surface area (Thorpe et al. 1999) and that transport oxygen-rich surface waters into deeper layers more efficiently than small scale turbulent mixing.

The contribution from these different processes cannot be quantified with our data. However, the total resulting DO input into the upwelled waters that will return to the deep layers is most likely substantially higher than the estimate given above.

It has to be noted that the strength of particle tracking simulations lies in their ability to identify trajectories and preferable pathways of upwelled water masses. Using particle tracking, one cannot determine the actual oxygen supply brought down to the deep layers, because particles have neither mass nor volume, and turbulent mixing between the upwelled and the surrounding waters cannot be assessed. A more robust quantification of the deep ventilation potential due to wintertime coastal upwelling, e.g., by means of numerical tracers (e.g., Matsumoto et al. 2015; Sun et al. 2017), goes beyond the scope of this study.

## 2.5 Summary and conclusions

Little is known about the physical dynamics of coastal upwelling in large lakes during wintertime. In order to investigate this transport process, we performed a detailed analysis of a full coastal upwelling event in Lake Geneva which occurred in January 2018 due to a strong southwesterly alongshore *Vent* wind event, and that lasted for 10 d. Field observations using moored current profilers and temperature nodes near the northern shore of the lake during winter 2017/2018 combined with 3D numerical modeling and Lagrangian particle tracking proved to be a powerful tool set that gave new insight into complex 3D lake hydrodynamic processes on a larger scale.

Field measurements showed that during the upwelling period, water masses from as deep as 200 m, well below the thermocline, were brought to the surface in the nearshore area and transported along the shore at high velocities. At the same time, short downwelling events, caused

by small directional changes in the wind field over the lake, transported warmer oxygen-saturated surface water towards the shore and down the slope. Near-bottom temperatures obtained from a DTS fiber-optic cable revealed that downwelling was limited to a depth of less than 50 m. The interplay of short downwelling events with the longer-lasting upwelling most likely causes vigorous mixing of the nearshore water masses, thus increasing the overall oxygen content.

Upwelling and temporary nearshore downwelling events were well reproduced by a 3D hydrodynamic model (RMSE 0.2°C), and thus allowed us to investigate the effects of the observed upwelling over a wider area of the lake. It should be noted that this would not have been possible using only the point measurements of the field observations. Computed surface temperatures suggest that upwelled waters spread out over up to 10% of the surface area of the *Grand Lac*. Lagrangian particle tracking based on the modeled 3D current velocity field confirmed that this water originated from the hypolimnion (maximum depth 200 m). Upwelled particles spend on average 1 d, and up to 5 d near the surface before descending again to the hypolimnion after the wind stress ceased. Once brought to the surface, upwelled hypolimnetic water (low in DO) is subject to gas (notably oxygen) exchange with the atmosphere. Considering the strong wind forcing and weak stratification, vigorous mixing between the upwelled hypolimnetic and DO-saturated epilimnetic water can also be expected.

Particle tracking showed that the upwelled water masses originated from a limited section of the slope in the vicinity of the study area, whereas water masses descending into the deep hypolimnion after the upwelling were caught in large-scale gyres and spread over a wide area of the hypolimnion, thus emphasizing the 3D structure of upwelling and deepwater renewal. Both field observations and particle tracking results suggest that coastal upwelling during the weakly stratified winter period provides an efficient pathway for deepwater renewal in Lake Geneva.

During our field observations between December 2017 and March 2018, four other upwelling periods, comparable in amplitude and duration, occurred (Figure S2.6). Recently, a study on climate change effects in Switzerland (CH2018 2018) reported that during their reference period (1981 to 2011), southwesterly winds (*Vent*) were the most important strong winds during winter in the Lake Geneva area. This further supports our findings that coastal upwelling produced by these winds is a significant contributor to deepwater dynamics. Historical continuous water temperature recordings from a nearshore station close to the present study site, dating

back several decades, provide additional evidence that full coastal upwelling is a frequently occurring transport process during the weakly stratified winter period.

Here, we provided for the first time in Lake Geneva details of the *Vent*-generated upwelling dynamics during winter over a section of the northern shore. Water mass movements related to upwelling similar to those observed in the study area take place simultaneously over other sections of the northern shore, thus reinforcing the lakewide effect of such a *Vent* event on deepwater renewal. Moreover, *Bise* wind events blowing from the opposite direction with comparable strength, duration, frequency and fetch also occur during winter (Figure 2.1c). They bring cold air from Northern Eurasia contributing to differential cooling and can produce coastal upwelling on the southern shore of the lake. Therefore, the integral effect of all these upwelling events on deepwater renewal during the weakly stratified winter season can potentially be substantial.

In the face of rising global surface water temperatures, our findings demonstrate that winter Ekman-type coastal upwelling, an overlooked transport process, could play an increasingly important role in deepwater renewal in Lake Geneva and possibly also in other large deep lakes with favorable wind conditions. It is less sensitive to climate change effects, as opposed to convective cooling, which is expected to continue weakening and thus become less efficient.

Our study has revealed that wintertime coastal upwelling in large lakes is a highly complex and transient, yet potentially significant 3D transport process contributing to deepwater renewal. Therefore, it cannot be adequately described by traditional 1D concepts or models. This should be taken into consideration when making long-term predictions of lake system dynamics, such as those related to climate change.

## Acknowledgments, Samples, and Data

This work was supported by the Swiss National Science Foundation (grant no. 159422) and the [Bois Chamblard Foundation](#). Meteorological data were provided by the Federal Office of Meteorology and Climatology in Switzerland (MeteoSwiss). Full-depth temperature and dissolved oxygen profile data were provided for station SHL2 by © OLA-IS, AnaEE-France, INRAE of Thonon-les-Bains, CIPEL. The Distributed Temperature Sensing (DTS) system was made available by Hendrik Huwald (Laboratory of Cryospheric Sciences, CRYOS, EPFL). We

would like to thank Htet Kyi Wynn for assisting with the fieldwork. The in situ data and model results supporting the findings of this study are available at <https://doi.org/10.5281/zenodo.3968410>.

## References

- Adrian, R., C. M. O'Reilly, H. Zagarese, S. B. Baines, D. O. Hessen, W. Keller, D. M. Livingstone, R. Sommaruga, D. Straile, E. V. Donk, G. A. Weyhenmeyer, and M. Winder. 2009. Lakes as sentinels of climate change. *Limnology and Oceanography* **54**: 2283–2297. doi:[10.4319/lo.2009.54.6\\_part\\_2.2283](https://doi.org/10.4319/lo.2009.54.6_part_2.2283)
- Amadori, M., S. Piccolroaz, L. Giovannini, D. Zardi, and M. Toffolon. 2018. Wind variability and Earth's rotation as drivers of transport in a deep, elongated subalpine lake: The case of Lake Garda. *Journal of Limnology* **77**: 505–521. doi:[10.4081/jlimnol.2018.1814](https://doi.org/10.4081/jlimnol.2018.1814)
- Ambrosetti, W., and L. Barbanti. 1999. Deep water warming in lakes: An indicator of climatic change. *Journal of Limnology* **58**: 1–9. doi:[10.4081/jlimnol.1999.1](https://doi.org/10.4081/jlimnol.1999.1)
- Bauer, S. W., W. H. Graf, C. H. Mortimer, and C. Perrinjaquet. 1981. Inertial motion in Lake Geneva (Le Léman). *Archives for meteorology, geophysics, and bioclimatology, Series A* **30**: 289–312. doi:[10.1007/BF02257850](https://doi.org/10.1007/BF02257850)
- Bohle-Carbonell, M. 1991. Wind and currents: Response patterns of Lake Geneva. *Annales Geophysicae* **9**: 82–90.
- Bouffard, D., I. Kiefer, A. Wüest, S. Wunderle, and D. Odermatt. 2018. Are surface temperature and chlorophyll in a large deep lake related? An analysis based on satellite observations in synergy with hydrodynamic modelling and in-situ data. *Remote Sensing of Environment* **209**: 510–523. doi:[10.1016/j.rse.2018.02.056](https://doi.org/10.1016/j.rse.2018.02.056)
- Bouffard, D., and U. Lemmin. 2013. Kelvin waves in Lake Geneva. *Journal of Great Lakes Research* **39**: 637–645. doi:[10.1016/j.jglr.2013.09.005](https://doi.org/10.1016/j.jglr.2013.09.005)
- CH2018. 2018. CH2018 – Climate Scenarios for Switzerland, Technical Report, National Centre for Climate Services, Zurich, 271 pp. ISBN: 978-3-9525031-4-0. Retrieved from <https://natursciences.ch/service/publications/107865-ch2018---climate-scenarios-for-switzerland-technical-report>, last accessed 30 May 2021.
- Cimatoribus, A. A. 2018. C-tracker. doi:[10.5281/zenodo.1034118](https://doi.org/10.5281/zenodo.1034118)
- Cimatoribus, A. A., U. Lemmin, and D. A. Barry. 2019. Tracking Lagrangian transport in Lake Geneva: A 3D numerical modeling investigation. *Limnology and Oceanography* **64**: 1–18. doi:[10.1002/lno.11111](https://doi.org/10.1002/lno.11111)
- Cimatoribus, A. A., U. Lemmin, D. Bouffard, and D. A. Barry. 2018. Nonlinear dynamics of the near-shore boundary layer of a large lake (Lake Geneva). *Journal of Geophysical Research: Oceans* **123**: 1016–1031. doi:[10.1002/2017JC013531](https://doi.org/10.1002/2017JC013531)
- CIPEL. 2019. Rapports sur les études et recherches entreprises dans le bassin lémanique, Campagne 2018. Commission internationale pour la protection des eaux du Léman (CIPEL), Nyon, Switzerland. Retrieved from [https://www.cipel.org/wp-content/uploads/2019/10/RapportScientifique\\_camp\\_2018-1.pdf](https://www.cipel.org/wp-content/uploads/2019/10/RapportScientifique_camp_2018-1.pdf), last accessed 30 May 2021.
- Coats, R., J. Perez-Losada, G. Schladow, R. Richards, and C. Goldman. 2006. The warming of Lake Tahoe. *Climatic Change* **76**: 121–148. doi:[10.1007/s10584-005-9006-1](https://doi.org/10.1007/s10584-005-9006-1)
- Coman, M. A., and M. G. Wells. 2012. Temperature variability in the nearshore benthic boundary layer of Lake Opeongo is due to wind-driven upwelling events. *Canadian Journal of Fisheries and Aquatic Sciences* **69**: 282–296. doi:[10.1139/f2011-167](https://doi.org/10.1139/f2011-167)
- Corman, J. R., P. B. McIntyre, B. Kuboja, W. Mbemba, D. Fink, C. W. Wheeler, C. Gans, E. Michel, and A. S. Flecker. 2010. Upwelling couples chemical and biological dynamics across the littoral and pelagic zones of Lake Tanganyika, East Africa. *Limnology and Oceanography* **55**: 214–224. doi:[10.4319/lo.2010.55.1.0214](https://doi.org/10.4319/lo.2010.55.1.0214)



- Cossu, R., and M. G. Wells. 2013. The interaction of large amplitude internal seiches with a shallow sloping lakebed: Observations of benthic turbulence in Lake Simcoe, Ontario, Canada. *PLoS ONE* **8**: e57444. doi:[10.1371/journal.pone.0057444](https://doi.org/10.1371/journal.pone.0057444)
- Csanady, G. T. 1977. Intermittent ‘full’ upwelling in Lake Ontario. *Journal of Geophysical Research* **82**: 397–419. doi:[10.1029/JC082i003p00397](https://doi.org/10.1029/JC082i003p00397)
- Djoumna, G., K. G. Lamb, and Y. R. Rao. 2014. Sensitivity of the parameterizations of vertical mixing and radiative heat fluxes on the seasonal evolution of the thermal structure of Lake Erie. *Atmosphere-Ocean* **52**: 294–313. doi:[10.1080/07055900.2014.939824](https://doi.org/10.1080/07055900.2014.939824)
- Döös, K., J. Kjellsson, and B. Jönsson. 2013. TRACMASS—A Lagrangian trajectory model, p. 225–249. *In* T. Soomere and E. Quak [eds.], *Preventive Methods for Coastal Protection: Towards the Use of Ocean Dynamics for Pollution Control*. Heidelberg: Springer International Publishing.
- Dorostkar, A., and L. Boegman. 2013. Internal hydraulic jumps in a long narrow lake. *Limnology and Oceanography* **58**: 153–172. doi:[10.4319/lo.2013.58.1.0153](https://doi.org/10.4319/lo.2013.58.1.0153)
- Dorostkar, A., L. Boegman, and A. Pollard. 2017. Three-dimensional simulation of high-frequency non-linear internal wave dynamics in Cayuga Lake. *Journal of Geophysical Research: Oceans* **122**: 2183–2204. doi:[10.1002/2016JC011862](https://doi.org/10.1002/2016JC011862)
- Ekman, V. W. 1905. On the influence of the earth’s rotation on ocean-currents. *Arkiv for Matematik, Astronomi, och Fysik* **2**: 1–52.
- Fer, I., U. Lemmin, and S. A. Thorpe. 2002. Winter cascading of cold water in Lake Geneva. *Journal of Geophysical Research* **107**: 13-1-13–16. doi:[10.1029/2001JC000828](https://doi.org/10.1029/2001JC000828)
- Forel, F. A. 1892. *Le Léman: Monographie Limnologique* 1, F. Rouge.
- Friedrich, J., F. Janssen, D. Aleynik, H. W. Bange, N. Boltacheva, M. N. Çagatay, A. W. Dale, G. Etiope, Z. Erdem, M. Geraga, A. Gilli, M. T. Gomoiu, P. O. J. Hall, D. Hansson, Y. He, M. Holtappels, M. K. Kirf, M. Kononets, S. Konovalov, A. Lichtschlag, D. M. Livingstone, G. Marinaro, S. Mazlumyan, S. Naeher, R. P. North, G. Papatheodorou, O. Pfannkuche, R. Prien, G. Rehder, C. J. Schubert, T. Soltwedel, S. Sommer, H. Stahl, E. V. Stanev, A. Teaca, A. Tengberg, C. Waldmann, B. Wehrli, and F. Wenzhöfer. 2014. Investigating hypoxia in aquatic environments: diverse approaches to addressing a complex phenomenon. *Biogeosciences* **11**: 1215–1259. doi:[10.5194/bg-11-1215-2014](https://doi.org/10.5194/bg-11-1215-2014)
- van de Giesen, N., S. C. Steele-Dunne, J. Jansen, O. Hoes, M. B. Hausner, S. Tyler, and J. Selker. 2012. Double-ended calibration of fiber-optic Raman spectra distributed temperature sensing data. *Sensors* **12**: 5471–5485. doi:[10.3390/s120505471](https://doi.org/10.3390/s120505471)
- Giovanoli, F. 1990. Horizontal Transport and Sedimentation by Interflows and Turbidity Currents in Lake Geneva, p. 175–195. *In* M.M. Tilzer and C. Serruya [eds.], *Large Lakes: Ecological Structure and Function*. Springer.
- Goldman, C. R., M. Kumagai, and R. D. Robarts, eds. 2013. *Climatic change and global warming of inland waters: Impacts and mitigation for ecosystems and societies*, Wiley-Blackwell.
- Hlevca, B., M. G. Wells, L. Cruz Font, S. E. Doka, R. Portiss, M. St. John, and S. J. Cooke. 2018. Water circulation in Toronto Harbour. *Aquatic Ecosystem Health & Management* **21**: 234–244. doi:[10.1080/14634988.2018.1500059](https://doi.org/10.1080/14634988.2018.1500059)
- Homma, H., T. Nagai, K. Shimizu, and H. Yamazaki. 2016. Early-winter mixing event associated with baroclinic motions in weakly stratified Lake Biwa. *Inland Waters* **6**: 364–378. doi:[10.1080/IW-6.3.898](https://doi.org/10.1080/IW-6.3.898)
- Jabbari, A., J. D. Ackerman, L. Boegman, and Y. Zhao. 2019. Episodic hypoxia in the western basin of Lake Erie. *Limnology and Oceanography* **64**: 2220–2236. doi:[10.1002/lno.11180](https://doi.org/10.1002/lno.11180)
- Lemmin, U. 2020. Insights into the dynamics of the deep hypolimnion of Lake Geneva as revealed by long-term temperature, oxygen, and current measurements. *Limnology and Oceanography* **65**: 2092–2107. doi:[10.1002/lno.11441](https://doi.org/10.1002/lno.11441)
- Lemmin, U., and N. D’Adamo. 1996. Summertime winds and direct cyclonic circulation: Observations from Lake Geneva. *Annales Geophysicae* **14**: 1207–1220. doi:[10.1007/s00585-996-1207-z](https://doi.org/10.1007/s00585-996-1207-z)
- Lemmin, U., C. H. Mortimer, and E. Bäuerle. 2005. Internal seiche dynamics in Lake Geneva. *Limnology and Oceanography* **50**: 207–216. doi:[10.4319/lo.2005.50.1.0207](https://doi.org/10.4319/lo.2005.50.1.0207)
- Likens, G. E., ed. 2010. *Biogeochemistry of inland waters: a derivative of Encyclopedia of inland waters*, Elsevier/Academic Press.

- Livingstone, D. M. 1993. Temporal structure in the deep-water temperature of four Swiss lakes: A short-term climatic change indicator? *Verhandlungen der Internationalen Vereinigung für Theoretische und Angewandte Limnologie* **25**: 75–81. doi:[10.1080/03680770.1992.11900062](https://doi.org/10.1080/03680770.1992.11900062)
- Marshall, J., A. Adcroft, C. Hill, L. Perelman, and C. Heisey. 1997. A finite-volume, incompressible Navier Stokes model for studies of the ocean on parallel computers. *Journal of Geophysical Research: Oceans* **102**: 5753–5766. doi:[10.1029/96JC02775](https://doi.org/10.1029/96JC02775)
- Matsumoto, K., K. S. Tokos, and C. Gregory. 2015. Ventilation and dissolved oxygen cycle in Lake Superior: Insights from a numerical model. *Geochemistry, Geophysics, Geosystems* **16**: 3097–3110. doi:[10.1002/2015GC005916](https://doi.org/10.1002/2015GC005916)
- McEwen, G. F. 1912. The distribution of ocean temperatures along the west coast of North America deduced from Ekman’s theory of the upwelling of cold water from the adjacent ocean depths. *Internationale Revue der gesamten Hydrobiologie und Hydrographie* **5**: 243–286. doi:[10.1002/iroh.19120050205](https://doi.org/10.1002/iroh.19120050205)
- McKinney, P., K. S. Tokos, and K. Matsumoto. 2018. Modeling nearshore-offshore exchange in Lake Superior. *PLOS ONE* **13**: e0193183. doi:[10.1371/journal.pone.0193183](https://doi.org/10.1371/journal.pone.0193183)
- Monsen, N. E., J. E. Cloern, L. V. Lucas, and S. G. Monismith. 2002. A comment on the use of flushing time, residence time, and age as transport time scales. *Limnology and Oceanography* **47**: 1545–1553. doi:[10.4319/lo.2002.47.5.1545](https://doi.org/10.4319/lo.2002.47.5.1545)
- Mortimer, C. H. 1952. Water movements in lakes during summer stratification; evidence from the distribution of temperature in Windermere. *Philosophical Transactions of the Royal Society of London. Series B, Biological Sciences* **236**: 355–404. doi:[10.1098/rstb.1952.0005](https://doi.org/10.1098/rstb.1952.0005)
- O’Reilly, C. M., S. Sharma, D. K. Gray, S. E. Hampton, J. S. Read, R. J. Rowley, P. Schneider, J. D. Lenters, P. B. McIntyre, B. M. Kraemer, G. A. Weyhenmeyer, D. Straile, B. Dong, R. Adrian, M. G. Allan, O. Anneville, L. Arvola, J. Austin, J. L. Bailey, J. S. Baron, J. D. Brookes, E. de Eyto, M. T. Dokulil, D. P. Hamilton, K. Havens, A. L. Hetherington, S. N. Higgins, S. Hook, L. R. Izmet’eva, K. D. Joehnk, K. Kangur, P. Kasprzak, M. Kumagai, E. Kuusisto, G. Leshkevich, D. M. Livingstone, S. MacIntyre, L. May, J. M. Melack, D. C. Mueller-Navarra, M. Naumenko, P. Noges, T. Noges, R. P. North, P.-D. Plisnier, A. Rigos, A. Rimmer, M. Rogora, L. G. Rudstam, J. A. Rusak, N. Salmaso, N. R. Samal, D. E. Schindler, S. G. Schladow, M. Schmid, S. R. Schmidt, E. Silow, M. E. Soylu, K. Teubner, P. Verburg, A. Voutilainen, A. Watkinson, C. E. Williamson, and G. Zhang. 2015. Rapid and highly variable warming of lake surface waters around the globe. *Geophysical Research Letters* **42**: 10,773–10,781. doi:[10.1002/2015GL066235](https://doi.org/10.1002/2015GL066235)
- Peeters, F., D. Finger, M. Hofer, M. Brennwald, D. M. Livingstone, and R. Kipfer. 2003. Deep-water renewal in Lake Issyk-Kul driven by differential cooling. *Limnology and Oceanography* **48**: 1419–1431. doi:[10.4319/lo.2003.48.4.1419](https://doi.org/10.4319/lo.2003.48.4.1419)
- Perroud, M., S. Goyette, A. Martynov, M. Beniston, and O. Anneville. 2009. Simulation of multiannual thermal profiles in deep Lake Geneva: A comparison of one-dimensional lake models. *Limnology and Oceanography* **54**: 1574–1594. doi:[10.4319/lo.2009.54.5.1574](https://doi.org/10.4319/lo.2009.54.5.1574)
- Pöschke, F., J. Lewandowski, C. Engelhardt, K. Preuß, M. Oczipka, T. Ruhtz, and G. Kirillin. 2015. Upwelling of deep water during thermal stratification onset—A major mechanism of vertical transport in small temperate lakes in spring? *Water Resources Research* **51**: 9612–9627. doi:[10.1002/2015WR017579](https://doi.org/10.1002/2015WR017579)
- Rao, Y. R., T. Howell, S. B. Watson, and S. Abernethy. 2014. On hypoxia and fish kills along the north shore of Lake Erie. *Journal of Great Lakes Research* **40**: 187–191. doi:[10.1016/j.jglr.2013.11.007](https://doi.org/10.1016/j.jglr.2013.11.007)
- Rao, Y. R., and C. R. Murthy. 2001. Nearshore currents and turbulent exchange processes during upwelling and downwelling events in Lake Ontario. *Journal of Geophysical Research: Oceans* **106**: 2667–2678. doi:[10.1029/2000JC900149](https://doi.org/10.1029/2000JC900149)
- Rimet, F., O. Anneville, D. Barbet, C. Chardon, L. Crépin, I. Domaizon, J.-M. Dorioz, L. Espinat, V. Frossard, J. Guillard, C. Goulon, V. Hamelet, J.-C. Hustache, S. Jacquet, L. Lainé, B. Montuelle, P. Perney, P. Quetin, S. Rasconi, A. Schellenberger, V. Tran-Khac, and G. Monet. 2020. The Observatory on LAkes (OLA) database: Sixty years of environmental data accessible to the public: The Observatory on LAkes (OLA) database. *Journal of Limnology* **79**. doi:[10.4081/jlimnol.2020.1944](https://doi.org/10.4081/jlimnol.2020.1944)

- Rivas, D., and R. M. Samelson. 2011. A numerical modeling study of the upwelling source waters along the Oregon Coast during 2005. *Journal of Physical Oceanography* **41**: 88–112. doi:[10.1175/2010JPO4327.1](https://doi.org/10.1175/2010JPO4327.1)
- Sahoo, G. B., S. G. Schladow, J. E. Reuter, R. Coats, M. Dettinger, J. Riverson, B. Wolfe, and M. Costa-Cabral. 2013. The response of Lake Tahoe to climate change. *Climatic Change* **116**: 71–95. doi:[10.1007/s10584-012-0600-8](https://doi.org/10.1007/s10584-012-0600-8)
- Schladow, S. G., S. Ö. Pálmarsson, T. E. Steissberg, S. J. Hook, and F. E. Prata. 2004. An extraordinary upwelling event in a deep thermally stratified lake. *Geophysical Research Letters* **31**: L15504. doi:[10.1029/2004GL020392](https://doi.org/10.1029/2004GL020392)
- Schulz, B. 1917. Die Auftrieberscheinungen an der Westküste Nordamerikas. *Naturwissenschaften* **5**: 713–719. doi:[10.1007/BF02447973](https://doi.org/10.1007/BF02447973)
- van Sebille, E., S. M. Griffies, R. Abernathey, T. P. Adams, P. Berloff, A. Biastoch, B. Blanke, E. P. Chassignet, Y. Cheng, C. J. Cotter, E. Deleersnijder, K. Döös, H. F. Drake, S. Drijfhout, S. F. Gary, A. W. Heemink, J. Kjellsson, I. M. Koszalka, M. Lange, C. Lique, G. A. MacGilchrist, R. Marsh, C. G. Mayorga Adame, R. McAdam, F. Nencioli, C. B. Paris, M. D. Piggott, J. A. Polton, S. Rührs, S. H. A. M. Shah, M. D. Thomas, J. Wang, P. J. Wolfram, L. Zanna, and J. D. Zika. 2018. Lagrangian ocean analysis: Fundamentals and practices. *Ocean Modelling* **121**: 49–75. doi:[10.1016/j.ocemod.2017.11.008](https://doi.org/10.1016/j.ocemod.2017.11.008)
- Selker, J. S., L. Thévenaz, H. Huwald, A. Mallet, W. Luxemburg, N. van de Giesen, M. Stejskal, J. Zeman, M. Westhoff, and M. B. Parlange. 2006. Distributed fiber-optic temperature sensing for hydrologic systems. *Water Resources Research* **42**: W12202. doi:[10.1029/2006WR005326](https://doi.org/10.1029/2006WR005326)
- Soullignac, F., P.-A. Danis, D. Bouffard, V. Chanudet, E. Dambrine, Y. Guénand, T. Harmel, B. W. Ibelings, D. Trevisan, R. Uittenbogaard, and O. Anneville. 2018. Using 3D modeling and remote sensing capabilities for a better understanding of spatio-temporal heterogeneities of phytoplankton abundance in large lakes. *Journal of Great Lakes Research* **44**: 756–764. doi:[10.1016/j.jglr.2018.05.008](https://doi.org/10.1016/j.jglr.2018.05.008)
- Steissberg, T. E., S. J. Hook, and S. G. Schladow. 2005. Characterizing partial upwellings and surface circulation at Lake Tahoe, California–Nevada, USA with thermal infrared images. *Remote Sensing of Environment* **99**: 2–15. doi:[10.1016/j.rse.2005.06.011](https://doi.org/10.1016/j.rse.2005.06.011)
- Sun, D., T. Ito, and A. Bracco. 2017. Oceanic uptake of oxygen during deep convection events through diffusive and bubble-mediated gas exchange. *Global Biogeochemical Cycles* **31**: 1579–1591. doi:[10.1002/2017GB005716](https://doi.org/10.1002/2017GB005716)
- Tamsitt, V., H. F. Drake, A. K. Morrison, L. D. Talley, C. O. Dufour, A. R. Gray, S. M. Griffies, M. R. Mazloff, J. L. Sarmiento, J. Wang, and W. Weijer. 2017. Spiraling pathways of global deep waters to the surface of the Southern Ocean. *Nature Communications* **8**: 172. doi:[10.1038/s41467-017-00197-0](https://doi.org/10.1038/s41467-017-00197-0)
- Thorade, H. 1909. Über die Kalifornischen Meeresströmungen, Oberflächentemperaturen und Strömungen, an der Westküste Nordamerikas. *Annalen der Hydrographie und maritimen Meteorologie* **37**: 17-34,63-77.
- Thorpe, S. A., U. Lemmin, C. Perrinjaquet, and I. Fer. 1999. Observations of the thermal structure of a lake using a submarine. *Limnology and Oceanography* **44**: 1575–1582. doi:[10.4319/lo.1999.44.6.1575](https://doi.org/10.4319/lo.1999.44.6.1575)
- Troy, C. D., S. Ahmed, N. Hawley, and A. Goodwell. 2012. Cross-shelf thermal variability in southern Lake Michigan during the stratified periods. *Journal of Geophysical Research: Oceans* **117**: C02028. doi:[10.1029/2011JC007148](https://doi.org/10.1029/2011JC007148)
- Valipour, R., Y. R. Rao, L. F. León, and D. Depew. 2019. Nearshore-offshore exchanges in multi-basin coastal waters: Observations and three-dimensional modeling in Lake Erie. *Journal of Great Lakes Research* **45**: 50–60. doi:[10.1016/j.jglr.2018.10.005](https://doi.org/10.1016/j.jglr.2018.10.005)
- Viglione, G. A., and A. F. Thompson. 2016. Lagrangian pathways of upwelling in the Southern Ocean. *Journal of Geophysical Research: Oceans* **121**: 6295–6309. doi:[10.1002/2016JC011773](https://doi.org/10.1002/2016JC011773)
- Voudouri, A., E. Avgoustoglou, and P. Kaufmann. 2017. Impacts of Observational Data Assimilation on Operational Forecasts. *Perspectives on Atmospheric Sciences*. Cham: Springer International Publishing. 143–149.

- Wahl, B., and F. Peeters. 2014. Effect of climatic changes on stratification and deep-water renewal in Lake Constance assessed by sensitivity studies with a 3D hydrodynamic model. *Limnology and Oceanography* **59**: 1035–1052. doi:[10.4319/lo.2014.59.3.1035](https://doi.org/10.4319/lo.2014.59.3.1035)
- Wang, Y., K. Hutter, and E. Bäuerle. 2000. Wind-induced baroclinic response of Lake Constance. *Annales Geophysicae* **18**: 1488–1501. doi:[10.1007/s005850000279](https://doi.org/10.1007/s005850000279)
- Woolf, D. K. 1993. Bubbles and the air-sea transfer velocity of gases. *Atmosphere-Ocean* **31**: 517–540. doi:[10.1080/07055900.1993.9649484](https://doi.org/10.1080/07055900.1993.9649484)

# Supporting Information for Chapter 2

---

Rafael Sebastian Reiss, Ulrich Lemmin, Andrea Cimatoribus, and David Andrew Barry

Ecological Engineering Laboratory (ECOL), Faculty of Architecture, Civil and Environmental Engineering (ENAC), Ecole Polytechnique Fédérale de Lausanne (EPFL), Lausanne, Switzerland

## Introduction

This Supporting Information section contains six figures, a text and one movie:

- Figure S2.1: Comparison of the SHL2 full-depth temperature profiles measured by [CIPEL](#) (red) and computed by the High Resolution (HR) 3D model (blue), approximately one month after the beginning of the HR simulation, i.e., on 21 November 2017.
- Figure S2.2: Nearshore area in which particles were released during the particle tracking simulations, referred to as the seeding area in the main text.
- Figure S2.3: Temperature time series recorded at the western moorings MW1, MW2, MW3 and the eastern moorings ME1, ME2, ME3 during the winter coastal upwelling event discussed in the main text.
- Figure S2.4: Full-depth temperature profiles taken along a north-south transect across the central basin of Lake Geneva during a coastal upwelling event in December 2018, as well as wind speed and direction measured at the nearby St. Prex MeteoSwiss station.
- Figure S2.5: Trajectories of particles released near the northern shore of Lake Geneva during the winter upwelling event discussed in the main text, obtained by backward and forward particle tracking based on 3D numerical modeling results. This is similar to Figure 2.9 in the main text but considers all 230,000 particles.
- Figure S2.6: Temperature time series recorded at the western mooring site at 10-m depth (MW2) from 7 December 2017 to 1 February 2018 showing a total of five coastal upwelling events.
- Text S2.1: A rough order-of-magnitude estimation of the wintertime coastal upwelling ventilation potential in Lake Geneva.
- Movie S2.1: Animation of the modeled current velocities, the COSMO-1 wind field, and the observed and modeled nearshore temperatures during the temporary nearshore downwelling events, which were caused by small changes in the wind direction (Section 2.4.1 in the main text). (file uploaded separately)

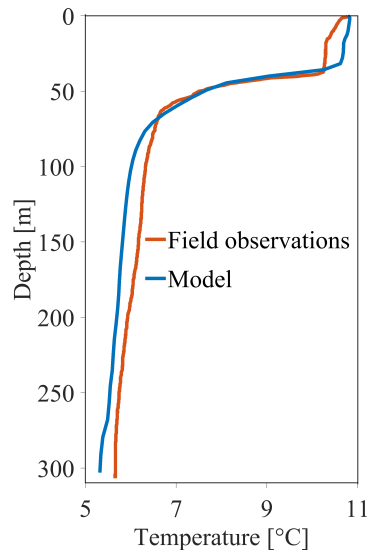


**Figure S2.1.** Full-depth temperature profiles at SHL2 measured by CIPEL on 21 November 2017 (red) and computed by the high resolution (HR) model (blue). For SHL2 station location, see Figure 2.1.

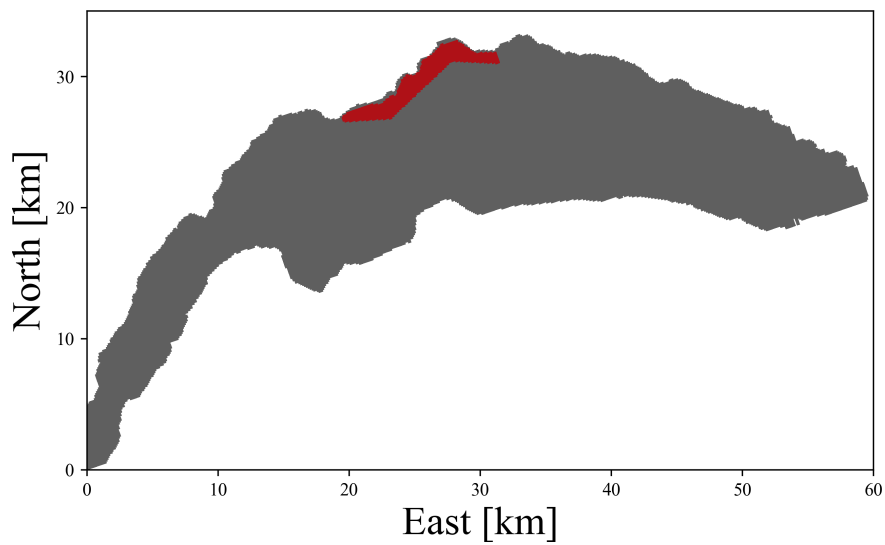


**Figure S2.2.** The red polygon marks the nearshore area in which particles were released during the particle tracking simulations, referred to as the seeding area in the main text.

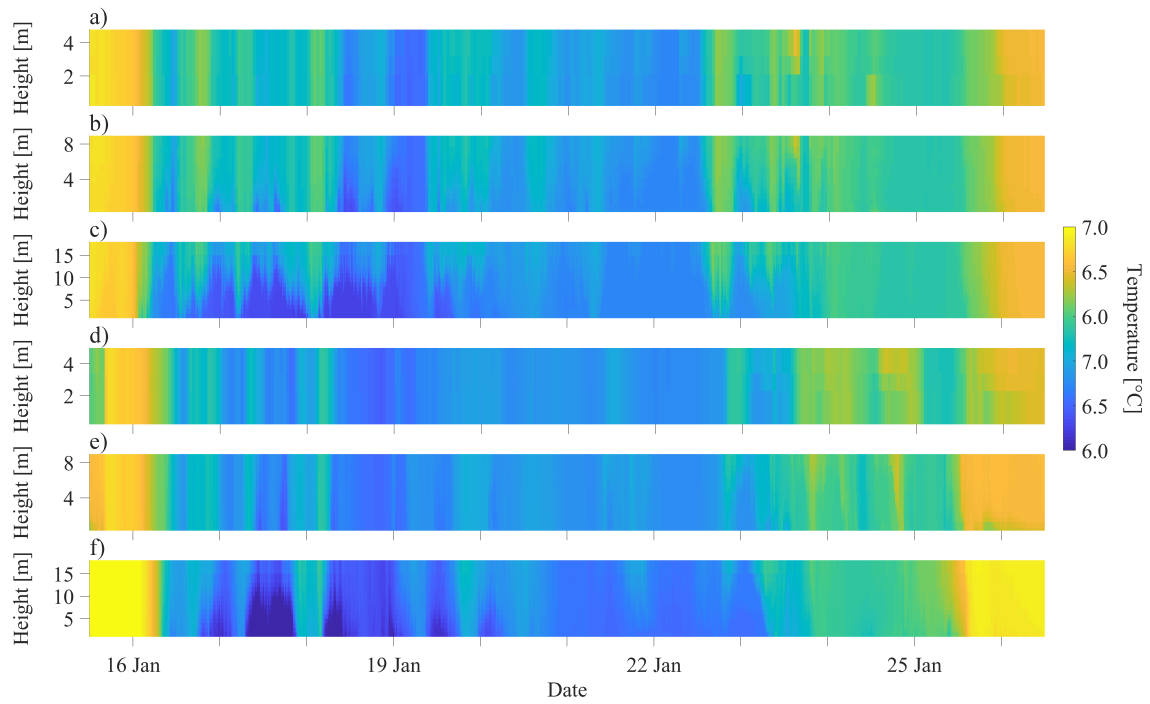


**Figure S2.3.** Temperature time series recorded during a coastal upwelling event in January 2018 at the western moorings MW1 (a), MW2 (b), MW3 (c) and the eastern moorings ME1 (d), ME2 (e), ME3 (f). Height is given in meters above the lakebed. The dates on the horizontal axis refer to the year 2018. The colorbar shows the temperature.



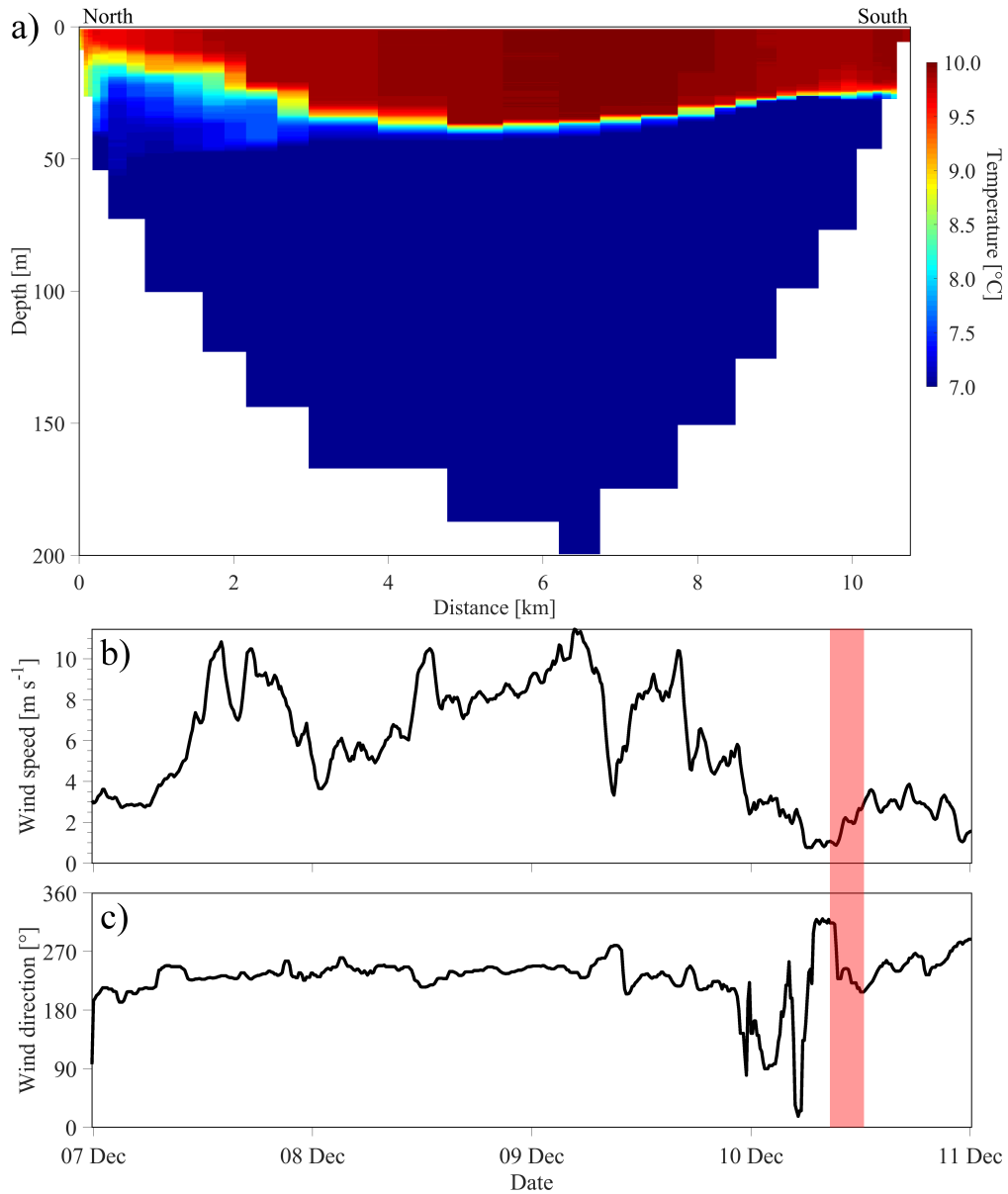


**Figure S2.4. a.** Full-depth temperature profiles taken along a north-south transect across the lake, starting in the study area on the northern shore marked in Figure 2.1, show an up-tilted thermocline near the northern shore of Lake Geneva during a coastal upwelling event in December 2018. Distance is given in km starting at the northern shore. The colorbar shows the temperature. This measured thermocline tilting compares well with results from numerical simulations in Figure 2.8). **b.** and **c.** Wind speed and wind direction, respectively, measured at the St. Prex MeteoSwiss station from 7 to 11 December 2018 (see Figure 2.1a for station location). The red shaded area marks the time during which the profiles in a) were taken. The dates on the horizontal axis refer to the year 2018.

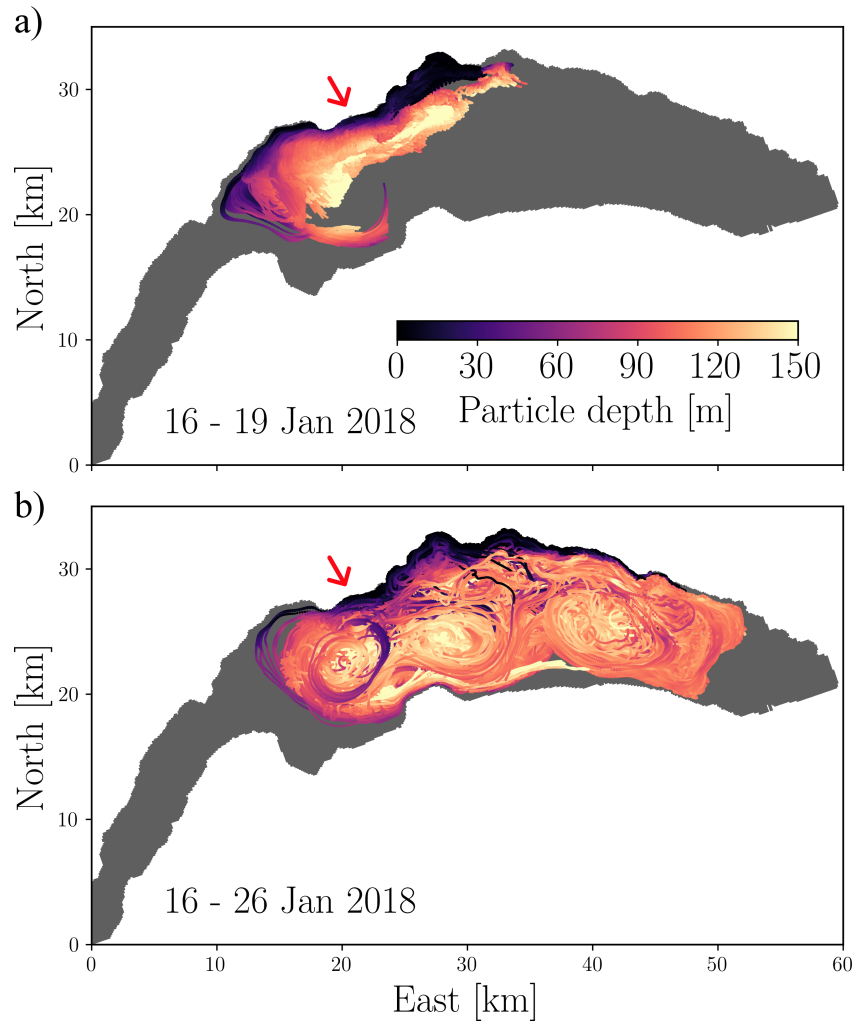


**Figure S2.5.** **a.** Backward tracking (from 19 to 16 January) and **b.** forward tracking (from 16 to 26 January) of all 230,000 particles released during the upwelling event from 16 to 26 January 2018. During the upwelling (panel a), particles from a limited area in close proximity to the study area are transported up into the near shore zone. During the descent (panel b) the trajectories of the downward motion spread out over a much wider region covering a large portion of the Grand Lac basin and are mainly caught in three large-scale gyres. Particles were continuously released in the nearshore study site (marked by the red arrow; see also Figure S2.2 for the location of the release area) within the upper 15 m of the water column (Section 2.2.4 in the main text). Only particles with an origin depth (backward tracking) or a final depth (forward tracking) of more than 100 m are displayed and all trajectories shown in b) end on 26 January. Particle depth is given in the colorbar legends.

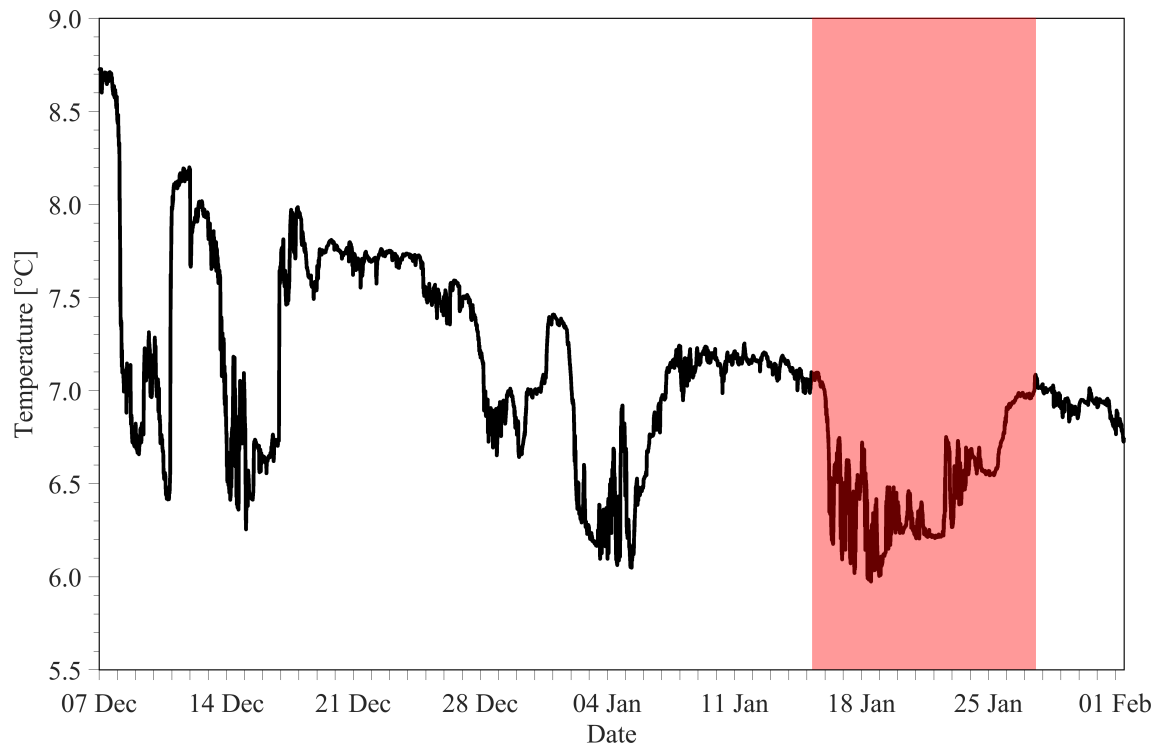


**Figure S2.6.** Temperature time series recorded at the western mooring site at 10-m depth (MW2) approximately 50 cm above the lakebed from 7 December 2017 to 1 February 2018. A total of five coastal upwelling events, characterized by sudden temperature drops, also seen at all other thermistor moorings near the northern shore, were identified during the observation period from December 2017 to March 2018. The red shaded area marks the coastal upwelling event investigated in this study.

## Text S2.1

### **A rough order-of-magnitude estimation of the wintertime coastal upwelling ventilation potential in Lake Geneva**

A rough order-of-magnitude estimation of the coastal upwelling ventilation potential in Lake Geneva during wintertime is carried out using some characteristic numbers determined in this study, and its suitability is discussed considering the 3D nature of this transport process.

### **Gas transfer velocity $k$ and saturation concentration of dissolved oxygen $C_s$**

Air-water gas exchange is often described by the gas transfer velocity  $k$ , also called piston velocity (e.g., Likens 2010). Due to its importance for estimating air-water gas exchange in surface waters, the development of empirical  $k$  models has received considerable attention in the past decades (e.g., Cole and Caraco 1998; Crusius and Wanninkhof 2003; Guérin et al. 2007; Vachon and Prairie 2013). Most of the models describe  $k$  as a function of wind speed and sometimes system-dependent parameters such as the lake surface area or fetch length. Klaus and Vachon (2020) compared the predictive performance of six widely used empirical models based on a large dataset of published  $k$  estimates obtained by various methods and found that they all performed poorly, especially if applied outside of their calibration range. Hence, care has to be taken when selecting a model. Using data collected from lakes of different sizes, Vachon and Prairie (2013) developed a lake-surface-area-dependent model describing the gas transfer velocity standardized to a Schmidt number of 600, i.e.,  $k_{600}$ , as

$$k_{600} = 2.51 (\pm 0.99) + 1.48 (\pm 0.34) U_{10} + 0.39 (\pm 0.08) U_{10} \log_{10} LA \quad [\text{cm h}^{-1}] \quad (2.1)$$

where  $U_{10}$  is wind speed at 10 m height in  $\text{m s}^{-1}$  and  $LA$  is the lake surface area in  $\text{km}^2$ . One of the cases incorporated into their model calibration was a large reservoir ( $LA = 602 \text{ km}^2$ ) under relatively high wind conditions (maximum wind speed  $U_{10} > 6 \text{ m s}^{-1}$ ), making it a reasonable choice for estimating the air-water oxygen exchange during wintertime coastal upwelling in Lake Geneva ( $LA = 580 \text{ km}^2$ ). A Schmidt number of 600 characterizes  $\text{CO}_2$  transfer at  $20^\circ\text{C}$  water temperature and is often used in the literature. To apply equation (2.1) for a given Schmidt number ( $Sc$ ), it needs to be scaled as

$$k = \left( \frac{Sc}{600} \right)^{-n} k_{600} \quad (2.2)$$

with  $n = 2/3$  for low wind speeds and  $n = 1/2$  for high wind speeds as suggested by Jähne et al. (1987). For oxygen transfer in fresh water at 7°C, we find  $Sc \approx 1000$  (e.g., Wanninkhof 2014). Using equations (2.1) and (2.2) with  $U_{10} = 7.2 \text{ m s}^{-1}$  (mean wind speed during the upwelling, Section 3.2),  $LA = 580 \text{ km}^2$ ,  $Sc = 1000$  and  $n = 1/2$ , we obtain a gas transfer velocity of  $k \approx 16 \text{ cm h}^{-1}$ . This value is comparable to those measured by Vachon and Prairie (2013) in the large reservoir under high wind conditions.

Knowing  $k$ , the DO flux across the air-water interface  $F_{DO}$  can be estimated as (e.g., Likens (2010))

$$F_{DO} = k (C_S - C) \quad (2.3)$$

where  $C_S$  and  $C$  are the saturation and in situ DO concentrations, respectively. The DO saturation concentration increases with decreasing temperature and can be described for freshwater lakes as (Mortimer 1981)

$$C_S = \exp(7.7117 - 1.31403 \ln(T + 45.93)) \quad (2.4)$$

where  $T$  is the water temperature in °C.

Using a typical epilimnetic water temperature of 7°C during the upwelling event we find  $C_S \approx 12 \text{ mg L}^{-1}$ . The  $C_S$  obtained by equation (2.4) needs be corrected for the altitude dependent partial pressure of oxygen in the atmosphere using the barometric formula. However, in the case of Lake Geneva (surface level at 372 m above sea level) the difference due to the altitude correction is less than 5% and will be neglected in the following order of magnitude calculations.

### **Dissolved oxygen flux $F_{DO}$ and total oxygen injection during the upwelling event**

The modeled particle trajectories revealed that a significant amount of the particles released in the nearshore study region originated from the hypolimnion, with a maximum origin depth of 200 m. [CIPEL](#) measurements taken on 21 December 2017 at the deepest point of the lake (SHL2, Figure 2.1a) show DO concentrations of  $C \approx 6 \text{ mg L}^{-1}$  at 200-m depth (CIPEL 2019; Rimet et al. 2020). With  $C_S \approx 12 \text{ mg L}^{-1}$  and  $k \approx 16 \text{ cm h}^{-1}$  the DO flux during the upwelling is calculated by equation (2.3) as  $F_{DO} \approx 23 \text{ t km}^{-2} \text{ d}^{-1}$ . Considering an exposed surface area of  $50 \text{ km}^2$  (Section 2.3.4) and an average surface exposure time of 1 d (Section 2.4.2), the total oxygen injection over the nearshore region is about 1150 t. This could contribute to a dissolved oxygen

increase of approximately  $0.04 \text{ mg L}^{-1}$  in the layer between 100 and 200-m depth. Bearing in mind that the actual extent of the nearshore area affected by coastal upwelling is much larger than our study area, an increase of  $0.1 \text{ mg L}^{-1}$  during an upwelling event can be expected in that layer. As indicated in the main text, several upwelling events occurred during the winter season and taken altogether, this could significantly contribute to oxygen renewal in the deep layers. The above figures, however, should be taken with great caution for the reasons discussed below.

### Remarks

The above estimation of the dissolved oxygen flux and the total oxygen injection into the near-surface layer based on model results and measured wind speed is only a rough, order-of-magnitude calculation. However, the DO flux estimate is also affected by the following:

- a) The particle tracking simulations carried out in this study focus on one nearshore region in the central basin where the coastal upwelling is the most evident in the hydrodynamic modeling results and where the moorings were located. However, under the discussed wind conditions, coastal upwelling occurs along a wide stretch of the northern shore where different particle trajectories, exposure times and affected surface areas can be expected.
- b) In equation (2.3), a key parameter determining  $F_{DO}$  is the in situ DO concentration. The value of  $6 \text{ mg L}^{-1}$  used here was measured in the center of the lake at 200-m depth, which approximately corresponds to the maximum upwelling depth. However, the upwelled water masses originate from a wide range of depth. Consequently, the in situ DO concentrations driving the gas transfer may also vary considerably, both in space and time. It is not possible to assess the volume flux or the contribution from each of the different depth layers. Hence, there remains a large uncertainty in the in situ oxygen concentrations of the water masses that are actually in contact with the atmosphere.
- c) The surface area affected by the upwelling was estimated to be 10% of the *Grand Lac* surface area, based on a modeled surface temperature anomaly of  $0.2^{\circ}\text{C}$ . While this certainly corresponds to the most affected region, i.e., the area with the coldest surface temperatures, the choice of  $0.2^{\circ}\text{C}$  is somewhat arbitrary, and a smaller value would result in a larger area. Therefore, the obtained value may best be seen as a lower bound for the affected area during the most intense period of the upwelling. Another complicating factor is that the coastal upwelling event discussed in this manuscript is a highly

three-dimensional and transient process. Consequently, the affected surface area is also a function of time.

- d) Our results clearly show that wintertime coastal upwelling in Lake Geneva is a highly three-dimensional and transient process. It is therefore questionable to what degree average values such as a mean surface exposure time, mean wind speed and mean oxygen concentration can be used to assess the DO flux and total oxygen injection.
- e) Particles return to the full depth range down to 200-m depth over a very wide area. Furthermore, the background oxygen concentrations of the surrounding waters into which the upwelled water masses return are highly spatially heterogeneous due to other hydrodynamic processes, such as large-scale gyre motions causing pelagic up- and downwelling and thus vertical oxygen transport in the off-shore waters (Figure 2.9d).

Unfortunately, the actual pathways of the oxygen transported into the different layers of the hypolimnion cannot be determined. Particle tracking is a tool used to reveal the dominant 3D pathways taken by hypolimnetic water parcels during the upwelling phase and their subsequent descent back into the deep layers. However, the passive particles employed in this study have no mass and no volume and can only trace the advective motion of water parcels. Therefore, nothing can be inferred about how oxygen is transported down into the deep layers or about the mixing between the upwelled water parcels and the surrounding waters along their path, both during the upwelling and the descent.

## References

- CIPEL. 2019. Rapports sur les études et recherches entreprises dans le bassin lémanique, Campagne 2018. Commission internationale pour la protection des eaux du Léman (CIPEL), Nyon, Switzerland. Retrieved from [https://www.cipel.org/wp-content/uploads/2019/10/RapportScientifique\\_camp\\_2018-1.pdf](https://www.cipel.org/wp-content/uploads/2019/10/RapportScientifique_camp_2018-1.pdf), last accessed 30 May 2021.
- Cole, J. J., and N. F. Caraco. 1998. Atmospheric exchange of carbon dioxide in a low-wind oligotrophic lake measured by the addition of SF<sub>6</sub>. *Limnology and Oceanography* **43**: 647–656. doi:[10.4319/lo.1998.43.4.0647](https://doi.org/10.4319/lo.1998.43.4.0647)
- Crusius, J., and R. Wanninkhof. 2003. Gas transfer velocities measured at low wind speed over a lake. *Limnology and Oceanography* **48**: 1010–1017. doi:[10.4319/lo.2003.48.3.1010](https://doi.org/10.4319/lo.2003.48.3.1010)
- Guérin, F., G. Abril, D. Serça, C. Delon, S. Richard, R. Delmas, A. Tremblay, and L. Varfalvy. 2007. Gas transfer velocities of CO<sub>2</sub> and CH<sub>4</sub> in a tropical reservoir and its river downstream. *Journal of Marine Systems* **66**: 161–172. doi:[10.1016/j.jmarsys.2006.03.019](https://doi.org/10.1016/j.jmarsys.2006.03.019)
- Jähne, B., K. O. Münnich, R. Börsinger, A. Dutzi, W. Huber, and P. Libner. 1987. On the parameters influencing air-water gas exchange. *Journal of Geophysical Research* **92**: 1937–1949. doi:[10.1029/JC092iC02p01937](https://doi.org/10.1029/JC092iC02p01937)

- Klaus, M., and D. Vachon. 2020. Challenges of predicting gas transfer velocity from wind measurements over global lakes. *Aquatic Sciences* **82**: 53. doi:[10.1007/s00027-020-00729-9](https://doi.org/10.1007/s00027-020-00729-9)
- Likens, G. E., ed. 2010. *Biogeochemistry of inland waters: a derivative of Encyclopedia of inland waters*, Elsevier/Academic Press.
- Mortimer, C. H. 1981. The oxygen content of air-saturated fresh waters over ranges of temperature and atmospheric pressure of limnological interest. *SIL Communications, 1953-1996* **22**: 1–23. doi:[10.1080/05384680.1981.11904000](https://doi.org/10.1080/05384680.1981.11904000)
- Rimet, F., O. Anneville, D. Barbet, C. Chardon, L. Crépin, I. Domaizon, J.-M. Dorioz, L. Espinat, V. Frossard, J. Guillard, C. Goulon, V. Hamelet, J.-C. Hustache, S. Jacquet, L. Lainé, B. Montuelle, P. Perney, P. Quetin, S. Rasconi, A. Schellenberger, V. Tran-Khac, and G. Monet. 2020. The Observatory on LAkes (OLA) database: Sixty years of environmental data accessible to the public: The Observatory on LAkes (OLA) database. *Journal of Limnology* **79**. doi:[10.4081/jlimnol.2020.1944](https://doi.org/10.4081/jlimnol.2020.1944)
- Vachon, D., and Y. T. Prairie. 2013. The ecosystem size and shape dependence of gas transfer velocity versus wind speed relationships in lakes. *Canadian Journal of Fisheries and Aquatic Sciences* **70**: 1757–1764. doi:[10.1139/cjfas-2013-0241](https://doi.org/10.1139/cjfas-2013-0241)
- Wanninkhof, R. 2014. Relationship between wind speed and gas exchange over the ocean revisited: Gas exchange and wind speed over the ocean. *Limnology and Oceanography: Methods* **12**: 351–362. doi:[10.4319/lom.2014.12.351](https://doi.org/10.4319/lom.2014.12.351)



# Chapter 3      Wind-induced      hypolimnetic upwelling between the multi-depth basins of Lake Geneva during winter: An overlooked deepwater renewal mechanism?

---

Rafael Sebastian Reiss, Ulrich Lemmin, and David Andrew Barry

Ecological Engineering Laboratory (ECOL), Faculty of Architecture, Civil and Environmental  
Engineering (ENAC), Ecole Polytechnique Fédérale de Lausanne (EPFL), Lausanne,  
Switzerland

## Abstract

Combining field observations, 3D hydrodynamic modeling, and particle tracking, we investigated wind-induced interbasin exchange between the *Petit Lac* (*PL*) (depth 75 m) and *Grand Lac* (*GL*) (depth 309 m) basins of Lake Geneva in early winter.

Following a strong 2.5-d wind event, a two-layer flow established, where the downwind surface drift into the *GL* was balanced by counterflowing hypolimnetic currents into the *PL*. Velocities in both layers exceeded  $20 \text{ cm s}^{-1}$ , with the highest values ( $27 \text{ cm s}^{-1}$ ) found near the bottom. For 3.5 d, hypolimnetic temperatures at the confluence decreased to values found in the deep *GL* hypolimnion at 180-m depth. Approximately 1.5 d after the wind event ceased, currents reversed and upwelled waters drained back into the deep *GL* hypolimnion. Coriolis force strongly modified the interbasin exchange dynamics, which were well represented by the model. Particle tracking revealed a “current loop,” i.e., water from below 150-m depth first upwelled into the *PL*, intruded approximately 10 km (half its length), and then descended back into the *GL* hypolimnion. Model results showed that the *PL* hypolimnetic volume doubled during the upwelling. Low model-based gradient Richardson numbers and temperature inversions in CTD profiles indicated turbulent mixing between the upwelled *GL* and surrounding *PL* waters.

Our findings demonstrate that hypolimnetic upwelling between the two basins frequently occurs during winter and is an important, but as yet, overlooked mechanism for hypolimnetic-epilimnetic exchange and deepwater renewal in Lake Geneva, and probably in other multi-depth basin lakes under similar wind conditions.

**Keywords:** Lake Geneva, upwelling, multi-basin lake, multi-depth basin lake, *Vent* wind, deepwater renewal, wind-induced interbasin exchange, hypolimnetic upwelling, particle tracking, 3D modeling

### 3.1 Introduction

Distinct sub-basins and large embayments are a ubiquitous feature of many lakes, e.g., Lake Huron (Bennett 1988; Nguyen et al. 2014), Lake Erie (Bartish 1987; Niu et al. 2015; Jabbari et al. 2019, 2021), Lake Simcoe (Nürnberg et al. 2013; Flood et al. 2020), Lake Constance (Kocsis et al. 1998; Appt et al. 2004) and Lake Geneva (Umlauf and Lemmin 2005; Cimatoribus et al. 2019). Horizontal gradients in water quality between basins can result from a number of processes. For example, different seasonal mixing regimes between basins with different maximum depths can produce biochemical gradients between their hypolimnia (e.g., Lake Geneva: CIPEL 2016; Lake Garda: Salmaso 2005). On the other hand, the thin and usually warmer hypolimnion of a shallow basin is prone to earlier oxygen depletion compared to the larger and colder hypolimnion of an adjacent deep basin (e.g., Cornett and Rigler 1979; Ahrensbrak and Wing 1998; Scavia et al. 2014). Consequently, interbasin exchange investigated in the present study can be an important transport process with potentially significant ecological consequences, both locally and basin-wide.

Interbasin exchange can be caused by diverse processes: Density-driven exchange not only can result from differential heating (Monismith et al. 1990; Wells and Sealock 2009) or cooling (Monismith et al. 1990; Okubo 1995; Oonishi 1995) of adjacent basins with different depths, but also from geochemical gradients between basins due to river inflow and/or differential vertical mixing due to non-uniform wind fields (Aeschbach-Hertig et al. 1996). In stratified systems, wind stress can act indirectly through internal wave pumping between basins (van Senden and Imboden 1989; Umlauf and Lemmin 2005; Flood et al. 2020) or directly via two-way advective exchange, whereby a mean downwind surface drift towards one basin is balanced by a subsurface counterflow towards the other basin (Boyce et al. 1980; Laval et al. 2008).

The importance of wind-driven coastal upwelling (and downwelling) in lakes due to its role in nutrient cycling, deepwater renewal, and vertical and horizontal exchange is well recognized and investigated (e.g., Rao and Murthy 2001; Coman and Wells 2012; Amadori et al. 2018; Piccolroaz et al. 2019; Reiss et al. 2020). On the other hand, wind-induced interbasin exchange, in particular, hypolimnetic upwelling between basins of different depths is less studied, with the exception of shallow Lake Erie, where most of the field efforts date back several decades (e.g., Boyce et al. 1980; Saylor and Miller 1987; Jabbari et al. 2021), as summarized in the

review by Bartish (1987). However, with increasing global warming and the consequent weakening of convective cooling, the potential of such an alternative deepwater renewal process needs to be urgently studied.

In the present study, we investigated wind-induced interbasin exchange during a typical, strong wind event in Lake Geneva, in particular, the as yet little-known dynamics of the exchange between its shallow basin called *Petit Lac* (maximum depth 75 m) and its deep basin called *Grand Lac* (maximum depth 309 m) during early winter. For this study, we combined extensive field observations, three-dimensional (3D) hydrodynamic modeling, and model-based Lagrangian particle tracking. Focusing on the hypolimnion layer, we addressed the following questions:

- What are the prevailing current patterns during wind-induced interbasin exchange and are they affected by the Coriolis force?
- Does this transport process produce deepwater upwelling from the deep *Grand Lac* into the shallow *Petit Lac* basin? If so, how far does the upwelled water penetrate into the *Petit Lac* basin, how much of the *Petit Lac* volume is affected, and what happens with the upwelled waters after the wind has ceased?
- Can such an upwelling between the two basins provide a potentially significant mechanism for hypolimnetic-epilimnetic exchange and deepwater renewal?
- Does the Coriolis force affect the flow of the upwelled water masses in the *Petit Lac*? If so, can it cause coastal upwelling, and what is the role of the topography?

Since the phenomenon investigated here is an interbasin exchange flow combined with topographic and coastal upwelling, it will hereinafter be referred to as “interbasin upwelling.”

Additional clarifications and details on certain topics mentioned in the text are provided in the Supporting Information (SI).

## 3.2 Materials and methods

### 3.2.1 Study site

Lake Geneva (local name: *Lac Léman*) is a large monomictic lake located between France and Switzerland. With a surface area of 580 km<sup>2</sup>, a total length of 73 km along its major axis, and a volume of about 89 km<sup>3</sup>, Lake Geneva is Western Europe's largest lake. It is crescent-shaped and consists of two basins: a small western basin, called *Petit Lac* (maximum depth 75 m, width 5 km, length 23 km) and a large eastern basin, called *Grand Lac* (maximum depth 309 m and width 14 km; Figure 3.1a). The “confluence” of the two basins is about 3.5 km wide (Figure 3.1b). River throughflow is small and results in a flushing time (also referred to as theoretical residence time in the literature; Monsen et al. 2002) of approximately 11 y (CIPEL 2019).

The shallow *Petit Lac* undergoes complete vertical mixing every winter, usually in late December or early January. In contrast, in the deep *Grand Lac*, a weak thermocline, typically in the range of 100 to 150-m depth, remains throughout the cold season and full-depth convective overturning only occurs during severely cold winters (CIPEL 2019). Although the latter has long been considered the only mechanism for deepwater renewal in Lake Geneva, recent studies suggest that 3D transport processes such as differential cooling or wind-driven coastal upwelling also play an important role (Lemmin 2020; Reiss et al. 2020). Furthermore, due to its annual complete vertical mixing, water quality parameters such as dissolved oxygen (higher values) and nutrient concentrations (lower values) in the *Petit Lac* differ considerably from those in the deep *Grand Lac* hypolimnion (e.g., CIPEL 2016; Lavigne and Nirel 2016). Therefore, hypolimnetic exchange between the two basins could have important effects on the lake's overall ecological state.

Observational and numerical studies show that Coriolis force effects strongly modify the lake's hydrodynamics (e.g., Bauer et al. 1981; Lemmin et al. 2005; Bouffard and Lemmin 2013; Cimatoribus et al. 2018, 2019; Lemmin 2020; Reiss et al. 2020). The inertial period is approximately 16.5 h.

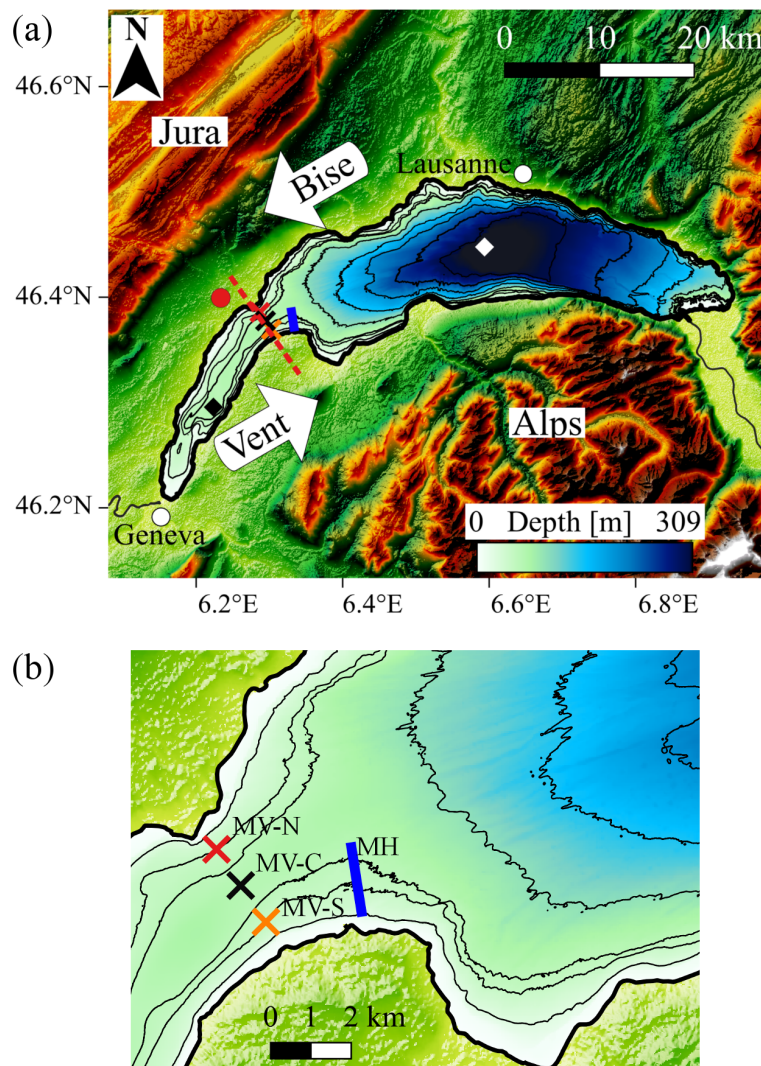


**Figure 3.1. a.** Bathymetric map of Lake Geneva including the surrounding topography. The red dashed line (confluence) approximately delimits the two basins, i.e., the small *Petit Lac* and the large *Grand Lac*. Two strong winds, namely the *Vent* from the southwest and the *Bise* from the northeast, channeled by the Alps and Jura mountains, blow over most of the lake surface. Full-depth temperature profiles are taken at CIPEL stations SHL2 (white diamond; depth 309 m) and GE3 (black diamond; depth 71 m). Meteorological data were recorded at the MeteoSwiss Nyon onshore station (red circle). Depth is given in meters in the colorbar legend and by the isobath contours (0, 25, 50, 60, 100, 150, 200, 250, 300 m). **b.** Close-up of the study site at the confluence of the two basins, with the moorings, MV-N (red cross), MV-C (black cross), MV-S (orange cross), and MH (blue line), deployed during winter 2018 to 2019. Isobath contours (0, 25, 50, 60, 100, 150, 200 m) are given.

Lake Geneva is surrounded by the Jura and Alp mountains, whose channeling effect results in two dominant large-scale wind fields, namely the *Vent* coming from the southwest and the *Bise* from the northeast (Figure 3.1a). Both winds usually last for several days, have a long fetch,

typically reach wind speeds of  $5 - 15 \text{ m s}^{-1}$ , and are almost aligned with the longitudinal axis of the *Petit Lac* and a large section of the *Grand Lac* shoreline (see example for *Vent* in Figure S3.5), all of which favors the occurrence of wind-driven coastal upwelling (Reiss et al. 2020) and interbasin exchange (Umlauf and Lemmin 2005) during such events.

### 3.2.2 Field observations

We conducted a field measurement campaign near the confluence between the *Petit Lac* and *Grand Lac* basins during winter 2018 to 2019 (Figure 3.1a). Three vertical moorings were deployed along the confluence: namely, MV-C at 65-m depth, MV-N at 50 m, and MV-S at 50 m. MV-C was in the center, with MV-N  $\sim 1$  km to the northwest, and MV-S  $\sim 1$  km to the southeast (see Figure 3.1b). Table S3.1 (S refers to Supporting Information) summarizes the mooring configurations and instrument settings. Full-depth current profiles at all three moorings were recorded by bottom-mounted Teledyne RDI Workhorse Sentinel (300 kHz) Acoustic Doppler Current Profilers (ADCPs). To investigate the interbasin exchange flow, current velocities were projected onto a vertical plane parallel to the isobaths at the confluence, i.e., a plane rotated by approximately 50 degrees eastwards from the north (Figure 3.1b). Temperature profiles between 1 and 10 m above the lakebed were obtained from vertical lines equipped with 10 temperature loggers spaced at 1-m intervals. Near-bottom temperatures were measured every 80 m along a 1.5 km long horizontal thermistor line (mooring MH) equipped with 20 RBRsolo T temperature loggers, which was laid down on the lakebed perpendicular to the shoreline between 25 and 65-m depth (Figure 3.1b). To avoid the risk of burying by sediment deposition, the tips of the thermistors at MH were made slightly buoyant, so that the instruments stood vertically on the lakebed.

In addition, we carried out Conductivity Temperature Depth (CTD) casts on 13 December 2018: (i) along a transect perpendicular to the shore near the confluence, and (ii) along the central axis of the *Petit Lac*, starting at the confluence and intruding as far as 7 km into the *Petit Lac* basin (Figure S3.1).

The data sets were complemented by full-depth CTD profiles taken on a regular basis by the Commission Internationale pour la Protection des Eaux du Léman (CIPEL, last accessed on 3 June 2021; Rimet et al. 2020) at the deepest point of the lake (309 m; SHL2 in Figure 3.1a) and at 70-m depth in the *Petit Lac* (GE3 in Figure 3.1a).

A meteorological station operated by the Swiss National Weather and Climate Service ([MeteoSwiss](#); last accessed on 3 June 2021) and located onshore approximately 5 km northwest of the study site in Nyon recorded wind speed and direction every 10 min (red circle in Figure 3.1a). Hourly moving averages were applied to the meteorological data prior to the analysis.

### 3.2.3 Hydrodynamic model

We employed a hydrostatic version of the MITgcm code solving the 3D Boussinesq Navier-Stokes equations (Marshall et al. 1997). Originating from the oceanographic community, this code has successfully been applied to lakes (Dorostkar and Boegman 2013; Djoumna et al. 2014; Dorostkar et al. 2017), and recently to Lake Geneva (Cimatoribus et al. 2018, 2019; Reiss et al. 2020). The model employed free-slip conditions at the lateral boundaries and quadratic bottom drag. It was configured with a uniform horizontal Cartesian grid with a resolution of 113 m, 100 size-varying  $z$ -layers (30 cm at the surface, 2.8 m and 4.8 m respectively at the deepest points of the confluence and the *Grand Lac*) and a time step of 8 s. Except for the increased vertical resolution to better resolve the bottom currents in both the *Petit Lac* and *Grand Lac*, the model configuration was similar to the one used by Reiss et al. (2020) to investigate wind-driven coastal upwelling during winter in Lake Geneva. A detailed calibration of the model for Lake Geneva was carried out by Cimatoribus et al. (2018).

Realistic two-dimensional (2D) surface forcing was obtained from the COSMO-1 numerical weather model of MeteoSwiss at a 1.1-km resolution (Voudouri et al. 2017) and was linearly interpolated onto the MITgcm grid. The model was initialized with zero velocity and a horizontally homogenous temperature field derived from the temperature profile measured at SHL2 on 12 September 2018 at 15:00 (local time). This starting date was chosen because the preceding days were calm, thus allowing the model to adjust to the initial conditions.

### 3.2.4 Particle tracking

Lagrangian particle tracking based on the velocity output of the validated MITgcm model was used to analyze pathways of water masses. The code employed in the present study was developed by Cimatoribus (2018) and is based on the algorithm described by Döös et al. (2013). The code was recently applied to Lake Geneva to study: (i) the dispersion of riverine



water from the lake's main tributary the Rhône River (Cimatoribus et al. 2019), and (ii) wind-driven coastal upwelling during winter at the northern shore of the *Grand Lac* basin (Reiss et al. 2020). Following Reiss et al. (2020), we used backward and forward particle tracking to determine the origin and fate of upwelled waters at different locations in the *Petit Lac*.

Three different particle tracking simulations, hereinafter referred to as simulations B (bottom), S (surface), and L (loop), were run to address aspects of the wind-driven circulation between the *Petit Lac* and *Grand Lac*. In each of the three simulations, a total of approximately 200,000 to 300,000 particles were released, either simultaneously or at regular time intervals, as discussed below. The corresponding seeding regions are given in Figure S3.2.

In simulation S, the coastal upwelling dynamics at the northern *Petit Lac* shore were investigated by releasing particles near the shore, in the upper 15 m of the water column at a 1-m depth interval (green area in Figure S3.2). Simulation B addressed the hypolimnetic upwelling of deep *Grand Lac* water into the bottom layers of the *Petit Lac*, by releasing particles in an approximately 3 km by 5 km wide area near the confluence at every vertical grid point below 40-m depth (red area in Figure S3.2). For simulations B and S, the seeding regions, depths, and times were determined based on the occurrence of low temperature signals in the hydrodynamic simulations, indicating upwelling of hypolimnetic water (e.g., Figure 3.4). Particles were released every 2 h from 8 December at 12:00 to 10 December 12:00 (simulation S) and from 8 December at 00:00 to 11 December 00:00 (simulation B), and tracked both backward and forward in time. The seeding locations in simulation L were inferred from the backward tracking results of simulation B by selecting the origin locations of all particles originating from below 50-m depth within the *Grand Lac* (blue area in Figure S3.2). In this case, approximately 200,000 particles were released simultaneously on 7 December 13:00 and forward tracked until 18 December 00:00, thus describing the complete loop of the particles, i.e., the upwelling from deep within the *Grand Lac* into the *Petit Lac* and the subsequent descent back into the hypolimnion of the *Grand Lac*.

To determine the origin and fate of upwelled waters in different regions of the *Petit Lac*, the backward and forward trajectories of simulations S and B were classified by initial and final depth, respectively. Furthermore, the distance that upwelled *Grand Lac* water penetrated into the *Petit Lac*, hereinafter referred to as intrusion length, was determined by analyzing the trajectories of simulation L. This also allowed estimation of the time that upwelled *Grand Lac* water spent in the *Petit Lac* before descending back into the *Grand Lac* hypolimnion.

### 3.3 Results and discussion

#### 3.3.1 Field observations

Temperatures recorded at mooring MV-C show that the *Petit Lac* remained weakly stratified until approximately 4 January 2019 (Figure S3.3). The mean thermocline depth could not be determined from full-depth temperature profiles at GE3 and SHL2 because the thermocline was strongly tilted between stations GE3 and SHL2 due to strong winds that preceded the sampling days closest to the upwelling event investigated here. Instead, a thermocline depth of approximately 35 m in early December 2018, i.e., before the wind event discussed here, was inferred from the measurements at the horizontal thermistor line MH (Figure S3.4).

A total of three strong comparable *Vent* wind events were observed in December 2018 (Figure S3.3). In the present study we will investigate the *Vent* event that lasted from 7 to 10 December 2018 in detail (Figure 3.2). During that event, the overall mean wind speed measured at the Nyon meteorological station (Figure 3.1a) was approximately  $5.5 \text{ m s}^{-1}$  with hourly-averaged maximum values of up to  $10.7 \text{ m s}^{-1}$ . The COSMO-1 data for that period confirmed that the wind field over the lake was spatially relatively homogenous and aligned with the main axes of the *Petit Lac* and the western and central parts of the *Grand Lac* (Figure S3.5).

Current velocities and temperatures recorded at the three vertical moorings, MV-S, MV-C, and MV-N, at the confluence of the two basins show that two phases (upwelling and relaxation) with distinctively different flow patterns can be identified during this *Vent* event (Figure 3.2), as discussed below.

#### ***Upwelling phase: 7 December at ~19:00 to 11 December at ~10:00***

Approximately half a day after the *Vent* wind started blowing, a two-layer flow pattern established at the central and northern moorings (MV-C, MV-N) and then persisted for 1.5 d after the wind had ceased. The northeastward-directed wind stress caused a strong epilimnetic flow from the *Petit Lac* into the *Grand Lac* (hereinafter referred to as outflow), which was balanced by a hypolimnetic counterflow from the *Grand Lac* into the *Petit Lac* (hereinafter referred to as inflow; Figure 3.2).

During this phase, *Grand Lac* water was continuously transported into the *Petit Lac* in a bottom current at the central and northern sections of the confluence. Inflowing current velocities near

the bottom exceeded  $27 \text{ cm s}^{-1}$  at both MV-C and MV-N. Temperatures at these moorings gradually decreased to below  $6^\circ\text{C}$  on 11 December at around noon (Figure 3.2c, e). This suggests that the inflowing water originated from the deep hypolimnion of the *Grand Lac*. The lowest value of  $5.96^\circ\text{C}$ , measured 1 m above the lakebed at MV-C, corresponds to temperatures found at 180-m depth, as indicated by the temperature profiles at SHL2 in November and December 2018 (Figure S3.6). This was the lowest temperature observed at the confluence during the entire observation period from November 2018 to April 2019.

The depth at which the separation between the in- and outflow occurred varied from 25 to 35 m at MV-C, and from 20 to 30 m at MV-N. At the latter mooring, this interface was observed generally at shallower depths, indicating that during the upwelling phase, the thermocline was upwardly tilted at the northern shore of the confluence (white color separating red and blue areas in Figure 3.2). This thermocline tilt, perpendicular to the wind stress resembles that of a Coriolis force-driven Ekman-type coastal upwelling at the northern shore (e.g., Reiss et al. 2020) and is discussed below in the Particle Tracking subsection.

At the southern mooring (MV-S), a vertically relatively uniform outflow prevailed with maximum current velocities reaching  $16 \text{ cm s}^{-1}$ . The measured near-bottom temperatures at this mooring also dropped during the upwelling phase. However, the decrease was not continuous and lagged behind that of MV-N, indicating that it was not caused by direct deepwater upwelling at this mooring location. Instead, it was probably caused by the sporadic outflow of colder water masses that had entered the *Petit Lac* north of MV-S. In contrast, the upper thermistors at this mooring showed increasing temperatures during the first two days of the upwelling. The maximum temperature of  $10.27^\circ\text{C}$  measured at the topmost thermistor, i.e., at 40-m depth, on 8 December 01:20 is the same as the one observed at the shallowest thermistor at MH, i.e., at 25-m depth in the epilimnion. This temperature pattern can be explained by a Coriolis force-driven coastal downwelling of the thermocline at the southern shore during the upwelling phase, as confirmed by the 3D model and the horizontal thermistor line (Figures 3.4b and S3.4).

### ***Relaxation phase: 11 December at ~14:00 to 15 December at ~14:00***

Approximately 1.5 d after the wind had ceased, the flow pattern reversed at all moorings. The two-layer structure at MV-N was replaced by a uniform inflow over most of the water column, with only sporadic weak outflow near the lakebed. On the other hand, at MV-C, the

current directions reversed in both layers, resulting in an epilimnetic inflow and a hypolimnetic outflow. A similar two-layer structure was observed at MV-S with current velocities higher than during the upwelling phase, and outflowing velocities reaching  $19 \text{ cm s}^{-1}$ .

This period was characterized by a continuous outflow in a bottom-hugging current in the southern and central sections of the confluence. The interfacial depth separating the in- and outflow was not steady. More importantly, at MV-S, the interface appeared at a shallower depth suggesting an upward tilt of the thermocline at the southern shore during the relaxation phase. This thermocline tilt was confirmed by north-south CTD casts at the confluence (Figure S3.1b) and is further analyzed in the Model Results and Particle Tracking subsections below. The prevailing current patterns during both the upwelling and relaxation phases are summarized in detail in Figures S3.7-S3.9.

Temperatures increased during the relaxation phase at all moorings, in agreement with the flow field, which indicated that the supply of the deep, cold upwelled *Grand Lac* water had ceased. However, compared to MV-N, the increase at MV-S and MV-C occurred more gradually and was uniform over the entire bottom layer (Figure 3.2).

The field observations demonstrated that the flow field during both phases of the interbasin upwelling was strongly affected by Coriolis force, even though the horizontal distance between the northern and southern moorings was only about 2 km.

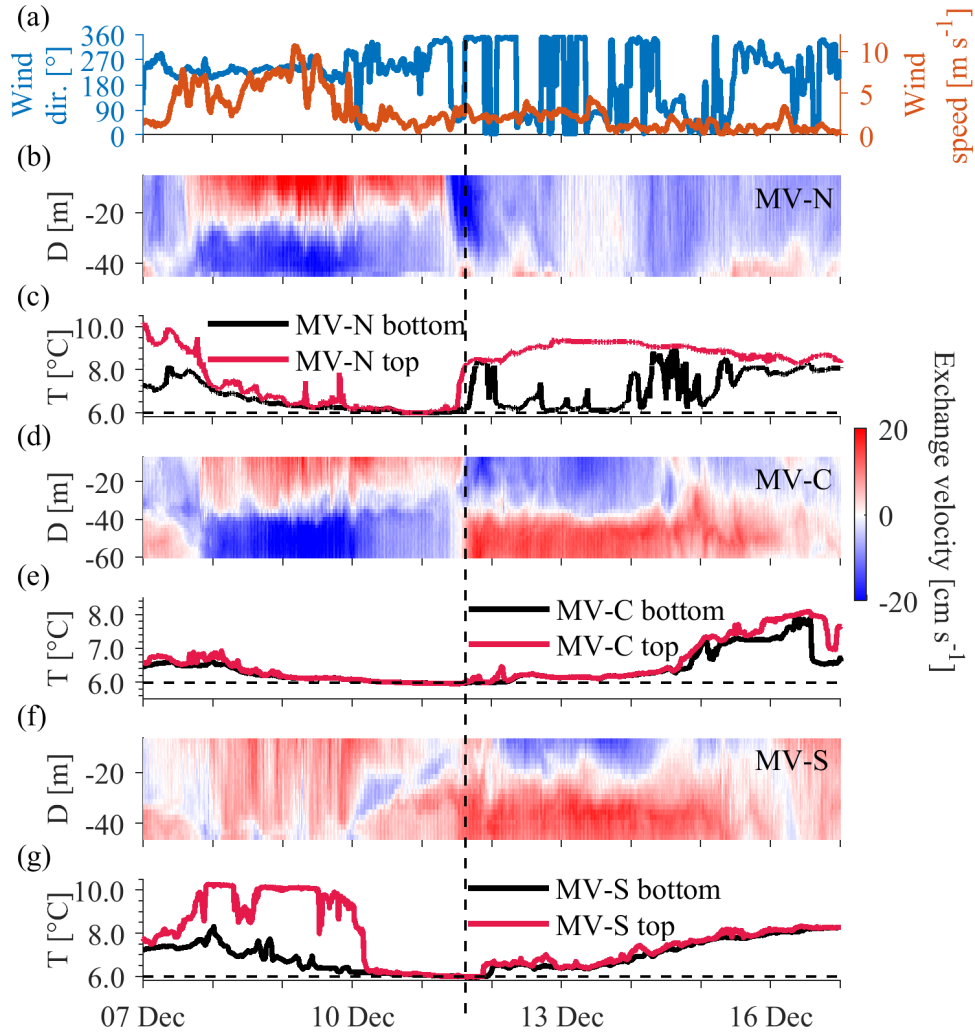


**Figure 3.2.** a. Wind direction (blue) and speed (red) measured at the Nyon meteorological station. b. to g. Temperatures (T) and current velocities (versus depth D) recorded at moorings MV-N (b, c), MV-C (d, e), and MV-S (f, g), respectively. Current velocities are given as “interbasin exchange velocities,” i.e., projected onto a vertical plane parallel to the isobaths at the confluence. The colorbar gives the magnitude of the interbasin exchange velocity. Positive values indicate flow out of the *Petit Lac*. The dashed horizontal line in c, e, and g marks 6°C. The dashed vertical line indicates the transition from the upwelling to the relaxation phase. All dates refer to 2018. Note that vertical axes scales are different.

### 3.3.2 Model results

The depth-averaged temperatures in the lowest 10 m of the water column as observed (black) and modeled (red) at the confluence from 7 to 17 December 2018 are compared in Figure 3.3. The model captured well the characteristics of the two regimes, namely: (i) the decreasing temperatures at the central and northern sections during the upwelling phase (Figure

3.3a, b), and (ii) the gradually rising temperatures at the central and southern sections during the relaxation phase (Figure 3.3b, c).

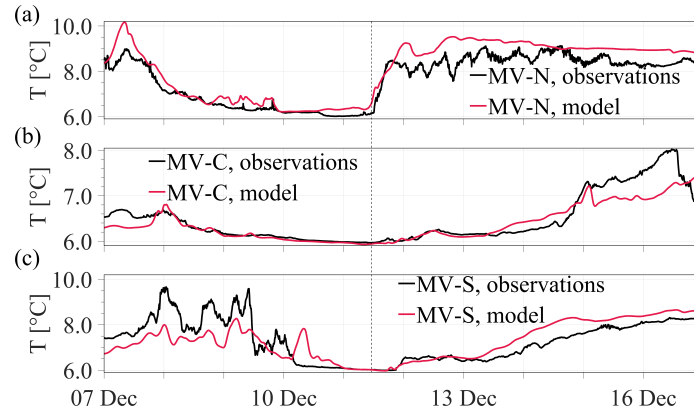


**Figure 3.3.** Depth-averaged temperatures in the lowest 10 m of the water column as observed (black) and modeled (red) from 7 to 17 December 2018 at moorings: **a.** MV-N, **b.** MV-C, and **c.** MV-S. For mooring locations, see Figure 3.1b. All dates refer to 2018.

The modeled and observed current velocities at the northern (MV-N), central (MV-C), and southern (MV-S) mooring locations are depicted as current roses in Figures S3.7-S3.9, respectively. Furthermore, the time series of the modeled current and temperature profiles at the same locations (similar to Figure 3.2) are presented in Figure S3.10. Good agreement between observation and model results is found. The model well reproduced the two dynamic regimes characterized by: (i) a bottom inflow and surface outflow at the central and northern sections during the upwelling phase, and (ii) a bottom outflow and surface inflow at the central and southern sections during the relaxation phase.

The good performance of the hydrodynamic model allowed using model results to further investigate the complex 3D structure of the interbasin upwelling event. Vertical temperature and current velocity slices at selected locations, as well as maps of the near-surface temperature anomalies at 1.5-m depth at different times are displayed in Figure 3.4. Here, temperature anomaly was taken as the difference between the local temperature and the basin-wide averaged temperature at the same depth.

The strong surface outflow and bottom inflow measured at the confluence during the upwelling phase prevailed in the entire *Petit Lac* basin, suggesting that upwelled cold *Grand Lac* water was transported far into the *Petit Lac* in a steady southwestward hypolimnetic current (Figures

3.4b and S3.11a). Consequently, the bottom temperatures at the confluence decreased continuously, and the hypolimnion in the *Petit Lac* gradually thickened (Figure 3.4d). Based on the modeled 3D temperature field, the volume of the *Petit Lac* hypolimnion was estimated by taking the depth of the maximum Brunt-Väisälä frequency as its upper limit (Figure 3.5a, b). This analysis suggests that the *Petit Lac* hypolimnion had almost doubled in volume by the end of the upwelling phase on 11 December 2018 at around 11:00 and then strongly decreased in volume during the relaxation phase (Figure 3.5c).

Furthermore, the model results revealed an upward tilt of the thermocline at the northern shore perpendicular to the wind stress during the upwelling phase (Figure 3.4b, d), indicating that the flow field was modified by the Coriolis force. This thermocline shape agrees with the ADCP measurements at MV-C and MV-N (Figure 3.2b, d). At the same time, patches of cold water appeared along the northern shore of the *Petit Lac*, indicating a surfacing of the thermocline (Figure 3.4a). While this temperature pattern resembles that of an Ekman-type coastal upwelling (e.g., Reiss et al. 2020), the underlying hydrodynamics appear to be different, as will be discussed below in the Particle Tracking subsection.

The current patterns reversed on 11 December around noon (Figure 3.2), signaling the start of the relaxation phase, and a northeastward hypolimnetic current was established in the entire *Petit Lac* (Figures 3.4f and S3.11b). During this period, the *Grand Lac* water that had previously been upwelled into the *Petit Lac*, flowed back into the *Grand Lac*, resulting in the thinning of the *Petit Lac* hypolimnion (Figure 3.4f). Furthermore, the volume estimation based on the Brunt-Väisälä frequency indicated that the *Petit Lac* hypolimnetic volume at the end of the relaxation phase was noticeably smaller than before the interbasin upwelling event (Figure 3.5c). This suggests that this process can efficiently flush most of the deep layers of the *Petit Lac* within only a few days. The highest current velocities, exceeding  $20 \text{ cm s}^{-1}$ , were found between 50 to 60-m depth near the confluence. The outflow then hugged the southern shore of the *Grand Lac* basin, indicating a Coriolis deflection. Accordingly, the thermocline now appeared to be tilted upward at the southern shore (Figure 3.4f), which was confirmed by north-south CTD transects taken across the confluence on 13 December at around noon (Figure S3.1b), as well as by the ADCP measurements at moorings MV-C and MV-S (Figure 3.2).

The complete spatio-temporal evolution of the modeled temperatures and current velocities during both the upwelling and relaxation phases is shown in the Movie S3.1.

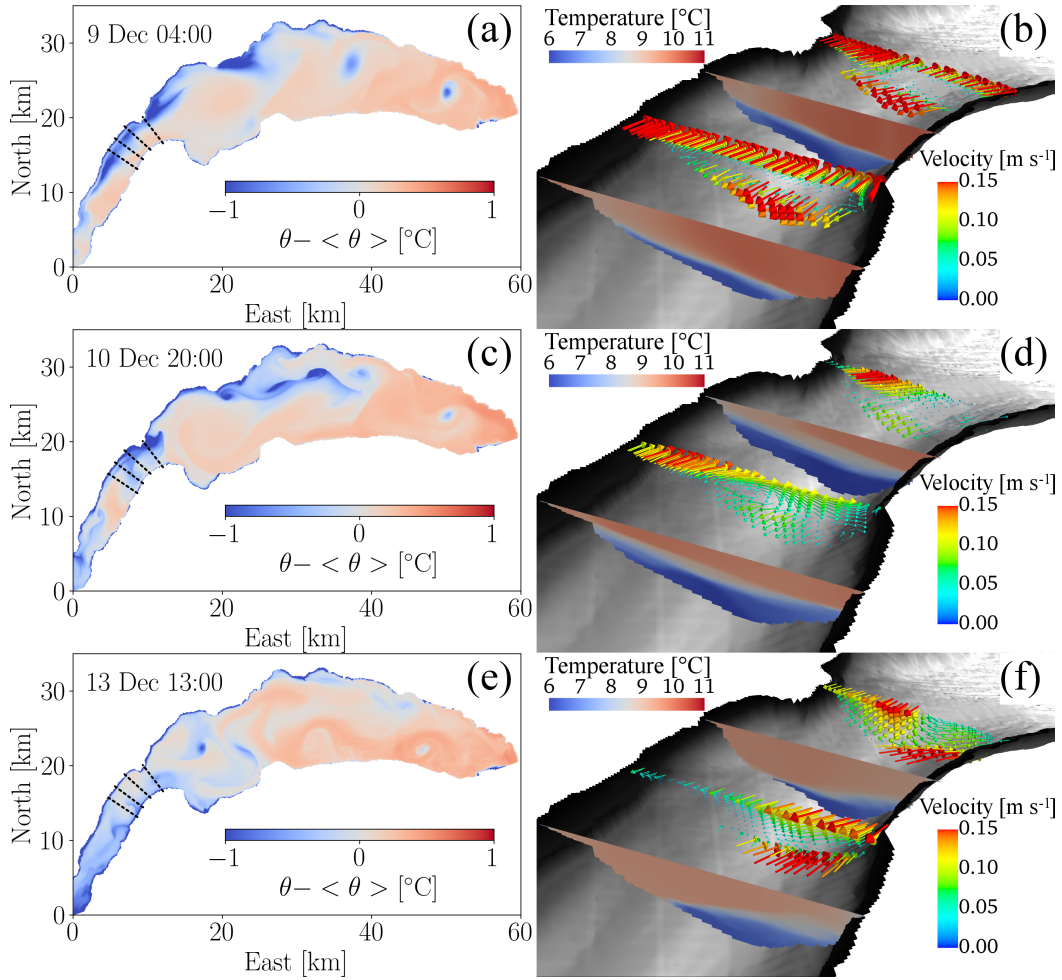


**Figure 3.4.** Modeled near-surface temperature anomaly at 1.5-m depth (a, c, e; see text for details) and current velocity and temperature slices at selected locations (b, d, f; looking towards the *Grand Lac* basin) at different times, i.e., the maximum coastal upwelling in the *Petit Lac* basin (a, b), approximately one day after the wind stopped (c, d), and the strongest outflowing bottom currents (e, f). The colorbars give the surface temperature anomaly, temperature, and current velocity, respectively. The locations of the vertical slices are marked in the surface contour plots by black dashed lines. The length of the velocity vectors is scaled with the velocity and for clarity, not all vectors are shown.



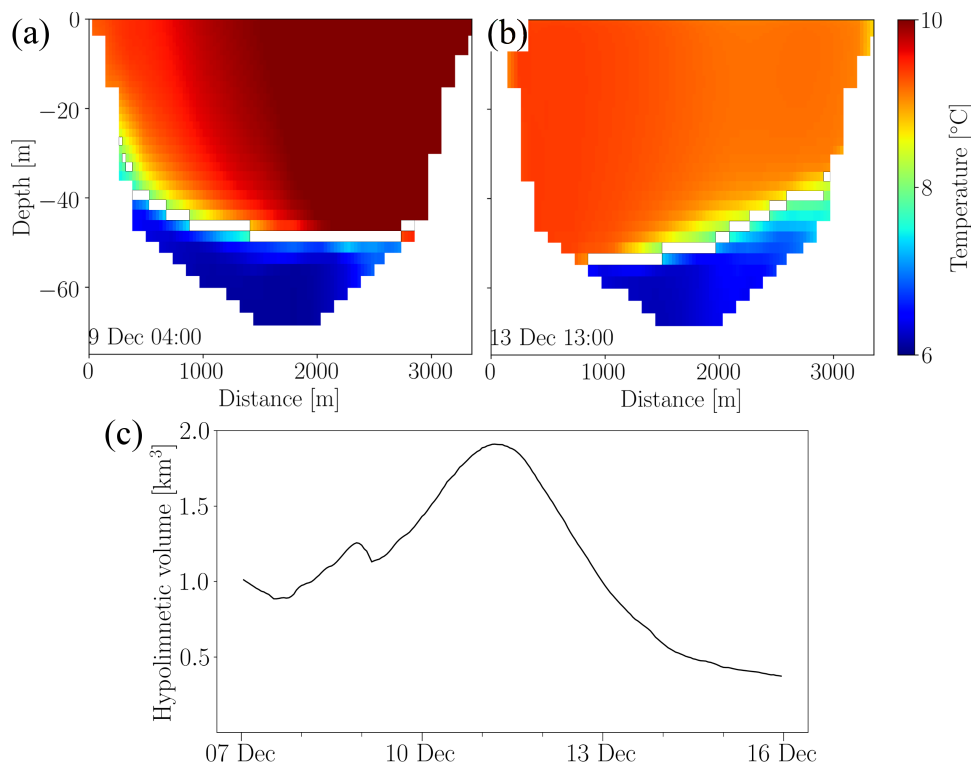


**Figure 3.5.** Modeled temperature at the confluence (red line in Figure 3.1a) between the *Petit Lac* and *Grand Lac* basins **a.** during the upwelling phase (9 December 2018 04:00) and **b.** during the relaxation phase (13 December 2018 13:00), respectively. Distance is given from the northern shore. The overlaid wide white pixel lines in (a) and (b) mark the depth of the maximum buoyancy frequency for every profile along the transect. This depth was continuously determined in the entire *Petit Lac* basin during the whole interbasin upwelling event and was used to estimate the volume of its hypolimnion. **c.** Time-series of the estimated volume of the *Petit Lac* hypolimnion from 7 to 16 December 2018. The colorbar gives the temperature.

### 3.3.3 Particle tracking

During the wind-driven interbasin upwelling event analyzed here, hypolimnetic water from the deep *Grand Lac* (max. depth 309 m) was transported into the shallow *Petit Lac* (max. depth 75 m) (Figures 3.2, 3.4). We investigated the pathways taken by the upwelled waters using backward and forward particle tracking simulations at different sites. Particles were released in two seeding regions to investigate: (i) the upwelling into the hypolimnion of the *Petit Lac* (simulation B, red area in Figure S3.2), and (ii) the coastal upwelling at its northern shore (simulation S, green area in Figure S3.2). Note that doubling or tripling the number of particles by doubling the seeding frequency and increasing the vertical seeding resolution did not change the results of the particle tracking analysis, thus indicating their statistical robustness.

### *Hypolimnetic upwelling along the bottom of the Petit Lac: The current loop*

The backward and forward trajectories of the particles released during the upwelling phase in the hypolimnion of the *Petit Lac* (simulation B) are depicted in Figure 3.6. For better visualization, random subsets of around 2500 (Figure 3.6a, c) and 10 particles (Figure 3.6b, d) are displayed here. In agreement with the observed and modeled inflowing bottom currents at the confluence, the backward tracking revealed that particles, i.e., water masses, were transported from the *Grand Lac* into the *Petit Lac* during this period. Furthermore, 44%, 25% and 6% of all particles originated from below 75, 100 and 150-m depths, respectively, confirming the deep origin of these waters, as suggested by the low temperatures observed near the bottom at the confluence (Figure 3.2). During the upwelling phase, the particle transport from the *Grand Lac* towards the confluence appeared to be concentrated in a bottom-hugging current following the southern shore, especially for particles originating from below 100-m depth (Figure 3.6a, b). This current structure, i.e., the strong bottom current directed towards the *Petit Lac*, was confirmed by moored ADCP measurements near the southern shore of the *Grand Lac* during a similar interbasin upwelling event in December 2019 (Figure S3.12).

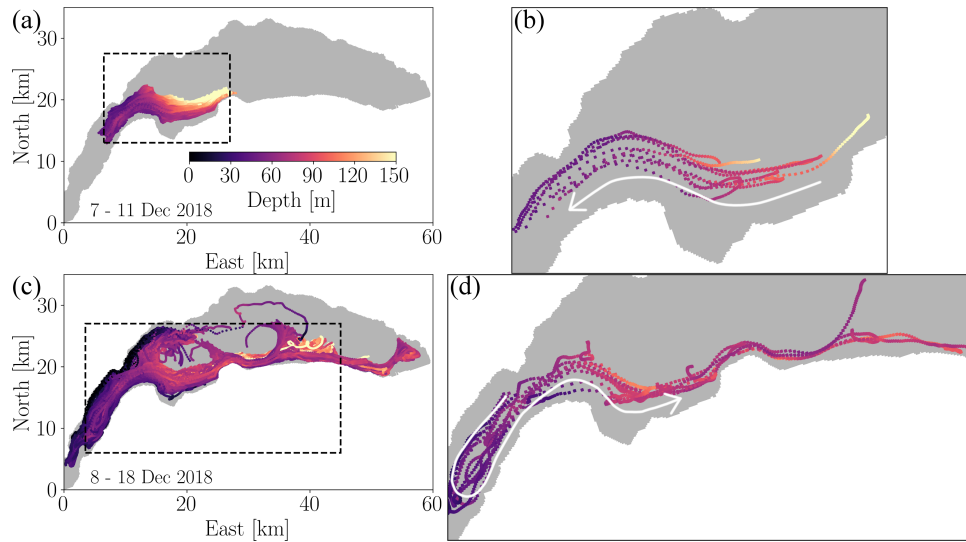


**Figure 3.6.** **a.** Backward trajectories and **c.** forward trajectories of particles released below 40-m depth in the hypolimnion of the *Petit Lac* (simulation B, Figure S3.2 red area). **b.** and **d.** Close-ups of the areas marked by the black dashed rectangles in (a) and (c) showing backward and forward trajectories for a random subset of 10 particles, respectively. The white arrows indicate the travel direction of the particles, reflecting the movement of water parcels. The colorbar gives the particle depth. Only particles with an origin (backward tracking) and final (forward tracking) depth below 75 m are displayed.

Further insight into the origin of the upwelled waters was gained by grouping the particles of backward tracking simulation B according to their seeding time. Notched boxplots show the particle origin depth as a function of the seeding time (Figure 3.7). The increasing medians of the origin depth over time suggest that as the interbasin upwelling advanced, *Grand Lac* water from progressively greater depths in the hypolimnion was transported into the *Petit Lac*. The increasing height of the boxes and the length of the whiskers with time and depth indicate that particles from a progressively wider depth range were drawn into the *Petit Lac*. This is in agreement with the continuously decreasing bottom temperatures observed at the confluence (Figure 3.3). Furthermore, the boxplots reveal that approximately 25% of the particles released on the last day of the upwelling phase originated from below 150-m depth. This is in good agreement with the estimated maximum origin depth of 180 m, based on lowest observed temperatures at MV-C (Figure 3.2e) and the full depth profiles at SHL2 (Figure S3.6). Once upwelled into the *Petit Lac*, strong southwestward bottom currents transported the water masses far into the *Petit Lac* along its thalweg, thus explaining the gradual thickening of the hypolimnion (Figures 3.4d; 3.5c; S3.11).

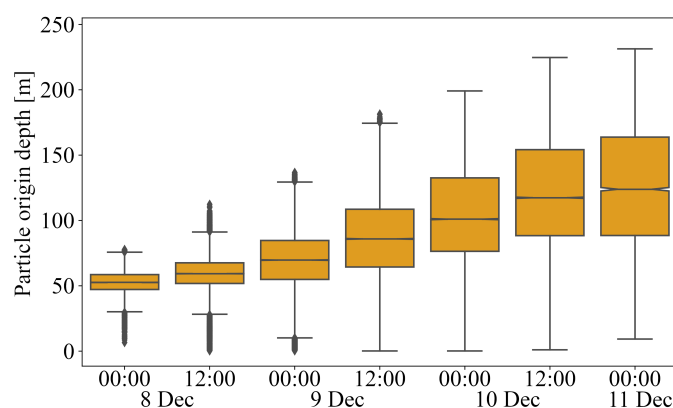


**Figure 3.7.** Notched box-plots of the particle origin depths during the upwelling phase obtained from the backward tracking results of simulation B as a function of the seeding time. The brown boxes give the interquartile range (1<sup>st</sup> and 3<sup>rd</sup> quartile). The maximum length of the whiskers is 1.5 times the interquartile range and the diamonds mark the outliers. Dates refer to 2018.

After the wind ceased and the currents reversed during the relaxation phase, the waters that had upwelled into the *Petit Lac* flowed back into the hypolimnion of the *Grand Lac*, as shown by the forward trajectories of simulation B (Figure 3.6c, d). Thus, the interbasin upwelling event effectively formed a current loop, i.e., over the course of more than one week, hypolimnetic

water from below 150-m depth first upwelled far into the *Petit Lac* and subsequently descended back into the *Grand Lac* hypolimnion mainly along the southern shore confirming the field measurements (Figure 3.2). At the end of the forward tracking simulation on 18 December 2018, i.e., approximately one week after the last particles had been released, 78% of all particles were again found in the *Grand Lac* basin. The rest remained in the *Petit Lac* either because: (i) they had intruded too far towards the southwestern end of the lake to be affected by the outflow during the relaxation phase, or (ii) they were entrained into basin-scale gyres (Movie S3.1). This indicates that there was a significant net exchange of hypolimnetic water between the two basins during the interbasin upwelling event.

To further analyze these current loops, approximately 200,000 particles were simultaneously released on 7 December 2018 at 13:00 below 50-m depth in the hypolimnion of the *Grand Lac* and forward tracked for approximately 10.5 d until 18 December 2018 00:00 (simulation L, blue area in Figure S3.2). Based on the backward tracking results of simulation B, the seeding locations and seeding time of simulation L were determined in such a way that all particles would upwell into the hypolimnion of the *Petit Lac* (see subsection Particle Tracking in Material and Methods for details). For each particle, the maximum intrusion length into the *Petit Lac* was determined, and the time that each particle spent in the *Petit Lac* before descending back into the *Grand Lac* was estimated (hereinafter referred to as intrusion time). A typical current loop trajectory, as well as the histograms of the intrusion length and time are shown in Figure 3.8.

Two peaks are evident in the intrusion length histogram (Figure 3.8b). The first one, at ~3 km, represents a small portion of the particles that only grazed the *Petit Lac*. They were immediately upwelled into its epilimnion and consequently flushed out back into the *Grand Lac* by the strong surface outflow. The second and more prominent peak shows that the majority of the particles intruded about 10 km or more into the *Petit Lac* (Figure 3.8b), i.e., approximately half its total length. Furthermore, these particles spent on average 3-4 d in the shallow basin before being flushed out again (Figure 3.8c). The small peak between 8 to 10 d and the sharp cut-off at the end of the time axis of the intrusion time histogram represent the fraction of the upwelled particles that had not left the *Petit Lac* by the end of the simulation.

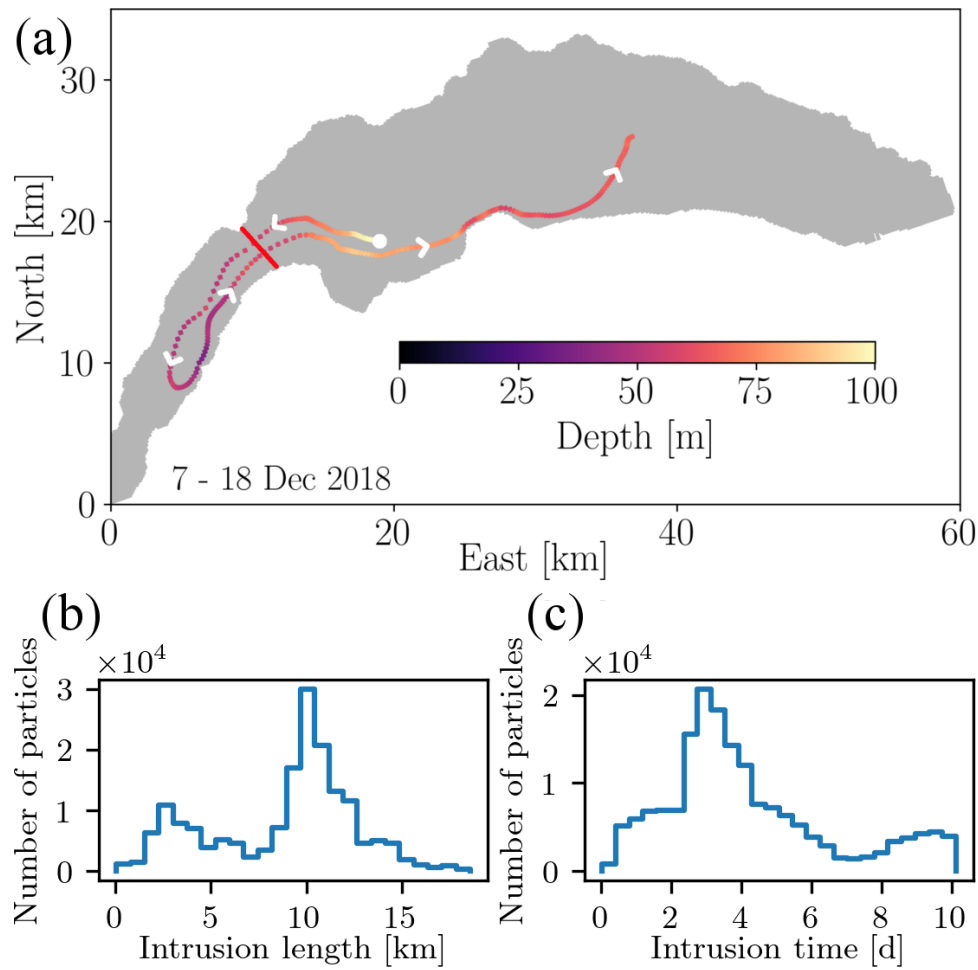


**Figure 3.8.** **a.** Typical particle trajectory obtained from simulation L showing the complete current loop. The red line marks the confluence between the *Petit Lac* and *Grand Lac* and was used to calculate the intrusion length and time. The colorbar gives the particle depth. The white circle marks the start of the trajectory with the white arrowheads indicating the travel direction of the particles. **b.** and **c.** Histograms of the intrusion length and time, respectively, obtained from simulation L.

Out of all the forward-tracked particles of simulation B that returned to the *Grand Lac*, 70% reached a maximum depth greater than 75 m, i.e., lower than the maximum depth of the *Petit Lac*, and 20%, greater than 100 m. Subject to the Coriolis force, the outflowing deep-reaching particles predominantly followed the southern shore of the *Grand Lac*, forming a strong shore-hugging current that reached the eastern end of Lake Geneva by the end of the simulation, traveling a distance of about 50 km (Figure 3.6c). The presence of this eastward narrow jet during the relaxation phase was confirmed by moored ADCP measurements at 100 and 150-m depth near the southern shore of the *Grand Lac* in December 2019 (Figure S3.12). A significant

number of these particles was entrained into basin-scale gyres and subsequently spread over large parts of the hypolimnion of the *Grand Lac* (Figure 3.6c, d).

During both the upwelling and relaxation phases, a two-layer current structure with opposing current directions in the epilimnion and hypolimnion of the *Petit Lac* prevailed, resulting in large vertical shear (Figures 3.2, 3.4). Furthermore, the moored ADCP measurements at MV-N and MV-C showed counterflowing bottom currents at the northern and southern sections of the confluence during both periods, suggesting enhanced horizontal shear (Figure 3.2). Considering this enhanced horizontal and vertical shear and the relatively low stability of the water column at that time of the year, turbulent mixing between the upwelled *Grand Lac* and surrounding *Petit Lac* water masses can be expected. Gradient Richardson numbers ( $Ri$ ) in the *Petit Lac* were computed from the modeled velocity and temperature field and are given for selected vertical transects during the upwelling phase on 9 December 2018 14:00 in Figure S3.13. Low  $Ri$  values are observed both near the bottom and at the northern shore, indicating turbulent mixing between the upwelled and ambient waters. Furthermore, significant temperature inversions in the hypolimnion and around the depth of the thermocline seen in the CTD transects taken on 13 December 2018 at ~11:00 at different locations in the *Petit Lac* suggest active overturns and hence mixing (Figure S3.1c, d). The time evolution of  $Ri$  during the entire interbasin upwelling event is shown in the Movie S3.1.

Field observations from January to March 2019 indicate that some stratification in the *Petit Lac* is necessary for deep interbasin upwelling to occur, because the observed two-layer current structure is imposed by the presence of a thermocline. This is in agreement with the findings on hypolimnetic exchange between Lake Erie's deep eastern and shallow central basins (Bartish 1987). The particle tracking results of simulations B and L confirm that during the *Vent* wind event discussed here, there was a net exchange of hypolimnetic water between the two basins during the interbasin upwelling event. The resulting current loop may thus be an important transport process for interbasin exchange and an efficient mechanism for advective vertical exchange within the hypolimnion of Lake Geneva. The results also show that turbulent mixing between the upwelled and ambient waters due to strong vertical and horizontal shear appears to occur during the entire interbasin upwelling event. Since water quality in the *Petit Lac* is generally better than that of the deep hypolimnion of the *Grand Lac* (i.e., higher dissolved oxygen and lower nutrient concentrations; CIPEL 2016), the enhanced hypolimnetic exchange

and mixing between the two basins induced by this regularly occurring wind-induced transport process can be regarded as ecologically beneficial.

### ***Coastal upwelling at the northern shore of the Petit Lac: Origin and dynamics***

Some particles, especially those seeded at earlier times and at shallower depths, were entrained by coastal upwelling currents and transported into the epilimnion along the northern shore of the *Petit Lac*, in agreement with the lower surface temperatures observed in the model results in that area (Figure 3.4a). To address this coastal upwelling, backward tracking was used to determine the origin of particles released during the upwelling phase between 0 and 15-m depth near the northern shore of the *Petit Lac* (simulation S, green area in Figure S3.2). The corresponding particle trajectories of subsets of approximately 2500 and 10 particles are shown in Figure 3.9a and b, respectively. Approximately 50% of all released particles originated from the epilimnion, i.e., between 0 and 35-m depth. The remaining half came from 35 to 65-m depth, i.e., from within the hypolimnion, thus confirming that the lower surface temperatures observed in the model results were due to coastal upwelling of hypolimnetic water (Figure 3.4a).

A further breakdown of the particle origin locations shows that approximately half of all coastally upwelled particles originating from the hypolimnion came from depths of 35 to 45 m, and the other half came from depths of 45 to 65 m. Figure 3.9 depicts the origin locations for both groups of particles in the form of 2D concentration maps and histograms of the distance from the particle origin to the confluence. The majority of the particles that originated from just below the thermocline, i.e., 35 to 45-m depth, came from within the *Petit Lac* (Figure 3.9c, d). On the other hand, the bulk of the particles that upwelled from below 45-m depth came from the *Grand Lac*. This can be readily explained by the observed strong southwestward bottom currents in the *Petit Lac* (Figure 3.9e, f). Before actually upwelling into the epilimnion, these hypolimnetic particles traveled southwestward along the main axis of the *Petit Lac* for several kilometers, following the strong bottom currents (Figure 3.9b). With a typical velocity of the bottom currents of  $20 \text{ cm s}^{-1}$  and a length scale of 3 km (minimum intrusion length into the *Petit Lac* before upwelling; Figure 3.10c), a Rossby number of  $\sim 0.6$ , i.e.  $< 1$  is obtained, indicating that Coriolis force is important.

The upwelling location of each particle was used to determine where along the shoreline the coastal upwelling occurred, and to pinpoint areas (hotspots) where upwelling is most likely to occur. This was achieved by finding the time and location where each particle initially rose and

then stayed above 25-m depth for at least four hours. Three trajectory examples with the upwelling location determined accordingly are given in Figure 3.10a. The corresponding concentration maps of the upwelling locations for all particles coming from 35 to 45-m and 45 to 65-m depths are shown in Figure 3.10b and c, respectively. The spatial patterns of the upwelling locations are significantly different for the two groups.

While the coastal upwelling from 35 to 45-m depth, i.e., just below the thermocline, was relatively uniform over a 1 km by 8 km wide area (Figure 3.10b), the upwelling from deeper within the hypolimnion was more localized. In particular, upwelling appeared to be focused in an area approximately 7 km southwest of the confluence (red arrow in Figure 3.10c). The overlaid isobaths in Figure 3.10c indicate that this location coincided with a region where the isobaths between 50 to 60-m depth stretched in the cross-shore direction and, conversely, the slope between 40 to 50-m depth steepens. The observed upwelling hotspot can be explained by the combined effects of: (i) the shoreward Coriolis deflection of the southwestward bottom currents and (ii) the shoreward-veering 50-m isobath which favors the onshore deflection of the bottom currents and thus locally enhances the coastal upwelling.

The subsequent fate of the particles released in the upper 15 m of the *Petit Lac* during the upwelling phase was determined by forward tracking. At the end of the simulation on 18 December 2018, 70% of all particles had been flushed back into the *Grand Lac*. Nearly all of these particles reached below 40-m depth, i.e., into the hypolimnion, with 16% of them descending temporarily to depths between 75 and 100 m. Furthermore, the particles reaching the *Grand Lac* hypolimnion accumulated along the southern shore at the end of simulation S (Figure S3.14), indicating that they were entrained in the eastward shore-hugging current discussed above (Figure 3.6c, d). This suggests that both phenomena, i.e., the deep upwelling along the *Petit Lac* thalweg and the coastal upwelling at its northern shore, are inherently connected.



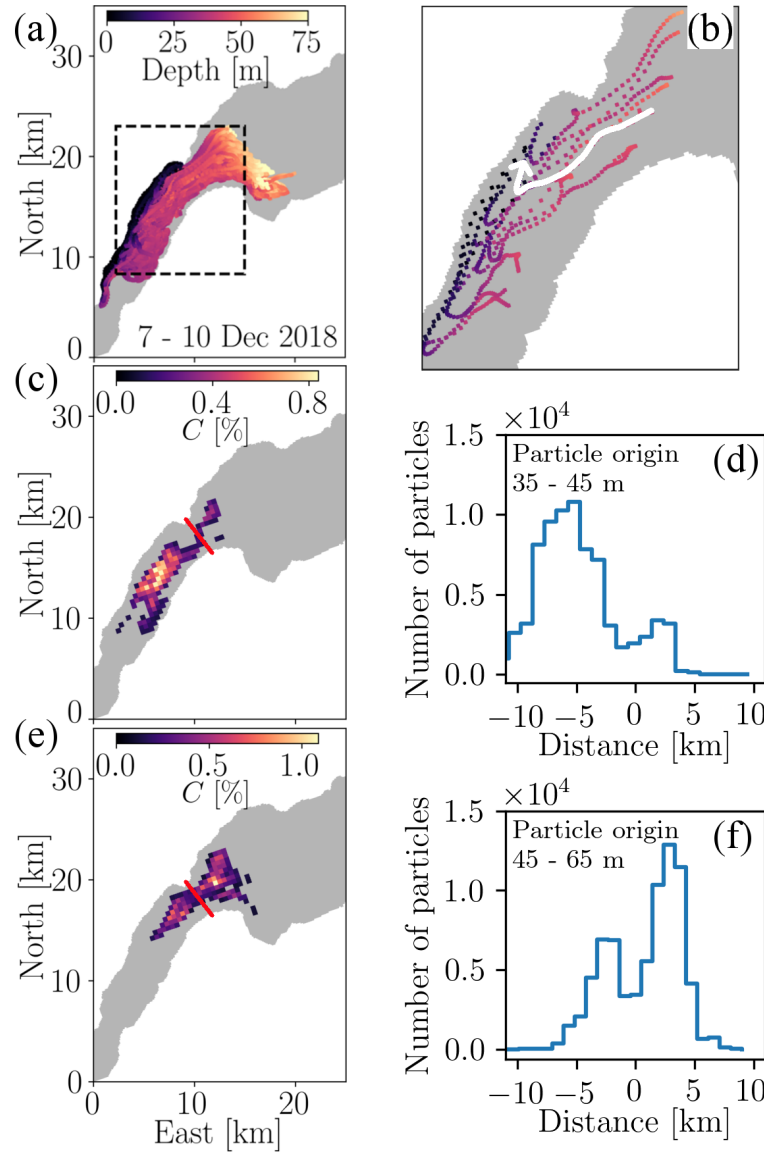


**Figure 3.9.** **a.** Backward trajectories of particles released between 0 to 15-m depth near the northern shore of the *Petit Lac* basin (simulation S; green area in Figure S3.2). **b.** Close-up of selected backward trajectories. The colorbar in (a) gives the particle depth. Only particles originating from below 35-m depth are displayed. The white arrow indicates the travel direction of the particles. **c.** and **e.** 2D maps of origin locations from particles originating from 35 to 45-m and 45 to 65-m depths, respectively, as inferred from the backward tracking of simulation S. **d.** and **f.** Histograms of the distance from the particle origin to the confluence (red lines in c and e), corresponding to the depth ranges in (c) and (e), respectively. Positive values indicate particles originating from the *Grand Lac*. The colorbars in (c) and (e) show the particle concentrations as percentages, i.e., the depth-accumulated number of particles per horizontal cell divided by the total number of particles originating from below 35-m depth. Each horizontal cell is comprised of 16 binned model grid cells, i.e.,  $4 \times 113$  m by  $4 \times 113$  m. For clarity, binned cells with less than 150 particles ( $C \leq 0.1\%$ ) are not shown.

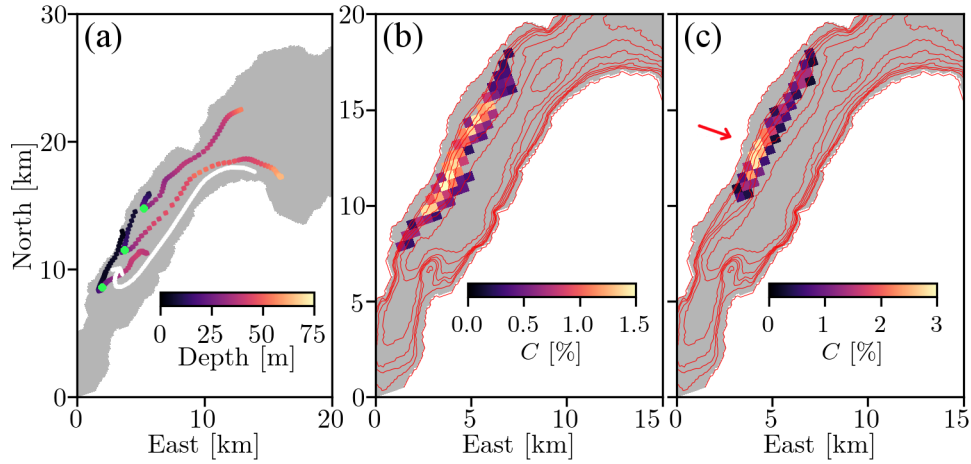


**Figure 3.10.** **a.** Examples of particle trajectories that upwelled at the northern shore of the *Petit Lac* basin with the estimated upwelling locations marked by the green dots. The colorbar gives the particle depth. The white arrow indicates the travel direction of the particles. **b.** and **c.** 2D concentration maps of the upwelling locations for particles originating from 35 to 45-m and 45 to 65-m depths, respectively, as inferred from the backward tracking results of simulation S. The overlaid red contours show the isobaths between 0 and 70-m depth at 10 m intervals. The colorbars in (b) and (c) indicate the upwelling occurrence as percentages, i.e., the number of upwelled particles per horizontal cell divided by the total number of particles originating from the considered depth range. Each horizontal cell is comprised of 16 binned model grid cells, i.e.,  $4 \times 113$  m by  $4 \times 113$  m. For clarity, binned cells with less than 380 particles ( $C \leq 0.25\%$ ) are not shown.

### 3.4 Summary and conclusions

In this study, we performed a detailed analysis of an interbasin hypolimnetic exchange event between the deep *Grand Lac* (max. depth 309 m) and shallow *Petit Lac* (max. depth 75 m) basins of Lake Geneva that occurred during the weakly stratified early winter period due to a strong along-axis wind event (*Vent*) from the southwest. Thus far, this potentially important interbasin exchange process has received little attention in the literature. For this analysis, we combined extensive field observations using moored current profilers and thermistor lines deployed at the confluence between the basins with 3D numerical modeling and Lagrangian particle tracking.

The results show that the wind-induced interbasin upwelling event effectively created a current loop whereby waters from the deep *Grand Lac* hypolimnion were drawn into the shallower *Petit Lac*. Once upwelled, these waters were advected far into the *Petit Lac*, then finally after the wind event had ceased, flowed back into the *Grand Lac* hypolimnion, where they spread

horizontally over a large area. In this current loop, upwelled waters spent in total  $\sim 3\text{--}4$  d in the *Petit Lac*. Coriolis force strongly modified the dynamics of the interbasin upwelling and the trajectories of the water masses.

During the interbasin upwelling event, hypolimnetic *Grand Lac* water from below 150-m depth was brought in contact with “fresher” *Petit Lac* water (i.e., higher dissolved oxygen and lower nutrient concentrations). Furthermore, strong shear and a relatively weak stratification suggested considerable turbulent mixing between these two different water masses, as indicated by low, model-based gradient Richardson numbers and temperature inversions measured both near the bottom and around the thermocline depth. Altogether, these findings demonstrate that wind-induced interbasin upwelling in Lake Geneva is potentially an important transport process for deepwater renewal, deep ventilation, and nutrient cycling.

At the same time that deep interbasin upwelling took place mainly in the hypolimnion of the *Petit Lac*, coastal upwelling occurred at its northern shore. Here, particle tracking revealed that water masses from as deep as 65 m in the *Grand Lac* hypolimnion were first drawn into the *Petit Lac* and subsequently upwelled at its northern shore. The latter appeared to be strongly affected by the irregular bottom topography, resulting in an upwelling hotspot approximately 7 km southwest of the confluence. The observed coastal upwelling in the *Petit Lac* further enhanced both interbasin and hypolimnetic-epilimnetic exchange and mixing and thus can have a positive effect on the deepwater renewal in the *Grand Lac* hypolimnion.

In this study, we discussed in detail one interbasin upwelling event and the accompanying coastal upwelling at the *Petit Lac* northern shore, which took place in mid-December 2018 under *Vent* wind conditions. Note, however, that the field observations showed that three comparable events occurred in December 2018 (Figure S3.3). Furthermore, model results suggest similar events in October and November, i.e., during the period when the *Petit Lac* was weakly stratified. Due to the surrounding mountainous topography, *Vent* winds from the southwest are the most frequent strong winds in the Lake Geneva region during winter (e.g., CH2018 2018). Based on these findings, hypolimnetic interbasin upwelling between the *Grand Lac* and *Petit Lac* basins caused by these winds can significantly affect the deepwater dynamics in Lake Geneva. Considering the deep origin of the upwelled waters, the great intrusion lengths, the long intrusion time, and the enhanced mixing by shear, the results indicate that these frequently occurring events can be an important mechanism for deepwater renewal and horizontal and vertical nutrient recycling in Lake Geneva, and thus can be regarded as ecologically beneficial.

In the light of global warming, our results suggest that wind-induced interbasin upwelling could become increasingly important for deepwater in Lake Geneva, as well as in other deep multi-basin lakes under favorable wind conditions. Unlike convective cooling, which is expected to further weaken due to climate change effects (increasing air temperatures), wind-driven interbasin upwelling is less susceptible to such changes. Moreover, while the complex topography around Lake Geneva makes long-term modeling of the local wind field a challenging endeavor, recent studies indicate that near-surface wind speeds in Switzerland will not change significantly by the end of the 21<sup>st</sup> century (CH2018 2018; Graf et al. 2019).

This study has demonstrated for the first time that mainly due to the effect of the Coriolis force, wind-induced hypolimnetic upwelling between the basins of Lake Geneva is a highly complex and transient 3D transport process, which cannot not be adequately described by traditional one-dimensional (1D) concepts. The findings of this study therefore should be taken into consideration when establishing long-term predictions of lake system dynamics related to climate change.

## Acknowledgments and data availability

This work was supported by the Swiss National Science Foundation (grant no. 159422) and the [Bois Chamblard Foundation](#) (last accessed on 3 June 2021). Meteorological data were provided by the Federal Office of Meteorology and Climatology in Switzerland (MeteoSwiss). Full-depth temperature profile data at SHL2 were provided by © OLA-IS, AnaEE-France, INRAE of Thonon-les-Bains, CIPEL. Temperature profile data at GE3 were provided by the Service de l'Ecologie de l'Eau (Département du territoire, Office cantonal de l'eau, SECOE, 1211 Genève, Suisse). We would like to thank Htet Kyi Wynn and Benjamin Graf for assisting with the fieldwork.

Conflicts of interest: none

## References

- Aeschbach-Hertig, W., R. Kipfer, M. Hofer, D. M. Imboden, and H. Baur. 1996. Density-driven exchange between the basins of Lake Lucerne (Switzerland) traced with the  $3\text{H}$ - $3\text{He}$  method. *Limnology and Oceanography* **41**: 707–721. doi:[10.4319/lo.1996.41.4.0707](https://doi.org/10.4319/lo.1996.41.4.0707)
- Ahrnsbrak, W. F., and M. R. Wing. 1998. Wind-induced hypolimnion exchange in Lake Ontario's Kingston basin: Potential effects on oxygen. *Journal of Great Lakes Research* **24**: 145–151. doi:[10.1016/S0380-1330\(98\)70806-8](https://doi.org/10.1016/S0380-1330(98)70806-8)
- Amadori, M., S. Piccolroaz, L. Giovannini, D. Zardi, and M. Toffolon. 2018. Wind variability and Earth's rotation as drivers of transport in a deep, elongated subalpine lake: The case of Lake Garda. *Journal of Limnology* **77**: 505–521. doi:[10.4081/jlimnol.2018.1814](https://doi.org/10.4081/jlimnol.2018.1814)
- Appt, J., J. Imberger, and H. Kobus. 2004. Basin-scale motion in stratified Upper Lake Constance. *Limnology and Oceanography* **49**: 919–933. doi:[10.4319/lo.2004.49.4.0919](https://doi.org/10.4319/lo.2004.49.4.0919)
- Bartish, T. 1987. A review of exchange processes among the three basins of Lake Erie. *Journal of Great Lakes Research* **13**: 607–618. doi:[10.1016/S0380-1330\(87\)71676-1](https://doi.org/10.1016/S0380-1330(87)71676-1)
- Bauer, S. W., W. H. Graf, C. H. Mortimer, and C. Perrinjaquet. 1981. Inertial motion in Lake Geneva (Le Léman). *Archives for meteorology, geophysics, and bioclimatology, Series A* **30**: 289–312. doi:[10.1007/BF02257850](https://doi.org/10.1007/BF02257850)
- Bennett, E. B. 1988. On the physical limnology of Georgian Bay, p. 21–34. *In* M. Munawar [ed.], *Limnology and fisheries of Georgian Bay and the North Channel ecosystems*. Dordrecht: Springer.
- Bouffard, D., and U. Lemmin. 2013. Kelvin waves in Lake Geneva. *Journal of Great Lakes Research* **39**: 637–645. doi:[10.1016/j.jglr.2013.09.005](https://doi.org/10.1016/j.jglr.2013.09.005)
- Boyce, F. M., F. Chiocchio, B. Eid, F. Penicka, and F. Rosa. 1980. Hypolimnion flow between the central and eastern basins of Lake Erie during 1977 (Interbasin hypolimnion flows). *Journal of Great Lakes Research* **6**: 290–306. doi:[10.1016/S0380-1330\(80\)72110-X](https://doi.org/10.1016/S0380-1330(80)72110-X)
- CH2018. 2018. CH2018 – Climate Scenarios for Switzerland, Technical Report, National Centre for Climate Services, Zurich, 271 pp. ISBN: 978-3-9525031-4-0. Retrieved from <https://natursciences.ch/service/publications/107865-ch2018---climate-scenarios-for-switzerland-technical-report>, last accessed 30 May 2021.
- Cimatoribus, A. A. 2018. C-tracker. doi:[10.5281/zenodo.1034118](https://doi.org/10.5281/zenodo.1034118)
- Cimatoribus, A. A., U. Lemmin, and D. A. Barry. 2019. Tracking Lagrangian transport in Lake Geneva: A 3D numerical modeling investigation. *Limnology and Oceanography* **64**: 1–18. doi:[10.1002/lno.11111](https://doi.org/10.1002/lno.11111)
- Cimatoribus, A. A., U. Lemmin, D. Bouffard, and D. A. Barry. 2018. Nonlinear dynamics of the near-shore boundary layer of a large lake (Lake Geneva). *Journal of Geophysical Research: Oceans* **123**: 1016–1031. doi:[10.1002/2017JC013531](https://doi.org/10.1002/2017JC013531)
- CIPEL. 2016. Rapports sur les études et recherches entreprises dans le bassin lémanique, Campagne 2015. Commission internationale pour la protection des eaux du Léman (CIPEL), Nyon, Switzerland. Retrieved from [http://www.cipel.org/wp-content/uploads/2016/10/RapportScientifique\\_camp\\_2015\\_VF.pdf](http://www.cipel.org/wp-content/uploads/2016/10/RapportScientifique_camp_2015_VF.pdf), last accessed 30 May 2021.
- CIPEL. 2019. Rapports sur les études et recherches entreprises dans le bassin lémanique, Campagne 2018. Commission internationale pour la protection des eaux du Léman (CIPEL), Nyon, Switzerland. Retrieved from [https://www.cipel.org/wp-content/uploads/2019/10/RapportScientifique\\_camp\\_2018-1.pdf](https://www.cipel.org/wp-content/uploads/2019/10/RapportScientifique_camp_2018-1.pdf), last accessed 30 May 2021.
- Coman, M. A., and M. G. Wells. 2012. Temperature variability in the nearshore benthic boundary layer of Lake Opeongo is due to wind-driven upwelling events. *Canadian Journal of Fisheries and Aquatic Sciences* **69**: 282–296. doi:[10.1139/f2011-167](https://doi.org/10.1139/f2011-167)
- Cornett, R., and F. Rigler. 1979. Hypolimnetic oxygen deficits: their prediction and interpretation. *Science (New York, N.Y.)* **205**: 580–581. doi:[10.1126/science.205.4406.580](https://doi.org/10.1126/science.205.4406.580)
- Djoumna, G., K. G. Lamb, and Y. R. Rao. 2014. Sensitivity of the parameterizations of vertical mixing and radiative heat fluxes on the seasonal evolution of the thermal structure of Lake Erie. *Atmosphere-Ocean* **52**: 294–313. doi:[10.1080/07055900.2014.939824](https://doi.org/10.1080/07055900.2014.939824)

- Döös, K., J. Kjellsson, and B. Jönsson. 2013. TRACMASS—A Lagrangian trajectory model, p. 225–249. *In* T. Soomere and E. Quak [eds.], *Preventive Methods for Coastal Protection: Towards the Use of Ocean Dynamics for Pollution Control*. Heidelberg: Springer International Publishing.
- Dorostkar, A., and L. Boegman. 2013. Internal hydraulic jumps in a long narrow lake. *Limnology and Oceanography* **58**: 153–172. doi:[10.4319/lo.2013.58.1.0153](https://doi.org/10.4319/lo.2013.58.1.0153)
- Dorostkar, A., L. Boegman, and A. Pollard. 2017. Three-dimensional simulation of high-frequency non-linear internal wave dynamics in Cayuga Lake. *Journal of Geophysical Research: Oceans* **122**: 2183–2204. doi:[10.1002/2016JC011862](https://doi.org/10.1002/2016JC011862)
- Flood, B., M. Wells, E. Dunlop, and J. Young. 2020. Internal waves pump waters in and out of a deep coastal embayment of a large lake. *Limnology and Oceanography* **65**: 205–223. doi:[10.1002/lno.11292](https://doi.org/10.1002/lno.11292)
- Graf, M., S. C. Scherrer, C. Schwierz, M. Begert, O. Martius, C. C. Raible, and S. Brönnimann. 2019. Near-surface mean wind in Switzerland: Climatology, climate model evaluation and future scenarios. *International Journal of Climatology* **39**: 4798–4810. doi:[10.1002/joc.6108](https://doi.org/10.1002/joc.6108)
- Jabbari, A., J. D. Ackerman, L. Boegman, and Y. Zhao. 2019. Episodic hypoxia in the western basin of Lake Erie. *Limnology and Oceanography* **64**: 2220–2236. doi:[10.1002/lno.11180](https://doi.org/10.1002/lno.11180)
- Jabbari, A., J. D. Ackerman, L. Boegman, and Y. Zhao. 2021. Increases in Great Lake winds and extreme events facilitate interbasin coupling and reduce water quality in Lake Erie. *Scientific Reports* **11**: 5733. doi:[10.1038/s41598-021-84961-9](https://doi.org/10.1038/s41598-021-84961-9)
- Kocsis, O., B. Mathis, M. Gloor, M. Schurter, and A. Wüest. 1998. Enhanced mixing in narrows: A case study at the Mainau sill (Lake Constance). *Aquatic Sciences* **60**: 236. doi:[10.1007/s000270050039](https://doi.org/10.1007/s000270050039)
- Laval, B. E., J. Morrison, D. J. Potts, E. C. Carmack, S. Vagle, C. James, F. A. McLaughlin, and M. Foreman. 2008. Wind-driven summertime upwelling in a fjord-type lake and its impact on downstream river conditions: Quesnel Lake and River, British Columbia, Canada. *Journal of Great Lakes Research* **34**: 189–203. doi:[10.3394/0380-1330\(2008\)34\[189:WSUIAF\]2.0.CO;2](https://doi.org/10.3394/0380-1330(2008)34[189:WSUIAF]2.0.CO;2)
- Lavigne, S., and P. Nirel. 2016. Physico-chemical and biological changes in the waters of the Petit Lac. Service de l'écologie de l'eau (SECOE). Geneva, Switzerland. Retrieved from [http://www.cipel.org/wp-content/uploads/2016/11/0\\_evolution\\_physico\\_chimique\\_biologique\\_petit-lac\\_camp\\_2015.pdf](http://www.cipel.org/wp-content/uploads/2016/11/0_evolution_physico_chimique_biologique_petit-lac_camp_2015.pdf), accessed 30 May 2021.
- Lemmin, U. 2020. Insights into the dynamics of the deep hypolimnion of Lake Geneva as revealed by long-term temperature, oxygen, and current measurements. *Limnology and Oceanography* **65**: 2092–2107. doi:[10.1002/lno.11441](https://doi.org/10.1002/lno.11441)
- Lemmin, U., C. H. Mortimer, and E. Bäuerle. 2005. Internal seiche dynamics in Lake Geneva. *Limnology and Oceanography* **50**: 207–216. doi:[10.4319/lo.2005.50.1.0207](https://doi.org/10.4319/lo.2005.50.1.0207)
- Marshall, J., A. Adcroft, C. Hill, L. Perelman, and C. Heisey. 1997. A finite-volume, incompressible Navier Stokes model for studies of the ocean on parallel computers. *Journal of Geophysical Research: Oceans* **102**: 5753–5766. doi:[10.1029/96JC02775](https://doi.org/10.1029/96JC02775)
- Monismith, S. G., J. Imberger, and M. L. Morison. 1990. Convective motions in the sidearm of a small reservoir. *Limnology and Oceanography* **35**: 1676–1702. doi:[10.4319/lo.1990.35.8.1676](https://doi.org/10.4319/lo.1990.35.8.1676)
- Monsen, N. E., J. E. Cloern, L. V. Lucas, and S. G. Monismith. 2002. A comment on the use of flushing time, residence time, and age as transport time scales. *Limnology and Oceanography* **47**: 1545–1553. doi:[10.4319/lo.2002.47.5.1545](https://doi.org/10.4319/lo.2002.47.5.1545)
- Nguyen, T. D., P. Thupaki, E. J. Anderson, and M. S. Phanikumar. 2014. Summer circulation and exchange in the Saginaw Bay-Lake Huron system. *Journal of Geophysical Research* **119**: 2713–2734. doi:[10.1002/2014JC009828](https://doi.org/10.1002/2014JC009828)
- Niu, Q., M. Xia, E. S. Rutherford, D. M. Mason, E. J. Anderson, and D. J. Schwab. 2015. Investigation of interbasin exchange and interannual variability in Lake Erie using an unstructured-grid hydrodynamic model. *Journal of Geophysical Research: Oceans* **120**: 2212–2232. doi:[10.1002/2014JC010457](https://doi.org/10.1002/2014JC010457)
- Nürnberg, G. K., L. A. Molot, E. O'Connor, H. Jarjanazi, J. Winter, and J. Young. 2013. Evidence for internal phosphorus loading, hypoxia and effects on phytoplankton in partially polymictic Lake Simcoe, Ontario. *Journal of Great Lakes Research* **39**: 259–270. doi:[10.1016/j.jglr.2013.03.016](https://doi.org/10.1016/j.jglr.2013.03.016)



- Okubo, K. 1995. Field observations of the dense bottom current between the north and south basins, p. 43–51. *In* S. Okuda, J. Imberger, and M. Kumagai [eds.], Physical processes in a large lake: Lake Biwa, Japan. American Geophysical Union (AGU).
- Oonishi, Y. 1995. Numerical simulation of density-induced currents between the north and south basins of lake biwa, p. 53–64. *In* S. Okuda, J. Imberger, and M. Kumagai [eds.], Physical processes in a large lake: Lake Biwa, Japan. American Geophysical Union (AGU).
- Piccolroaz, S., M. Amadori, M. Toffolon, and H. A. Dijkstra. 2019. Importance of planetary rotation for ventilation processes in deep elongated lakes: Evidence from Lake Garda (Italy). *Scientific Reports* **9**: 8290. doi:[10.1038/s41598-019-44730-1](https://doi.org/10.1038/s41598-019-44730-1)
- Rao, Y. R., and C. R. Murthy. 2001. Nearshore currents and turbulent exchange processes during upwelling and downwelling events in Lake Ontario. *Journal of Geophysical Research: Oceans* **106**: 2667–2678. doi:[10.1029/2000JC900149](https://doi.org/10.1029/2000JC900149)
- Reiss, R. S., U. Lemmin, A. A. Cimadoribus, and D. A. Barry. 2020. Wintertime coastal upwelling in Lake Geneva: An efficient transport process for deepwater renewal in a large, deep lake. *Journal of Geophysical Research: Oceans* **125**. doi:[10.1029/2020JC016095](https://doi.org/10.1029/2020JC016095)
- Rimet, F., O. Anneville, D. Barbet, C. Chardon, L. Crépin, I. Domaizon, J.-M. Dorioz, L. Espinat, V. Frossard, J. Guillard, C. Goulon, V. Hamelet, J.-C. Hustache, S. Jacquet, L. Lainé, B. Montuelle, P. Perney, P. Quetin, S. Rasconi, A. Schellenberger, V. Tran-Khac, and G. Monet. 2020. The Observatory on LAkes (OLA) database: Sixty years of environmental data accessible to the public: The Observatory on LAkes (OLA) database. *Journal of Limnology* **79**. doi:[10.4081/jlimnol.2020.1944](https://doi.org/10.4081/jlimnol.2020.1944)
- Salmaso, N. 2005. Effects of climatic fluctuations and vertical mixing on the interannual trophic variability of Lake Garda, Italy. *Limnology and Oceanography* **50**: 553–565. doi:[10.4319/lo.2005.50.2.0553](https://doi.org/10.4319/lo.2005.50.2.0553)
- Saylor, J. H., and G. S. Miller. 1987. Studies of large-scale currents in Lake Erie, 1979–80. *Journal of Great Lakes Research* **13**: 487–514. doi:[10.1016/S0380-1330\(87\)71668-2](https://doi.org/10.1016/S0380-1330(87)71668-2)
- Scavia, D., J. David Allan, K. K. Arend, S. Bartell, D. Beletsky, N. S. Bosch, S. B. Brandt, R. D. Briland, I. Daloğlu, J. V. DePinto, D. M. Dolan, M. A. Evans, T. M. Farmer, D. Goto, H. Han, T. O. Höök, R. Knight, S. A. Ludsın, D. Mason, A. M. Michalak, R. Peter Richards, J. J. Roberts, D. K. Rucinski, E. Rutherford, D. J. Schwab, T. M. Sesterhenn, H. Zhang, and Y. Zhou. 2014. Assessing and addressing the re-eutrophication of Lake Erie: Central basin hypoxia. *Journal of Great Lakes Research* **40**: 226–246. doi:[10.1016/j.jglr.2014.02.004](https://doi.org/10.1016/j.jglr.2014.02.004)
- van Senden, D. C., and D. M. Imboden. 1989. Internal seiche pumping between sill-separated basins. *Geophysical & Astrophysical Fluid Dynamics* **48**: 135–150. doi:[10.1080/03091928908219530](https://doi.org/10.1080/03091928908219530)
- Umlauf, L., and U. Lemmin. 2005. Interbasin exchange and mixing in the hypolimnion of a large lake: The role of long internal waves. *Limnology and Oceanography* **50**: 1601–1611. doi:[10.4319/lo.2005.50.5.1601](https://doi.org/10.4319/lo.2005.50.5.1601)
- Voudouri, A., E. Avgoustoglou, and P. Kaufmann. 2017. Impacts of Observational Data Assimilation on Operational Forecasts. *Perspectives on Atmospheric Sciences*. Cham: Springer International Publishing. 143–149.
- Wells, M. G., and L. Sealock. 2009. Summer water circulation in Frenchman’s Bay, a shallow coastal embayment connected to Lake Ontario. *Journal of Great Lakes Research* **35**: 548–559. doi:[10.1016/j.jglr.2009.08.009](https://doi.org/10.1016/j.jglr.2009.08.009)





# Supporting Information for Chapter 3

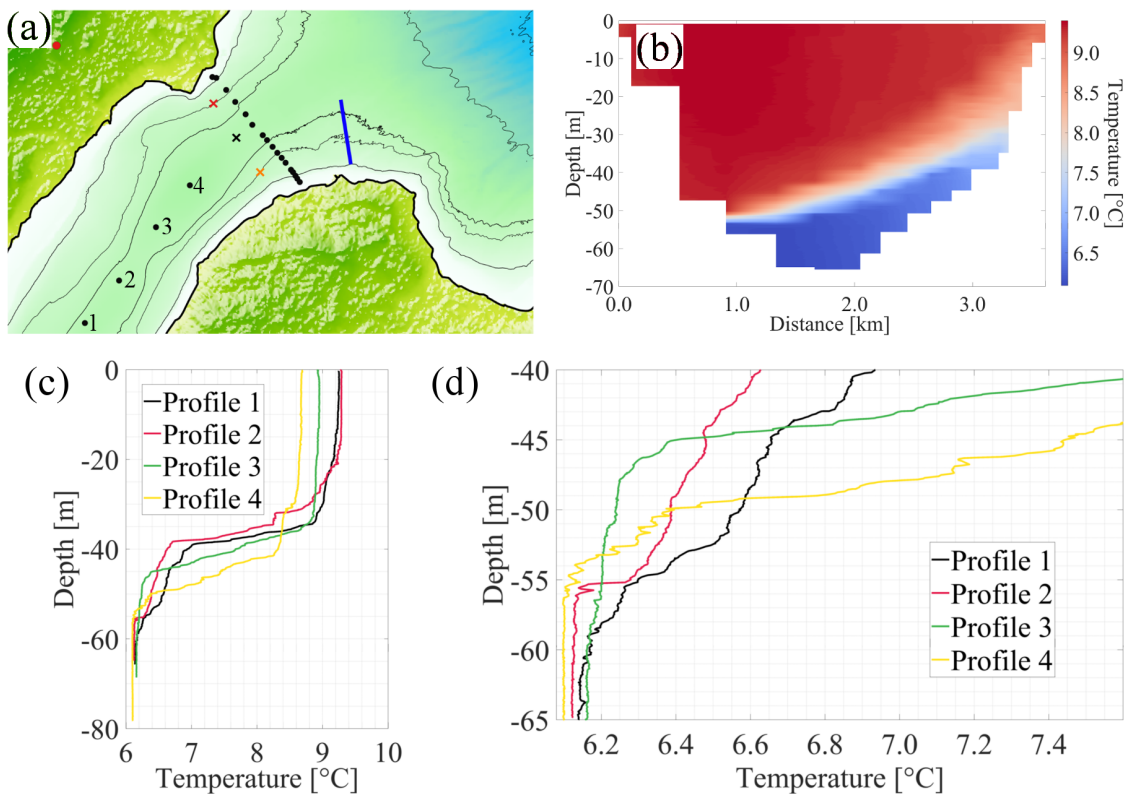
---

Rafael Sebastian Reiss, Ulrich Lemmin, and David Andrew Barry

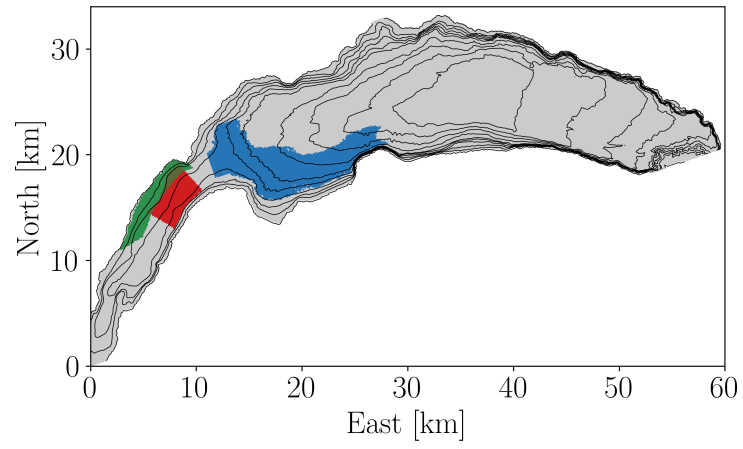
Ecological Engineering Laboratory (ECOL), Faculty of Architecture, Civil and Environmental Engineering (ENAC), Ecole Polytechnique Fédérale de Lausanne (EPFL), Lausanne, Switzerland

Table S3.1. Details of the moorings

Mooring	Depth [m]	Instruments and settings
MV-N	50	10 Seabird SBE-39, vertical spacing 1 m, sampling interval 5 min Teledyne RDI Workhorse Sentinel (300 kHz): 21 bins of 2 m, 20 min ensemble interval, 180 pings per ensemble
MV-C	65	10 Seabird SBE-56, vertical spacing 1 m, sampling interval 5 s Teledyne RDI Workhorse Sentinel (300 kHz): 29 bins of 2 m, 20 min ensemble interval, 180 pings per ensemble
MV-S	50	10 RBRsolo T, vertical spacing 1 m, sampling interval 1 s Teledyne RDI Workhorse Sentinel (300 kHz): 21 bins of 2 m, 20 min ensemble interval, 180 pings per ensemble
MH	25 – 65	20 RBRsolo T, horizontal spacing 80 m, sampling interval 1 s



**Figure S3.1.** **a.** Bathymetric map of Lake Geneva showing the mooring locations during winter 2018/2019, i.e., MV-N (red cross), MV-C (black cross), MV-S (orange cross), and MH (blue line), as well as the locations of the CTD casts performed on 13 December 2018 (black dots). **b.** Temperatures at the confluence between the *Petit Lac* and *Grand Lac* basins inferred from the CTD casts from 13 December 2018. Compare to Figure 3.4f in the main text. The distance is given from the northern shore. **c.** Temperature profiles taken in the *Petit Lac* at stations 1 to 4 on 13 December 2018 (see panel a). **d.** Close-up of the lower 25 m of the profiles in (c).



**Figure S3.2.** Regions in Lake Geneva where particles were released during the particle tracking simulations: B (red), S (green) in the *Petit Lac* basin, and L (blue) in the *Grand Lac* basin.

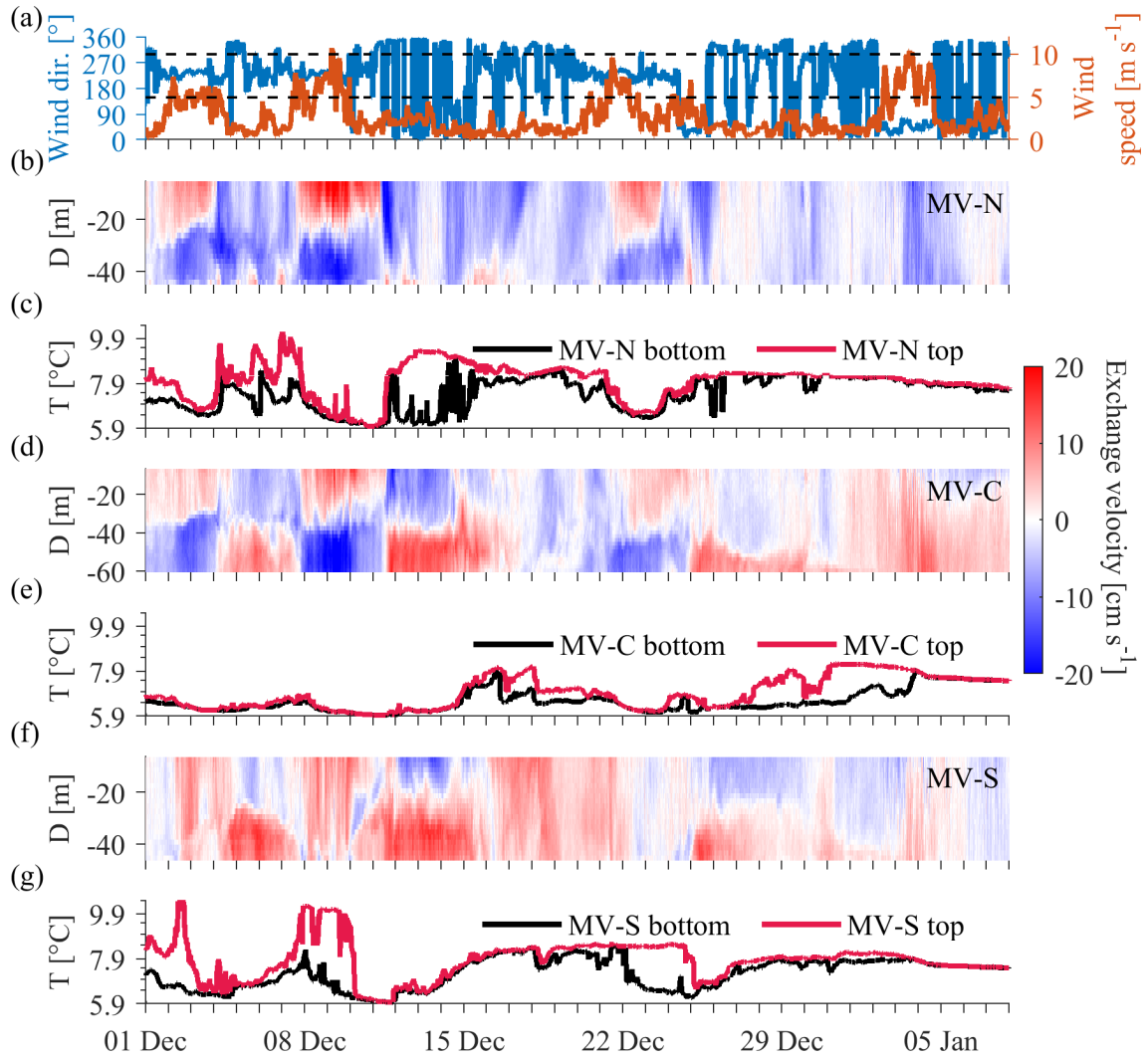


**Figure S3.3.** For the period 1 December 2018 to 8 January 2019: **a.** Wind speed (red) and wind direction (blue) measured at the Nyon meteorological station. **b. to g.** Current velocities (versus depth  $D$ ) and temperatures ( $T$ ) recorded at moorings MV-N (**b, c**), MV-C (**d, e**), and MV-S (**f, g**), respectively. Current velocities are shown as “interbasin exchange velocities,” i.e., projected onto a plane parallel to the isobaths at the confluence. The colorbar gives the magnitude of the interbasin exchange velocity. Positive values indicate flow out of the *Petit Lac*. Note that a sequence of strong two-layer current patterns is established (particularly at mooring MV-C in panel **d**) as a result of strong wind events (panel **a**) that reverse after the wind ceased. Horizontal dashed lines in (**a**) mark a wind speed of 5 and 10  $\text{m s}^{-1}$ . For mooring locations, see Figure S3.1a.

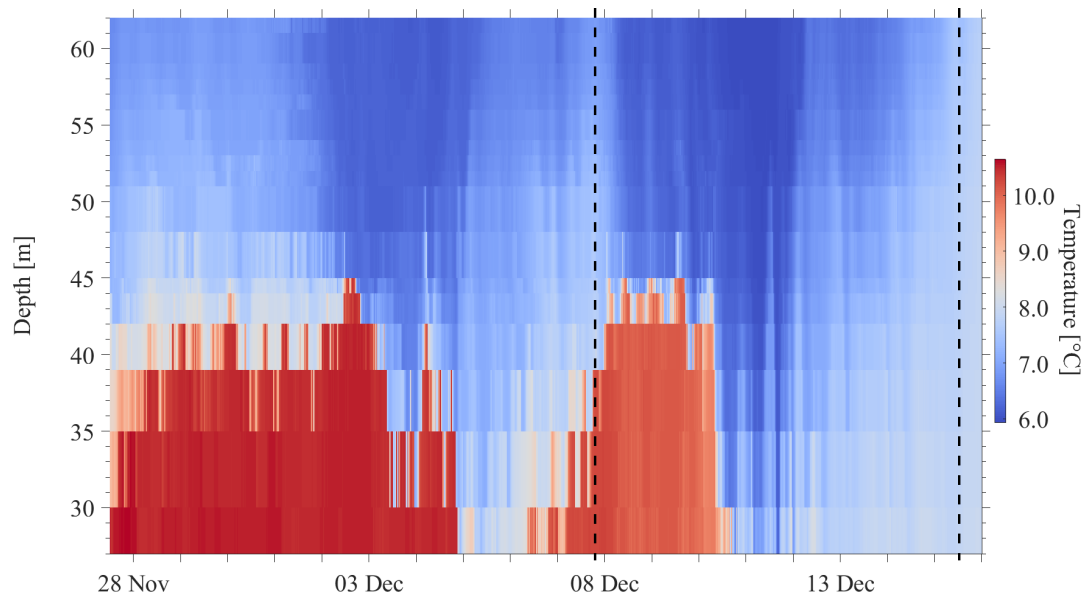


**Figure S3.4.** Temperatures recorded near the bottom at the horizontal thermistor line (mooring MH) from 27 November 2018 to 16 December 2018. The vertical dashed lines mark the beginning and end of the interbasin upwelling event detailed in this study. See Figure S3.1a for mooring location. The colorbar gives the temperature range.

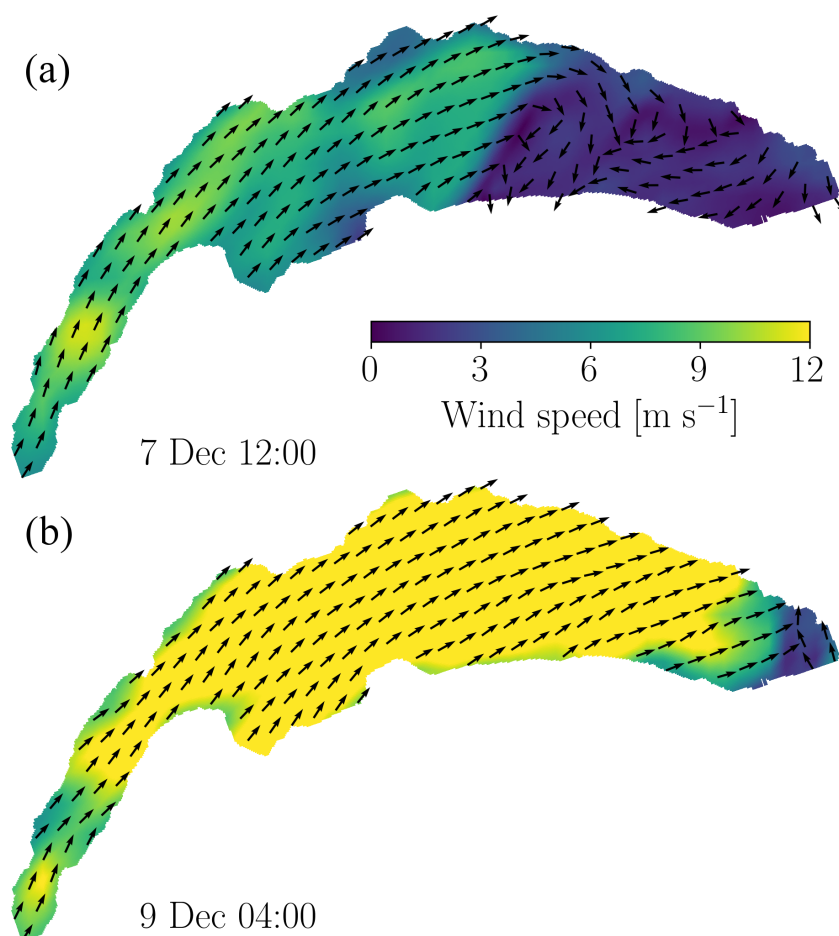


**Figure S3.5.** Two-dimensional COSMO-1 wind field at (a) the beginning and (b) the peak of the *Vent* wind event. The normalized black arrows show the *Vent* wind direction (from the southwest) over most of the lake. The colorbar gives the wind speed. For clarity, not all wind vectors are shown.

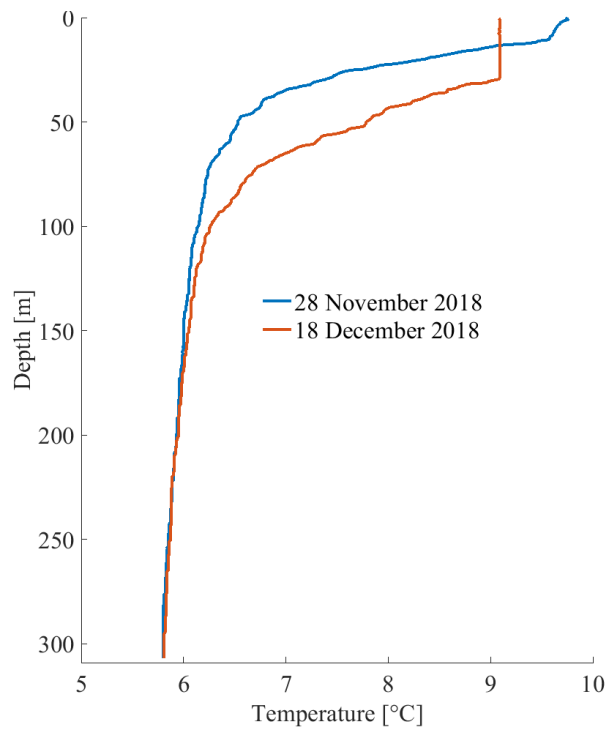


**Figure S3.6.** Full-depth temperature profiles taken by CIPEL at station SHL2 on 28 November 2018 (blue) and 18 December 2018 (red). See Figure S3.1a for station location.

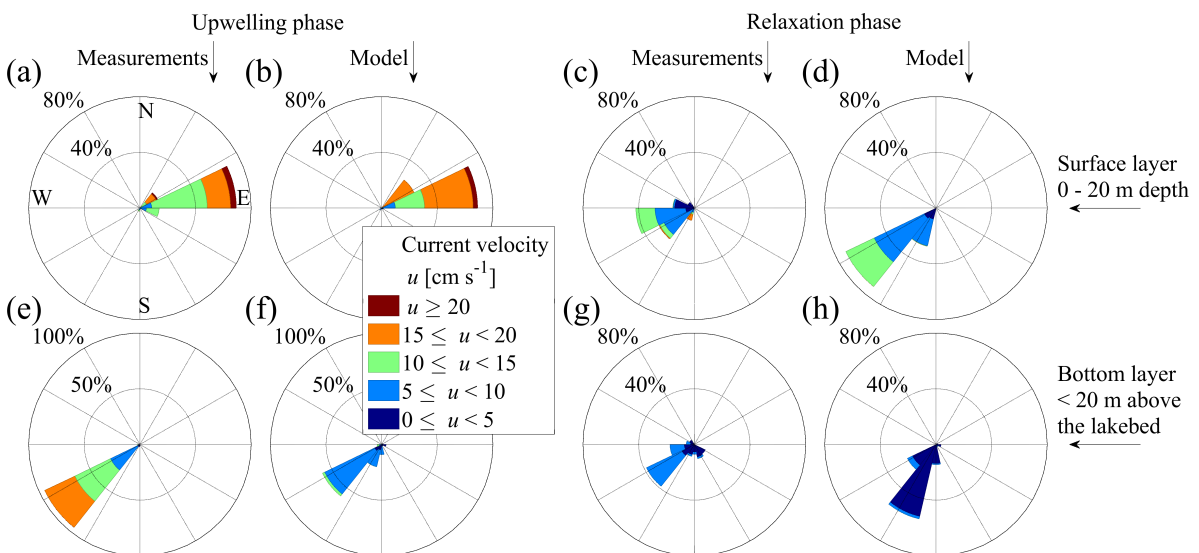


**Figure S3.7.** Current velocities measured (a, c, e, g) and modeled (b, d, f, h) in the surface (0 to 20-m depth; upper panels) and bottom layers (0 to 20 m above the lakebed; lower panels) at the northern mooring MV-N. The four current roses to the left (a, b, e, f) show the current velocities during the upwelling phase, and the four to the right (c, d, g, h), during the relaxation phase. For mooring location, see Figure S3.1a.

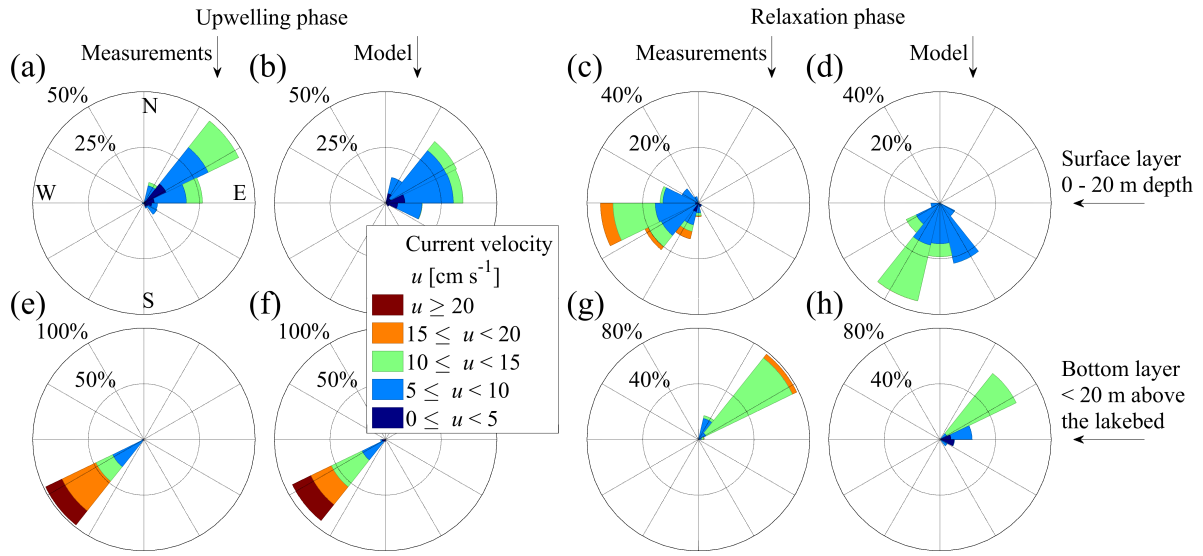


**Figure S3.8.** Current velocities measured (a, c, e, g) and modeled (b, d, f, h) in the surface (0 to 20-m depth; upper panels) and bottom layers (0 to 20 m above the lakebed; lower panels) at the central mooring MV-C. The four current roses to the left (a, b, e, f) show the current velocities during the upwelling phase, and the four to the right (c, d, g, h), during the relaxation phase. For mooring location, see Figure S3.1a.

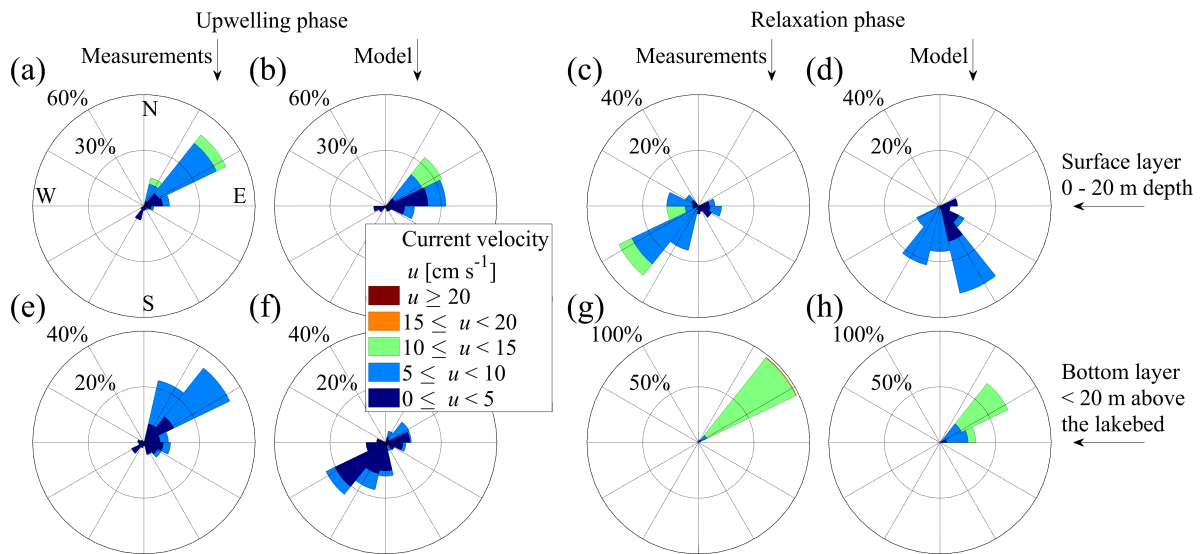


**Figure S3.9.** Current velocities measured (a, c, e, g) and modeled (b, d, f, h) in the surface (0 to 20-m depth; upper panels) and bottom layers (0 to 20 m above the lakebed; lower panels) at the southern mooring MV-S. The four current roses to the left (a, b, e, f) show the current velocities during the upwelling phase, and the four to the right (c, d, g, h), during the relaxation phase. For mooring location, see Figure S3.1a.



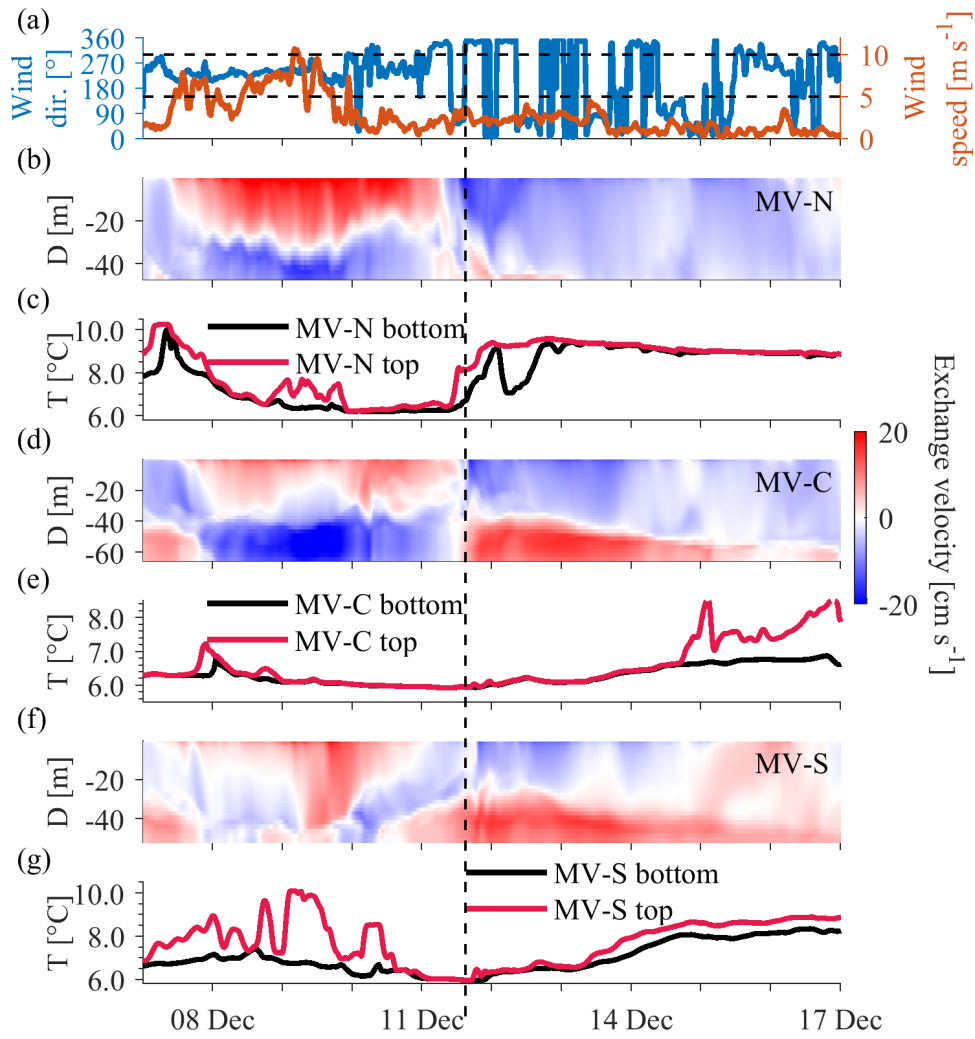


**Figure S3.10.** **a.** Wind direction (blue) and wind speed (red) measured at the Nyon meteorological station. **b. to g.** Modeled current velocities (versus depth  $D$ ) and temperatures ( $T$ ) at moorings MV-N (b, c), MV-C (d, e), and MV-S (f, g), respectively. Current velocities are given as “interbasin exchange velocities,” i.e., projected onto a vertical plane parallel to the isobaths at the confluence. The colorbar gives the magnitude of the interbasin exchange velocity. Positive values indicate flow out of the *Petit Lac*. All dates refer to 2018. Horizontal dashed lines in (a) mark a wind speed of 5 and 10 m s<sup>-1</sup>. For mooring location, see Figure S3.1a

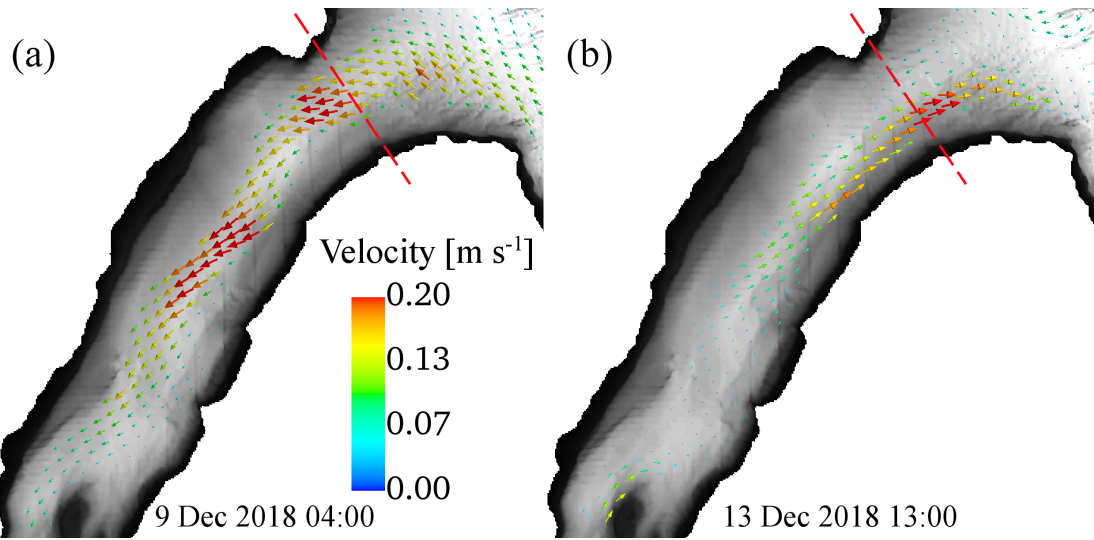


**Figure S3.11.** Modeled current velocities at 50-m depth in the *Petit Lac* basin of Lake Geneva **a.** during the upwelling phase (9 December 2018 04:00), and **b.** during the relaxation phase (13 December 2018 13:00). The colorbar gives the current velocity. The dashed red line indicates the confluence of the two lake basins (maximum depth in the center: 65 m); see Figure 3.1a in the main text for location.

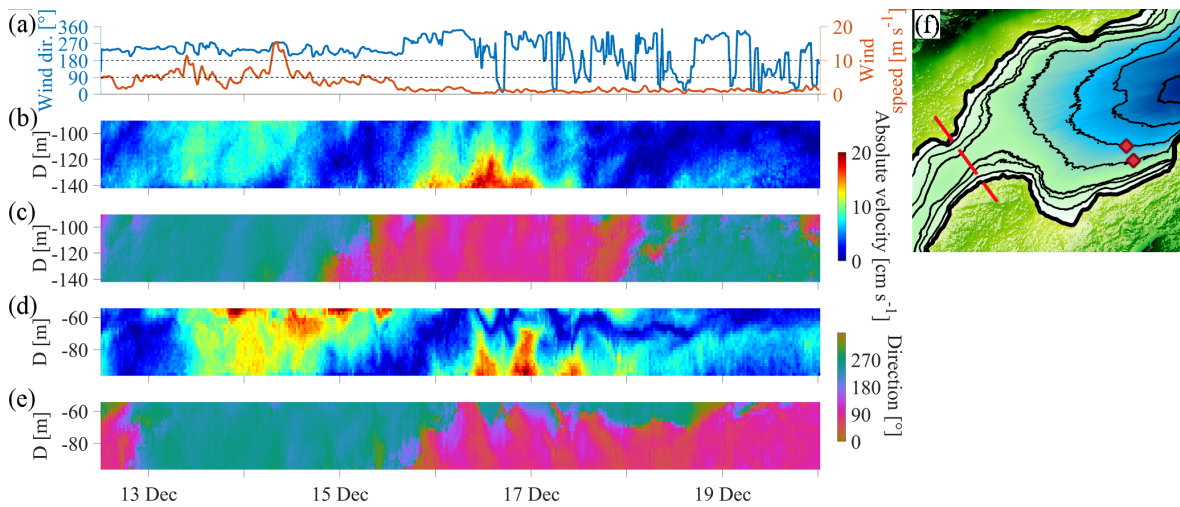


**Figure S3.12.** **a.** Wind direction (blue) and wind speed (red) measured at the Nyon meteorological station (see Figure S3.1a for station location). **b.** and **c.** Current velocity and current direction measured at a vertical mooring at 150-m depth during December 2019. **d.** and **e.** Current velocity and direction measured at a vertical mooring at 100-m depth in December 2019. **f.** Map indicating the locations of the moorings at 100 and 150-m depth (red diamonds). Depth contours are given at 0, 25, 50, 60, 100, 150, 200, and 250 m. The dashed red line indicates the confluence of the two lake basins of Lake Geneva (see Figure 3.1a in the main text for location). The colorbars give the absolute current velocity and the current direction. Current directions are given as “flowing towards,” with 0° and 90 ° being north and east, respectively. All dates refer to 2019. Horizontal dashed lines in (a) mark a wind speed of 5 and 10 m s<sup>-1</sup>.

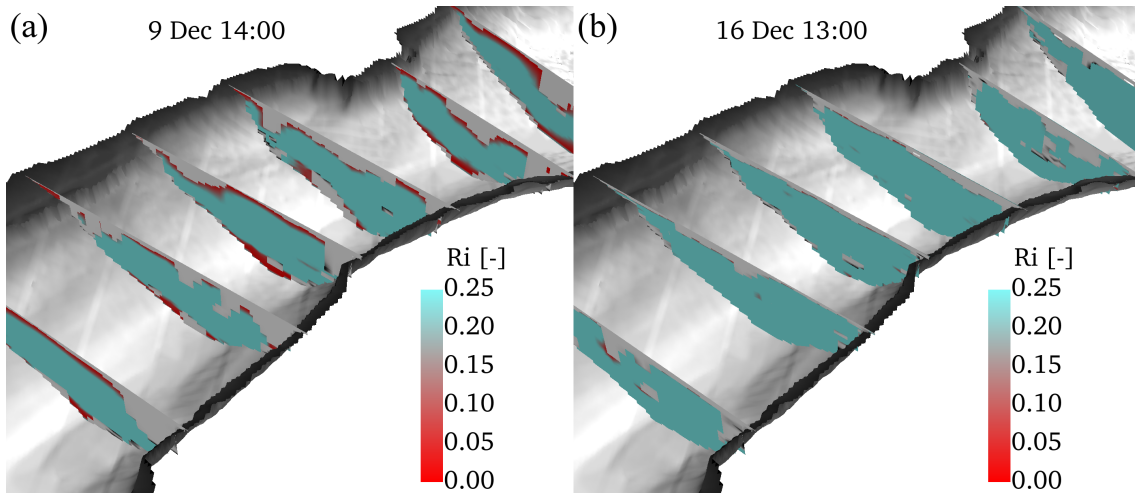


**Figure S3.13.** Gradient Richardson numbers ( $Ri$ ) inferred from the modeled 3D current velocity and temperature fields at selected vertical slices in the *Petit Lac* basin and near the confluence (second transect from the right) **a.** during the upwelling phase of the interbasin upwelling event (9 December 2018 14:00), and **b.** after the event (16 December 2018 13:00). The colorbar gives the gradient Richardson number ( $Ri$ ) between 0 and 0.25, with values below 0.25 indicating turbulent mixing by shear instabilities. Negative  $Ri$  values can occur: (i) under unstable stratified conditions leading to convective mixing, and (ii) due to small numerical errors in the modeled temperature field of a well-mixed layer. Here, negative  $Ri$  values are marked in grey.

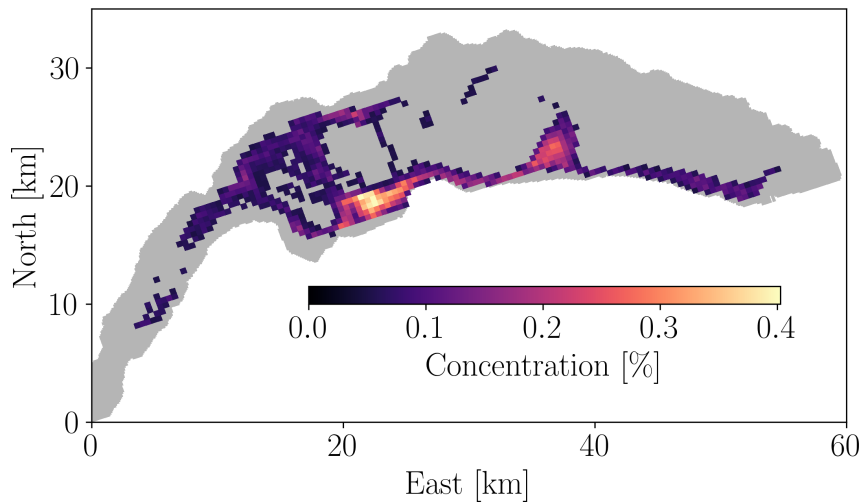


**Figure S3.14.** Two-dimensional (2D) map showing the final locations of the forward tracked particles that reached the hypolimnion, i.e., below 40-m depth (simulation S). The particles were released in the epilimnion of the *Petit Lac* near its northern shore (see Figure S3.2 for release location; green area). Particle concentrations (see colorbar) are given as the depth-accumulated number of particles per horizontal cell divided by the total number of particles that reached the hypolimnion. Each horizontal cell is comprised of 16 binned model grid cells, i.e.,  $4 \times 113$  m by  $4 \times 113$  m. For clarity, binned cells with less than 70 particles ( $C \leq 0.05\%$ ) are not shown.



# Chapter 4    What role does stratification play in wind-induced hypolimnetic upwelling between the multi-depth basins of Lake Geneva during winter?

---

Rafael Sebastian Reiss, Ulrich Lemmin, and David Andrew Barry

Ecological Engineering Laboratory (ECOL), Faculty of Architecture, Civil and Environmental Engineering (ENAC), Ecole Polytechnique Fédérale de Lausanne (EPFL), Lausanne, Switzerland

## Abstract

The effect of stratification on wind-induced exchange between the *Petit Lac* (*PL*) (max. depth 75 m) and *Grand Lac* (*GL*) (max. depth 309 m) basins of Lake Geneva was investigated with field observations and 3D numerical modeling and particle tracking. Under comparable strong, along-axis wind forcing, early (weakly stratified) and late (fully-mixed) winter conditions in the *PL* were considered.

For early winter, we previously found a two-layer exchange pattern with downwind surface outflow into the *GL* balanced by strong, steady bottom inflow that brings deep, cold hypolimnetic *GL* water into the *PL*. Here, we show that this bottom inflow is driven by baroclinic pressure gradients caused by upwind upwelling in the *GL*. Furthermore, after an adjustment phase, barotropic pressure gradients due to water level setup at the right shore, largely balance the Coriolis acceleration acting on the epilimnetic outflow, yielding a unidirectional net current structure, aligned with the wind.

In late winter, when the thermocline is below the *PL* depth, upwelling in the *GL* does not reach the *PL* bottom and baroclinicity does not enhance the exchange. Therefore, exchange currents are weaker and the upper layer currents show a depth-veering structure due to Coriolis force. As a consequence, the net volume exchange reduces by 50%. More striking is that the deep hypolimnetic upwelling from the *GL* into the *PL* is suppressed altogether. Based on our results, prolonged winter stratification due to global warming can be expected to make hypolimnetic interbasin-upwelling an increasingly important deepwater renewal mechanism in multi-depth basin lakes.

**Keywords:** Lake Geneva, upwelling, stratification, interbasin exchange, Coriolis force, multi-basin lake, multi-depth basin, hypolimnion, deepwater renewal, momentum budget

## 4.1 Introduction

Water quality in lakes is closely linked to hydrodynamics and is often strongly affected by (thermal) stratification, which limits the vertical exchange between the hypolimnion and epilimnion. Thus, horizontal exchange and mixing processes, leading to the vertical redistribution of biogeochemical tracers such as dissolved oxygen and nutrients are of great ecological importance. In multi-basin lakes, interbasin gradients in water quality can exist, for example, due to (i) localized nutrient loading (e.g., Lake Michigan: Hamidi et al. 2015), (ii) differences in the thermal structure and productivity (e.g., Lake Erie: Bartish 1987), or (iii) different seasonal mixing regimes in adjacent basins of different depths (e.g., Lake Garda: Salmaso 2005; Lake Geneva: CIPEL 2016). Consequently, exchange processes between sub-basins, especially between their hypolimnia, can have significant ecological consequences (Jabbari et al. 2019, 2021), and can contribute to deepwater renewal (Boyce et al. 1980; Ahrnsbrak and Wing 1998; Reiss et al. 2021).

One important driver for interbasin exchange is wind stress, which can act indirectly through internal wave pumping (van Senden and Imboden 1989; Umlauf and Lemmin 2005; Flood et al. 2020) or geostrophic adjustment processes after the relaxation of coastal upwelling fronts (Jabbari et al. 2021). Coastal upwelling near the junction between basins can also give rise to baroclinic pressure gradients that drive hypolimnetic exchange flows (Lawrence et al. 2004; Schertzer et al. 2008; Liu et al. 2018). Furthermore, in the presence of stratification, along-axis winds can produce direct two-way advective exchange, where the mean downwind surface drift towards one basin is balanced by a hypolimnetic counterflow into the other basin (Laval et al. 2008; Niu et al. 2015; Reiss et al. 2021). In large lakes, the two-layer exchange pattern is modified by the Coriolis force, resulting in a tilted current-reversal interface, perpendicular to the flow direction (Bartish 1987; Anderson and Schwab 2017; Reiss et al. 2021). Interbasin exchange is often governed by a combination of the aforementioned processes (e.g., Anderson and Schwab 2017).

Overall, stratification plays an important role in wind-induced interbasin exchange processes, not only by imposing a vertical two-layer structure of the velocity field, but also by producing baroclinic pressure gradients between the basins.

Numerous studies have shown that climate change-induced warming has and will continue to alter the thermal structure of lakes, for example, by reducing the maximum mixed-layer depth

and prolonging the stratified period (e.g., Perroud and Goyette 2012; Goldman et al. 2013; Mesman et al. 2021). This raises the question of how changes in stratification will be reflected in interbasin exchange processes, for example, by modulating the strength of the net volume exchange or by suppressing hypolimnetic exchange altogether.

Recently, Reiss et al. (2021) investigated wind-induced interbasin exchange and upwelling between the deep *Grand Lac* and shallow *Petit Lac* basins of Lake Geneva (Figure 4.1) during early winter when both basins are still weakly stratified. It was demonstrated that under these conditions, strong winds from the southwest produced a “current loop,” whereby deep, hypolimnetic *Grand Lac* water was first drawn into the *Petit Lac*, then transported far into the shallow basin by vigorous bottom currents, before finally descending back into the *Grand Lac* hypolimnion. In addition, it was shown that strong bottom currents in the *Petit Lac* can persist for more than 1 d after the wind ceased, maintaining a steady inflow of upwelled water, and that Coriolis-induced rightward veering of the latter simultaneously produces coastal upwelling in the shallow and narrow *Petit Lac*.

In the present study, we examine how the wind-induced exchange between the basins of Lake Geneva is modified by the presence or absence of thermal stratification in its shallow basin (*Petit Lac*). To achieve this, we combined field observations, three-dimensional (3D) numerical modeling and particle tracking. Furthermore, model-based momentum budget analyses allowed determining the role of baroclinicity and rotational effects on the wind-induced exchange flow. To our knowledge, such an investigation of these aspects under these conditions has not been carried out on a lake before. Thus, our findings can be expected to make a significant contribution to understanding these lesser-known alternative deepwater renewal mechanisms that are expected to become increasingly important as convective cooling weakens due to global warming.

The following questions are addressed:

- What are the driving mechanisms behind the strong, steady bottom currents carrying cold hypolimnetic waters into the *Petit Lac* that were observed by Reiss et al. (2021)?
- How are the axial and transversal circulation patterns in the *Petit Lac* affected by stratification, and what are the implications on the strength of the interbasin exchange?



- Is the vertical structure of the exchange modified by stratification? If so, can hypolimnetic upwelling between the basins occur when the *Petit Lac* is fully mixed?
- How is the wind-induced circulation between the basins modified by Coriolis force and is there a difference between the fully-mixed and stratified situation?

Additional clarifications and details on certain topics mentioned in the text are provided in a Supporting Information (SI) section (figures, tables marked with prefix S).

## 4.2 Materials and methods

### 4.2.1 Study site

Lake Geneva (local name: *Lac Léman*), Western Europe's largest freshwater lake, is a deep, monomictic lake between Switzerland and France. It has a volume of 89 km<sup>3</sup>, a surface area of 580 km<sup>2</sup>, and a theoretical residence time of 11 y (CIPEL 2019).

The lake has a total length of 73 km and is composed of two basins: (i) the large, eastern *Grand Lac* (maximum width 14 km and depth 309 m), and (ii) the small, western *Petit Lac* (maximum width 5 km and depth 75 m), joined at a 3.5-km wide and 65-m deep “confluence” (Figure 4.1). The shallow *Petit Lac* annually destratifies completely, typically by early January, whereas the deeper *Grand Lac* remains weakly stratified throughout most seasons with the maximum mixing depth reaching 100 to 150 m in late February or early March. Complete convective overturning in the *Grand Lac* only occurs during severely cold winters (CIPEL 2019).

The different mixing regimes result in biochemical gradients between the hypolimnia of the two basins, notably in dissolved oxygen (higher values in the *Petit Lac*) and nutrient concentrations (higher values in the *Grand Lac*) (e.g., CIPEL 2016; Lavigne and Nirel 2016). This implies that hypolimnetic exchange processes between the basins may have important effects on the lake's overall ecological state.

The lake is bordered by the Alps in the south and the Jura mountains in the northwest. Two large-scale, strong wind fields that are guided by this topography dominate the region, namely the *Bise* coming from the northeast and the *Vent* from the southwest; both approximately aligned with the main axis of the *Petit Lac* (Graf and Prost 1980; Wanner and Furger 1990; Lemmin and D'Adamo 1996). These winds are characterized by high wind speeds (5 – 15 m s<sup>-1</sup>) often lasting for several days, thus considerably impacting the lake's hydrodynamics, for

example, in the form of deep coastal upwelling (Reiss et al. 2020), enhanced interbasin exchange due to internal Kelvin waves (Umlauf and Lemmin 2005), and wind-induced interbasin upwelling (Reiss et al. 2021).

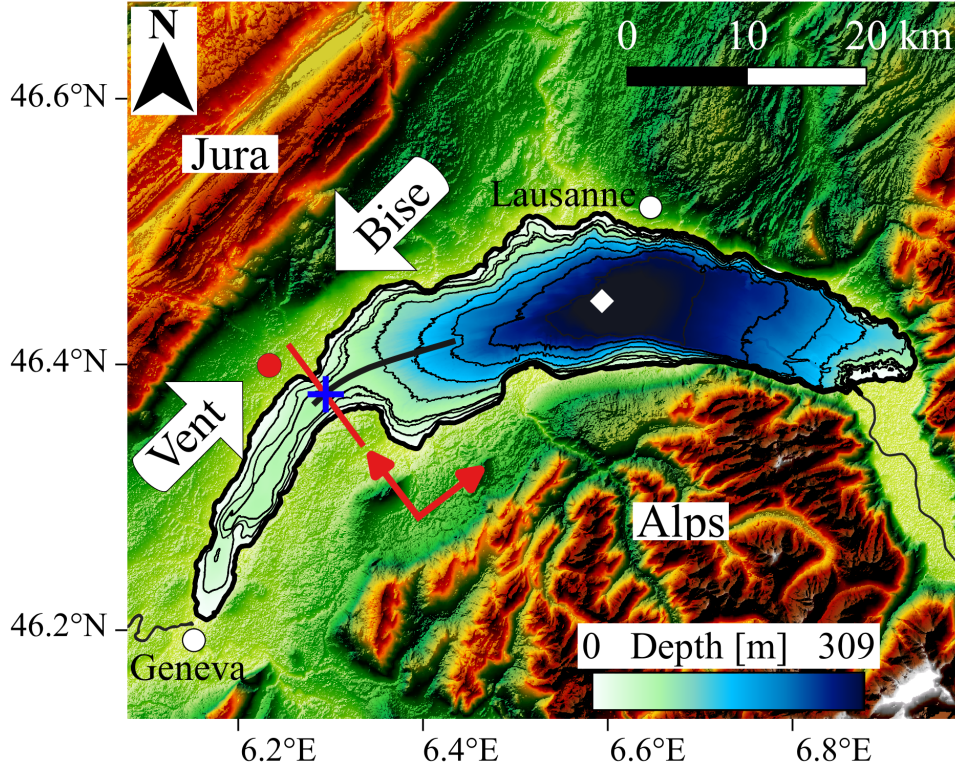


**Figure 4.1.** Bathymetric map of Lake Geneva including the surrounding topography. The white arrows indicate the direction of the two strong dominant winds called *Bise* and *Vent*, channeled by the Alps and Jura mountains, that frequently blow over large areas of the lake. The red line approximately delimits the confluence between the two basins composing Lake Geneva, i.e., the small *Petit Lac* and the large *Grand Lac*. The blue cross in the center of the confluence shows the mooring location. Meteorological data were recorded at the MeteoSwiss station in Nyon (red circle) and the white diamond marks the location of the CIPEL monitoring station SHL2 (depth 309 m). Depth is given in meters in the colorbar legend and by the isobath contours (0, 25, 50, 60, 100, 150, 200, 250, 300 m). The model results shown in Figures 4.5 and 4.6 were evaluated along the black and red lines, with the red arrows giving the positive transversal and axial directions referred to in the momentum budget analysis.

#### 4.2.2 Field observations

In the present study, we use data from a mooring deployed at 65-m depth in the center of the confluence between the *Petit Lac* and *Grand Lac* basins (Figure 4.1, blue cross) that was part of a field campaign carried out in Lake Geneva during winter 2018/2019 (Reiss et al. 2021).

The mooring consisted of a bottom-mounted, upward-looking 300 kHz Teledyne-RDI Workhorse Sentinel ADCP (Acoustic Doppler Current Profiler), with a 10-m long thermistor line (vertical sensor spacing 1 m) attached to the top. The coordinate system for the current velocities was rotated to be aligned with the along- and cross-axis directions of the *Petit Lac*, herein after referred to as axial and transversal directions, respectively (Figure 4.1). Prior to the analysis, 2-h and 10-min moving averages were applied to the ADCP and thermistor data, respectively. The instrument settings are summarized in Table S4.1 in the Supporting Information (SI).

The typical depth of the thermocline in Lake Geneva during early and late winter was inferred from Conductivity Temperature Depth (CTD) profiles provided by the Commission Internationale pour la Protection des Eaux du Léman ([CIPEL](#), last accessed on 3 June 2021; Rimet et al. 2020) at the deepest point of the lake (309 m; SHL2 in Figure 4.1)

Wind speed and direction were recorded every 10 min at a meteorological station maintained by the Swiss National Weather and Climate Service ([MeteoSwiss](#); last accessed on 3 June 2021) located in Nyon, approximately 5 km northwest of the confluence.

#### 4.2.3 Hydrodynamic model

The three dimensional (3D) hydrodynamic model used in this study is based on a hydrostatic version of the MITgcm code (Marshall et al. 1997), with a configuration similar to that employed by Cimadoribus et al. (2018), who performed a detailed validation based on various field observations around the lake. Furthermore, the model was recently applied to Lake Geneva to investigate wind-driven coastal upwelling (Reiss et al. 2020) and wind-induced interbasin exchange (Reiss et al. 2021) during winter. Except for the initial conditions and external forcing, the model configurations used in this study are the same as those detailed in Reiss et al. (2021).

The domain was discretized by a uniform horizontal Cartesian grid with a resolution of 113 m and 100 size-varying z-layers, ranging from 30 cm at the surface to 2.8 m at the deepest point of the confluence and 4.8 m at the bottom of the *Grand Lac*.

To determine the effect of stratification on wind-induced interbasin exchange, two simulations were run, with identical external forcing, but different initial lake temperature fields. Two idealized temperature profiles were generated (Figure 4.2), representing the lake’s typical stratification in December and February/March, hereinafter referred to as early and late winter, respectively.

Realistic surface forcing for a typical winter *Vent* wind event was obtained from the COSMO-1 numerical weather model provided by MeteoSwiss (Voudouri et al. 2017). To allow a comparison of the results obtained in the present study for early winter with the ones discussed in Reiss et al. (2021), we used the COSMO-1 data for the same period, i.e., from 7 to 18 December 2018.

This period included a 2.5-d *Vent* event, with mean and maximum wind speeds of approximately  $6 \text{ m s}^{-1}$  and  $11 \text{ m s}^{-1}$ , respectively (Reiss et al. 2021). The MITgcm internal calendar was set such that the early winter simulation ran from 7 to 18 December 2018 and the late winter one from 7 to 18 March 2019.

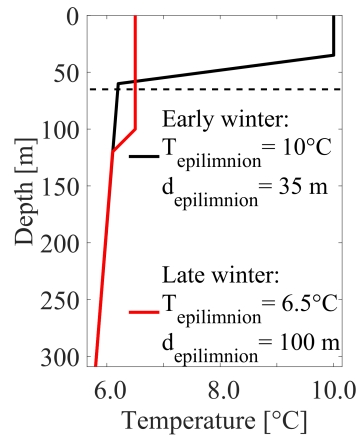


**Figure 4.2.** Idealized temperature profiles, representing the typical early (December; black line, epilimnion depth,  $d_{\text{epilimnion}}$  of 35 m) and late (March; red line,  $d_{\text{epilimnion}}$  of 100 m) winter stratification in Lake Geneva, used to initialize the hydrodynamic model. The dashed horizontal line marks the maximum depth of the confluence.

The simulations were initialized with zero velocity. Considering the strong, persistent wind stress that rapidly induces a strong circulation, this did not notably affect the results, as confirmed by the good agreement with the results discussed in Reiss et al. (2021), whose model was run with a 3-month spin-up period.

To shed light on the driving mechanisms behind interbasin exchange in Lake Geneva under different stratifications, we considered momentum balances at the confluence (Figure 4.1). The diagnostics module of the MITgcm model allows storing all terms of the momentum budget equations in both horizontal directions of the grid, and at all grid cells in the domain. The vector terms were linearly interpolated onto the (vertical) confluence transect and rotated to be aligned with the along- and cross-axis directions of the *Petit Lac*, hereinafter referred to as axial and transversal directions, respectively (Figure 4.1). The full momentum budget equation considered here takes the form:

$$\frac{\partial \mathbf{v}_h}{\partial t} = P_c + P_t + C + A + D, \quad (4.1)$$

where  $\partial \mathbf{v}_h / \partial t$  is the horizontal acceleration vector,  $P_c$  the baroclinic and  $P_t$  the barotropic pressure gradients,  $C$  is the Coriolis acceleration,  $A$  is the nonlinear advection term, and  $D$  represents the dissipation due to bulk and bottom friction (hereinafter referred to as friction). Note that the external forcing term acting on the surface cells (e.g., Cimatoribus et al. 2018), is not explicitly included since it is not relevant for the cell-wise momentum balances in the interior. Instead, the effect of the external forcing can be seen in the frictional terms.

#### 4.2.4 Particle tracking

The particle tracking code used here, developed by Cimatoribus (2018) and based on the method described by Döös et al. (2013), was previously applied to Lake Geneva to study: (i) the transport of inflowing water from the lake’s main tributary (Rhône River) (Cimatoribus et al. 2019), (ii) wind-driven coastal upwelling at the northern *Grand Lac* shore (Reiss et al. 2020), and (iii) wind-induced interbasin exchange and upwelling between the *Grand Lac* and *Petit Lac* in early winter (Reiss et al. 2021). Our simulation approach closely followed that of Reiss et al. (2021) and is therefore only briefly be outlined here.

The origin of the deep *Petit Lac* waters could be traced by backward tracking of particles released in the bottom layers of the shallow basin. Particles were released every 4 h during the first 5 d of the wind event, in an approximately 3 km by 5 km wide area near the confluence, at every vertical grid point below 40-m depth (Figure S4.1), resulting in a total of more than 200,000 particles.

## 4.3 Results and discussion

Reiss et al. (2021) investigated *Vent* wind-induced interbasin exchange and coastal upwelling in the weakly stratified *Petit Lac* during early winter. Under these conditions, deep hypolimnetic waters from the *Grand Lac* can upwell into the *Petit Lac*, where they form a current loop by first being transported far into the shallow basin, and then descending back into the *Grand Lac* hypolimnion, over the course of one week. In this section, we first revisit parts of the same observational data set to highlight the differences between early and late winter stratification. Then, we determine how stratification affects the *Vent*-induced circulation near the confluence by means of hydrodynamic modeling and particle tracking.

### 4.3.1 Field observations

Figure 4.3 shows hourly-averaged wind speeds and directions measured at the Nyon station (Figure 4.1) near the confluence, as well as currents and temperatures recorded in the center of the confluence (Figure 4.1, blue cross) from 8 to 10 December 2018 (hereinafter referred to as early winter; left panels) and from 9 to 11 March 2019 (hereinafter referred to as late winter; right panels), respectively. Full-depth current velocity and direction profiles for both periods are given in Figure 4.4.

The two *Vent* wind events were comparable in duration and strength, with overall mean wind speeds of 5.5 and 4.9 m s<sup>-1</sup> and maximum hourly averages of 10.7 and 9.4 m s<sup>-1</sup> in early and late winter, respectively. Typical of *Vent* conditions, the wind fields were spatially relatively homogeneous and approximately aligned with the main axis of the *Petit Lac*, as shown by the COSMO-1 model wind fields (Figure S4.2).

Prior to the early winter *Vent* wind event, there was a weak thermocline at approximately 35-m depth, with temperatures in the *Petit Lac* epilimnion and hypolimnion of ~10°C and 6.3°C, respectively (Reiss et al. 2021). In March, on the other hand, temperatures in the *Petit Lac* were nearly homogeneous around 6.5°C, and a weak thermocline in the *Grand Lac* was formed below 100-m depth (Figure S4.3).

In early winter, a few hours after the wind started, a distinct two-layer flow pattern, with opposing current directions and a sharp reversal at the thermocline depth, was established (Figures 4.3d and 4.4). While the currents in the epilimnion were approximately aligned with the wind (Figure 4.3a) and directed towards the *Grand Lac* (hereinafter referred to as outflow, Figure

4.3d, e), a countercurrent into the *Petit Lac* prevailed in the hypolimnion (hereinafter referred to as inflow, Figure 4.3d, g). In both layers, current velocities exceeded  $20 \text{ cm s}^{-1}$ . However, the bottom currents were considerably steadier and stronger, with maximum velocities above  $27 \text{ cm s}^{-1}$  (Figure 4.3b). Even though the bottom inflow became weaker after the wind stopped, it persisted for approximately another 1.5 d (Figure S4.4). The flow in both the epi- and hypolimnion was vertically unidirectional, i.e., there was little variation in the current direction with depth in each layer (Figure 4.4b). Shortly after the onset of the bottom inflow, temperatures gradually and continuously decreased. This is due to upwelling of cold, deep *Grand Lac* water, as discussed by Reiss et al. (2021).

Despite comparable external forcing, in March, the currents at the confluence were weaker and less steady than in December. The highest velocities of  $\sim 10 \text{ cm s}^{-1}$  were observed in the topmost ADCP bin at approximately 6-m depth, coinciding with the period of maximum wind speeds (Figure 4.3h, i). The measured velocities showed significant variability and no apparent two-layer structure. However, it was observed that: (i) the currents in the upper layers were more often directed towards the *Grand Lac* than those in the interior (Figure 4.3k), (ii) unlike in early winter, they were never aligned with the wind, but instead were deflected approximately  $30^\circ$  to  $90^\circ$  to the right, and (iii) the rightward deflection increased with depth, producing a veering current structure resembling that of a surface Ekman spiral (Figures 4.3h, l, m and 4.4).

The temperatures in the lower layer of the confluence remained fairly stable throughout the late winter wind event, except for small fluctuations at around 23:00 (local time) on 9 March. These were associated with increased current velocities in the middle of the water column (Figure 4.3i, j, m) and were most pronounced at the topmost thermistor, i.e., 10 m above the lakebed, suggesting the temporary downwelling of slightly warmer surface waters. The temperatures 1 m above the lakebed remained nearly constant (within  $\pm 0.03^\circ\text{C}$ ) during the entire period (not shown). Altogether, the observations during late winter showed no signs of upwelling of cold, hypolimnetic *Grand Lac* water into the *Petit Lac* (compare Figure 4.3c and j). Furthermore, the currents in the entire water column were significantly weaker, with their vertical structure in the upper layers apparently strongly influenced by Coriolis force.

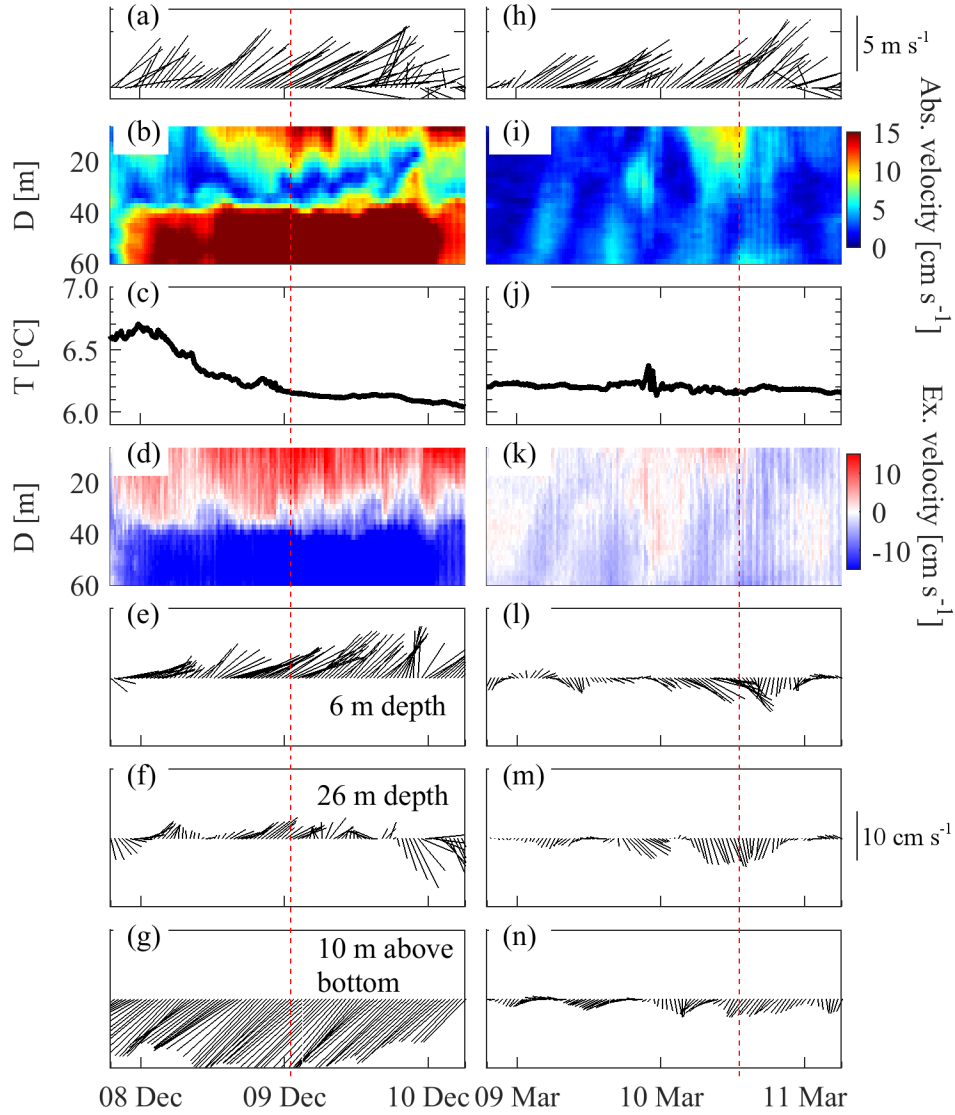


**Figure 4.3.** Wind vectors (a, h) and mooring data (b-g, i-n) recorded from 8 to 10 December 2018 (a-g; left panels) and 9 to 11 March 2019 (h-n; right panels), respectively. The mooring data panels from top to bottom show: absolute current velocity (b, i), depth-averaged temperature (T) in the bottom-most 10 m (D is depth) (c, j), “interbasin exchange velocity” (d, k), as well as current velocity and direction at 6-m depth (e, l), 26-m depth (f, m), and 10 m above the bottom (g, n). Interbasin exchange velocities were obtained by projecting the velocity vectors onto a plane perpendicular to the confluence transect (Figure 4.1, red arrow). The colorbars give the magnitude of the absolute and interbasin exchange velocities. The scale of the wind and current quivers is the same for both periods and is given next to panels h and m. The quiver heads point in the direction of travel, with the positive y- and x-direction corresponding to north ( $0^\circ$ ) and east ( $90^\circ$ ). The red dashed lines mark the times of the velocity profiles shown in Figure 4.4. Meteorological data were recorded at the MeteoSwiss station in Nyon (Figure 4.1, red circle). See Figure 4.1 (blue cross) for mooring location.



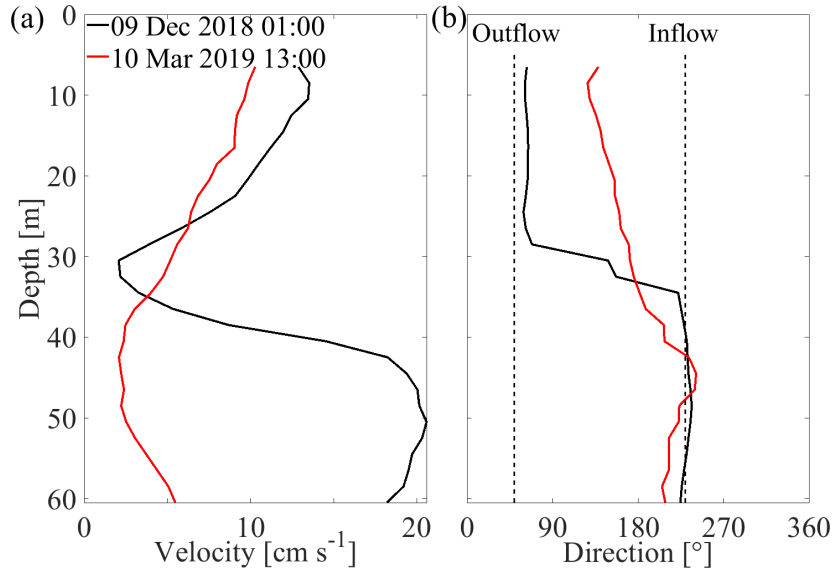


**Figure 4.4.** Current velocity (a) and direction (b) recorded at the confluence center (Figure 4.1, blue cross) during the *Vent* wind events in December 2018 (solid black lines) and March 2019 (red lines), respectively. The exact dates are given in the legend in (a). The dashed black lines mark the outflow and inflow directions. The times of the profiles are marked in Figure 4.3 by the red dashed lines.

#### 4.3.2 Model results

The field observations showed that the *Vent*-induced flow patterns at the confluence strongly differed between early stratified and late destratified winter. In the following sections, the effect of stratification on the temporal development of the wind-induced circulation at the confluence between the two basins is further investigated with the 3D hydrodynamic model. Four-hour moving averages were applied to the model results (temperature, velocities, and momentum budget terms) prior to the analysis.

#### *Temperature field*

Figure 4.5 shows the modeled temperatures near the confluence along the transect marked in Figure 4.1, before and 1.5 d after the wind started. In early winter, the lake was stratified, with a thermocline at approximately 35-m depth (Figure 4.5a). By late winter, the thermocline had descended to approximately 100-m depth, yielding a fully mixed *Petit Lac* and a hypolimnion in the *Grand Lac* (Figure 4.5b). Note that the initial temperature fields below 120-m depth were identical in both simulations, as illustrated by the dashed 6.1°C isotherm lines in Figure 4.5a, b (see also Figure 4.2).

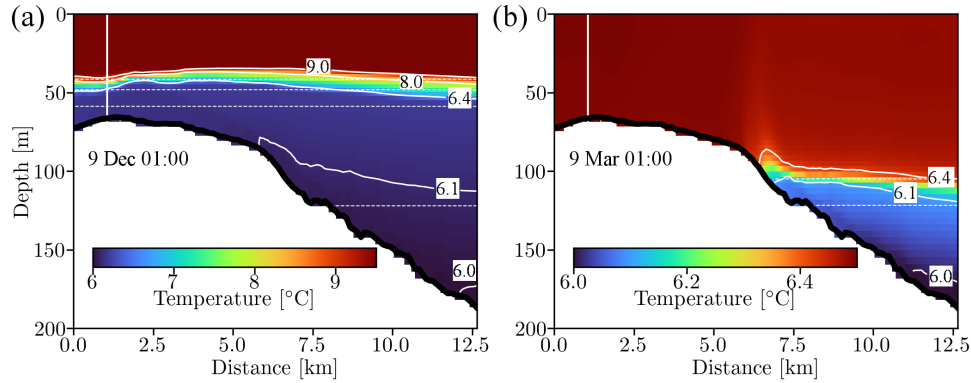


**Figure 4.5.** Modeled temperatures along a curved transect, approximately following the central axis of the lake and perpendicular to the confluence (Figure 4.1, black line), during early (a) and late (b) winter. The white vertical lines mark the location of the confluence center, i.e., where the mooring was deployed (Figure 4.1, blue cross). Temperatures are given by the colorbars. The white lines depict selected isotherms, both before (dashed white lines) and 1.5 d after (solid white lines) the *Vent* wind started. Distance is given along the transect starting at its southwestern end, approximately 500 m west of the confluence (Figure 4.1, black line).

Under both stratifications, the *Vent* wind (from the southwest; approximately blowing from left to right in Figure 4.5), caused upward tilting of the isotherms towards the western end of the *Grand Lac*, i.e., towards the confluence.

In early winter, the maximum isotherm tilt occurred ~2 to 4 km east of the confluence where the mooring was deployed. West of the mooring location, i.e., further into the *Petit Lac*, the isotherms were also displaced upwards compared to pre-wind conditions, but to a lesser extent (Figure 4.5a). The upwelling at the western end of the *Grand Lac* and the discontinuous upward tilt of the isotherms across the confluence can be explained by the significantly different widths of the two basins: The wind-induced surface drift in the narrow *Petit Lac* was not sufficient to balance the one in the wider *Grand Lac*, resulting in upwind upwelling in that basin, similar to what was observed previously in Lake Constance (Appt et al. 2004).

With the greater thermocline depth in late winter, the two basins were decoupled, and the upwind upwelling was limited to the *Grand Lac*, with the maximum isotherm tilt occurring below the deepest point of the confluence (Figure 4.5b). As a consequence, the stratification at the confluence and in the *Petit Lac* was not affected by the *Grand Lac* upwelling and the shallow basin remained well-mixed, as confirmed by field measurements (Figure 4.3).

### ***Development of the axial and transversal circulations at the confluence***

To illustrate the temporal development that leads to the measured bottom-intensified inflow and unidirectional outflow in early winter, as well as the veering surface currents in late winter (Figure 4.4), the following three phases are discussed below in detail: (i) Initialization phase:  $\sim 4$  h after wind started, (ii) adjustment phase:  $\sim 12$  h after wind started, and (iii) fully-developed circulation:  $\sim 1.5$  d after wind started. Note that the selected times do not necessarily mark the start or end of each phase, but instead are representative for the prevailing currents.

The modeled current velocities at the confluence during the three phases, both in the axial (in- and outflow; blue and red colors) and transversal (cross-shore flow at the confluence; black arrows) directions are shown in Figure 4.6. Hereinafter, unless stated otherwise, rightward and leftward transversal currents are with respect to the outflow direction into the *Grand Lac*, that is, when looking into the page in Figure 4.6. Corresponding full-depth modeled current velocity and direction profiles at the confluence center are presented in Figure 4.7. The corresponding profiles of the axial and transversal velocity components are given in Figure S4.5.

#### ***Initialization phase***

A few hours after the wind started, the current patterns were similar in both the early and late winter stratification cases (Figure 4.6a, b). The strong wind stress initiated an outflow towards the *Grand Lac* in the uppermost 10 m, which was balanced by a weaker inflow distributed over the entire depth range below. The current velocities were highest near the surface, reaching  $10 \text{ cm s}^{-1}$  in early winter and  $8 \text{ cm s}^{-1}$  in late winter.

A weaker secondary circulation developed in the transversal direction, with the highest velocities  $\sim 1.5 \text{ cm s}^{-1}$  found close to the surface in both cases (Figure S4.5a, b). The transversal currents in the upper layers were oriented to the right, i.e., towards the southern shore, and were balanced by weaker leftward currents, towards the northern shore, in the layers below (Figure 4.6a, b).

In both cases, the net currents in the upper layers at the center of the confluence described a spiraling motion, i.e., with increasing depth, magnitudes decreased and directions veered to the right (Figure 4.7 black curves). In early winter, the initially horizontal isotherms began to tilt slightly upward towards the northern shore (Figure 4.6a).

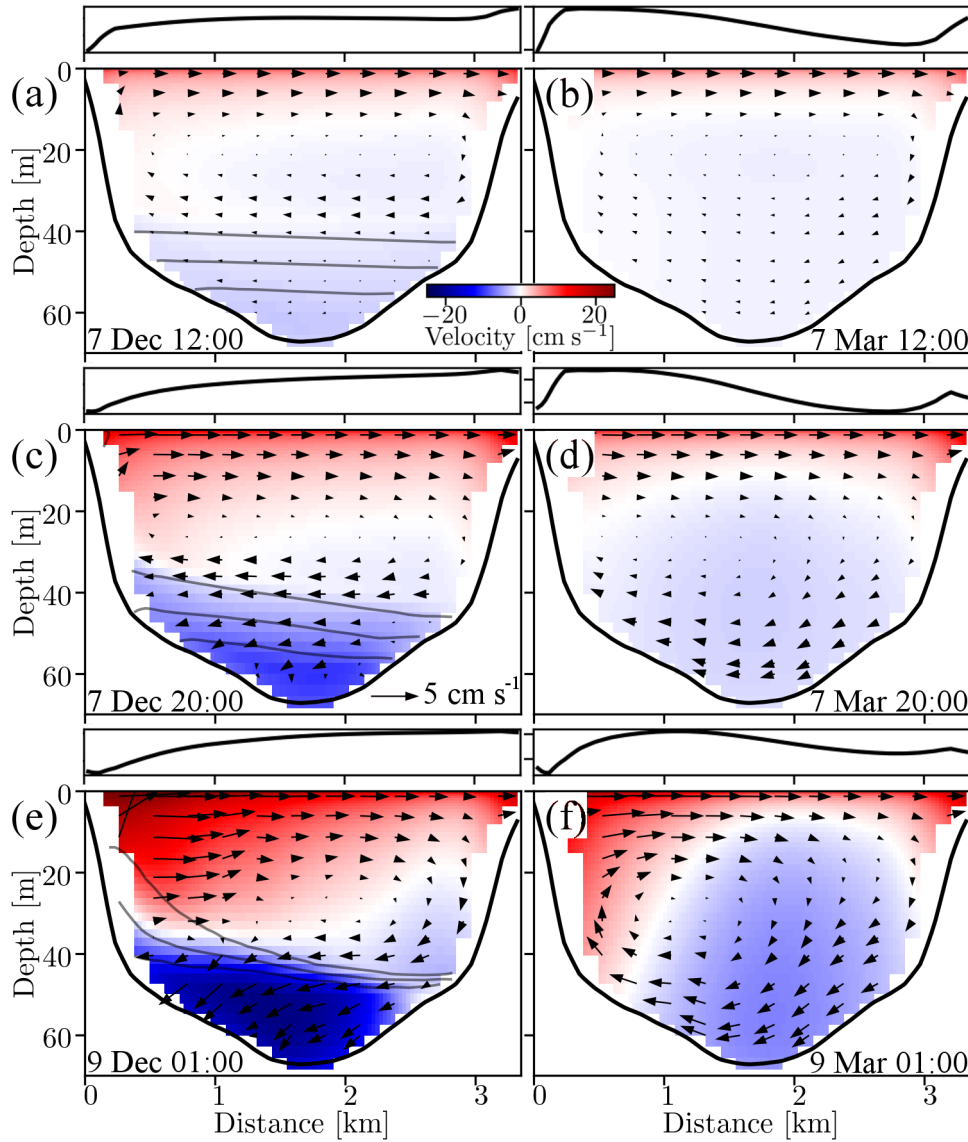


**Figure 4.6.** Modeled current velocities at the confluence, during the initialization (a, b) and adjustment (c, d) phases, and when the circulation was fully developed (e, f), in early winter (left panels) and late winter (right panels), respectively. Axial and transversal velocities are depicted by color (see colorbar in panels a-b) and black arrows, respectively. The grey contour lines in the left panels mark the 7, 8 and 9°C isotherms (from bottom to top). Red color indicates outflow into the *Grand Lac* and blue color inflow into the *Petit Lac*. The black curve above each 2D transect shows the shape of the corresponding modeled free surface elevation. Distance is given along the transect from the northern shore. The location of the transect and orientation of the axial and transversal directions are shown in Figure 4.1. The transversal velocity scale is given in panel (c). For better visualization, vertical velocities are scaled up by a factor of 20.

### *Adjustment phase*

As the wind stress continued, both the axial and transversal circulations became stronger, and differences between the two simulations emerged (Figure 4.6c, d).

In early winter, the stratification imposed a clear two-layer flow with strong, bottom-intensified inflow currents in the hypolimnion balancing the wind-driven epilimnetic outflow. The thermocline continued tilting upwards towards the northern shore (Figures 4.6c and 4.7a, b).

In the fully-mixed late winter case, the downwind outflow was more pronounced in the shallow regions near the shores, where it extended over the entire water column until a depth of 30 m. Away from the shores, the outflow at the confluence center was limited to the uppermost 10 m and an upwind inflow prevailed in most of the transect. This resulted in a dome-shaped zero isotach (white region separating the in- and outflow in Figure 4.6d). Furthermore, the inflow in late winter was weaker than in early winter, and almost uniform in strength over depth (Figure 4.7c).

In both cases, the transversal circulation resembled a clockwise vortical motion, with near-zero velocities in the center, leftward currents in the lower layers balanced by the rightward near-surface currents, and down- and upwelling at the right and left boundaries, respectively. While this transversal vortex spanned the entire water column in the fully-mixed case, it was confined to the epilimnion when stratification was present (Figure 4.6c, d).

The magnitudes of the transversal currents near the surface were similar in both cases. However, due to the stronger and deeper-reaching outflow in early winter, the net currents in the epilimnion gradually approached a more unidirectional structure, whereas they continued veering with depth in late winter (Figures 4.7b, d and S4.5c, d).

### *Fully-developed circulation*

In early winter, the two-layer structure further strengthened and 1.5 d after the wind started, inflowing and outflowing velocities were comparable and both exceeded  $20 \text{ cm s}^{-1}$  (Figures 4.6e and 4.7a). The net currents in the two layers were nearly unidirectional and aligned with the axial direction, with a sharp current reversal around the thermocline depth (Figure 4.7b). Furthermore, the core of the bottom inflow was shifted towards the northern shore and the thermocline upwelling continued, with the  $9^\circ\text{C}$  isotherm, which was initially at

42-m depth, almost reaching 10-m depth. This shows that the bottom inflow was strongly modified by Coriolis force, as will be discussed below in the momentum budget analysis (see also Reiss et al. 2021).

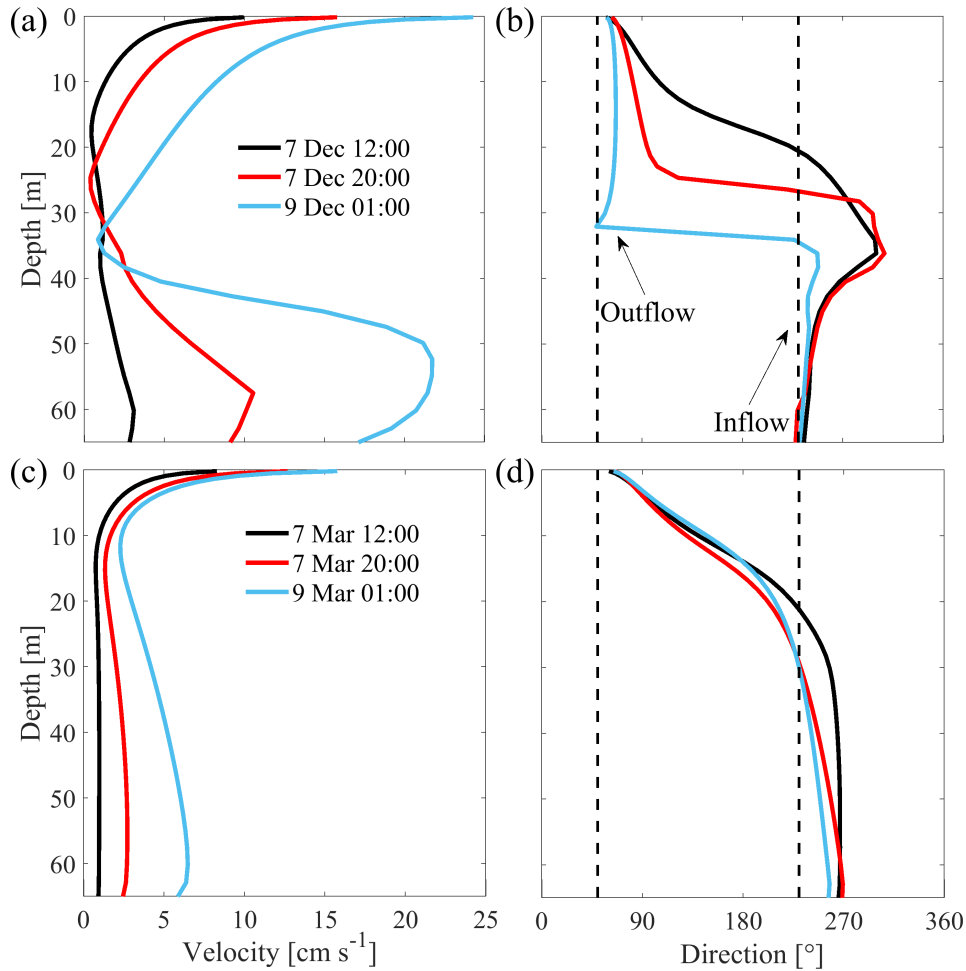


**Figure 4.7.** Modeled current velocity (**a**, **c**) and direction (**b**, **d**) at the confluence center during the initialization (black) and adjustment (red) phases, and when the circulation was fully developed (blue), in early winter (upper panels) and late winter (lower panels). The exact dates are given in the legend in (**a**) and (**c**). The vertical black dashed lines in (**b**) and (**d**) mark the outflow and inflow directions, respectively.

In late winter, the wide dome-shaped zero-isotach developed into an inverse U-shaped one, which was slanted to the right. The strongest downwind currents were found in the shallow regions near the shores, especially towards the northern shore, and the interior was dominated by upwind inflow (Figure 4.6f). At the center, the net currents near the surface maintained their

depth-veering structure, confining the outflow to the uppermost 5 to 10 m, and were approximately three times as strong as the inflow (Figure 4.7c, d). The transversal vortex grew stronger, with its center slightly shifted to the left (Figure 4.6f).

In both simulations, the outflow and rightward transversal currents at the northern shore were significantly stronger than along the southern shore (Figure 4.6e, f). This is probably due to: (i) gentler slopes and shallower banks along the northern *Petit Lac* shore, which cause stronger downwind currents in the north in both cases (Figure S4.6), and (ii) nearshore divergence at the northwestern end of the *Grand Lac* in early winter, which results in a surface depression northeast of the confluence, producing strong barotropic pressure gradients that accelerated the flow towards the *Grand Lac* in this section of the confluence (Figures S4.6, S4.7, and S4.8). This is further discussed in the Momentum budget analysis section below.

### ***Comparison of model results with observations***

The main features and differences of the *Vent*-induced circulation observed at the center of the confluence during December 2018 and March 2019 (Figure 4.4) were well reproduced by the numerical model (Figure 4.7).

The fully-developed early winter circulation was characterized by a two-layer pattern, with comparably strong outflows in the epilimnion and inflows in the hypolimnion. The currents were aligned with the main axis of the *Petit Lac* and unidirectional over each layer, with a sharp current reversal around the thermocline depth. The flow adjustment in the upper layers during the first hours of the wind, i.e., from initially veering to unidirectional, was also observed in the ADCP measurements (compare Figures 4.7b and S4.10).

In late winter, currents at the confluence center were generally weaker and the highest velocities were found near the surface. Furthermore, the currents in the upper layer maintained a veering structure throughout the entire wind event.

### ***Momentum budget analysis***

In this section, the mechanisms that produce the observed and modeled current patterns at the confluence center are investigated by model-based momentum budgets. The temporal development is discussed by considering the three phases (initialization, adjustment and fully developed circulation) introduced in the previous section. Figures 4.8 and 4.9 show the leading terms in the axial and transversal momentum balances, respectively, along a full-depth profile

at the confluence center in early (left panels) and late (right panels) winter. Positive terms in the axial balances are directed into the *Grand Lac* and towards the northern shore in the transversal balances (Figure 4.1, red arrows). For clarity, only the total pressure gradient (barotropic and baroclinic) is shown in the axial balances, with any deviation from the value at the surface indicating baroclinicity. In the transversal balances, the baroclinic pressure gradient is explicitly given. The nonlinear advection term is not shown because it was generally not of leading order (exceptions are discussed below). Two-dimensional (2D) transects of the time-averaged axial momentum terms at the confluence are given in Figures S4.8 and S4.9.

### *Initialization phase*

Shortly after the wind started, the axial momentum balances in the upper layer were similar in both simulations. The wind stress-induced friction was by far dominant, penetrating down to a depth of approximately 30 m (Figure 4.8a, b). The positive friction term was partly balanced by a negative barotropic pressure gradient, due to a water level setup induced by downwind surface drift (Figure S4.7). The transversal currents near the surface (to the right) induced an axial, negative Coriolis acceleration (into the *PL*). Its magnitude decreased with depth, until it changed sign below 20-m depth, which was the depth where the transversal currents changed from right- to leftward (Figure 4.6a, b). The net axial balance in the upper 15 to 20 m produced a strong acceleration (i.e.,  $\partial \mathbf{v}_h / \partial t$  in Eq. (4.1)) towards the *Grand Lac*.

In the fully-mixed late winter case, all axial terms below 30-m depth were constant, with the balance between the barotropic pressure gradient and the Coriolis acceleration resulting in an acceleration into the *Petit Lac*, approximately uniform in strength with depth. Note the constant total pressure gradient throughout the water column, which confirms that baroclinicity was negligible in late winter (Figure 4.8b). In contrast, in early winter, a negative baroclinic pressure gradient was evident below 35-m depth, i.e., below the thermocline, resulting in an enhanced acceleration into the *Petit Lac* near the bottom (Figure 4.8a).

As for the axial direction, the transversal momentum terms in the upper layers had a similar structure under both stratifications. In the uppermost 10 m, the wind-driven outflow produced a strong, negative Coriolis acceleration, which was largely balanced by positive wind-induced friction, indicating that the wind stress was not perfectly aligned with the along-axis direction (Figure 4.9a, b). Except for immediately below the surface, there was a weak negative net acceleration, explaining the rightward, transversal circulation in the upper layers (Figure 4.6a, b).



In late winter, all transversal terms were small below the wind-affected surface layers, with the barotropic pressure gradient opposing the Coriolis acceleration caused by the weak inflow in the interior. In early winter, due to the bottom-intensified inflow, the Coriolis acceleration towards the northern shore was approximately in geostrophic balance with the baroclinic pressure gradient induced by the onset of an upwards tilt of the thermocline (Figures 4.6a and 4.9a).

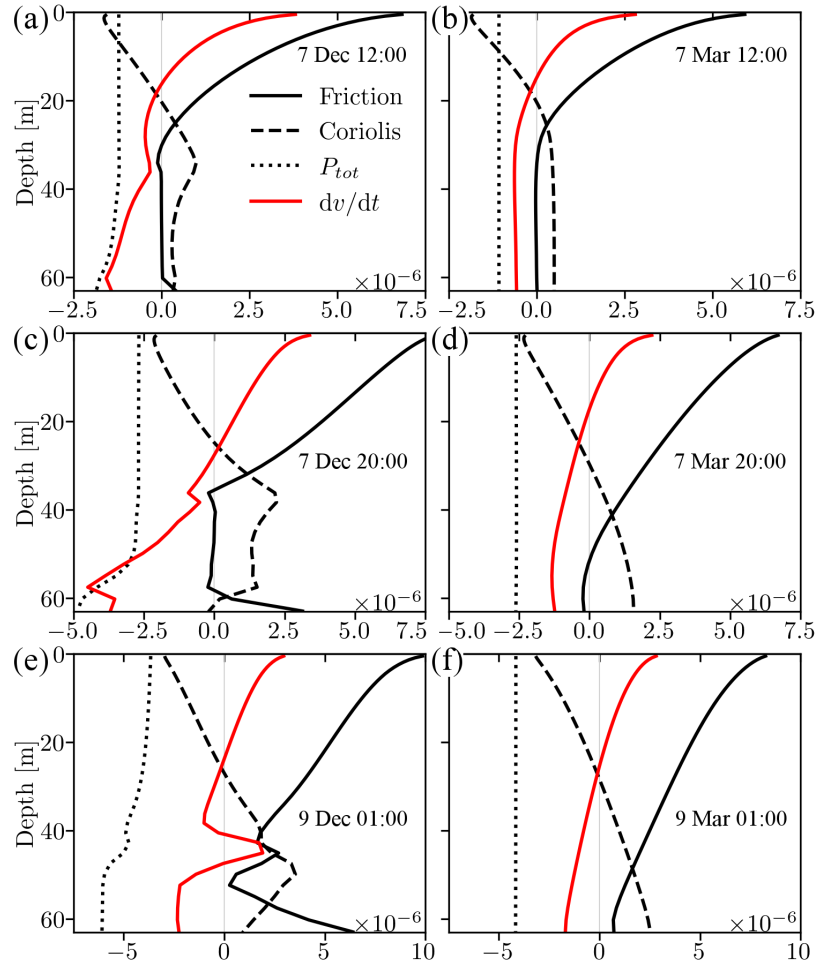


**Figure 4.8.** Leading terms of the axial momentum balance at the confluence center during the initialization (**a**, **b**) and adjustment (**c**, **d**) phases, and when the circulation was fully developed (**e**, **f**), in early winter (left panels) and late winter (right panels). The red curve gives the left-hand-side of the momentum balance equation, i.e., the local net acceleration (see Eq. (4.1)). The unit of the values on the x-axis is  $\text{m s}^{-2}$ . The orientation of the axial axis is shown in Figure 4.1. Lines are defined in panel (a), with  $P_{tot}$  giving the total pressure gradient term (baroclinic and barotropic) and any deviation from its value at the surface indicating baroclinicity. For clarity, the nonlinear advection term is not shown. Date and time are indicated in each panel.

### *Adjustment phase*

As in the initial phase, the increasing wind-induced axial friction was only partially balanced by the Coriolis and barotropic pressure gradient terms, resulting in a net acceleration of near-surface waters into the *Grand Lac* (Figure 4.8c, d). In the fully-mixed late winter case, the wind stress penetrated almost the entire water column, whereas it was confined to the epilimnion when stratification was present. Since the same wind energy was distributed over a smaller volume of water, this resulted in overall higher axial frictional forces in the upper layers, thus explaining the stronger near-surface outflow in early winter (Figures 4.6 and 4.7). As a consequence, the transversal Coriolis acceleration towards the southern shore was considerably higher in early winter (Figure 4.9c, d). This would imply stronger, Coriolis-induced, rightward currents in the upper layers. However, as discussed above, the transversal velocities were comparable in both cases (Figure 4.6c, d), which can be explained by the different signs of the transversal barotropic pressure gradients at the confluence center as follows:

In early winter, the relatively uniform outflow in the entire epilimnion and the accompanying rightward Ekman transport caused an upward tilt of the free surface from left to right (Figure 4.6c), resulting in positive transversal barotropic pressure gradients opposing the Coriolis acceleration (Figure 4.9c).

In late winter, on the other hand, transversal convergence and divergence between the outflow-dominated lateral shallows and the inflow-dominated interior produced an undulating free surface (Figure 4.6d). This resulted in negative transversal barotropic pressure gradients at the confluence center, acting together with the Coriolis acceleration (Figure 4.9d).

The opposing signs of the transversal barotropic pressure gradients, acting either with or against the Coriolis acceleration, can explain the differences in the vertical structure of the upper currents during the adjustment phase. While the net currents in the fully-mixed late winter case continued to veer strongly with depth, they approached a more unidirectional structure under early winter stratification (Figure 4.7b, d, red curves).

In the lower layers, the momentum balances during the adjustment phase showed a continuation of the trends observed during the first hours after the wind started. In early winter, the negative, axial baroclinic pressure gradients near the bottom, caused by upwind upwelling in the *Grand Lac* (Figure 4.5a) increased, further accelerating the hypolimnetic inflow. The stronger bottom

inflow resulted in higher axial bottom friction (Figure 4.8c) and transversal Coriolis acceleration (Figure 4.9c). This caused the thermocline to tilt further upward at the northern shore (Figure 4.6c), while maintaining a geostrophic balance with the resulting transversal baroclinic pressure gradients. In late winter, the weak inflow in the interior was mostly due to the axial barotropic pressure gradient, which was balanced by the friction and Coriolis terms (Figure 4.8d). The transversal terms were qualitatively similar to the initialization phase.

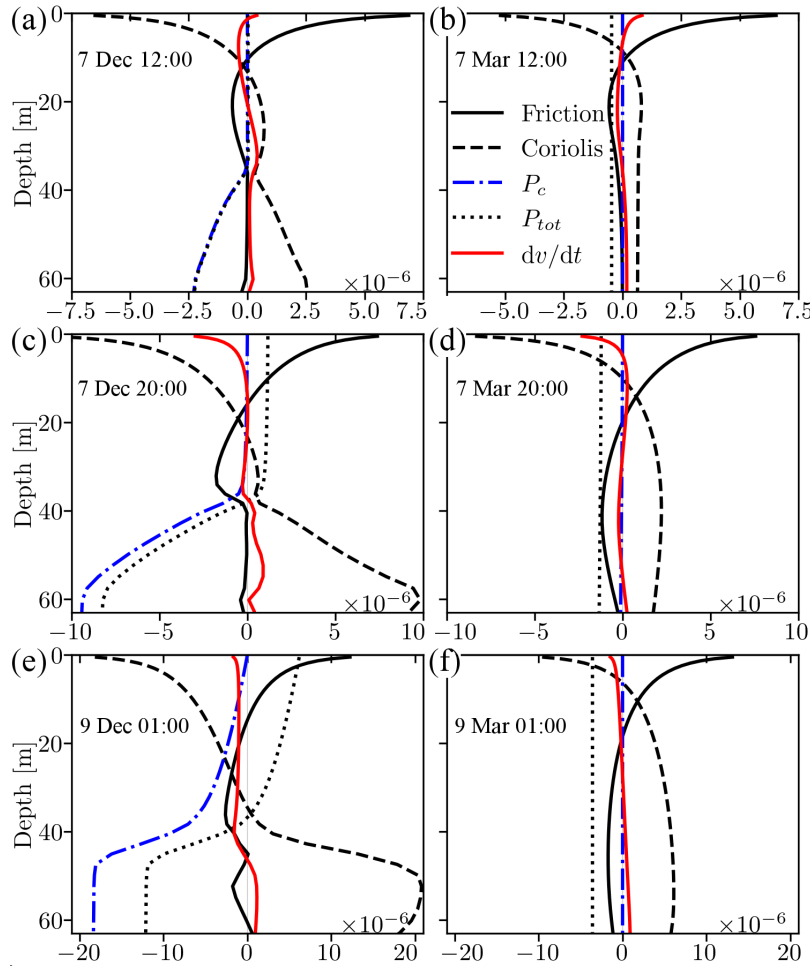


**Figure 4.9.** Leading terms of the transversal momentum balance at the confluence center during the initialization (a, b) and adjustment (c, d) phases, and when the circulation was fully developed (e, f), in early winter (left panels) and late winter (right panels). The red curve gives the left-hand-side of the momentum balance equation, i.e., the local net acceleration (see Eq. (4.1)). The unit of the values on the x-axis is  $\text{m s}^{-2}$ . The orientation of the transversal axis is shown in Figure 4.1. Lines are defined in panel (a). For clarity, the nonlinear advection term is not shown. Date and time are indicated in each panel.

### *Fully-developed circulation*

In the fully-mixed late winter case, the axial momentum balance of the fully-developed circulation was characterized by smooth profiles of the frictional and Coriolis terms, approximately linearly decreasing and increasing from top to bottom, respectively (Figure 4.8f). Transversally, the balance between the Coriolis, barotropic pressure gradient, and friction terms resulted in negative accelerations in the upper layers and positive accelerations in the lower layers, in agreement with the fully developed transversal, clockwise vortex (Figures 4.6f and 4.9f).

In contrast, in the stratified early winter case, axial baroclinicity grew more important as the wind stress continued, affecting almost the entire water column (Figure 4.8e) and indicating sustained upwind upwelling in the *Grand Lac* (Figure 4.5a). The thickness of the frictional bottom boundary layer also increased, which was reflected in the approximately logarithmic velocity profile in the lowest 15 m (Figures 4.4a and 4.7a). Note the “bump” in the net acceleration between 40 and 50-m depth (Figure 4.8e), which was caused by strong advection (not shown). This indicates that nonlinearity could be of leading order in the fully-developed, energetic early winter circulation, especially in the lower layers. The latter was likely due to the interaction of the strong currents with the local bottom topography (Cimatoribus et al. 2018), which is a known phenomenon in estuarine exchange (e.g., Giddings and MacCready 2017).

In the upper layers, the transversal Coriolis acceleration in early winter was almost twice as high as in late winter (Figure 4.9e, f). However, since it was largely balanced by the barotropic pressure gradient caused by the transversal free surface tilt (Figures 4.6e and 4.9e), the net currents in early winter were unidirectional throughout the epilimnion (Figure 4.7b blue curve), but they remained depth-veering in late winter (Figure 4.7d blue curve).

Furthermore, the transversal baroclinic pressure gradients, induced by coastal upwelling, and the Coriolis acceleration due to the bottom-intensified inflow, both doubled in strength, while maintaining a near-geostrophic balance (Figures 4.6e and 4.9e). As in the axial direction, the transversal nonlinear term near the bottom was substantial during early winter (not shown).

The fully-developed axial circulation in late winter resembled the wind-driven circulation in a non-rotating, elongated, non-stratified basin with sloping boundaries, as discussed, for example, by Winant (2004) and Sanay and Valle-Levinson (2005). This circulation is characterized

by intense downwind flow over the shallow banks and everywhere else near the surface, which is balanced by an upwind flow in the interior (e.g., Figure 11 in Winant 2004). In a rotating basin, deeper than one Ekman depth, the axial circulation is similar, but with reduced magnitude, while transversally a clockwise vortex (when looking downwind) develops that spans most of the cross-section (e.g., Winant 2004; Sanay and Valle-Levinson 2005; Ponte et al. 2012). Here, the Ekman depth is a measure relating frictional force to Coriolis force and is defined as  $d_E = \sqrt{2 K_v f^{-1}}$ , where  $f$  is the latitude-dependent Coriolis parameter,  $O(10^{-4} \text{ s}^{-1})$ , and  $K_v$  is the vertical eddy viscosity (e.g., Amadori et al. 2020). In the model employed in this study,  $K_v$  is computed by the K-profile parameterization (often referred to as KPP; Large et al. 1994) and can be output from MITgcm as a diagnostics term. Taking a typical value of  $K_v = 300 \text{ cm}^2 \text{ s}^{-1}$  for the eddy viscosity during the late winter *Vent* event as the cross-sectional average at the confluence, 1.5 d after the wind started (Sanay and Valle-Levinson 2005), we obtain an Ekman depth of  $d_E \approx 15 \text{ m}$ .

Considering a typical Ekman depth smaller than the maximum confluence depth (65 m), the elongated shape of the *Petit Lac*, and the spatially fairly homogeneous and steady *Vent*-wind, the late winter case studied here is comparable to those in the basins described in the literature, and can explain the general circulation patterns (Figure 4.6f). For a uniform wind acting on a symmetric basin and ignoring nonlinear effects, the resulting axial circulation is symmetrical with respect to the cross-section center (Winant 2004). However, Ponte et al. (2012) showed that the core of the upwind interior flow can shift towards the shores when nonlinear effects are included and a spatially varying wind field is imposed. This results in a slanted inverse-U-shaped zero-isotach, and is similar to the pattern observed here. In this case, the stronger downwind currents at the northern shore of the *Petit Lac*, caused by the gentler slopes and shallower banks, are probably the reason for the observed asymmetries in the axial and transversal circulation patterns (Figures 4.6f and S4.6). Note that the undulating free surface at the confluence (Figure 4.6, right panels) was also observed by Sanay and Valle-Levinson (2005) when considering rotation.

#### 4.3.3 Effect of stratification on interbasin exchange and hypolimnetic upwelling

##### ***Strength of interbasin exchange***

The observed differences in the circulation patterns between the stratified early winter and fully-mixed late winter cases have important consequences for the wind-induced interbasin

exchange in Lake Geneva during winter. Based on the modeled velocity field, the volume exchange across the confluence transect was estimated by integrating the inflowing (or outflowing) velocities in time and space (blue and red color areas, respectively in Figure 4.6). When considering the 2.5-d wind period, the accumulated volume transport into the *Petit Lac* was  $Q_{in,early} \approx 0.88 \text{ km}^3$  during early winter and  $Q_{in,late} \approx 0.46 \text{ km}^3$  during late winter. Furthermore, driven by the baroclinic pressure gradients at the confluence, the bottom inflow in early winter continued to flow for approximately 1.5 d, maintaining velocities of  $\sim 10 \text{ cm s}^{-1}$  (cf. Reiss et al. 2021). In late winter, however, the inflow rapidly weakened to 1 to  $3 \text{ cm s}^{-1}$  after the wind stress ceased. Taking this into account, we obtain  $Q_{in,early} \approx 1.64 \text{ km}^3$  and  $Q_{in,late} \approx 0.71 \text{ km}^3$ . The former suggests, that during a single early-winter *Vent* event, more than half of the total *Petit Lac* volume ( $\sim 3 \text{ km}^3$ ) was exchanged across the confluence. These findings are in agreement with Reiss et al. (2021), who showed by numerical modeling, that the strong, steady bottom inflow of cold, deep *Grand Lac* water during a December *Vent*-event resulted in a temporary doubling of the *Petit Lac* hypolimnetic volume. In late winter, however, the accumulated interbasin exchange was reduced by a factor of  $\sim 2.3$ , due to the weaker and veering currents.

### ***Horizontal and vertical exchange patterns and hypolimnetic upwelling***

Following Reiss et al. (2021), the origin of the deep *Petit Lac* waters was determined by backward tracking of particles released in the bottom layers of the shallow basin during the first days of the wind event. Figure 4.10 shows histograms of the particle origin depth, as well as the dominant pathways taken by particles coming from below 65-m depth, i.e., the maximum depth at the confluence, in the form of probability maps (e.g., van Sebille et al. 2018).

In early winter, more than half of the particles originated from below 65-m depth, with a significant number coming from depths between 100 to 200 m (Figure 4.10b), illustrating the upwelling of deep, hypolimnetic *Grand Lac* water. Furthermore, the upwelled particles traveled up to 20 km in the *Grand Lac* before entering the *Petit Lac*, suggesting that large areas of the *Grand Lac* hypolimnion were affected by the exchange (Figure 4.10a). These results are similar to those discussed in detail by Reiss et al. (2021), who showed that the *Vent*-induced circulation in Lake Geneva during early winter forms a “current loop,” whereby deep, hypolimnetic *Grand Lac* waters first upwell into the *Petit Lac*, are then transported more than 10 km into the *Petit Lac* basin, before finally descending back into the hypolimnion of the *Grand Lac*.

In contrast, in late winter, only 5% of the particles originated from below 65-m depth in the *Grand Lac*, with virtually none coming from below the thermocline (Figure 4.10d). This confirms that the upwind upwelling in the *Grand Lac* did not extend into the *Petit Lac*, as indicated by the modeled temperature field (Figure 4.5). Furthermore, this agrees with the measurements taken during a comparable *Vent*-event in March 2019, when constant near-bottom temperatures were observed at the confluence (Figure 4.3).

In early winter, more than 75% of all particles originated from within the *Grand Lac*. In late winter, on the other hand, only 50% of all particles originated from within the *Grand Lac*, with the bulk of these particles coming from the immediate vicinity of the confluence (Figure 4.10c). This suggests that the interbasin exchange was more local in late winter.

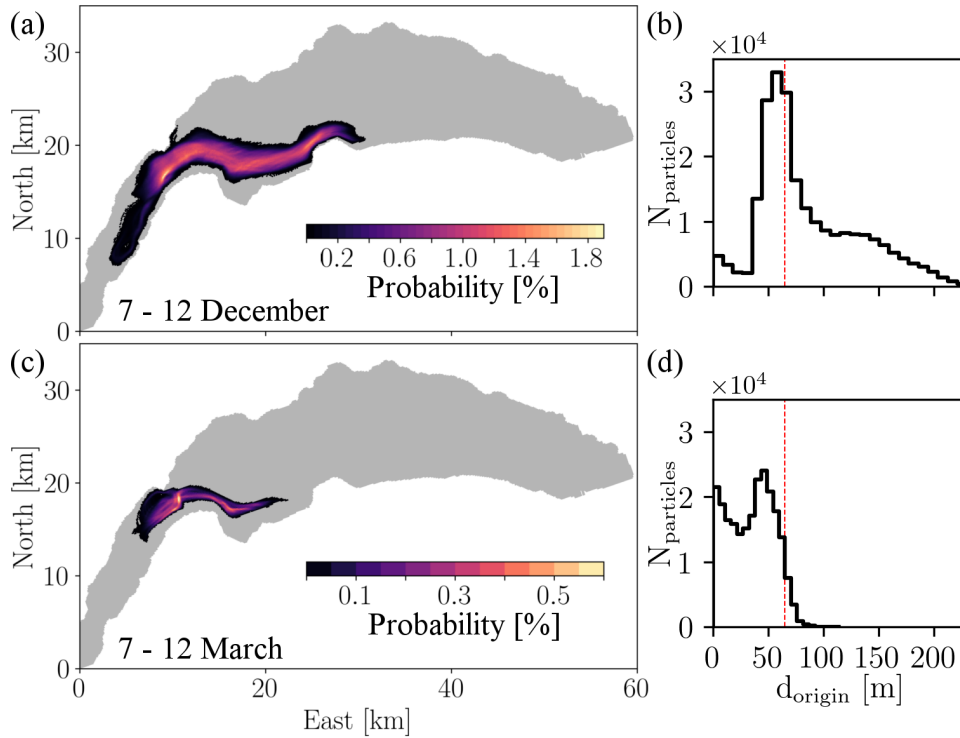


**Figure 4.10.** **a.** and **c.** Probability maps derived from the backward particle tracking simulations showing dominant particle pathways during early and late winter cases. **b.** and **d.** Histograms of the particle origin depths during early and late winter. The red dashed lines in (b) and (d) mark the maximum depth of the confluence (65 m). Probabilities are shown by the colorbars and reflect the total number of different particles that visited each 113 m × 113 m model grid cell during the entire simulation, divided by the total number of particles.

## 4.4 Summary and conclusions

Combining field observations, three-dimensional (3D) hydrodynamic modeling, particle tracking, and model-based momentum budget analysis, we demonstrated for the first time, the significant effect of stratification on wind-induced interbasin exchange between the shallow *Petit Lac* and deep *Grand Lac* basins of Lake Geneva during winter.

Current profiles taken at the confluence between the basins showed markedly different current patterns during two comparably strong *Vent* wind events (from the southwest) in December 2018 when the *Petit Lac* was weakly stratified, and in March 2019 when it was fully-mixed.

The circulation in December (early winter) was characterized by a two-layer flow, where downwind currents in the epilimnion flowing into the *Grand Lac* (outflow) were balanced by hypolimnetic currents flowing into the *Petit Lac* (inflow). The flow was approximately unidirectional in each layer, with the outflow roughly aligned with the wind, i.e., the main axis of the basin.

In March (late winter), the observed currents were considerably weaker, less steady, and showed more directional variability. While the currents in the upmost 20 m were roughly directed towards the *Grand Lac*, they were never aligned with the wind. Instead, they were deflected to the right by at least  $30^\circ$ . In the lower layers, a weak inflow prevailed most of the time.

To identify the effect of stratification on the exchange between the two lake basins, we carried out two 3D simulations with identical external forcing, but different initial stratification, representing typical early and late winter conditions. The observed differences were well reproduced by the numerical model, which allowed us to investigate the driving mechanisms behind the two circulation patterns by means of a momentum budget analysis.

Based on our results, the key features and differences in the interbasin exchange of a weakly stratified or fully-mixed *Petit Lac* can be summarized as follows:

- In both cases, the *Vent* wind from the southwest causes upwind upwelling at the western end of the *Grand Lac* basin, i.e., near the confluence.
- In early winter, the upwelling in the *Grand Lac* produces significant axial baroclinic pressure gradients in the *Petit Lac* hypolimnion. These gradients are the driving force behind the strong, steady bottom inflow that persisted for more than one day



after the wind had ceased. Furthermore, the transversal Coriolis acceleration, acting on the bottom inflow, generates coastal upwelling at the northern *Petit Lac* shore, in near-geostrophic balance with the transversal baroclinic pressure gradients.

- In early winter, there is downwind outflow in the entire epilimnion, with the rightward Ekman transport producing an upward tilt of the free surface towards the southern *Petit Lac* shore. This gives rise to barotropic pressure gradients that largely balance the Coriolis acceleration due to the epilimnetic outflow, thus resulting in a unidirectional current structure aligned with the wind.
- In late winter, the thermocline is well below the *Petit Lac* depth and the upwind upwelling at the western end of the *Grand Lac* does not reach the bottom of the confluence. Baroclinicity, therefore, no longer plays a role, and both interbasin exchange and the circulation in the *Petit Lac*, are purely wind-driven.
- The *Vent*-induced late winter circulation in the *Petit Lac* resembles that of a steady, wind-driven circulation in a rotating, fully-mixed, elongated basin with sloping boundaries and a depth greater than one Ekman depth, as described in the literature (e.g., Winant 2004). The modeling results show that this circulation is characterized by downwind flow over the shallow nearshore regions and near the surface, and upwind flow in the interior of the cross section. In the transversal plane, a clockwise rotating vortex (when looking downwind) develops, and the net currents near the surface veer to the right with depth, resembling the motion described by an Ekman spiral.

*Vent*-induced interbasin exchange during stratified early winter was studied in detail in Reiss et al. (2021), where it was demonstrated that under these conditions, hypolimnetic interbasin upwelling provides a potentially important mechanism for deepwater renewal in Lake Geneva.

The present study shows that in late winter, when the *Petit Lac* basin is fully mixed, wind-induced currents are not only weaker, but also continuously changing direction with depth (depth-veering) in the upper layers of the water column. As a result, the net exchange is less than half of that observed during early winter. Furthermore, particle tracking revealed that the exchange is more local, affecting only the *Grand Lac* waters in the immediate vicinity of the confluence. Even more striking was that no upwelling of hypolimnetic *Grand Lac* water into the *Petit Lac* occurred.

The present analysis demonstrates that the extent to which wind-induced interbasin exchange can contribute to deepwater renewal in the *Grand Lac* basin strongly depends on the stratification dynamics of the *Petit Lac* basin. Climate change-induced warming is expected to reduce the efficiency of convective cooling in Lake Geneva, resulting not only in less frequent complete overturning, but also in a shallower thermocline depth (e.g., Perroud and Goyette 2012; Schwefel et al. 2016). Likewise, globally higher epilimnion-hypolimnion temperature differences and stronger and longer stratification periods in lakes have been recorded (Arvola et al. 2010; Woolway et al. 2020). Therefore, prolonged winter stratification in the *Petit Lac* will make interbasin upwelling an increasingly important process for deepwater renewal in the deep hypolimnion of the *Grand Lac* as convective cooling weakens.

This study demonstrated that wind-induced interbasin exchange in Lake Geneva is a complex 3D process that is strongly affected by Coriolis force. This exchange appears to be a significant deepwater renewal process in Lake Geneva, in particular, during early winter stratification conditions. Such a deepwater renewal process can also be expected to play a key role in other multi-basin lakes under comparable conditions.

## Acknowledgments and data availability

This work was supported by the Swiss National Science Foundation (grant no. 159422) and the [Bois Chamblard Foundation](#) (last accessed on 3 June 2021). Meteorological data were provided by the Federal Office of Meteorology and Climatology in Switzerland (MeteoSwiss). Full-depth temperature profile data at SHL2 were provided by © OLA-IS, AnaEE-France, INRAE of Thonon-les-Bains, CIPEL. We would like to thank Htet Kyi Wynn and Benjamin Graf for assisting with the fieldwork.

Conflicts of interest: none

## References

- Ahrnsbrak, W. F., and M. R. Wing. 1998. Wind-induced hypolimnion exchange in Lake Ontario's Kingston basin: Potential effects on oxygen. *Journal of Great Lakes Research* **24**: 145–151. doi:[10.1016/S0380-1330\(98\)70806-8](https://doi.org/10.1016/S0380-1330(98)70806-8)
- Amadori, M., S. Piccolroaz, H. A. Dijkstra, and M. Toffolon. 2020. What makes an elongated lake 'large'? Scales from wind-driven steady circulation on a rotating Earth. *Journal of Great Lakes Research* **46**: 703–717. doi:[10.1016/j.jglr.2019.10.013](https://doi.org/10.1016/j.jglr.2019.10.013)
- Anderson, E. J., and D. J. Schwab. 2017. Meteorological influence on summertime baroclinic exchange in the Straits of Mackinac. *Journal of Geophysical Research: Oceans* **122**: 2171–2182. doi:[10.1002/2016JC012255](https://doi.org/10.1002/2016JC012255)
- Appt, J., J. Imberger, and H. Kobus. 2004. Basin-scale motion in stratified Upper Lake Constance. *Limnology and Oceanography* **49**: 919–933. doi:[10.4319/lo.2004.49.4.0919](https://doi.org/10.4319/lo.2004.49.4.0919)
- Arvola, L., G. George, D. M. Livingstone, M. Järvinen, T. Blenckner, M. T. Dokulil, E. Jennings, C. N. Aonghusa, P. Nöges, T. Nöges, and G. A. Weyhenmeyer. 2010. The impact of the changing climate on the thermal characteristics of lakes, p. 85–101. In G. George [ed.], *The Impact of Climate Change on European Lakes*. Dordrecht: Springer.
- Bartish, T. 1987. A review of exchange processes among the three basins of Lake Erie. *Journal of Great Lakes Research* **13**: 607–618. doi:[10.1016/S0380-1330\(87\)71676-1](https://doi.org/10.1016/S0380-1330(87)71676-1)
- Boyce, F. M., F. Chiocchio, B. Eid, F. Penicka, and F. Rosa. 1980. Hypolimnion flow between the central and eastern basins of Lake Erie during 1977 (Interbasin hypolimnion flows). *Journal of Great Lakes Research* **6**: 290–306. doi:[10.1016/S0380-1330\(80\)72110-X](https://doi.org/10.1016/S0380-1330(80)72110-X)
- Cimatoribus, A. A. 2018. C-tracker. doi:[10.5281/zenodo.1034118](https://doi.org/10.5281/zenodo.1034118)
- Cimatoribus, A. A., U. Lemmin, and D. A. Barry. 2019. Tracking Lagrangian transport in Lake Geneva: A 3D numerical modeling investigation. *Limnology and Oceanography* **64**: 1–18. doi:[10.1002/lno.11111](https://doi.org/10.1002/lno.11111)
- Cimatoribus, A. A., U. Lemmin, D. Bouffard, and D. A. Barry. 2018. Nonlinear dynamics of the near-shore boundary layer of a large lake (Lake Geneva). *Journal of Geophysical Research: Oceans* **123**: 1016–1031. doi:[10.1002/2017JC013531](https://doi.org/10.1002/2017JC013531)
- CIPEL. 2016. Rapports sur les études et recherches entreprises dans le bassin lémanique, Campagne 2015. Commission internationale pour la protection des eaux du Léman (CIPEL), Nyon, Switzerland. Retrieved from [http://www.cipel.org/wp-content/uploads/2016/10/RapportScientifique\\_camp\\_2015\\_VF.pdf](http://www.cipel.org/wp-content/uploads/2016/10/RapportScientifique_camp_2015_VF.pdf), last accessed 30 May 2021.
- CIPEL. 2019. Rapports sur les études et recherches entreprises dans le bassin lémanique, Campagne 2018. Commission internationale pour la protection des eaux du Léman (CIPEL), Nyon, Switzerland. Retrieved from [https://www.cipel.org/wp-content/uploads/2019/10/RapportScientifique\\_camp\\_2018-1.pdf](https://www.cipel.org/wp-content/uploads/2019/10/RapportScientifique_camp_2018-1.pdf), last accessed 30 May 2021.
- Döös, K., J. Kjellsson, and B. Jönsson. 2013. TRACMASS—A Lagrangian trajectory model, p. 225–249. In T. Soomere and E. Quak [eds.], *Preventive Methods for Coastal Protection: Towards the Use of Ocean Dynamics for Pollution Control*. Heidelberg: Springer International Publishing.
- Flood, B., M. Wells, E. Dunlop, and J. Young. 2020. Internal waves pump waters in and out of a deep coastal embayment of a large lake. *Limnology and Oceanography* **65**: 205–223. doi:[10.1002/lno.11292](https://doi.org/10.1002/lno.11292)
- Giddings, S. N., and P. MacCready. 2017. Reverse estuarine circulation due to local and remote wind forcing, enhanced by the presence of along-coast estuaries. *Journal of Geophysical Research: Oceans* **122**: 10184–10205. doi:[10.1002/2016JC012479](https://doi.org/10.1002/2016JC012479)
- Goldman, C. R., M. Kumagai, and R. D. Robarts, eds. 2013. *Climatic change and global warming of inland waters: Impacts and mitigation for ecosystems and societies*, Wiley-Blackwell.
- Graf, W. H., and J. P. Prost. 1980. Aerodynamic drag and its relation to the sea state: With data from Lake Geneva. *Archiv für Meteorologie, Geophysik und Bioklimatologie, Serie A* **29**: 67–87. doi:[10.1007/BF02247734](https://doi.org/10.1007/BF02247734)

- Hamidi, S. A., H. R. Bravo, J. V. Klump, and J. T. Waples. 2015. The role of circulation and heat fluxes in the formation of stratification leading to hypoxia in Green Bay, Lake Michigan. *Journal of Great Lakes Research* **41**: 1024–1036. doi:[10.1016/j.jglr.2015.08.007](https://doi.org/10.1016/j.jglr.2015.08.007)
- Jabbari, A., J. D. Ackerman, L. Boegman, and Y. Zhao. 2019. Episodic hypoxia in the western basin of Lake Erie. *Limnology and Oceanography* **64**: 2220–2236. doi:[10.1002/lno.11180](https://doi.org/10.1002/lno.11180)
- Jabbari, A., J. D. Ackerman, L. Boegman, and Y. Zhao. 2021. Increases in Great Lake winds and extreme events facilitate interbasin coupling and reduce water quality in Lake Erie. *Scientific Reports* **11**: 5733. doi:[10.1038/s41598-021-84961-9](https://doi.org/10.1038/s41598-021-84961-9)
- Large, W. G., J. C. McWilliams, and S. C. Doney. 1994. Oceanic vertical mixing: A review and a model with a nonlocal boundary layer parameterization. *Reviews of Geophysics* **32**: 363–403. doi:[10.1029/94RG01872](https://doi.org/10.1029/94RG01872)
- Laval, B. E., J. Morrison, D. J. Potts, E. C. Carmack, S. Vagle, C. James, F. A. McLaughlin, and M. Foreman. 2008. Wind-driven summertime upwelling in a fjord-type lake and its impact on downstream river conditions: Quesnel Lake and River, British Columbia, Canada. *Journal of Great Lakes Research* **34**: 189–203. doi:[10.3394/0380-1330\(2008\)34\[189:WSUIAF\]2.0.CO;2](https://doi.org/10.3394/0380-1330(2008)34[189:WSUIAF]2.0.CO;2)
- Lavigne, S., and P. Nirel. 2016. Physico-chemical and biological changes in the waters of the Petit Lac. Service de l'écologie de l'eau (SECOE). Geneva, Switzerland. Retrieved from [http://www.cipel.org/wp-content/uploads/2016/11/0\\_evolution\\_physico\\_chimique\\_biologique\\_petit-lac\\_camp\\_2015.pdf](http://www.cipel.org/wp-content/uploads/2016/11/0_evolution_physico_chimique_biologique_petit-lac_camp_2015.pdf), accessed 30 May 2021.
- Lawrence, G., R. Pieters, L. Zaremba, T. Tedford, L. Gu, S. Greco, and P. Hamblin. 2004. Summer exchange between Hamilton Harbour and Lake Ontario. *Deep Sea Research Part II: Topical Studies in Oceanography* **51**: 475–487. doi:[10.1016/j.dsr2.2003.09.002](https://doi.org/10.1016/j.dsr2.2003.09.002)
- Lemmin, U., and N. D'Adamo. 1996. Summertime winds and direct cyclonic circulation: Observations from Lake Geneva. *Annales Geophysicae* **14**: 1207–1220. doi:[10.1007/s00585-996-1207-z](https://doi.org/10.1007/s00585-996-1207-z)
- Liu, Q., E. J. Anderson, Y. Zhang, A. D. Weinke, K. L. Knapp, and B. A. Biddanda. 2018. Modeling reveals the role of coastal upwelling and hydrologic inputs on biologically distinct water exchanges in a Great Lakes estuary. *Estuarine, Coastal and Shelf Science* **209**: 41–55. doi:[10.1016/j.ecss.2018.05.014](https://doi.org/10.1016/j.ecss.2018.05.014)
- Marshall, J., A. Adcroft, C. Hill, L. Perelman, and C. Heisey. 1997. A finite-volume, incompressible Navier Stokes model for studies of the ocean on parallel computers. *Journal of Geophysical Research: Oceans* **102**: 5753–5766. doi:[10.1029/96JC02775](https://doi.org/10.1029/96JC02775)
- Mesman, J. P., J. A. A. Stelzer, V. Dakos, S. Goyette, I. D. Jones, J. Kasparian, D. F. McGinnis, and B. W. Ibelings. 2021. The role of internal feedbacks in shifting deep lake mixing regimes under a warming climate. *Freshwater Biology* **66**: 1021–1035. doi:[10.1111/fwb.13704](https://doi.org/10.1111/fwb.13704)
- Niu, Q., M. Xia, E. S. Rutherford, D. M. Mason, E. J. Anderson, and D. J. Schwab. 2015. Investigation of interbasin exchange and interannual variability in Lake Erie using an unstructured-grid hydrodynamic model. *Journal of Geophysical Research: Oceans* **120**: 2212–2232. doi:[10.1002/2014JC010457](https://doi.org/10.1002/2014JC010457)
- Perroud, M., and S. Goyette. 2012. Interfacing a one-dimensional lake model with a single-column atmospheric model: 2. Thermal response of the deep Lake Geneva, Switzerland under a  $2 \times \text{CO}_2$  global climate change. *Water Resources Research* **48**: W06522. doi:[10.1029/2011WR011222](https://doi.org/10.1029/2011WR011222)
- Ponte, A. L., G. Gutiérrez de Velasco, A. Valle-Levinson, K. B. Winters, and C. D. Winant. 2012. Wind-driven subinertial circulation inside a semienclosed bay in the Gulf of California. *Journal of Physical Oceanography* **42**: 940–955. doi:[10.1175/JPO-D-11-0103.1](https://doi.org/10.1175/JPO-D-11-0103.1)
- Reiss, R. S., U. Lemmin, and D. A. Barry. 2021. Wind-induced hypolimnetic upwelling between the multi-depth basins of Lake Geneva during winter: An overlooked deep-water renewal mechanism?. *Limnology and Oceanography*: Submitted
- Reiss, R. S., U. Lemmin, A. A. Cimattoribus, and D. A. Barry. 2020. Wintertime coastal upwelling in Lake Geneva: An efficient transport process for deepwater renewal in a large, deep lake. *Journal of Geophysical Research: Oceans* **125**. doi:[10.1029/2020JC016095](https://doi.org/10.1029/2020JC016095)
- Rimet, F., O. Anneville, D. Barbet, C. Chardon, L. Crépin, I. Domaizon, J.-M. Dorioz, L. Espinat, V. Frossard, J. Guillard, C. Goulon, V. Hamelet, J.-C. Hustache, S. Jacquet, L. Lainé, B. Montuelle, P. Perney, P. Quetin, S. Rasconi, A. Schellenberger, V. Tran-Khac, and G. Monet. 2020. The

- Observatory on Lakes (OLA) database: Sixty years of environmental data accessible to the public: The Observatory on Lakes (OLA) database. *Journal of Limnology* **79**. doi:[10.4081/jlimnol.2020.1944](https://doi.org/10.4081/jlimnol.2020.1944)
- Salmaso, N. 2005. Effects of climatic fluctuations and vertical mixing on the interannual trophic variability of Lake Garda, Italy. *Limnology and Oceanography* **50**: 553–565. doi:[10.4319/lo.2005.50.2.0553](https://doi.org/10.4319/lo.2005.50.2.0553)
- Sanay, R., and A. Valle-Levinson. 2005. Wind-induced circulation in semienclosed homogeneous, rotating basins. *Journal of Physical Oceanography* **35**: 2520–2531. doi:[10.1175/JPO2831.1](https://doi.org/10.1175/JPO2831.1)
- Schertzer, W. M., R. A. Assel, D. Beletsky, T. E. C. Li, B. M. Lofgren, and D. J. Schwab. 2008. Lake Huron climatology, inter-lake exchange and mean circulation. *Aquatic Ecosystem Health and Management* **11**: 144–152. doi:[10.1080/14634980802098705](https://doi.org/10.1080/14634980802098705)
- Schwefel, R., A. Gaudard, A. Wüest, and D. Bouffard. 2016. Effects of climate change on deepwater oxygen and winter mixing in a deep lake (Lake Geneva): Comparing observational findings and modeling. *Water Resources Research* **52**: 8811–8826. doi:[10.1002/2016WR019194](https://doi.org/10.1002/2016WR019194)
- van Sebille, E., S. M. Griffies, R. Abernathey, T. P. Adams, P. Berloff, A. Biastoch, B. Blanke, E. P. Chassignet, Y. Cheng, C. J. Cotter, E. Deleersnijder, K. Döös, H. F. Drake, S. Drijfhout, S. F. Gary, A. W. Heemink, J. Kjellsson, I. M. Koszalka, M. Lange, C. Lique, G. A. MacGilchrist, R. Marsh, C. G. Mayorga Adame, R. McAdam, F. Nencioli, C. B. Paris, M. D. Piggott, J. A. Polton, S. Rühs, S. H. A. M. Shah, M. D. Thomas, J. Wang, P. J. Wolfram, L. Zanna, and J. D. Zika. 2018. Lagrangian ocean analysis: Fundamentals and practices. *Ocean Modelling* **121**: 49–75. doi:[10.1016/j.ocemod.2017.11.008](https://doi.org/10.1016/j.ocemod.2017.11.008)
- van Senden, D. C., and D. M. Imboden. 1989. Internal seiche pumping between sill-separated basins. *Geophysical & Astrophysical Fluid Dynamics* **48**: 135–150. doi:[10.1080/03091928908219530](https://doi.org/10.1080/03091928908219530)
- Umlauf, L., and U. Lemmin. 2005. Interbasin exchange and mixing in the hypolimnion of a large lake: The role of long internal waves. *Limnology and Oceanography* **50**: 1601–1611. doi:[10.4319/lo.2005.50.5.1601](https://doi.org/10.4319/lo.2005.50.5.1601)
- Voudouri, A., E. Avgoustoglou, and P. Kaufmann. 2017. Impacts of Observational Data Assimilation on Operational Forecasts. *Perspectives on Atmospheric Sciences*. Cham: Springer International Publishing. 143–149.
- Wanner, H., and M. Furger. 1990. The Bise - Climatology of a regional wind north of the Alps. *Meteorology and Atmospheric Physics* **43**: 105–115. doi:[10.1007/BF01028113](https://doi.org/10.1007/BF01028113)
- Winant, C. D. 2004. Three-dimensional wind-driven flow in an elongated, rotating basin. *Journal of Physical Oceanography* **34**: 462–476. doi:[10.1175/1520-0485\(2004\)034<0462:TWFIAE>2.0.CO;2](https://doi.org/10.1175/1520-0485(2004)034<0462:TWFIAE>2.0.CO;2)
- Woolway, R. I., B. M. Kraemer, J. D. Lenters, C. J. Merchant, C. M. O'Reilly, and S. Sharma. 2020. Global lake responses to climate change. *Nature Reviews Earth & Environment* **1**: 388–403. doi:[10.1038/s43017-020-0067-5](https://doi.org/10.1038/s43017-020-0067-5)



# Supporting Information for Chapter 4

---

Rafael Sebastian Reiss, Ulrich Lemmin, and David Andrew Barry

Ecological Engineering Laboratory (ECOL), Faculty of Architecture, Civil and Environmental Engineering (ENAC), Ecole Polytechnique Fédérale de Lausanne (EPFL), Lausanne, Switzerland

Table S4.1. Details of the mooring.

Depth [m]	Instruments and settings
65	10 Seabird SBE-56, vertical spacing 1 m, sampling interval 5 s Teledyne RDI Workhorse Sentinel (300 kHz): 29 bins of 2 m, 20 min ensemble interval, 180 pings per ensemble

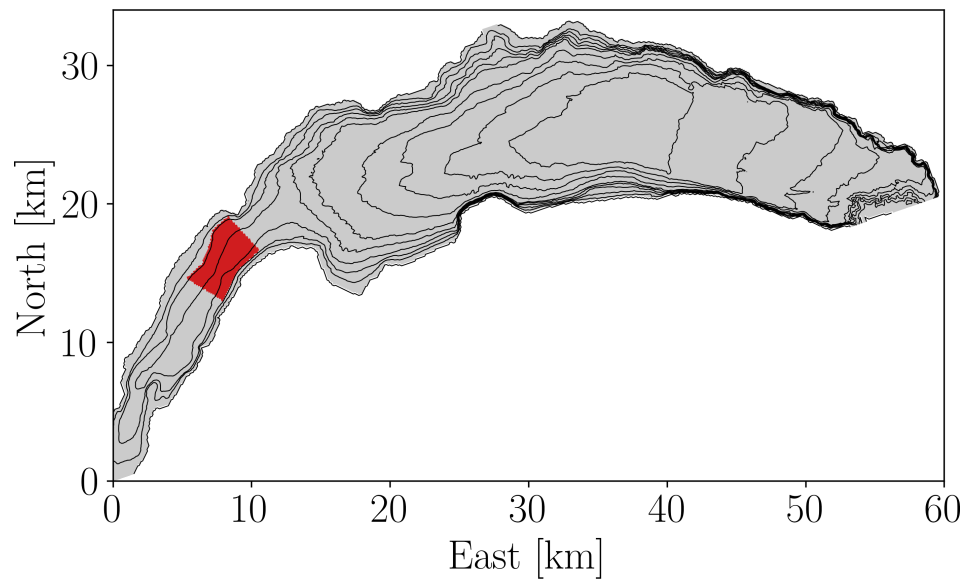


**Figure S4.1.** Seeding area (red) in the *Petit Lac* basin of Lake Geneva where particles were released during the particle tracking simulation.



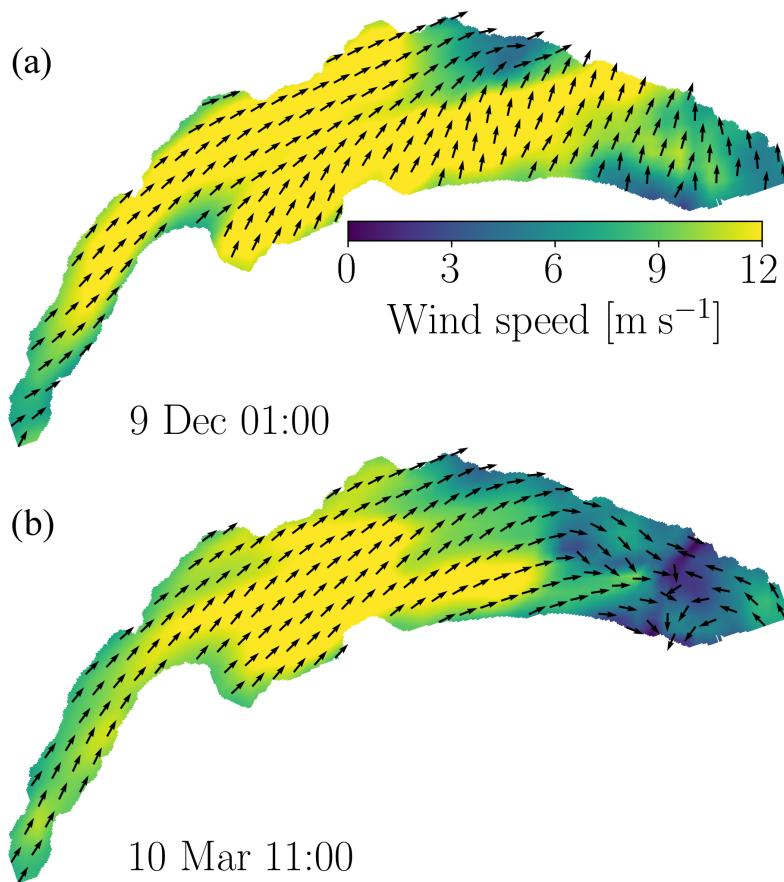


**Figure S4.2.** Snapshots of the two-dimensional (2D) COSMO wind field of a *Vent* wind event lasting several days during (a) early and (b) late winter (see Figure 4.3 in the main text). The normalized black arrows show the *Vent* wind direction (from the southwest) that blows over most of the lake surface. The colorbar gives the wind speed. For clarity, not all wind vectors are shown.

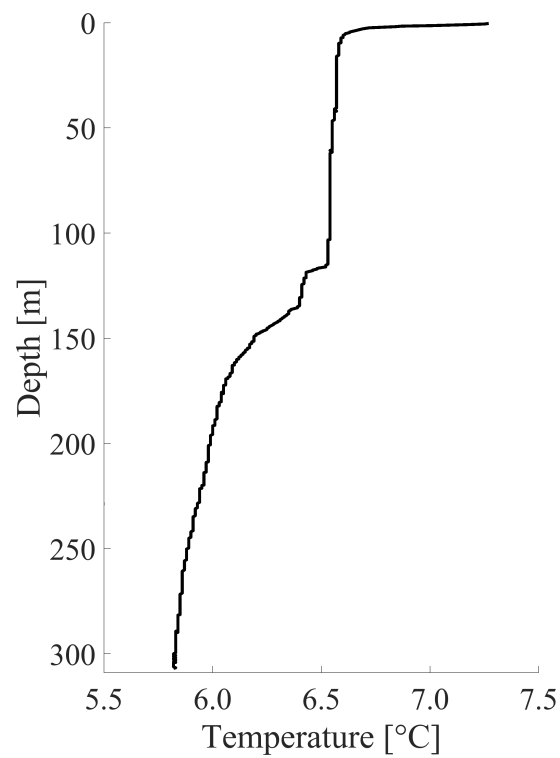


**Figure S4.3.** Temperature profile taken by CIPEL at station SHL2 on 14 February 2019 (for location, see Figure 4.1 in main text).

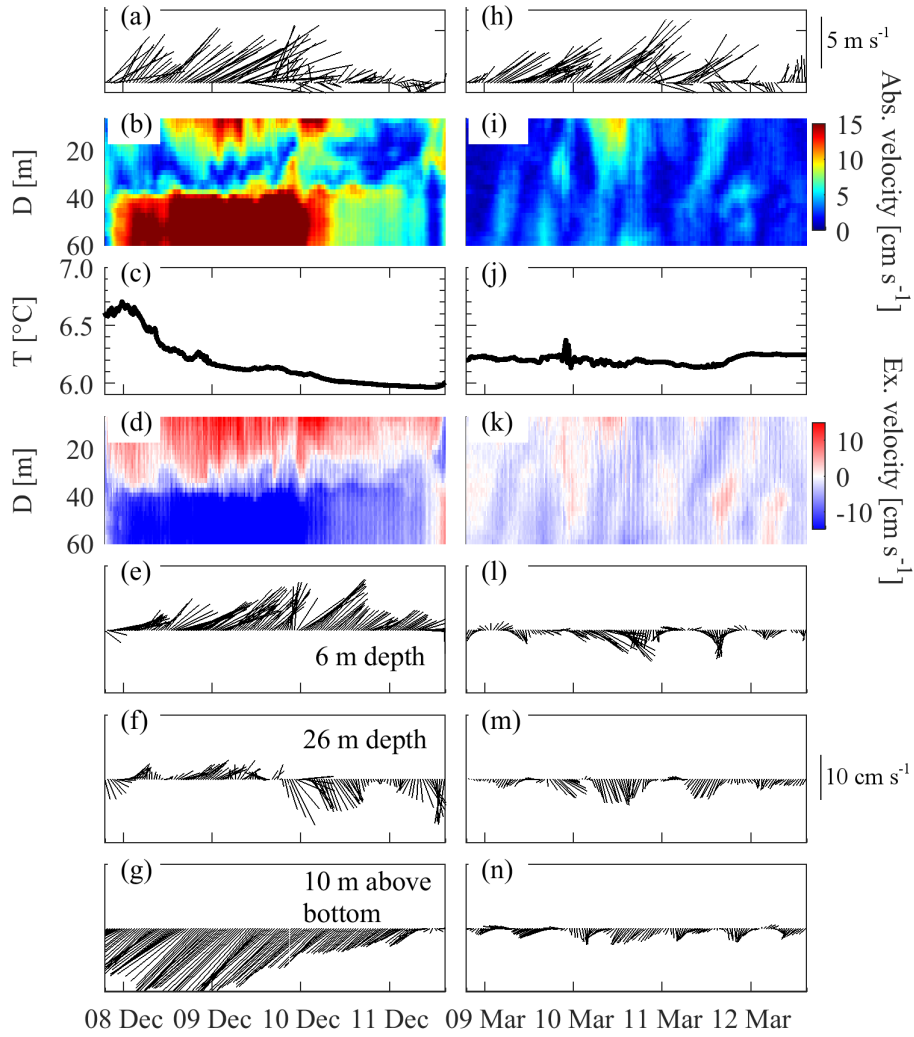


**Figure S4.4.** Wind vectors (**a**, **h**) and mooring data (**b**-**g**, **i**-**n**) recorded from 8 to 11 December 2018 (**a**-**g**; left panels) and 9 to 12 March 2019 (**h**-**n**; right panels), respectively. The mooring data panels from top to bottom show: absolute current velocity (**b**, **i**), depth-averaged temperature ( $T$ ) in the bottom-most 10 m ( $D$  is depth) (**c**, **j**), “interbasin exchange velocity” (**d**, **k**), as well as current velocity and direction at 6-m depth (**e**, **l**), 26-m depth (**f**, **m**), and 10 m above the bottom (**g**, **n**). Interbasin exchange velocities were obtained by projecting the velocity vectors onto a vertical plane perpendicular to the confluence transect (Figure 4.1 in the main text, red arrow). The colorbars give the magnitude of the absolute and interbasin exchange velocities. The scale of the wind and current quivers is the same for both periods and is given next to panels **h** and **m**. The quiver heads point in the direction of travel, with the positive  $y$ - and  $x$ -direction corresponding to north ( $0^\circ$ ) and east ( $90^\circ$ ). Meteorological data were recorded at the MeteoSwiss station in Nyon (Figure 4.1 in the main text, red circle).

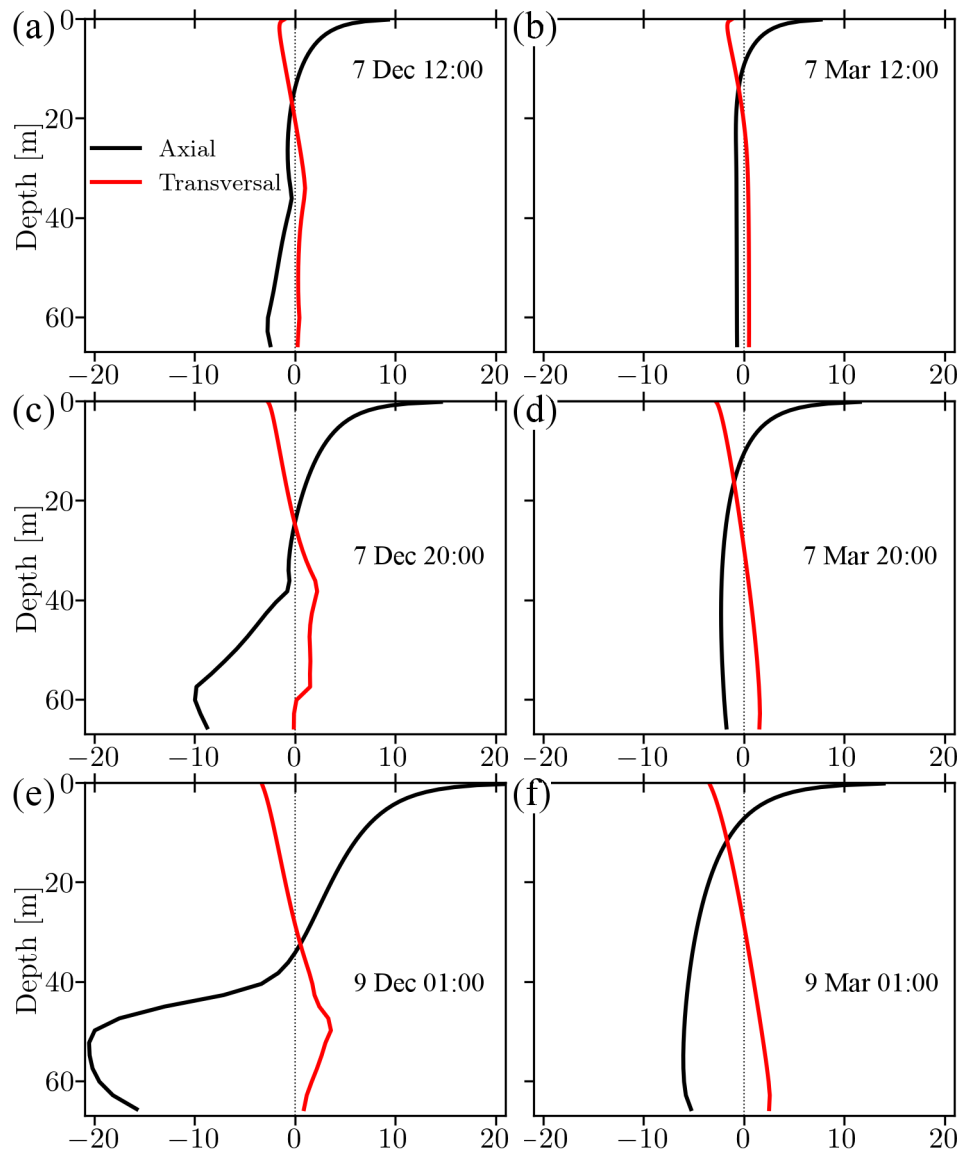


**Figure S4.5.** Modeled axial (black) and transversal (red) velocity components at the mooring in the confluence center (blue cross in Figure 4.1 in the main text) during the initialization (a, b) and adjustment (c, d) phases, and when the circulation was fully developed (e, f), in early winter (left panels) and late winter (right panels). The orientation of the axial and transversal axes is shown in Figure 4.1 in the main text (red arrows). Date and time are indicated in each panel.

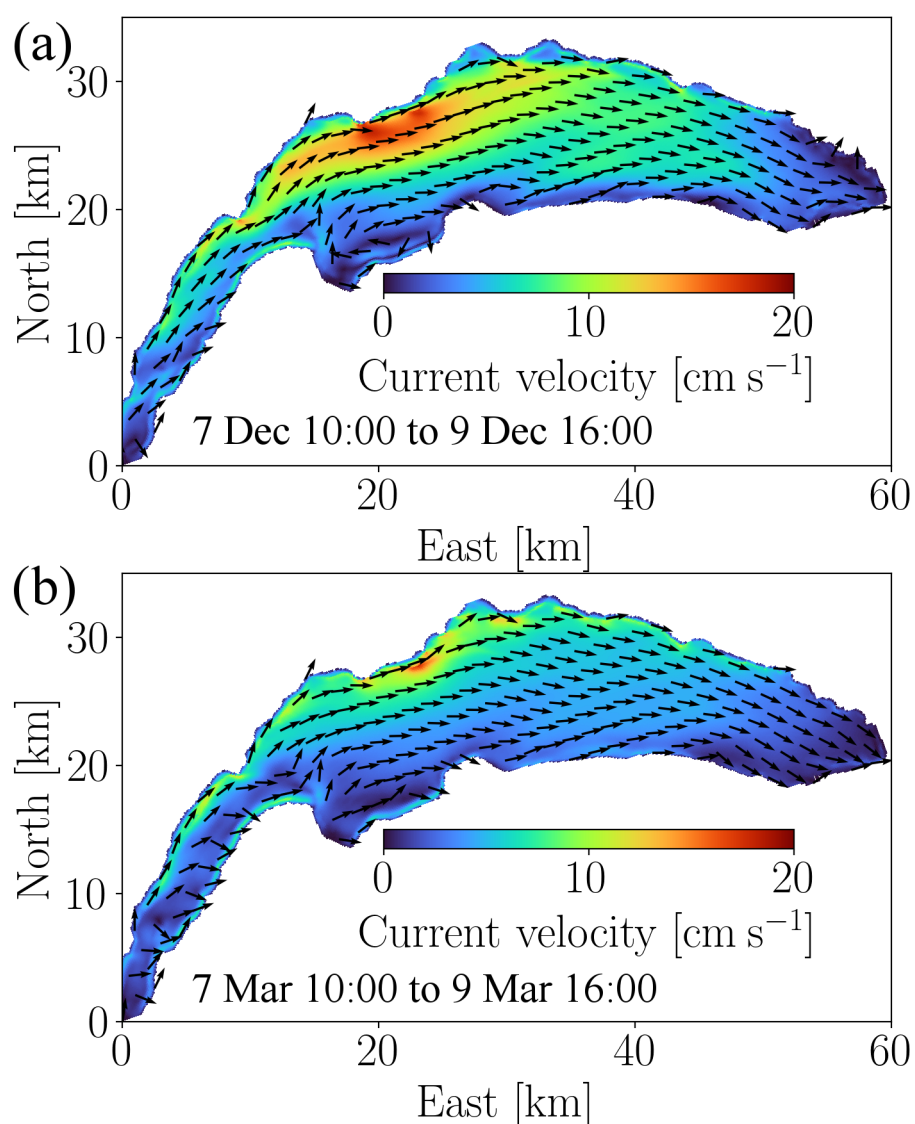


**Figure S4.6.** Depth-averaged modeled currents (0 – 20-m depth) averaged over the entire *Vent* wind event in (a) early and (b) late winter in Lake Geneva. The normalized black arrows show the current direction. The colorbar gives the absolute velocity. For clarity, not all current vectors are shown.

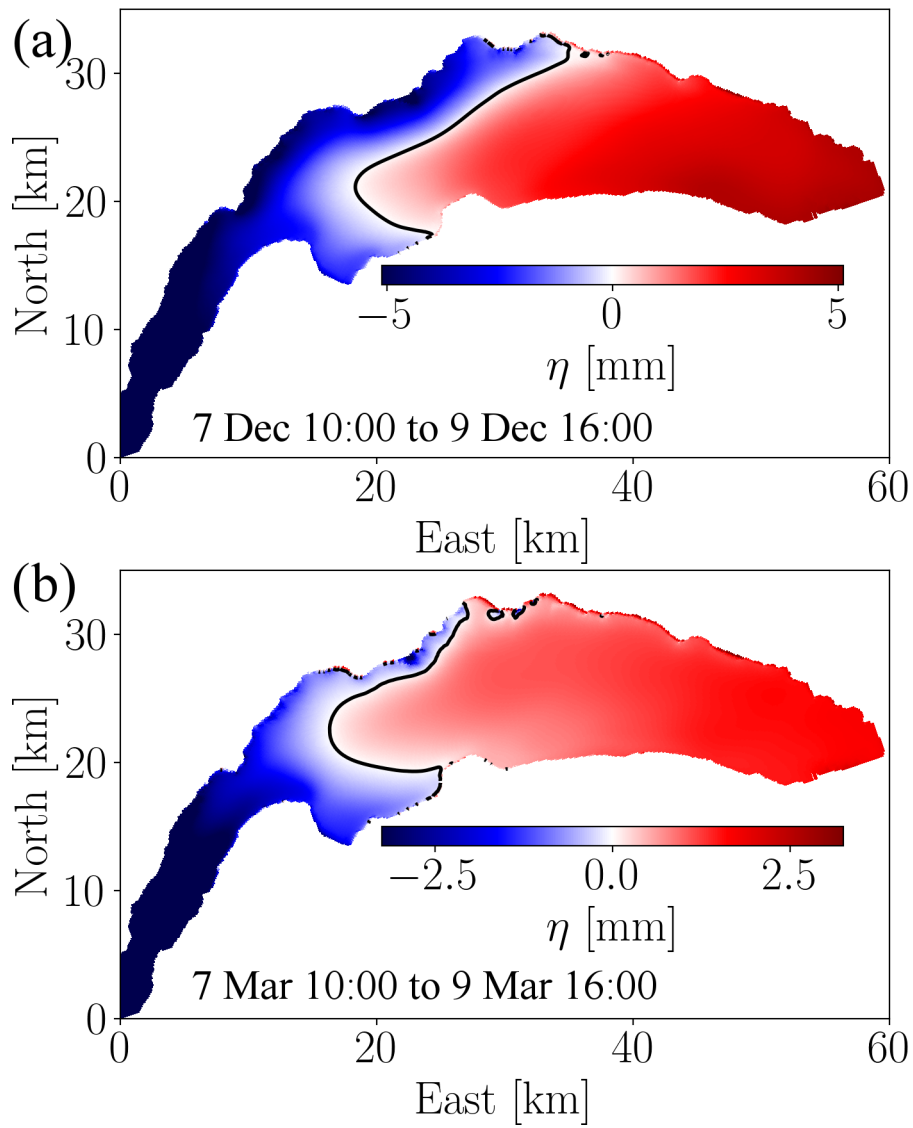


**Figure S4.7.** Mean modeled free surface elevation averaged over the entire *Vent* wind event in (a) early and (b) late winter. The black contour line marks the zero crossing, i.e., the level of the free surface before the wind started. The colorbars indicate the net surface elevation.

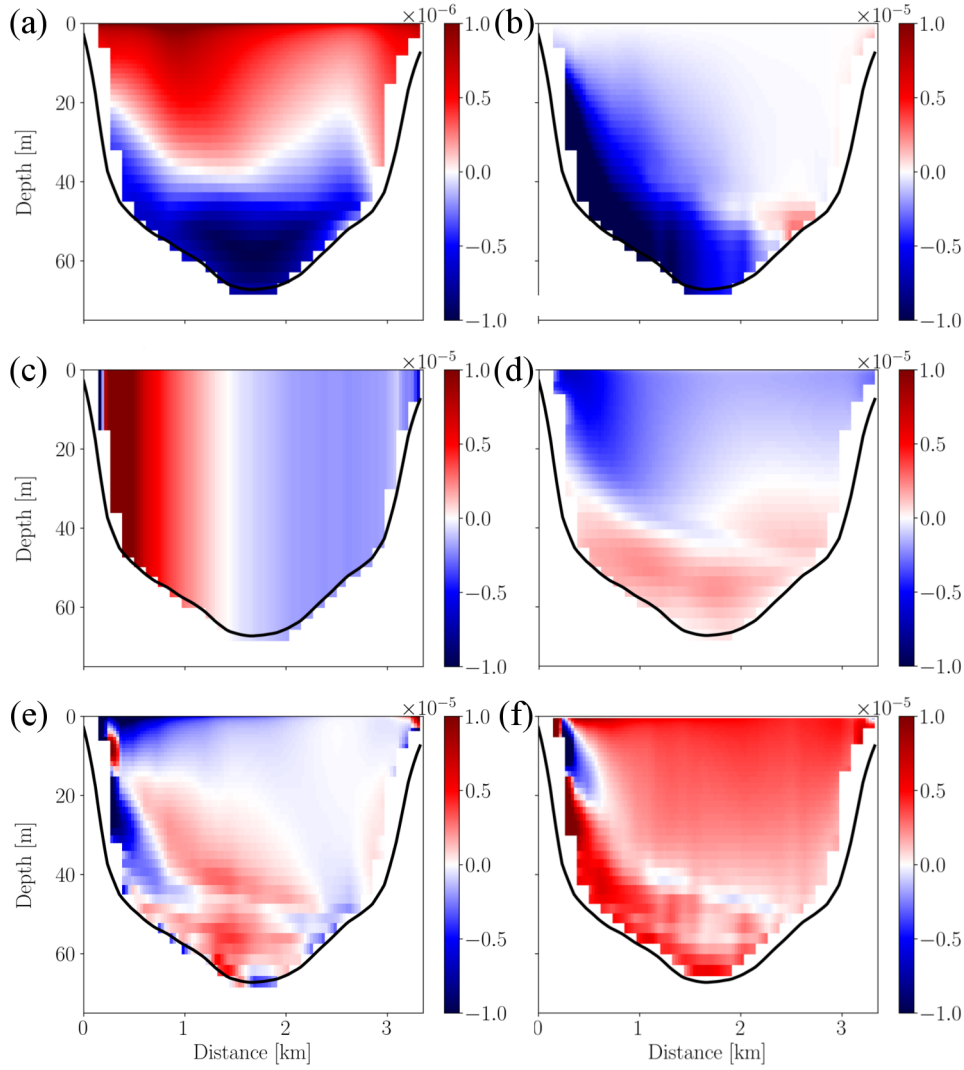


**Figure S4.8.** Mean axial momentum budget terms at the confluence of the *Petit Lac* and *Grand Lac* basins of Lake Geneva (for location, see Figure 4.1 in the main text) during early winter, averaged over the entire *Vent* wind event (7 December 10:00 to 9 December 16:00). The panels show: **(a)** net acceleration, **(b)** baroclinic pressure gradient, **(c)** barotropic pressure gradient, **(d)** Coriolis acceleration, **(e)** advection, and **(f)** friction. The unit of the values given in the colorbars is  $\text{m s}^{-2}$ . Distance is given along the transect from the northern shore.

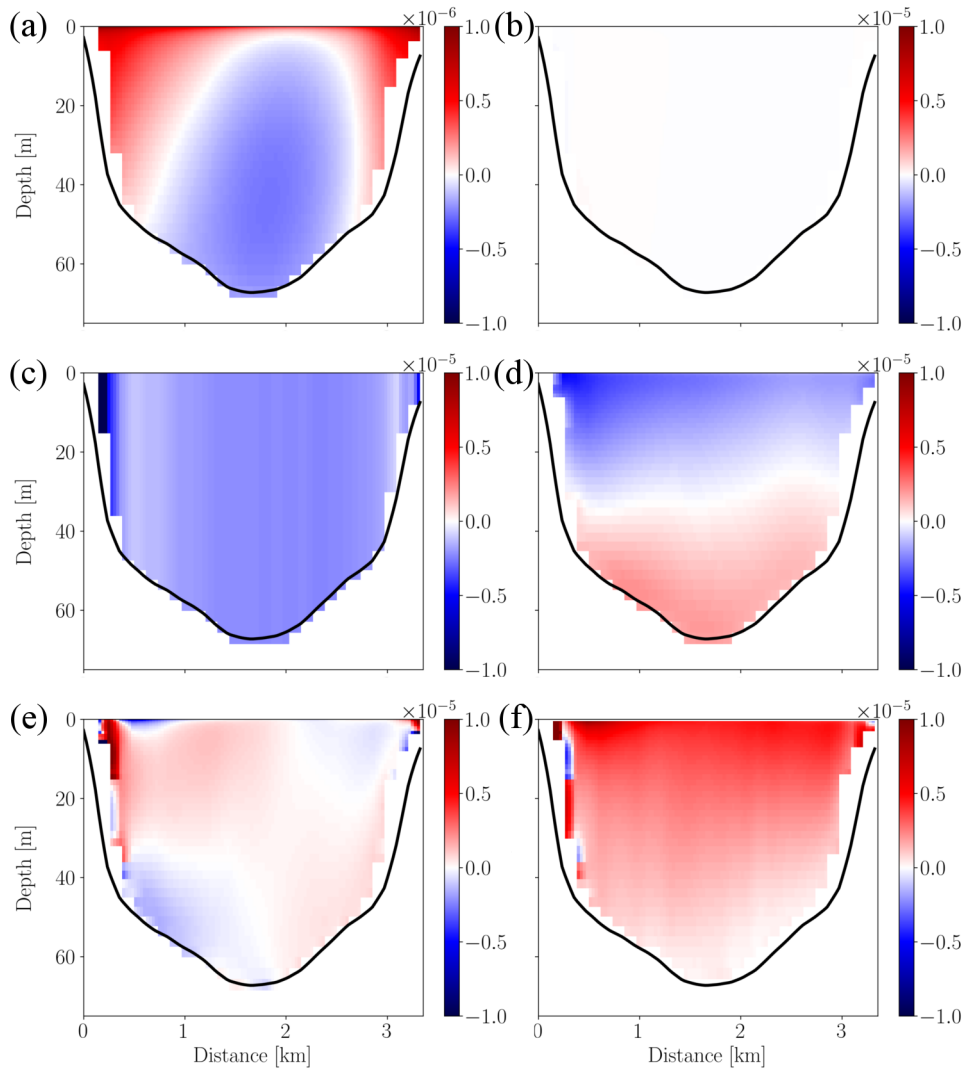


**Figure S4.9.** Mean axial momentum budget terms at the confluence of the *Petit Lac* and *Grand Lac* basins of Lake Geneva (for location, see Figure 4.1 in the main text) during late winter, averaged over the entire *Vent* event (7 March 10:00 to 9 March 16:00). The panels show: **(a)** net acceleration, **(b)** baroclinic pressure gradient, **(c)** barotropic pressure gradient, **(d)** Coriolis acceleration, **(e)** advection, and **(f)** friction. The unit of the values given in the colorbars is  $\text{m s}^{-2}$ . Distance is given along the transect from the northern shore.



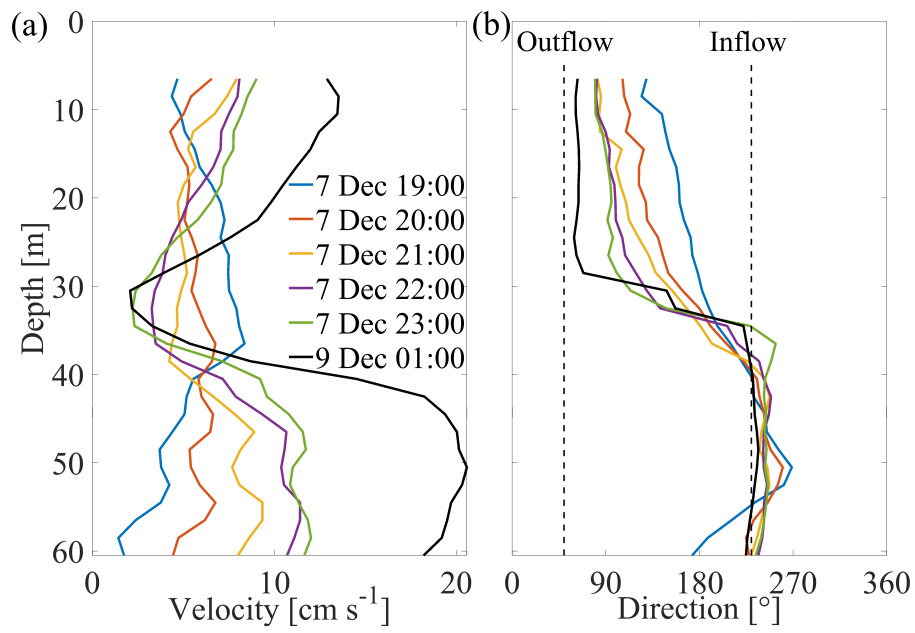


**Figure S4.10.** Current velocity (a) and direction (b) recorded at the mooring in the confluence center (Figure 4.1 in the main text, blue cross) during the *Vent* wind event in December 2018. The exact dates are given in the legend in (a). The dashed black lines mark the outflow and inflow directions.



## Chapter 5    Conclusions and Outlook

---

## 5.1 Summary and conclusions

This thesis explored the dynamics and ecological implications of wind-induced coastal upwelling and interbasin exchange processes in Lake Geneva during the weakly stratified winter period. The combination of systematic field observation campaigns, 3D hydrodynamic modeling, Lagrangian particle tracking, and model-based momentum budget analysis proved a powerful toolset to address the complex, transient, and three-dimensional nature of these processes.

In chapter 2, it was demonstrated that frequently occurring, strong winds from the southwest (local name: *Vent*) generate Ekman-type coastal upwelling at the central northern shore of Lake Geneva. Field measurements during one such upwelling event in January 2018 showed that hypolimnetic water from as deep as 200 m was brought into the shallow nearshore region and advected downwind along the shore at high velocities ( $> 25 \text{ cm s}^{-1}$ ) for several days. At the same time, several short-lived downwelling events, limited to a depth of  $\sim 50$  m and caused by small directional changes in the wind field over the lake, occurred. The 3D numerical model well reproduced the observed upwelling dynamics. Model results indicated that the upwelled, cold water spread over approximately 10% of the surface area of Lake Geneva's main basin. The deep origin of the upwelled waters, suggested by the field observations, was confirmed by particle tracking based on the modeled current field. Furthermore, upwelled particles spent on average 1 day, and up to 5 days near the surface, before descending back to around 150 to 200-m depth after the wind subsided, spreading over a wide area in the deep hypolimnion.

In chapter 3, the southwesterly *Vent* winds causing coastal upwelling in the *Grand Lac* (chapter 2) were identified for the first time as drivers for frequent topographic upwelling between the deep *Grand Lac* (max. depth 309 m) and shallow *Petit Lac* (max. depth 75 m) basins of Lake Geneva during early winter, i.e., when the *Petit Lac* is weakly stratified. Under these conditions, winds from the southwest (*Vent*) generate a two-layer flow, where the downwind surface drift towards the *Grand Lac* is balanced by a hypolimnetic counterflow into the *Petit Lac*. Field observations from December 2018 and modeling showed that the strong bottom currents carry cold, hypolimnetic *Grand Lac* waters from below 150-m depth into the bottom layers of the *Petit Lac*. Once upwelled, these waters are transported far into the *Petit Lac* (around 10 km, i.e.,  $\sim$  half its length) before finally, after the wind has subsided, draining back into the *Grand Lac* hypolimnion. Particle tracking results suggest that the upwelled *Grand Lac* waters spend on average several days in the *Petit Lac*. Low model-based gradient Richardson numbers and significant temperature inversions in the *Petit Lac* hypolimnion and around the thermocline

depth seen in CTD profiles suggest turbulent mixing between the upwelled *Grand Lac* and surrounding *Petit Lac* waters. Furthermore, model results indicate a temporary doubling of the *Petit Lac* hypolimnetic volume during the upwelling. At the same time, coastal upwelling occurs at the northern shore of the *Petit Lac*. Here, particle tracking showed that waters from the upper *Grand Lac* hypolimnion (down to 65-m depth) are first drawn into the *Petit Lac* by the strong bottom currents discussed above, and subsequently upwell at its northern shore. This type of coastal upwelling appears to be related to Coriolis force-induced veering of the upwelled bottom currents, and is locally enhanced by basin topography.

The findings of chapters 2 and 3 illustrate that *Vent* wind-induced coastal upwelling and hypolimnetic upwelling between the two basins of Lake Geneva are frequently occurring processes during winter that are strongly modified by Coriolis effects. They cause intense horizontal and vertical exchange between the epilimnion and hypolimnion of Lake Geneva, with vertical excursions often exceeding 150 m, and thus can be important mechanisms for deepwater renewal and horizontal and vertical nutrient recycling. Furthermore, these findings indicate that these processes play a crucial role in the energy budget of the deep layers. In the light of global warming and the associated weakening of wintertime convective mixing, the findings of chapters 2 and 3 demonstrate that wind-induced coastal and interbasin upwelling could become increasingly important for deepwater renewal in Lake Geneva, as well as in other deep (multi-basin) lakes under favorable wind conditions. Furthermore, due to their complex, transient, and three-dimensional nature, wind-induced coastal and interbasin upwelling processes cannot be represented by one-dimensional models typically employed to predict climate change-induced shifts, and thus merit further attention when assessing deepwater renewal and dynamics in large, deep (multi-basin) lakes.

In chapter 4, the effect of stratification on the previously discussed *Vent* wind-induced interbasin upwelling (chapter 3) in Lake Geneva was investigated with field observations and 3D numerical modeling. Early (weakly stratified) and late (fully-mixed) winter conditions in the *Petit Lac* were considered under comparably strong *Vent* wind forcing. For early winter, it was shown that the observed strong, steady bottom currents that carry deep, cold hypolimnetic *Grand Lac* water into the *Petit Lac* (chapter 3) are driven by baroclinic pressure gradients caused by upwind upwelling at the western end of the *Grand Lac*. The persistence of the latter causes this bottom inflow to continue for more than one day after the wind has stopped, enhancing the total exchange between the basins considerably. Furthermore, Ekman transport due to the downwind outflow in the epilimnion towards the *Grand Lac* induces a water level setup

at the right (i.e., southern) shore of the *Petit Lac*. After an adjustment phase, the resulting barotropic pressure gradients largely balance the Coriolis acceleration acting on the outflow, yielding a unidirectional net current structure in the upper layers that is aligned with the wind. In late winter, on the other hand, with the thermocline below the *Petit Lac* depth, the upwind upwelling in the western *Grand Lac* does not reach the *Petit Lac* bottom and baroclinicity does therefore not enhance the interbasin exchange. As a result, exchange currents are considerably weaker, with the currents in the upper layer showing a depth-veering structure due to Coriolis effects, both resulting in a reduction of the net volume exchange between the basins by 50% compared to early winter. More strikingly, deep hypolimnetic upwelling from the *Grand Lac* into the *Petit Lac* (chapter 3) is suppressed altogether in late winter. It is important to note that the *Vent*-induced late winter circulation in the *Petit Lac* resembles that of a steady, wind-driven circulation in a rotating, fully-mixed, elongated basin with sloping boundaries and a depth greater than one Ekman depth, as described in the literature (e.g., Winant 2004; Sanay and Valle-Levinson 2005).

The reduced efficiency of wintertime convective cooling in Lake Geneva due to global warming is expected to not only cause less frequent complete overturning, but also a shallower thermocline depth during winter (e.g., Perroud and Goyette 2012; Schwefel et al. 2016). Likewise, longer stratification periods in lakes have been recorded (e.g., Arvola et al. 2010). The findings of chapter 4 suggest that, as convective cooling weakens due to climate change, prolonged winter stratification in the *Petit Lac* will make wind-induced interbasin upwelling an increasingly important process for deepwater renewal in Lake Geneva, as well as in other multi-basin lakes under comparable conditions.

Finally, this thesis has demonstrated the potential of combining detailed field observations with high-resolution 3D numerical modeling and Lagrangian particle tracking to untangle the dynamics of complex, transient, and three-dimensional hydrodynamic processes in large, deep lakes.

## 5.2 Future work

### 5.2.1 The role of wind-induced upwelling processes in energizing and mixing the deep hypolimnion layers in Lake Geneva

The effects of wind-induced interbasin and coastal upwelling processes on deepwater dynamics in deep (multi-basin) lakes are manifold: On the one hand, as discussed in this thesis, upwelling provides an efficient advective pathway for deep waters to come in contact and mix with “fresher” surface waters, thus providing a direct means for aerating the deeper layers and recycling nutrients. However, in lakes as deep as Lake Geneva (max. depth 309 m), only rare, extreme winds can cause full upwelling of the bottom waters (Schladow et al. 2004), if at all. On the other hand, lakes act as a continuum. Hence, strong, wind-induced upwelling events set large parts of the water column in motion, thus potentially generating currents and shear even in the lowest layers of the hypolimnion that are not upwelled to the surface. This appears to be the case in Lake Geneva during Ekman-type coastal upwelling in winter, as indicated by the near-bottom temperatures recorded by the Distributed Temperature Sensing (DTS) system in January 2018 (Figure 2.5). During the coastal upwelling event discussed in chapter 2, near-bottom temperatures recorded at 130-m depth decreased to values found at 270-m depth before the upwelling, suggesting that, albeit not having reached the surface, even the deepest layers of the lake were affected. Likewise, bimonthly CTD profiles taken at the deepest point of Lake Geneva (309 m depth, Figure 2.1) by CIPEL often show well-mixed bottom layers with thicknesses of ~20 to 30 m after windy periods (*Vent* and *Bise*) during winter.

Furthermore, this thesis demonstrated that wind-induced upwelling processes in Lake Geneva during winter frequently induce large isotherm displacements, with vertical excursions of 100 to 150 m. Upon relaxation of the wind, the upwelled thermocline “collapses” and baroclinic motions such as standing and progressive internal waves are generated that can lead to hypolimnetic mixing in the bottom boundary layer (e.g., van Haren et al. 2020; Simoncelli et al. 2020) and interior of deep lakes (e.g., van Haren et al. 2020). Recently, Lemmin (2020) showed that turbulent mixing in the deep hypolimnion of Lake Geneva during summer stratification appears to be due to breaking internal waves and frictional decay of inertial motions.

Considering the frequent occurrence and large vertical thermocline displacements associated with wind-induced coastal and interbasin upwelling events during winter, it appears likely that these processes significantly contribute to the dynamics of the deep hypolimnion of Lake Geneva. In this context, moored in situ measurements of temperature and current velocity

profiles at different locations in the deep hypolimnion, combined with systematic CTD profiling campaigns before and after strong *Vent* events, guided by 3D numerical modeling, would provide valuable insights. Based on the findings of this thesis, the northwestern and southwestern regions of the central 300 m deep plateau (Figure 1.2) appear to be the most promising mooring sites, as this is where the observed upwelling processes are initiated (Figures 2.9 and 3.6).

### 5.2.2 Field observations of deepwater ventilation by wind-induced upwelling processes in Lake Geneva

Recently, Lemmin (2020) showed that: (i) DO concentrations in the deep hypolimnion of Lake Geneva show considerable spatial and temporal variability, and (ii) over the past 40 years, DO concentrations in the deepest part of the lake (309 m depth) increased every year between December and March, even during years of incomplete convective overturning. These patterns cannot be explained by convective vertical mixing, but instead must be due to 3D processes such as density currents caused by differential cooling (Fer et al. 2002a; b), or regular wind-induced coastal and interbasin upwelling processes, as discussed in this thesis.

The findings of this thesis provide the mechanistic framework for understanding how frequently occurring wind-induced upwelling processes can contribute to deepwater renewal in Lake Geneva during winter, and in other large, deep lakes under similar conditions. A rough, order-of-magnitude estimation of the ventilation potential by Ekman-type coastal upwelling was provided using some characteristic numbers obtained from the 3D hydrodynamic model and particle tracking results (chapter 2). However, detailed, systematic in situ DO measurements are necessary to confirm the aeration of the deep hypolimnion layers by wind-induced upwelling during winter.

### 5.2.3 The role of *Bise* winds in generating coastal upwelling in Lake Geneva

This thesis focused on upwelling processes induced by *Vent* winds coming from the southwest, and their potential to contribute to deepwater renewal during winter. However, another comparably strong and steady large-scale wind exists in the Lake Geneva region, namely the *Bise* coming from the northeast and blowing over large parts of the central and western part of the lake (Figure 1.2). Analogously to *Vent* winds, *Bise* winds might produce Ekman-type



coastal upwelling at the southern shore of the central *Grand Lac* and thus contribute to deep-water renewal and dynamics during winter. Moored field observations at the southern shore of Lake Geneva (between the towns of Yvoire and Thonon-les-Bains, France), guided by careful analysis of the 3D model results produced in this thesis (winters 2017/2018 and 2018/2019), would help to answer the question to what extent *Bise* winds contribute to wintertime upwelling and deepwater renewal in Lake Geneva.



# Bibliography

- Adrian, R., C. M. O'Reilly, H. Zagarese, S. B. Baines, D. O. Hessen, W. Keller, D. M. Livingstone, R. Sommaruga, D. Straile, E. V. Donk, G. A. Weyhenmeyer, and M. Winder. 2009. Lakes as sentinels of climate change. *Limnology and Oceanography* **54**: 2283–2297. doi:[10.4319/lo.2009.54.6\\_part\\_2.2283](https://doi.org/10.4319/lo.2009.54.6_part_2.2283)
- Aeschbach-Hertig, W., R. Kipfer, M. Hofer, D. M. Imboden, and H. Baur. 1996. Density-driven exchange between the basins of Lake Lucerne (Switzerland) traced with the 3H-3He method. *Limnology and Oceanography* **41**: 707–721. doi:[10.4319/lo.1996.41.4.0707](https://doi.org/10.4319/lo.1996.41.4.0707)
- Ahrnsbrak, W. F., and M. R. Wing. 1998. Wind-induced hypolimnion exchange in Lake Ontario's Kingston basin: Potential effects on oxygen. *Journal of Great Lakes Research* **24**: 145–151. doi:[10.1016/S0380-1330\(98\)70806-8](https://doi.org/10.1016/S0380-1330(98)70806-8)
- Amadori, M., S. Piccolroaz, H. A. Dijkstra, and M. Toffolon. 2020. What makes an elongated lake 'large'? Scales from wind-driven steady circulation on a rotating Earth. *Journal of Great Lakes Research* **46**: 703–717. doi:[10.1016/j.jglr.2019.10.013](https://doi.org/10.1016/j.jglr.2019.10.013)
- Amadori, M., S. Piccolroaz, L. Giovannini, D. Zardi, and M. Toffolon. 2018. Wind variability and Earth's rotation as drivers of transport in a deep, elongated subalpine lake: The case of Lake Garda. *Journal of Limnology* **77**: 505–521. doi:[10.4081/jlimnol.2018.1814](https://doi.org/10.4081/jlimnol.2018.1814)
- Ambrosetti, W., and L. Barbanti. 1999. Deep water warming in lakes: An indicator of climatic change. *Journal of Limnology* **58**: 1–9. doi:[10.4081/jlimnol.1999.1](https://doi.org/10.4081/jlimnol.1999.1)
- Ambrosetti, W., L. Barbanti, and E. A. Carrara. 2010. Mechanisms of hypolimnion erosion in a deep lake (Lago Maggiore, N. Italy). *Journal of Limnology* **69**: 3–14. doi:[10.3274/JL10-69-1-01](https://doi.org/10.3274/JL10-69-1-01)
- Anderson, E. J., and D. J. Schwab. 2017. Meteorological influence on summertime baroclinic exchange in the Straits of Mackinac. *Journal of Geophysical Research: Oceans* **122**: 2171–2182. doi:[10.1002/2016JC012255](https://doi.org/10.1002/2016JC012255)
- Anneville, O., M. Beniston, N. Gallina, C. Gillet, S. Jacquet, J. Lazzarotto, and M. Perroud. 2013. L'empreinte du changement climatique sur le Léman. *Archives des sciences* **66**: 157.
- Antenucci, J. 2009. Currents in stratified water bodies 3: Effects of rotation, p. 559–567. *In* G.E. Likens [ed.], *Encyclopedia of inland waters*. Oxford: Elsevier.
- Appt, J., J. Imberger, and H. Kobus. 2004. Basin-scale motion in stratified Upper Lake Constance. *Limnology and Oceanography* **49**: 919–933. doi:[10.4319/lo.2004.49.4.0919](https://doi.org/10.4319/lo.2004.49.4.0919)
- Arvola, L., G. George, D. M. Livingstone, M. Järvinen, T. Blenckner, M. T. Dokulil, E. Jennings, C. N. Aonghusa, P. Nöges, T. Nöges, and G. A. Weyhenmeyer. 2010. The impact of the changing climate on the thermal characteristics of lakes, p. 85–101. *In* G. George [ed.], *The Impact of Climate Change on European Lakes*. Dordrecht: Springer.
- Austin, J., and S. Colman. 2008. A century of temperature variability in Lake Superior. *Limnology and Oceanography* **53**: 2724–2730. doi:[10.4319/lo.2008.53.6.2724](https://doi.org/10.4319/lo.2008.53.6.2724)
- Baracchini, T., A. Wüest, and D. Bouffard. 2020. Meteolakes: An operational online three-dimensional forecasting platform for lake hydrodynamics. *Water Research* **172**: 115529. doi:[10.1016/j.watres.2020.115529](https://doi.org/10.1016/j.watres.2020.115529)
- Bartish, T. 1987. A review of exchange processes among the three basins of Lake Erie. *Journal of Great Lakes Research* **13**: 607–618. doi:[10.1016/S0380-1330\(87\)71676-1](https://doi.org/10.1016/S0380-1330(87)71676-1)
- Bauer, S. W., W. H. Graf, C. H. Mortimer, and C. Perrinjaquet. 1981. Inertial motion in Lake Geneva (Le Léman). *Archives for meteorology, geophysics, and bioclimatology, Series A* **30**: 289–312. doi:[10.1007/BF02257850](https://doi.org/10.1007/BF02257850)
- Beletsky, D., W. P. O'Connor, D. J. Schwab, and D. E. Dietrich. 1997. Numerical simulation of internal Kelvin waves and coastal upwelling fronts. *Journal of Physical Oceanography* **27**: 1197–1215. doi:[10.1175/1520-0485\(1997\)027<1197:NSOIKW>2.0.CO;2](https://doi.org/10.1175/1520-0485(1997)027<1197:NSOIKW>2.0.CO;2)

- Bengtsson, L., R. W. Herschy, and R. W. Fairbridge, eds. 2012. *Encyclopedia of lakes and reservoirs*, Springer.
- Bennett, E. B. 1988. On the physical limnology of Georgian Bay, p. 21–34. *In* M. Munawar [ed.], *Limnology and fisheries of Georgian Bay and the North Channel ecosystems*. Dordrecht: Springer.
- Boegman, L. 2009. Currents in stratified water bodies 2: Internal waves, p. 539–558. *In* G.E. Likens [ed.], *Encyclopedia of inland waters*. Oxford: Elsevier.
- Boehrer, B., and M. Schultze. 2009. Density stratification and stability, p. 583–593. *In* G.E. Likens [ed.], *Encyclopedia of inland waters*. Oxford: Elsevier.
- Bohle-Carbonell, M. 1991. Wind and currents: Response patterns of Lake Geneva. *Annales Geophysicae* **9**: 82–90.
- Bouffard, D., L. Boegman, and Y. R. Rao. 2012. Poincaré wave-induced mixing in a large lake. *Limnology and Oceanography* **57**: 1201–1216. doi:[10.4319/lo.2012.57.4.1201](https://doi.org/10.4319/lo.2012.57.4.1201)
- Bouffard, D., I. Kiefer, A. Wüest, S. Wunderle, and D. Odermatt. 2018. Are surface temperature and chlorophyll in a large deep lake related? An analysis based on satellite observations in synergy with hydrodynamic modelling and in-situ data. *Remote Sensing of Environment* **209**: 510–523. doi:[10.1016/j.rse.2018.02.056](https://doi.org/10.1016/j.rse.2018.02.056)
- Bouffard, D., and U. Lemmin. 2013. Kelvin waves in Lake Geneva. *Journal of Great Lakes Research* **39**: 637–645. doi:[10.1016/j.jglr.2013.09.005](https://doi.org/10.1016/j.jglr.2013.09.005)
- Boyce, F. M., F. Chiocchio, B. Eid, F. Penicka, and F. Rosa. 1980. Hypolimnion flow between the central and eastern basins of Lake Erie during 1977 (Interbasin hypolimnion flows). *Journal of Great Lakes Research* **6**: 290–306. doi:[10.1016/S0380-1330\(80\)72110-X](https://doi.org/10.1016/S0380-1330(80)72110-X)
- CH2018. 2018. CH2018 – Climate Scenarios for Switzerland, Technical Report, National Centre for Climate Services, Zurich, 271 pp. ISBN: 978-3-9525031-4-0., Retrieved from <https://natural-sciences.ch/service/publications/107865-ch2018---climate-scenarios-for-switzerland-technical-report>, last accessed 30 May 2021.
- Cimatoribus, A. A. 2018. C-tracker. doi:[10.5281/zenodo.1034118](https://doi.org/10.5281/zenodo.1034118)
- Cimatoribus, A. A., U. Lemmin, and D. A. Barry. 2019. Tracking Lagrangian transport in Lake Geneva: A 3D numerical modeling investigation. *Limnology and Oceanography* **64**: 1–18. doi:[10.1002/lno.11111](https://doi.org/10.1002/lno.11111)
- Cimatoribus, A. A., U. Lemmin, D. Bouffard, and D. A. Barry. 2018. Nonlinear dynamics of the near-shore boundary layer of a large lake (Lake Geneva). *Journal of Geophysical Research: Oceans* **123**: 1016–1031. doi:[10.1002/2017JC013531](https://doi.org/10.1002/2017JC013531)
- CIPEL. 2016. Rapports sur les études et recherches entreprises dans le bassin lémanique, Campagne 2015. Commission internationale pour la protection des eaux du Léman (CIPEL), Nyon, Switzerland. Retrieved from [http://www.cipel.org/wp-content/uploads/2016/10/RapportScientifique\\_camp\\_2015\\_VF.pdf](http://www.cipel.org/wp-content/uploads/2016/10/RapportScientifique_camp_2015_VF.pdf), last accessed 30 May 2021.
- CIPEL. 2019. Rapports sur les études et recherches entreprises dans le bassin lémanique, Campagne 2018. Commission internationale pour la protection des eaux du Léman (CIPEL), Nyon, Switzerland. Retrieved from [https://www.cipel.org/wp-content/uploads/2019/10/RapportScientifique\\_camp\\_2018-1.pdf](https://www.cipel.org/wp-content/uploads/2019/10/RapportScientifique_camp_2018-1.pdf), last accessed 30 May 2021.
- Coats, R., J. Perez-Losada, G. Schladow, R. Richards, and C. Goldman. 2006. The warming of Lake Tahoe. *Climatic Change* **76**: 121–148. doi:[10.1007/s10584-005-9006-1](https://doi.org/10.1007/s10584-005-9006-1)
- Cole, J. J., and N. F. Caraco. 1998. Atmospheric exchange of carbon dioxide in a low-wind oligotrophic lake measured by the addition of SF<sub>6</sub>. *Limnology and Oceanography* **43**: 647–656. doi:[10.4319/lo.1998.43.4.0647](https://doi.org/10.4319/lo.1998.43.4.0647)
- Coman, M. A., and M. G. Wells. 2012. Temperature variability in the nearshore benthic boundary layer of Lake Opeongo is due to wind-driven upwelling events. *Canadian Journal of Fisheries and Aquatic Sciences* **69**: 282–296. doi:[10.1139/f2011-167](https://doi.org/10.1139/f2011-167)
- Corman, J. R., P. B. McIntyre, B. Kuboja, W. Mbemba, D. Fink, C. W. Wheeler, C. Gans, E. Michel, and A. S. Flecker. 2010. Upwelling couples chemical and biological dynamics across the littoral and pelagic zones of Lake Tanganyika, East Africa. *Limnology and Oceanography* **55**: 214–224. doi:[10.4319/lo.2010.55.1.0214](https://doi.org/10.4319/lo.2010.55.1.0214)
- Cornett, R., and F. Rigler. 1979. Hypolimnetic oxygen deficits: their prediction and interpretation. *Science (New York, N.Y.)* **205**: 580–581. doi:[10.1126/science.205.4406.580](https://doi.org/10.1126/science.205.4406.580)

- Cossu, R., and M. G. Wells. 2013. The interaction of large amplitude internal seiches with a shallow sloping lakebed: Observations of benthic turbulence in Lake Simcoe, Ontario, Canada. *PLoS ONE* **8**: e57444. doi:[10.1371/journal.pone.0057444](https://doi.org/10.1371/journal.pone.0057444)
- Crusius, J., and R. Wanninkhof. 2003. Gas transfer velocities measured at low wind speed over a lake. *Limnology and Oceanography* **48**: 1010–1017. doi:[10.4319/lo.2003.48.3.1010](https://doi.org/10.4319/lo.2003.48.3.1010)
- Csanady, G. T. 1977. Intermittent ‘full’ upwelling in Lake Ontario. *Journal of Geophysical Research* **82**: 397–419. doi:[10.1029/JC082i003p00397](https://doi.org/10.1029/JC082i003p00397)
- Cushman-Roisin, B., and J.-M. Beckers. 2011. *Introduction to geophysical fluid dynamics: physical and numerical aspects*, Academic Press.
- Djoumna, G., K. G. Lamb, and Y. R. Rao. 2014. Sensitivity of the parameterizations of vertical mixing and radiative heat fluxes on the seasonal evolution of the thermal structure of Lake Erie. *Atmosphere-Ocean* **52**: 294–313. doi:[10.1080/07055900.2014.939824](https://doi.org/10.1080/07055900.2014.939824)
- Döös, K., J. Kjellsson, and B. Jönsson. 2013. TRACMASS—A Lagrangian trajectory model, p. 225–249. *In* T. Soomere and E. Quak [eds.], *Preventive Methods for Coastal Protection: Towards the Use of Ocean Dynamics for Pollution Control*. Heidelberg: Springer International Publishing.
- Dorostkar, A., and L. Boegman. 2013. Internal hydraulic jumps in a long narrow lake. *Limnology and Oceanography* **58**: 153–172. doi:[10.4319/lo.2013.58.1.0153](https://doi.org/10.4319/lo.2013.58.1.0153)
- Dorostkar, A., L. Boegman, and A. Pollard. 2017. Three-dimensional simulation of high-frequency non-linear internal wave dynamics in Cayuga Lake. *Journal of Geophysical Research: Oceans* **122**: 2183–2204. doi:[10.1002/2016JC011862](https://doi.org/10.1002/2016JC011862)
- Ekman, V. W. 1905. On the influence of the earth’s rotation on ocean-currents. *Arkiv for Matematik, Astronomi, och Fysik* **2**: 1–52.
- Fer, I., U. Lemmin, and S. A. Thorpe. 2002a. Winter cascading of cold water in Lake Geneva. *Journal of Geophysical Research* **107**: 13-1-13–16. doi:[10.1029/2001JC000828](https://doi.org/10.1029/2001JC000828)
- Fer, I., U. Lemmin, and S. A. Thorpe. 2002b. Contribution of entrainment and vertical plumes to the winter cascading of cold shelf waters in a deep lake. *Limnology and Oceanography* **47**: 576–580. doi:[10.4319/lo.2002.47.2.0576](https://doi.org/10.4319/lo.2002.47.2.0576)
- Flood, B., M. Wells, E. Dunlop, and J. Young. 2020. Internal waves pump waters in and out of a deep coastal embayment of a large lake. *Limnology and Oceanography* **65**: 205–223. doi:[10.1002/lno.11292](https://doi.org/10.1002/lno.11292)
- Forel, F. A. 1892. *Le Léman: Monographie Limnologique* 1, F. Rouge.
- Friedrich, J., F. Janssen, D. Aleynik, H. W. Bange, N. Boltacheva, M. N. Çagatay, A. W. Dale, G. Etiope, Z. Erdem, M. Geraga, A. Gilli, M. T. Gomoiu, P. O. J. Hall, D. Hansson, Y. He, M. Holtappels, M. K. Kirf, M. Kononets, S. Konovalov, A. Lichtschlag, D. M. Livingstone, G. Marinaro, S. Mazlumyan, S. Naeher, R. P. North, G. Papatheodorou, O. Pfannkuche, R. Prien, G. Rehder, C. J. Schubert, T. Soltwedel, S. Sommer, H. Stahl, E. V. Stanev, A. Teaca, A. Tengberg, C. Waldmann, B. Wehrli, and F. Wenzhöfer. 2014. Investigating hypoxia in aquatic environments: diverse approaches to addressing a complex phenomenon. *Biogeosciences* **11**: 1215–1259. doi:[10.5194/bg-11-1215-2014](https://doi.org/10.5194/bg-11-1215-2014)
- Giddings, S. N., and P. MacCready. 2017. Reverse estuarine circulation due to local and remote wind forcing, enhanced by the presence of along-coast estuaries. *Journal of Geophysical Research: Oceans* **122**: 10184–10205. doi:[10.1002/2016JC012479](https://doi.org/10.1002/2016JC012479)
- van de Giesen, N., S. C. Steele-Dunne, J. Jansen, O. Hoes, M. B. Hausner, S. Tyler, and J. Selker. 2012. Double-ended calibration of fiber-optic Raman spectra distributed temperature sensing data. *Sensors* **12**: 5471–5485. doi:[10.3390/s120505471](https://doi.org/10.3390/s120505471)
- Giovanoli, F. 1990. Horizontal Transport and Sedimentation by Interflows and Turbidity Currents in Lake Geneva, p. 175–195. *In* M.M. Tilzer and C. Serruya [eds.], *Large Lakes: Ecological Structure and Function*. Springer.
- Goldman, C. R., M. Kumagai, and R. D. Robarts, eds. 2013. *Climatic change and global warming of inland waters: Impacts and mitigation for ecosystems and societies*, Wiley-Blackwell.
- Graf, W. H., and J. P. Prost. 1980. Aerodynamic drag and its relation to the sea state: With data from Lake Geneva. *Archiv für Meteorologie, Geophysik und Bioklimatologie, Serie A* **29**: 67–87. doi:[10.1007/BF02247734](https://doi.org/10.1007/BF02247734)

- Graf, M., S. C. Scherrer, C. Schwierz, M. Begert, O. Martius, C. C. Raible, and S. Brönnimann. 2019. Near-surface mean wind in Switzerland: Climatology, climate model evaluation and future scenarios. *International Journal of Climatology* **39**: 4798–4810. doi:[10.1002/joc.6108](https://doi.org/10.1002/joc.6108)
- Guérin, F., G. Abril, D. Serça, C. Delon, S. Richard, R. Delmas, A. Tremblay, and L. Varfalvy. 2007. Gas transfer velocities of CO<sub>2</sub> and CH<sub>4</sub> in a tropical reservoir and its river downstream. *Journal of Marine Systems* **66**: 161–172. doi:[10.1016/j.jmarsys.2006.03.019](https://doi.org/10.1016/j.jmarsys.2006.03.019)
- Hamidi, S. A., H. R. Bravo, J. V. Klump, and J. T. Waples. 2015. The role of circulation and heat fluxes in the formation of stratification leading to hypoxia in Green Bay, Lake Michigan. *Journal of Great Lakes Research* **41**: 1024–1036. doi:[10.1016/j.jglr.2015.08.007](https://doi.org/10.1016/j.jglr.2015.08.007)
- van Haren, H., S. Piccolroaz, M. Amadori, M. Toffolon, and H. A. Dijkstra. 2020. Moored observations of turbulent mixing events in deep Lake Garda, Italy. *Journal of Limnology* **80**. doi:[10.4081/jlimnol.2020.1983](https://doi.org/10.4081/jlimnol.2020.1983)
- Hlevca, B., M. G. Wells, L. Cruz Font, S. E. Doka, R. Portiss, M. St. John, and S. J. Cooke. 2018. Water circulation in Toronto Harbour. *Aquatic Ecosystem Health & Management* **21**: 234–244. doi:[10.1080/14634988.2018.1500059](https://doi.org/10.1080/14634988.2018.1500059)
- Homma, H., T. Nagai, K. Shimizu, and H. Yamazaki. 2016. Early-winter mixing event associated with baroclinic motions in weakly stratified Lake Biwa. *Inland Waters* **6**: 364–378. doi:[10.1080/TW-6.3.898](https://doi.org/10.1080/TW-6.3.898)
- Hutter, K., Y. Wang, and I. P. Chubarenko. 2011. *Physics of Lakes Volume 1*, Springer Berlin Heidelberg.
- Jabbari, A., J. D. Ackerman, L. Boegman, and Y. Zhao. 2019. Episodic hypoxia in the western basin of Lake Erie. *Limnology and Oceanography* **64**: 2220–2236. doi:[10.1002/lno.11180](https://doi.org/10.1002/lno.11180)
- Jabbari, A., J. D. Ackerman, L. Boegman, and Y. Zhao. 2021. Increases in Great Lake winds and extreme events facilitate interbasin coupling and reduce water quality in Lake Erie. *Scientific Reports* **11**: 5733. doi:[10.1038/s41598-021-84961-9](https://doi.org/10.1038/s41598-021-84961-9)
- Jähne, B., K. O. Münnich, R. Börsinger, A. Dutzi, W. Huber, and P. Libner. 1987. On the parameters influencing air-water gas exchange. *Journal of Geophysical Research* **92**: 1937–1949. doi:[10.1029/JC092iC02p01937](https://doi.org/10.1029/JC092iC02p01937)
- Jazi, S. D., M. G. Wells, J. Peakall, R. M. Dorrell, R. E. Thomas, G. M. Keevil, S. E. Darby, J. Sommeria, S. Viboud, and T. Valran. 2020. Influence of Coriolis force upon bottom boundary layers in a large-scale gravity current experiment: Implications for evolution of sinuous deep-water channel systems. *Journal of Geophysical Research: Oceans* **125**: e2019JC015284. doi:[10.1029/2019JC015284](https://doi.org/10.1029/2019JC015284)
- Kämpf, J. 2010. *Advanced Ocean Modelling*, Berlin, Heidelberg: Springer.
- Kämpf, J., and P. Chapman. 2016. The functioning of coastal upwelling systems, p. 31–65. *In Upwelling systems of the world*. Cham: Springer International Publishing.
- Klaus, M., and D. Vachon. 2020. Challenges of predicting gas transfer velocity from wind measurements over global lakes. *Aquatic Sciences* **82**: 53. doi:[10.1007/s00027-020-00729-9](https://doi.org/10.1007/s00027-020-00729-9)
- Kocsis, O., B. Mathis, M. Gloor, M. Schurter, and A. Wüest. 1998. Enhanced mixing in narrows: A case study at the Mainau sill (Lake Constance). *Aquatic Sciences* **60**: 236. doi:[10.1007/s000270050039](https://doi.org/10.1007/s000270050039)
- Kraemer, B. M., O. Anneville, S. Chandra, M. Dix, E. Kuusisto, D. M. Livingstone, A. Rimmer, S. G. Schladow, E. Silow, L. M. Sitoki, R. Tamatamah, Y. Vadeboncoeur, and P. B. McIntyre. 2015. Morphometry and average temperature affect lake stratification responses to climate change. *Geophysical Research Letters* **42**: 4981–4988. doi:[10.1002/2015GL064097](https://doi.org/10.1002/2015GL064097)
- Krishna, S., H. N. Ulloa, O. Kerimoglu, C. Minaudo, O. Anneville, and A. Wüest. 2021. Model-based data analysis of the effect of winter mixing on primary production in a lake under reoligotrophication. *Ecological Modelling* **440**: 109401. doi:[10.1016/j.ecolmodel.2020.109401](https://doi.org/10.1016/j.ecolmodel.2020.109401)
- Lambert, A., and F. Giovanoli. 1988. Records of riverborne turbidity currents and indications of slope failures in the Rhone delta of Lake Geneva. *Limnology and Oceanography* **33**: 458–468. doi:[10.4319/lo.1988.33.3.0458](https://doi.org/10.4319/lo.1988.33.3.0458)
- Large, W. G., J. C. McWilliams, and S. C. Doney. 1994. Oceanic vertical mixing: A review and a model with a nonlocal boundary layer parameterization. *Reviews of Geophysics* **32**: 363–403. doi:[10.1029/94RG01872](https://doi.org/10.1029/94RG01872)



- Laval, B. E., J. Morrison, D. J. Potts, E. C. Carmack, S. Vagle, C. James, F. A. McLaughlin, and M. Foreman. 2008. Wind-driven summertime upwelling in a fjord-type lake and its impact on downstream river conditions: Quesnel Lake and River, British Columbia, Canada. *Journal of Great Lakes Research* **34**: 189–203. doi:[10.3394/0380-1330\(2008\)34\[189:WSUIAF\]2.0.CO;2](https://doi.org/10.3394/0380-1330(2008)34[189:WSUIAF]2.0.CO;2)
- Lavigne, S., and P. Nirel. 2016. Physico-chemical and biological changes in the waters of the Petit Lac. Service de l'écologie de l'eau (SECOE). Geneva, Switzerland. Retrieved from [http://www.cipel.org/wp-content/uploads/2016/11/0\\_evolution\\_physico\\_chimique\\_biologique\\_petit-lac\\_camp\\_2015.pdf](http://www.cipel.org/wp-content/uploads/2016/11/0_evolution_physico_chimique_biologique_petit-lac_camp_2015.pdf), accessed 30 May 2021.
- Lawrence, G., R. Pieters, L. Zaremba, T. Tedford, L. Gu, S. Greco, and P. Hamblin. 2004. Summer exchange between Hamilton Harbour and Lake Ontario. *Deep Sea Research Part II: Topical Studies in Oceanography* **51**: 475–487. doi:[10.1016/j.dsr2.2003.09.002](https://doi.org/10.1016/j.dsr2.2003.09.002)
- Lemmin, U. 2020. Insights into the dynamics of the deep hypolimnion of Lake Geneva as revealed by long-term temperature, oxygen, and current measurements. *Limnology and Oceanography* **65**: 2092–2107. doi:[10.1002/lno.11441](https://doi.org/10.1002/lno.11441)
- Lemmin, U., and A. Amouroux. 2013. The influence of climate change on Lake Geneva, p. 201–217. In C.R. Goldman, M. Kumagai, and R.D. Robarts [eds.], *Climatic change and global warming of inland waters*. Chichester: John Wiley.
- Lemmin, U., and N. D'Adamo. 1996. Summertime winds and direct cyclonic circulation: Observations from Lake Geneva. *Annales Geophysicae* **14**: 1207–1220. doi:[10.1007/s00585-996-1207-z](https://doi.org/10.1007/s00585-996-1207-z)
- Lemmin, U., C. H. Mortimer, and E. Bäuerle. 2005. Internal seiche dynamics in Lake Geneva. *Limnology and Oceanography* **50**: 207–216. doi:[10.4319/lo.2005.50.1.0207](https://doi.org/10.4319/lo.2005.50.1.0207)
- Likens, G. E., ed. 2010. *Biogeochemistry of inland waters: a derivative of Encyclopedia of inland waters*, Elsevier/Academic Press.
- Liu, Q., E. J. Anderson, Y. Zhang, A. D. Weinke, K. L. Knapp, and B. A. Biddanda. 2018. Modeling reveals the role of coastal upwelling and hydrologic inputs on biologically distinct water exchanges in a Great Lakes estuary. *Estuarine, Coastal and Shelf Science* **209**: 41–55. doi:[10.1016/j.ecss.2018.05.014](https://doi.org/10.1016/j.ecss.2018.05.014)
- Livingstone, D. M. 1993. Temporal structure in the deep-water temperature of four Swiss lakes: A short-term climatic change indicator? *Verhandlungen der Internationalen Vereinigung für Theoretische und Angewandte Limnologie* **25**: 75–81. doi:[10.1080/03680770.1992.11900062](https://doi.org/10.1080/03680770.1992.11900062)
- Livingstone, D. M. 1997. An example of the simultaneous occurrence of climate-driven “sawtooth” deep-water warming/cooling episodes in several Swiss lakes. *SIL Proceedings, 1922–2010* **26**: 822–828. doi:[10.1080/03680770.1995.11900832](https://doi.org/10.1080/03680770.1995.11900832)
- Livingstone, D. M. 2003. Impact of secular climate change on the thermal structure of a large temperate Central European lake. *Climatic Change* **57**: 205–225. doi:[10.1023/A:1022119503144](https://doi.org/10.1023/A:1022119503144)
- Loizeau, J.-L., and J. Dominik. 2000. Evolution of the Upper Rhone River discharge and suspended sediment load during the last 80 years and some implications for Lake Geneva. *Aquatic Sciences* **62**: 54. doi:[10.1007/s000270050075](https://doi.org/10.1007/s000270050075)
- Marshall, J., A. Adcroft, C. Hill, L. Perelman, and C. Heisey. 1997. A finite-volume, incompressible Navier Stokes model for studies of the ocean on parallel computers. *Journal of Geophysical Research: Oceans* **102**: 5753–5766. doi:[10.1029/96JC02775](https://doi.org/10.1029/96JC02775)
- Matsumoto, K., K. S. Tokos, and C. Gregory. 2015. Ventilation and dissolved oxygen cycle in Lake Superior: Insights from a numerical model. *Geochemistry, Geophysics, Geosystems* **16**: 3097–3110. doi:[10.1002/2015GC005916](https://doi.org/10.1002/2015GC005916)
- McEwen, G. F. 1912. The distribution of ocean temperatures along the west coast of North America deduced from Ekman's theory of the upwelling of cold water from the adjacent ocean depths. *Internationale Revue der gesamten Hydrobiologie und Hydrographie* **5**: 243–286. doi:[10.1002/iroh.19120050205](https://doi.org/10.1002/iroh.19120050205)
- McKinney, P., K. S. Tokos, and K. Matsumoto. 2018. Modeling nearshore-offshore exchange in Lake Superior. *PLOS ONE* **13**: e0193183. doi:[10.1371/journal.pone.0193183](https://doi.org/10.1371/journal.pone.0193183)
- Mesman, J. P., J. A. A. Stelzer, V. Dakos, S. Goyette, I. D. Jones, J. Kasparian, D. F. McGinnis, and B. W. Ibelings. 2021. The role of internal feedbacks in shifting deep lake mixing regimes under a warming climate. *Freshwater Biology* **66**: 1021–1035. doi:[10.1111/fwb.13704](https://doi.org/10.1111/fwb.13704)

- Molinero, J. C., O. Anneville, S. Souissi, L. Lainé, and D. Gerdeaux. 2007. Decadal changes in water temperature and ecological time series in Lake Geneva, Europe—relationship to subtropical Atlantic climate variability. *Climate Research* **34**: 15–23. doi:[10.3354/cr034015](https://doi.org/10.3354/cr034015)
- Monismith, S. G., J. Imberger, and M. L. Morison. 1990. Convective motions in the sidearm of a small reservoir. *Limnology and Oceanography* **35**: 1676–1702. doi:[10.4319/lo.1990.35.8.1676](https://doi.org/10.4319/lo.1990.35.8.1676)
- Monsen, N. E., J. E. Cloern, L. V. Lucas, and S. G. Monismith. 2002. A comment on the use of flushing time, residence time, and age as transport time scales. *Limnology and Oceanography* **47**: 1545–1553. doi:[10.4319/lo.2002.47.5.1545](https://doi.org/10.4319/lo.2002.47.5.1545)
- Mortimer, C. H. 1952. Water movements in lakes during summer stratification; evidence from the distribution of temperature in Windermere. *Philosophical Transactions of the Royal Society of London. Series B, Biological Sciences* **236**: 355–404. doi:[10.1098/rstb.1952.0005](https://doi.org/10.1098/rstb.1952.0005)
- Mortimer, C. H. 1981. The oxygen content of air-saturated fresh waters over ranges of temperature and atmospheric pressure of limnological interest. *SIL Communications, 1953-1996* **22**: 1–23. doi:[10.1080/05384680.1981.11904000](https://doi.org/10.1080/05384680.1981.11904000)
- Nguyen, T. D., P. Thupaki, E. J. Anderson, and M. S. Phanikumar. 2014. Summer circulation and exchange in the Saginaw Bay-Lake Huron system. *Journal of Geophysical Research* **119**: 2713–2734. doi:[10.1002/2014JC009828](https://doi.org/10.1002/2014JC009828)
- Niu, Q., M. Xia, E. S. Rutherford, D. M. Mason, E. J. Anderson, and D. J. Schwab. 2015. Investigation of interbasin exchange and interannual variability in Lake Erie using an unstructured-grid hydrodynamic model. *Journal of Geophysical Research: Oceans* **120**: 2212–2232. doi:[10.1002/2014JC010457](https://doi.org/10.1002/2014JC010457)
- Nürnberg, G. K., L. A. Molot, E. O'Connor, H. Jarjanazi, J. Winter, and J. Young. 2013. Evidence for internal phosphorus loading, hypoxia and effects on phytoplankton in partially polymictic Lake Simcoe, Ontario. *Journal of Great Lakes Research* **39**: 259–270. doi:[10.1016/j.jglr.2013.03.016](https://doi.org/10.1016/j.jglr.2013.03.016)
- Okubo, K. 1995. Field observations of the dense bottom current between the north and south basins, p. 43–51. *In* S. Okuda, J. Imberger, and M. Kumagai [eds.], *Physical processes in a large lake: Lake Biwa, Japan*. American Geophysical Union (AGU).
- Oonishi, Y. 1995. Numerical simulation of density-induced currents between the north and south basins of lake biwa, p. 53–64. *In* S. Okuda, J. Imberger, and M. Kumagai [eds.], *Physical processes in a large lake: Lake Biwa, Japan*. American Geophysical Union (AGU).
- O'Reilly, C. M., S. Sharma, D. K. Gray, S. E. Hampton, J. S. Read, R. J. Rowley, P. Schneider, J. D. Lenters, P. B. McIntyre, B. M. Kraemer, G. A. Weyhenmeyer, D. Straile, B. Dong, R. Adrian, M. G. Allan, O. Anneville, L. Arvola, J. Austin, J. L. Bailey, J. S. Baron, J. D. Brookes, E. de Eyto, M. T. Dokulil, D. P. Hamilton, K. Havens, A. L. Hetherington, S. N. Higgins, S. Hook, L. R. Izmet'seva, K. D. Joehnk, K. Kangur, P. Kasprzak, M. Kumagai, E. Kuusisto, G. Leshkevich, D. M. Livingstone, S. MacIntyre, L. May, J. M. Melack, D. C. Mueller-Navarra, M. Naumenko, P. Noges, T. Noges, R. P. North, P.-D. Plisnier, A. Rigosi, A. Rimmer, M. Rogora, L. G. Rudstam, J. A. Rusak, N. Salmaso, N. R. Samal, D. E. Schindler, S. G. Schladow, M. Schmid, S. R. Schmidt, E. Silow, M. E. Soylu, K. Teubner, P. Verburg, A. Voutilainen, A. Watkinson, C. E. Williamson, and G. Zhang. 2015. Rapid and highly variable warming of lake surface waters around the globe. *Geophysical Research Letters* **42**: 10,773–10,781. doi:[10.1002/2015GL066235](https://doi.org/10.1002/2015GL066235)
- Peeters, F., D. Finger, M. Hofer, M. Brennwald, D. M. Livingstone, and R. Kipfer. 2003. Deep-water renewal in Lake Issyk-Kul driven by differential cooling. *Limnology and Oceanography* **48**: 1419–1431. doi:[10.4319/lo.2003.48.4.1419](https://doi.org/10.4319/lo.2003.48.4.1419)
- Perroud, M., and S. Goyette. 2012. Interfacing a one-dimensional lake model with a single-column atmospheric model: 2. Thermal response of the deep Lake Geneva, Switzerland under a  $2 \times \text{CO}_2$  global climate change. *Water Resources Research* **48**: W06522. doi:[10.1029/2011WR011222](https://doi.org/10.1029/2011WR011222)
- Perroud, M., S. Goyette, A. Martynov, M. Beniston, and O. Anneville. 2009. Simulation of multiannual thermal profiles in deep Lake Geneva: A comparison of one-dimensional lake models. *Limnology and Oceanography* **54**: 1574–1594. doi:[10.4319/lo.2009.54.5.1574](https://doi.org/10.4319/lo.2009.54.5.1574)
- Piccolroaz, S., M. Amadori, M. Toffolon, and H. A. Dijkstra. 2019. Importance of planetary rotation for ventilation processes in deep elongated lakes: Evidence from Lake Garda (Italy). *Scientific Reports* **9**: 8290. doi:[10.1038/s41598-019-44730-1](https://doi.org/10.1038/s41598-019-44730-1)



- Plattner, S., D. M. Mason, G. A. Leshkevich, D. J. Schwab, and E. S. Rutherford. 2006. Classifying and forecasting coastal upwellings in Lake Michigan using satellite derived temperature images and buoy data. *Journal of Great Lakes Research* **32**: 63–76. doi:[10.3394/0380-1330\(2006\)32\[63:CAFCUI\]2.0.CO;2](https://doi.org/10.3394/0380-1330(2006)32[63:CAFCUI]2.0.CO;2)
- Ponte, A. L., G. Gutiérrez de Velasco, A. Valle-Levinson, K. B. Winters, and C. D. Winant. 2012. Wind-driven subinertial circulation inside a semienclosed bay in the Gulf of California. *Journal of Physical Oceanography* **42**: 940–955. doi:[10.1175/JPO-D-11-0103.1](https://doi.org/10.1175/JPO-D-11-0103.1)
- Pöschke, F., J. Lewandowski, C. Engelhardt, K. Preuß, M. Oczipka, T. Ruhtz, and G. Kirillin. 2015. Upwelling of deep water during thermal stratification onset—A major mechanism of vertical transport in small temperate lakes in spring? *Water Resources Research* **51**: 9612–9627. doi:[10.1002/2015WR017579](https://doi.org/10.1002/2015WR017579)
- Rao, Y. R., T. Howell, S. B. Watson, and S. Abernethy. 2014. On hypoxia and fish kills along the north shore of Lake Erie. *Journal of Great Lakes Research* **40**: 187–191. doi:[10.1016/j.jglr.2013.11.007](https://doi.org/10.1016/j.jglr.2013.11.007)
- Rao, Y. R., and C. R. Murthy. 2001. Nearshore currents and turbulent exchange processes during upwelling and downwelling events in Lake Ontario. *Journal of Geophysical Research: Oceans* **106**: 2667–2678. doi:[10.1029/2000JC900149](https://doi.org/10.1029/2000JC900149)
- Reiss, R. S., U. Lemmin, and D. A. Barry. 2021. Wind-induced hypolimnetic upwelling between the multi-depth basins of Lake Geneva during winter: An overlooked deep-water renewal mechanism?. *Limnology and Oceanography*: Submitted
- Reiss, R. S., U. Lemmin, A. A. Cimattoribus, and D. A. Barry. 2020. Wintertime coastal upwelling in Lake Geneva: An efficient transport process for deepwater renewal in a large, deep lake. *Journal of Geophysical Research: Oceans* **125**. doi:[10.1029/2020JC016095](https://doi.org/10.1029/2020JC016095)
- Rimet, F., O. Anneville, D. Barbet, C. Chardon, L. Crépin, I. Domaizon, J.-M. Dorioz, L. Espinat, V. Frossard, J. Guillard, C. Goulon, V. Hamelet, J.-C. Hustache, S. Jacquet, L. Lainé, B. Montuelle, P. Perney, P. Quetin, S. Rasconi, A. Schellenberger, V. Tran-Khac, and G. Monet. 2020. The Observatory on LAkes (OLA) database: Sixty years of environmental data accessible to the public: The Observatory on LAkes (OLA) database. *Journal of Limnology* **79**. doi:[10.4081/jlimnol.2020.1944](https://doi.org/10.4081/jlimnol.2020.1944)
- Rivas, D., and R. M. Samelson. 2011. A numerical modeling study of the upwelling source waters along the Oregon Coast during 2005. *Journal of Physical Oceanography* **41**: 88–112. doi:[10.1175/2010JPO4327.1](https://doi.org/10.1175/2010JPO4327.1)
- Roberts, D. C., G. C. Egan, A. L. Forrest, J. L. Largier, F. A. Bombardelli, B. E. Laval, S. G. Monismith, and G. Schladow. 2021. The setup and relaxation of spring upwelling in a deep, rotationally influenced lake. *Limnology and Oceanography* **66**: 1168–1189. doi:[10.1002/lno.11673](https://doi.org/10.1002/lno.11673)
- Roget, E., and J. Colomer. 1996. Flow characteristics of a gravity current induced by differential cooling in a small lake. *Aquatic sciences* **58**: 367–377. doi:[10.1007/BF00877476](https://doi.org/10.1007/BF00877476)
- Rowe, M. D., E. J. Anderson, D. Beletsky, C. A. Stow, S. D. Moegling, J. D. Chaffin, J. C. May, P. D. Collingsworth, A. Jabbari, and J. D. Ackerman. 2019. Coastal upwelling influences hypoxia spatial patterns and nearshore dynamics in Lake Erie. *Journal of Geophysical Research: Oceans* **124**: 6154–6175. doi:[10.1029/2019JC015192](https://doi.org/10.1029/2019JC015192)
- Sahoo, G. B., S. G. Schladow, J. E. Reuter, R. Coats, M. Dettinger, J. Riverson, B. Wolfe, and M. Costa-Cabral. 2013. The response of Lake Tahoe to climate change. *Climatic Change* **116**: 71–95. doi:[10.1007/s10584-012-0600-8](https://doi.org/10.1007/s10584-012-0600-8)
- Salmaso, N. 2005. Effects of climatic fluctuations and vertical mixing on the interannual trophic variability of Lake Garda, Italy. *Limnology and Oceanography* **50**: 553–565. doi:[10.4319/lo.2005.50.2.0553](https://doi.org/10.4319/lo.2005.50.2.0553)
- Sanay, R., and A. Valle-Levinson. 2005. Wind-induced circulation in semienclosed homogeneous, rotating basins. *Journal of Physical Oceanography* **35**: 2520–2531. doi:[10.1175/JPO2831.1](https://doi.org/10.1175/JPO2831.1)
- Saylor, J. H., and G. S. Miller. 1987. Studies of large-scale currents in Lake Erie, 1979–80. *Journal of Great Lakes Research* **13**: 487–514. doi:[10.1016/S0380-1330\(87\)71668-2](https://doi.org/10.1016/S0380-1330(87)71668-2)
- Scavia, D., J. David Allan, K. K. Arend, S. Bartell, D. Beletsky, N. S. Bosch, S. B. Brandt, R. D. Briland, I. Daloğlu, J. V. DePinto, D. M. Dolan, M. A. Evans, T. M. Farmer, D. Goto, H. Han, T. O. Höök, R. Knight, S. A. Ludsin, D. Mason, A. M. Michalak, R. Peter Richards, J. J. Roberts, D. K. Rucinski, E. Rutherford, D. J. Schwab, T. M. Sesterhenn, H. Zhang, and Y. Zhou. 2014.

- Assessing and addressing the re-eutrophication of Lake Erie: Central basin hypoxia. *Journal of Great Lakes Research* **40**: 226–246. doi:[10.1016/j.jglr.2014.02.004](https://doi.org/10.1016/j.jglr.2014.02.004)
- Schertzer, W. M., R. A. Assel, D. Beletsky, T. E. C. Li, B. M. Lofgren, and D. J. Schwab. 2008. Lake Huron climatology, inter-lake exchange and mean circulation. *Aquatic Ecosystem Health and Management* **11**: 144–152. doi:[10.1080/14634980802098705](https://doi.org/10.1080/14634980802098705)
- Schladow, S. G., S. Ó. Pálmarrsson, T. E. Steissberg, S. J. Hook, and F. E. Prata. 2004. An extraordinary upwelling event in a deep thermally stratified lake. *Geophysical Research Letters* **31**: L15504. doi:[10.1029/2004GL020392](https://doi.org/10.1029/2004GL020392)
- Schulz, B. 1917. Die Auftrieberscheinungen an der Westküste Nordamerikas. *Naturwissenschaften* **5**: 713–719. doi:[10.1007/BF02447973](https://doi.org/10.1007/BF02447973)
- Schwefel, R., A. Gaudard, A. Wüest, and D. Bouffard. 2016. Effects of climate change on deepwater oxygen and winter mixing in a deep lake (Lake Geneva): Comparing observational findings and modeling. *Water Resources Research* **52**: 8811–8826. doi:[10.1002/2016WR019194](https://doi.org/10.1002/2016WR019194)
- Schwefel, R., M. Hondzo, A. Wüest, and D. Bouffard. 2017. Scaling oxygen microprofiles at the sediment interface of deep stratified waters. *Geophysical Research Letters* **44**: 1340–1349. doi:[10.1002/2016GL072079](https://doi.org/10.1002/2016GL072079)
- Schwefel, R., T. Steinsberger, D. Bouffard, L. D. Bryant, B. Müller, and A. Wüest. 2018. Using small-scale measurements to estimate hypolimnetic oxygen depletion in a deep lake. *Limnology and Oceanography* **63**: S54–S67. doi:[10.1002/lno.10723](https://doi.org/10.1002/lno.10723)
- van Sebille, E., S. M. Griffies, R. Abernathey, T. P. Adams, P. Berloff, A. Biastoch, B. Blanke, E. P. Chassignet, Y. Cheng, C. J. Cotter, E. Deleersnijder, K. Döös, H. F. Drake, S. Drijfhout, S. F. Gary, A. W. Heemink, J. Kjellsson, I. M. Koszalka, M. Lange, C. Lique, G. A. MacGilchrist, R. Marsh, C. G. Mayorga Adame, R. McAdam, F. Nencioli, C. B. Paris, M. D. Piggott, J. A. Polton, S. Rühs, S. H. A. M. Shah, M. D. Thomas, J. Wang, P. J. Wolfram, L. Zanna, and J. D. Zika. 2018. Lagrangian ocean analysis: Fundamentals and practices. *Ocean Modelling* **121**: 49–75. doi:[10.1016/j.ocemod.2017.11.008](https://doi.org/10.1016/j.ocemod.2017.11.008)
- Selker, J. S., L. Thévenaz, H. Huwald, A. Mallet, W. Luxemburg, N. van de Giesen, M. Stejskal, J. Zeman, M. Westhoff, and M. B. Parlange. 2006. Distributed fiber-optic temperature sensing for hydrologic systems. *Water Resources Research* **42**: W12202. doi:[10.1029/2006WR005326](https://doi.org/10.1029/2006WR005326)
- van Senden, D. C., and D. M. Imboden. 1989. Internal seiche pumping between sill-separated basins. *Geophysical & Astrophysical Fluid Dynamics* **48**: 135–150. doi:[10.1080/03091928908219530](https://doi.org/10.1080/03091928908219530)
- Shimoda, Y., M. E. Azim, G. Perhar, M. Ramin, M. A. Kenney, S. Sadraddini, A. Gudimov, and G. B. Arhonditsis. 2011. Our current understanding of lake ecosystem response to climate change: What have we really learned from the north temperate deep lakes? *Journal of Great Lakes Research* **37**: 173–193. doi:[10.1016/j.jglr.2010.10.004](https://doi.org/10.1016/j.jglr.2010.10.004)
- Simoncelli, S., G. Valerio, M. Hupfer, S. Jordan, M. Pilotti, and G. Kirillin. 2020. Sources and scales of near-bottom turbulent mixing in large meromictic Lake Iseo. *Journal of Great Lakes Research* **46**: 1581–1594. doi:[10.1016/j.jglr.2020.09.013](https://doi.org/10.1016/j.jglr.2020.09.013)
- Soulignac, F., P.-A. Danis, D. Bouffard, V. Chanudet, E. Dambrine, Y. Guénand, T. Harmel, B. W. Ibelings, D. Trevisan, R. Uittenbogaard, and O. Anneville. 2018. Using 3D modeling and remote sensing capabilities for a better understanding of spatio-temporal heterogeneities of phytoplankton abundance in large lakes. *Journal of Great Lakes Research* **44**: 756–764. doi:[10.1016/j.jglr.2018.05.008](https://doi.org/10.1016/j.jglr.2018.05.008)
- Steissberg, T. E., S. J. Hook, and S. G. Schladow. 2005. Characterizing partial upwellings and surface circulation at Lake Tahoe, California–Nevada, USA with thermal infrared images. *Remote Sensing of Environment* **99**: 2–15. doi:[10.1016/j.rse.2005.06.011](https://doi.org/10.1016/j.rse.2005.06.011)
- Sun, D., T. Ito, and A. Bracco. 2017. Oceanic uptake of oxygen during deep convection events through diffusive and bubble-mediated gas exchange. *Global Biogeochemical Cycles* **31**: 1579–1591. doi:[10.1002/2017GB005716](https://doi.org/10.1002/2017GB005716)
- Tamsitt, V., H. F. Drake, A. K. Morrison, L. D. Talley, C. O. Dufour, A. R. Gray, S. M. Griffies, M. R. Mazloff, J. L. Sarmiento, J. Wang, and W. Weiher. 2017. Spiraling pathways of global deep waters to the surface of the Southern Ocean. *Nature Communications* **8**: 172. doi:[10.1038/s41467-017-00197-0](https://doi.org/10.1038/s41467-017-00197-0)

- Thorade, H. 1909. Über die Kalifornischen Meeresströmungen, Oberflächentemperaturen und Strömungen, an der Westküste Nordamerikas. *Annalen der Hydrographie und maritimen Meteorologie* **37**: 17-34,63-77.
- Thoreau, H. D. 1854. *Walden, or, life in the woods*, Boston: Ticknor and Fields.
- Thorpe, S. A., J. M. Keen, R. Jiang, and U. Lemmin. 1996. High-frequency internal waves in Lake Geneva. *Philosophical Transactions of the Royal Society of London A: Mathematical, Physical and Engineering Sciences* **354**: 237–257. doi:[10.1098/rsta.1996.0008](https://doi.org/10.1098/rsta.1996.0008)
- Thorpe, S. A., U. Lemmin, C. Perrinjaquet, and I. Fer. 1999. Observations of the thermal structure of a lake using a submarine. *Limnology and Oceanography* **44**: 1575–1582. doi:[10.4319/lo.1999.44.6.1575](https://doi.org/10.4319/lo.1999.44.6.1575)
- Toffolon, M. 2013. Ekman circulation and downwelling in narrow lakes. *Advances in Water Resources* **53**: 76–86. doi:[10.1016/j.advwatres.2012.10.003](https://doi.org/10.1016/j.advwatres.2012.10.003)
- Troitskaya, E., V. Blinov, V. Ivanov, A. Zhdanov, R. Gnatovsky, E. Sutyryna, and M. Shimaraev. 2015. Cyclonic circulation and upwelling in Lake Baikal. *Aquatic Sciences* **77**: 171–182. doi:[10.1007/s00027-014-0361-8](https://doi.org/10.1007/s00027-014-0361-8)
- Troy, C. D., S. Ahmed, N. Hawley, and A. Goodwell. 2012. Cross-shelf thermal variability in southern Lake Michigan during the stratified periods. *Journal of Geophysical Research: Oceans* **117**: C02028. doi:[10.1029/2011JC007148](https://doi.org/10.1029/2011JC007148)
- Umlauf, L., and U. Lemmin. 2005. Interbasin exchange and mixing in the hypolimnion of a large lake: The role of long internal waves. *Limnology and Oceanography* **50**: 1601–1611. doi:[10.4319/lo.2005.50.5.1601](https://doi.org/10.4319/lo.2005.50.5.1601)
- Vachon, D., and Y. T. Prairie. 2013. The ecosystem size and shape dependence of gas transfer velocity versus wind speed relationships in lakes. *Canadian Journal of Fisheries and Aquatic Sciences* **70**: 1757–1764. doi:[10.1139/cjfas-2013-0241](https://doi.org/10.1139/cjfas-2013-0241)
- Valipour, R., Y. R. Rao, L. F. León, and D. Depew. 2019. Nearshore-offshore exchanges in multi-basin coastal waters: Observations and three-dimensional modeling in Lake Erie. *Journal of Great Lakes Research* **45**: 50–60. doi:[10.1016/j.jglr.2018.10.005](https://doi.org/10.1016/j.jglr.2018.10.005)
- Viglione, G. A., and A. F. Thompson. 2016. Lagrangian pathways of upwelling in the Southern Ocean. *Journal of Geophysical Research: Oceans* **121**: 6295–6309. doi:[10.1002/2016JC011773](https://doi.org/10.1002/2016JC011773)
- Voudouri, A., E. Avgoustoglou, and P. Kaufmann. 2017. Impacts of Observational Data Assimilation on Operational Forecasts. *Perspectives on Atmospheric Sciences*. Cham: Springer International Publishing. 143–149.
- Wahl, B., and F. Peeters. 2014. Effect of climatic changes on stratification and deep-water renewal in Lake Constance assessed by sensitivity studies with a 3D hydrodynamic model. *Limnology and Oceanography* **59**: 1035–1052. doi:[10.4319/lo.2014.59.3.1035](https://doi.org/10.4319/lo.2014.59.3.1035)
- Wang, Y., K. Hutter, and E. Bäuerle. 2000. Wind-induced baroclinic response of Lake Constance. *Annales Geophysicae* **18**: 1488–1501. doi:[10.1007/s005850000279](https://doi.org/10.1007/s005850000279)
- Wanner, H., and M. Furger. 1990. The Bise - Climatology of a regional wind north of the Alps. *Meteorology and Atmospheric Physics* **43**: 105–115. doi:[10.1007/BF01028113](https://doi.org/10.1007/BF01028113)
- Wanninkhof, R. 2014. Relationship between wind speed and gas exchange over the ocean revisited: Gas exchange and wind speed over the ocean. *Limnology and Oceanography: Methods* **12**: 351–362. doi:[10.4319/lom.2014.12.351](https://doi.org/10.4319/lom.2014.12.351)
- Wells, M. G., and L. Sealock. 2009. Summer water circulation in Frenchman's Bay, a shallow coastal embayment connected to Lake Ontario. *Journal of Great Lakes Research* **35**: 548–559. doi:[10.1016/j.jglr.2009.08.009](https://doi.org/10.1016/j.jglr.2009.08.009)
- Winant, C. D. 2004. Three-dimensional wind-driven flow in an elongated, rotating basin. *Journal of Physical Oceanography* **34**: 462–476. doi:[10.1175/1520-0485\(2004\)034<0462:TWFIAE>2.0.CO;2](https://doi.org/10.1175/1520-0485(2004)034<0462:TWFIAE>2.0.CO;2)
- Woolf, D. K. 1993. Bubbles and the air-sea transfer velocity of gases. *Atmosphere-Ocean* **31**: 517–540. doi:[10.1080/07055900.1993.9649484](https://doi.org/10.1080/07055900.1993.9649484)
- Woolway, R. I., B. M. Kraemer, J. D. Lenters, C. J. Merchant, C. M. O'Reilly, and S. Sharma. 2020. Global lake responses to climate change. *Nature Reviews Earth & Environment* **1**: 388–403. doi:[10.1038/s43017-020-0067-5](https://doi.org/10.1038/s43017-020-0067-5)



Rafael S.  
**REISS**

10.06.1988



Faubourg de l'hôpital 90  
2000 Neuchâtel, Suisse



rafael-reiss@web.de

## LANGUAGES

German ●●●●●  
English ●●●●●  
French ●●●○○

## IT & PROGRAMMING

Windows, Linux (headless  
+ desktop)  
MATLAB  
Python: data analysis and  
embedded systems,  
e.g., Raspberry Pi  
C++, C (basic)  
MITgcm (on HPC clusters)  
Abaqus FEA, Autodesk In-  
ventor, CATIA  
QGIS

## COMPETENCES

Organization of complex ex-  
periments and measurement  
campaigns  
Solid background in physics  
and mechanics, as well as  
sensor technologies, pro-  
gramming, numerical mode-  
ling, and data analysis  
Good with my hands  
Good with people and work-  
ing in teams

## HOBBIES

(Multi-day) hiking, running,  
kayaking, football/soccer  
Home brewing

*I enjoy combining practical (experimental or observational) work with numerical modeling to understand complex physical processes.*

*I am passionate about the environment and keen to help improving our understanding of aquatic systems, by employing my skills to study the various physical processes therein, including their ecological implications.*

## Education

- July 2016 **PhD, Environmental Sciences**  
July 2021 *Ecole Polytechnique Fédérale de Lausanne, EPFL (Switzerland)*  
*Ecological Engineering Laboratory, ECOL*
- "Dynamics of wind-induced coastal upwelling and interbasin exchange in Lake Geneva during winter: Implications for deepwater renewal"
  - Design, preparation and conduction of complex field measurement/mooring campaigns
  - 3D hydrodynamic modeling, Lagrangian particle tracking
  - Data analysis using Python and MATLAB
- Oct. 2009 **Diplom, Environmental Engineering (equiv. Master's)**  
Feb. 2014 *University of Stuttgart (Germany)*
- Vibration mechanics, fluid mechanics, simulation methods
    - **Thesis at Robert Bosch GmbH, Gerlingen (Germany)**  
"Simulation and optimization of multi-element ultrasonic transducers"
- Aug. 2012 **Semester abroad**  
May 2013 *McMaster University, Hamilton, ON (Canada)*
- Oct. 2007 **Vordiplom, Mechanical Engineering** ("intermediate diploma")  
Oct. 2009 *Karlsruhe Institute of Technology, KIT (Germany)*

## Professional Experience

- Sept. 2014 **Development Engineer**  
May 2016 *Robert Bosch GmbH, Leonberg (Germany)*
- Development of new ultrasonic sensors for parking and maneuvering systems
  - Design, mechanical simulation (FEM), prototype realization and experimental validation of new sensor concepts
  - Implementation and optimization of signal filters
- Oct. 2011 **Intern Department of Structural Mechanics and Acoustics**  
June 2012 *Robert Bosch GmbH, Gerlingen (Germany)*
- Assembly and experimental validation of ultrasonic sensors
  - Vibration and acoustic measurements

## Teaching Experience

- 2016 **Teaching assistant**  
2019 *Ecole Polytechnique Fédérale de Lausanne EPFL (Switzerland)*
- Soil science (Fall 2016 – 2019)
  - Limnology (Spring 2018)
- Dec. 2009 **Student assistant**  
May 2011 *Institute of Applied and Experimental Mechanics, IAM*  
*University of Stuttgart (Germany)*

## Publications:

### *Published:*

**Reiss, R. S.,** U. Lemmin, A. A. Cimadoribus, and D. A. Barry. 2020. Wintertime coastal upwelling in Lake Geneva: An efficient transport process for deepwater renewal in a large, deep lake. *Journal of Geophysical Research: Oceans* **125**. doi:[10.1029/2020JC016095](https://doi.org/10.1029/2020JC016095)

### *Submitted:*

**Reiss, R. S.,** U. Lemmin, and D. A. Barry. Wind-induced hypolimnetic upwelling between the multi-depth basins of Lake Geneva during winter: An overlooked deepwater renewal mechanism?. Submitted for publication

**Reiss, R. S.,** U. Lemmin, and D. A. Barry. What role does stratification play in wind-induced hypolimnetic upwelling between the multi-depth basins of Lake Geneva during winter?. Submitted for publication

## Conference contributions:

**Reiss, R. S.,** U. Lemmin, and D. A. Barry. 2021. *Wind-driven interbasin exchange and hypolimnetic upwelling during wintertime in a large, deep lake (Lake Geneva)*. vEGU General Assembly 2021 (virtual). vPICO

**Reiss, R. S.,** A. A. Cimadoribus, U. Lemmin, and D. A. Barry. 2019. *Deep-water coastal upwelling events during wintertime in a large lake (Lake Geneva)*. EGU General Assembly 2019. Vienna, Austria. Oral presentation.

**Reiss, R. S.,** U. Lemmin, and D. A. Barry. 2018. *Differential cooling and near-shore dynamics in a large lake (Lake Geneva)*. Physical Processes in Natural Waters (PPNW) 2018. Solothurn, Switzerland. Poster presentation.

## Patents:

Ultraschallsensorvorrichtung zur Anordnung an einem Verkleidungsbauteil eines Fahrzeugs

Patent no.:	Germany:	DE102015212599B3	(2016-06-23)
	Europe:	EP3320362B1	(2020-09-23)

Ultrasonic sensor device for arrangement on a cladding component of a vehicle

Patent no.:	U.S.	20180180725	(2018-06-28)
-------------	------	-------------	--------------